eman ta zabal zazu

Universidad del País Vasco
Euskal Herriko Unibertsitatea

Doctoral Programme in Electrical Energy Systems

Doctoral thesis

# Optimisation-based Approaches for Evaluating the Aggregation of EVs and PVs in Unbalanced Low-Voltage Networks

*Andrés Felipe Cortés Borray*

Supervisors

Dra. Esther Torres Iglesias
Dr. Jose Emilio Rodríguez Seco

2021


Inter-university Doctoral Programme in Electrical Energy Systems

# Dedication

For the Lord Jesus Christ, who always inspired me with his wisdom and knowledge.

*"If any of you lacks wisdom, let him ask God, who gives generously to all without reproach, and it will be given him."*

*James 1:5*

This thesis is also dedicated to my beloved wife, who was with me at all times, giving me her support and strength. To my parents for their love and hope. To my beautiful daughter Isabella.

I want to present a special dedication with affection to my friend and supervisor, Dr Julia Merino Fernández. For all these years of work, she always encouraged me to go beyond the limits of the circumstances no matter how strong they were, as she did until the end.

# Acknowledgements

First of all, I would like to express my gratefulness to my supervisors and friends, Dr Julia Merino and Dr Esther Torres for giving me all the necessary support to complete this amazing research process. Also, I would like to thank Dr Javier Mazón for his kindness and guidance for all these years, for sharing his valuable knowledge and help me with new opportunities. Thanks also to Dr Emilio Rodríguez for serving as the supervisor in the name of Dr Julia Merino.

I am really thankful to Dr Alejandro Garcés because of his dedication as a teacher and for having given me such valuables advice to improve my models, as well as the discussions and reviewing time of my methodology and written articles.

I would also thank Dr Kalle Rauma from the Institute of Energy Systems, Energy Efficiency and Energy Economics at the TU Dortmund in Germany, for allowing a short stay in the laboratory where I learnt about how to test in real-time the algorithms to control the EV charging stations, as well as the usage of different power assets for real-time simulation.

On the other hand, I have to thank Dr Jhon Fredy Franco from the São Paulo State University UNESP and Dr Marc Petit from the Centrale-Supélec for their valuable comments as international reviewers to improve my manuscript.

Finally, I want to thank TECNALIA Member of Basque Research and Technology Alliance (BRTA) for the opportunity to perform my research through its PhD scholarship program.

tecnalia

MEMBER OF BASQUE RESEARCH
& TECHNOLOGY ALLIANCE

# Abstract

In the near future, it is expected that the distribution system operators face different technical challenges derived from the massification of electric mobility and renewable energy sources in the low voltage networks. The purpose of this thesis is to define different smart coordination strategies among different agents involved in the low voltage networks such as the distribution system operator, the aggregators and the end-users when significant penetration levels of these resources are adopted. New models for representing the uncertainty of the photovoltaic output power and the connection of the electric vehicles are introduced. A new energy boundary model for representing the flexibility of electric vehicles is also proposed. In combination with the above models, four optimisation models were proposed as coordination strategies into three different approaches: individual, population, and hybrid. The first model was defined at the aggregator level, whereas the others models were proposed at the distribution system operator level. Complementary experimental cases about the proposed optimisation model in the individual-based approach and the quadratic formulation in the hybrid approach for the PV power curtailment were carried out to test its response in real-time. Simulations results demonstrated that the proposed coordination strategies could effectively manage critical insertion levels of electric vehicles and photovoltaic units in unbalanced low voltage networks.

# Resumen

En un futuro próximo, se espera que los operadores del sistema de distribución enfrenten diferentes desafíos técnicos derivados de la masificación de la movilidad eléctrica y las fuentes de energía renovables en las redes de baja tensión. El propósito de esta tesis es definir diferentes estrategias de coordinación inteligente entre los diferentes agentes involucrados en las redes de baja tensión como el operador del sistema de distribución, los agregadores y los usuarios finales cuando se adoptan niveles de penetración significativos de estos recursos. Se introducen nuevos modelos para representar la incertidumbre de la potencia de salida fotovoltaica y la conexión de los vehículos eléctricos. También se propone un nuevo modelo de límites de energía para representar la flexibilidad de los vehículos eléctricos. En combinación con los modelos anteriores, se propusieron cuatro modelos de optimización como estrategias de coordinación en tres enfoques diferentes: individual, poblacional e híbrido. El primer modelo se definió a nivel de agregador, mientras que los otros modelos se propusieron a nivel de operador del sistema de distribución. Se llevaron a cabo casos experimentales complementarios sobre el modelo de optimización propuesto en el enfoque individual y la formulación cuadrática en el enfoque híbrido para la reducción de energía fotovoltaica para probar su respuesta en tiempo real. Los resultados de las simulaciones demostraron que las estrategias de coordinación propuestas podrían gestionar eficazmente los niveles críticos de inserción de vehículos eléctricos y unidades fotovoltaicas en redes de baja tensión desequilibradas.

# Contents

# List of Figures

# List of Tables

# Nomenclature

**Abbreviations**

| | |
|---|---|
| AM | Air Mass |
| CAPSO | Coordinated Aggregation-based PSO |
| DERs | Distributed Energy Resources |
| DSO | Distribution System Operators |
| ECR | Energy Consumption Rate |
| EMS | Energy Management System |
| ESP | Energy Service Provider |
| ESS | Energy Storage Systems |
| EV | Electric Vehicle |
| FACTS | Flexible Alternating Current Transmission System |
| HPSOM | Hybrid Particle Swarm Optimiser with Mutation |
| HV | High Voltage |
| ICE | Internal Combustion Engine |
| IEA | International Energy Agency |
| IQR | Interquartile Range |
| LFM | Local Flexibility Markets |
| LLF | Least Laxity First |
| LP | Linear Programming |
| LSA | Local Sensitivity Analysis |
| LV | Low Voltage |
| MILP | Mixed-Integer Linear Programming |
| MINLP | Mixed-Integer Nonlinear Programming |

| | |
|---|---|
| MIQP | Mixed-Integer Quadratic Programming |
| MV | Medium Voltage |
| NHTS | National Household Travel Survey |
| NLL | Negative Log-Likelihood |
| NLP | Nonlinear Programming |
| OPF | Optimal Power Flow |
| P&O | Perturb-and-Observe |
| PCC | Point of Common Coupling |
| PHEV | Plug-in Hybrid Electric Vehicles |
| PNNL | Pacific Northwest National Laboratory |
| PSO | Particle Swarm Optimisation |
| QCQP | Quadratically Constrained Quadratic Programming |
| QP | Quadratic Programming |
| SC | Sensitivity Coefficients |
| SOC | State of Charge |
| SQP | Sequential Quadratic Programming |
| STC | Standard Test Conditions |
| TE | Transactive Energy |
| TOU | Time-of-Use |
| TSO | Transmission System Operator |
| V2G | Vehicle-to-grid |
| VPP | Virtual Power Plant |

**Physics Constants**

| | | |
|---|---|---|
| $q$ | Electron's charge | $1.60217646\times10^{-19}\,C$ |
| $k$ | Boltzmann Constant | $1.3806503\times10^{-23}\,J/K$ |

**Parameters**

| | | |
|---|---|---|
| $\cos(\varphi)$ | load power factor | p.u. |
| $\eta_{ch}$ | charging efficiency | p.u. |
| $\eta_{dch}$ | discharging efficiency | p.u. |
| $BC_{k,j}$ | rated battery capacity for the $jth$ EV under aggregator $k$ | kWh |

| | | |
|---|---|---|
| $d_{k,j}$ | daily travelled distance by the $jth$ EV under aggregator $k$ | km |
| $ECR_{k,j}$ | energy consumption rate for the $jth$ EV under aggregator $k$ | kWh/km |
| $G_{eff}$ | effective irradiance | $W/m^2$ |
| $G_{STC}$ | irradiance level under the standard test conditions | $W/m^2$ |
| $I_{\text{mpp}}$ | cell's current at maximum power | $A$ |
| $k_0, k_1, k_2$ | efficiency parameters of the power inverter | |
| $N_{\text{cell}}$ | number of solar cells for the PV module. | |
| $N_p$ | number of PV modules connected in parallel | |
| $N_s$ | number of PV modules connected in series | |
| $p_{AC}^{\text{rated}}$ | inverter AC rated power | kVA |
| $p_{ch}^{\text{DC}}$ | maximum charging power at the battery side | kW |
| $p_{ch}^{\max}$ | maximum charging power from the grid side | kW |
| $p_{Line_{k,\phi}}^{\text{rated}}$ | rated capacity of the feeder main cable per phase $\phi$ for aggregator $k$ | kW |
| $S_{\text{Line}_k}^{\text{rated}}$ | rated capacity of the feeder main cable for aggregator $k$ | kVA |
| $S_{\text{Trans}_j}^{\text{rated}}$ | rated capacity of the distribution transformer $j$ | kVA |
| $SOC_{\max}$ | maximum state-of-charge | p.u. |
| $SOC_{\min}$ | minimum state-of-charge | p.u. |
| $SOC_{\text{obj}}$ | desired state-of-charge | p.u. |
| $T$ | test period | h |
| $t_s$ | time step | min |
| $T_a$ | ambient temperature | $^{\circ}C$ |
| $t_{k,j}^{\text{arr}}$ | arrival time at home for an EV $j$ under aggregator $k$ | |
| $V_{\text{mpp}}$ | cell's voltage at maximum power | $V$ |
| $V_T$ | thermal junction voltage of the cell | |
| $x_{k,i,t}$ | availability of EV in the household $i$ under aggregator $k$ at time $t$ | |
| $\alpha$ | voltage sensitivity matrix for load changes | V/kW |
| $\beta$ | voltage sensitivity matrix for generation changes | V/kW |
| $\mu$ | loading sensitivity matrix on lines for load changes | kW/kW |
| $\lambda$ | loading sensitivity matrix on lines for generation changes | kW/kW |
| $\delta$ | loading sensitivity matrix on distribution transformers for load changes | kW/kW |

| | | |
|---|---|---|
| $\epsilon$ | loading sensitivity matrix on distribution transformers for generation changes | kW/kW |

**Sets**

| | | |
|---|---|---|
| $H$ | number of households of the network | |
| $H_{k,\phi}^{EV}$ | households connected at phase $\phi$ which have an EV managed by the aggregator $k$ | |
| $H_{k,\phi}^{PV}$ | households connected at phase $\phi$ which have an PV managed by the aggregator $k$ | |
| $K$ | number of aggregators | |
| $N$ | number of nodes of the network without the slack nodes | |
| $N_k^{p_{\text{int}}}$ | number of parking time intervals for aggregator $k$ | |
| $N_{ph}$ | number of phases | |
| $Trans$ | number of distribution transformers | |

**Variables**

| | | |
|---|---|---|
| $\Delta t$ | interval length | |
| $\Delta_{k,i,t}^{P_{\text{inc}}}$ | increase in the rate of charge for the EV connected to the household $i$ under aggregator $k$ at time $t$ | kW |
| $\Delta_{k,t}^{P}$ | increase in the rate of charge for the aggregator $k$ at time $t$ | kW |
| $\eta_{\text{inv}}$ | efficiency of the power inverter | p.u. |
| $\upsilon_{oc}$ | normalised open circuit voltage of the cell | |
| $\zeta_{k,i,t}$ | export limit of the PV power for the household $i$ under aggregator $k$ at time $t$ | |
| $\zeta_{k,t}$ | export limit of the aggregated PV power for aggregator $k$ at time $t$ | |
| $e_{k,j}^{\text{obj}}$ | energy level desired for the $jth$ EV under aggregator $k$ | kWh |
| $e_{k,j}^{\text{req}}$ | energy level required for the $jth$ EV under aggregator $k$ | kWh |
| $e_{k,j}^{\text{arr}}$ | arrival energy state for the $jth$ EV under aggregator $k$ | kWh |
| $e_{k,j}^{\text{lower}}$ | lower energy boundary for the $jth$ EV under aggregator $k$ | kWh |
| $e_{k,j}^{\text{upper}}$ | upper energy boundary for the $jth$ EV under aggregator $k$ | kWh |
| $e_{k,j}^{B_{\max}}$ | battery capacity upper limit of the $jth$ EV under aggregator $k$ | kWh |
| $e_{k,j}^{B_{\min}}$ | battery capacity lower limit of the $jth$ EV under aggregator $k$ | kWh |
| $E_k^{\text{upper/lower}}(t)$ | aggregated upper/lower energy boundaries for the aggregator $k$ at time $t$ | kWh |

| | | |
|---|---|---|
| $FF$ | fill factor of the cell | |
| $FF_0$ | normalised fill factor of the cell | |
| $I_{\text{mpp(new)}}$ | corrected maximum current | $A$ |
| $I_{sc\text{(new)}}$ | corrected short-circuit current | $A$ |
| $N_{\text{slots}}$ | number of time slots | |
| $O^{ph}_{k,\phi,t}$ | overload condition in phase $\phi$ under aggregator $k$ at time $t$ | kW |
| $O_{k,t}$ | overload condition for the aggregator $k$ at time $t$ | kW |
| $p_{\text{out}}$ | normalised inverter AC output power | |
| $p_{AC}$ | power injected to the grid from the inverter | kW |
| $P^{\max}_{k,\phi,t}$ | maximum aggregated charging power per phase $\phi$ of the $kth$ aggregator at time $t$ in | kW |
| $P^{EV}_{k,i,t}$ | optimal EV charging power for the household $i$ under aggregator $k$ at time $t$ | $kW$ |
| $p^{PV}_{k,i}(t)$ | power at $t$ from the PV unit connected at household $i$ under aggregator $k$ | kW |
| $p^{\text{lower}}_{k,j}(t)$ | lower power boundary for the $jth$ EV at time $t$ under aggregator $k$ | kW |
| $p^{\text{upper}}_{k,j}(t)$ | upper power boundary for the $jth$ EV at time $t$ under aggregator $k$ | kW |
| $P^{\max}_{k,t}$ | maximum aggregated charging power of the $kth$ aggregator at time $t$ in | kW |
| $P^{\text{upper/lower}}_{k}(t)$ | aggregated upper/lower power boundaries for the aggregator $k$ at time $t$ | kW |
| $P^{PV}_{k}(t)$ | aggregated PV power for aggregator $k$ at time $t$ | kW |
| $r_s$ | normalised resistance of the cell | |
| $S^{\text{re}}_{PV_i}$ | active power of the PV unit connected at node $i$ | p.u. |
| $T_c$ | temperature of the cell | $^{\circ}C$ |
| $t^{\text{delay}}_{k,j}$ | maximum charging time delay for an EV $j$ under aggregator $k$ | |
| $t^{\text{dis}}_{k,j}$ | disconnection time for an EV $j$ under aggregator $k$ | |
| $t^{\text{int}}_{k,j}$ | discrete-time intervals for an EV $j$ parked at home under aggregator $k$ | |
| $V_{\text{mpp}(Tc)}$ | corrected maximum voltage to $T_c$ | $V$ |
| $Voc_{(Tc)}$ | corrected open circuit voltage to $T_c$ | $V$ |

# Chapter 1

# Introduction

## 1.1 General overview and context

The adoption of EVs is encouraged by governments and institutions to gradually replace the standard internal combustion engine (ICE) vehicles, particularly in large cities, where pollution is a critical issue. The use of EVs, along with increasing renewable energy generation, can help reduce greenhouse gas emissions and fulfil the ambitious goals of achieving a 45% reduction in emissions in the European Union by 2030 as compared with 1990 (European Commission, 2019). This approach was also expressed in the 2018 Global Status Report (Renewable Energy Policy Network - REN21, 2018), where the importance of incorporating new renewable energy sources and transitioning to new transport modes to achieve decarbonisation in electrical power systems was recognised. For example, in 2019, renewable energy sources such as PV solar and wind power generated an estimated 8.7% of global electricity, while all renewables satisfied 27.3% of global generation, highlighting an increased utilisation of solar PV to electrify end-uses in transport (Renewable Energy Policy Network - REN21, 2020).

According to Cluzel et al. (2015), Ertrac et al. (2017) and the European Commission (2011), a massive deployment of light-duty EVs and their charging infrastructure about 70% by 2030 and 80% by 2050 is expected in the European Union. This trend was evidenced by the International Energy Agency (IEA) (2018), whereby in 2017, the global electric car stock of EVs and plug-in hybrid electric vehicles (PHEVs) surpassed one million units more than in 2016, thereby keeping growth similar to that in 2015. In 2019, the global stock of EVs grew more than 40%, *i.e.*, two million more than in 2018. Nevertheless, that percentage was lower compared with 63%

in 2018. This growth is exemplified in Figure 1.1. Here, it can be observed that China is the most significant electric car market, followed by the United States and Japan, and subsequently, by other key European markets such as Norway and UK.

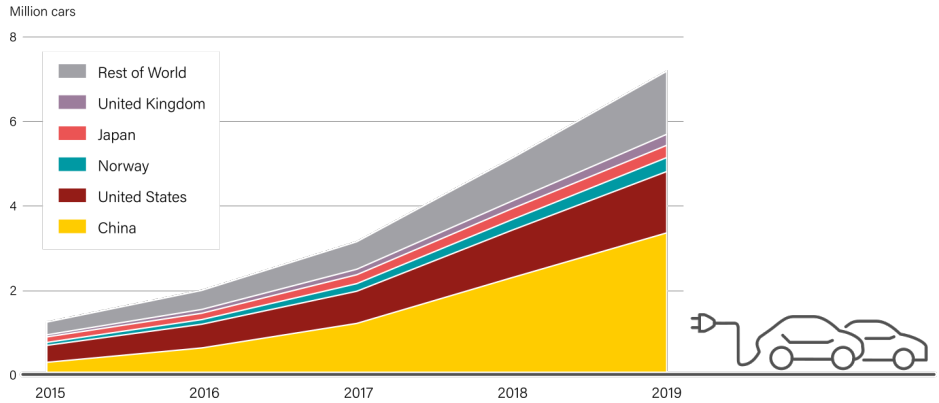


Figure 1.1: Electric car global stock 2015-2019 (top countries and rest of world). Taken from Renewable Energy Policy Network - REN21 (2020)

The progressive trend of introducing several distributed energy resources (DERs), especially in the distribution network, opens a new horizon of complexity to power system management because of the numerous technical problems that these devices may cause. The electrification of the transport is expected to produce a massive penetration level of EVs in the low voltage (LV) networks, increasing their stress during high demand periods, and bringing new challenges to the distribution system operator (DSO) such as overloading on transformers and lines, voltage deviations, increase in power losses, lower system efficiency, power quality issues and higher investments in new assets (Habib et al., 2015, Pieltain Fernandez et al., 2011) if proper control actions are not defined. Besides, the intermittent nature of renewable energy sources like PV systems brings new challenges to the distribution system in terms of power and voltage fluctuations, especially in residential areas. Those challenges are becoming more evident due to the growth of PV installations around the world. For instance, in 2019, 26 of 28 countries in the EU installed more PV capacity than in 2018, highlighting five countries such as Spain (4.8 GW), Germany (3.8 GW), the Netherlands (2.4 GW), France (0.9 GW) and Poland (0.8 MW) (Renewable Energy Policy Network - REN21, 2020). The addition of PV capacity from the top ten countries along with the rest of the world can be seen in Figure 1.2.

In this context, residential PV self-consumption is becoming exploited by several households to take advantage of the energy-cost reduction that

it provides to the owners, which is strongly related to the self-consumption policies of each country. For example, installation of PV rooftop systems in Spain rose considerably after eliminating the "Sun Tax" in November 2018 and streamlining the permitting process (Renewable Energy Policy Network - REN21, 2020). This has boosted self-consumption from individual PV systems and shared installations in the residential sector. Especially for those households with an EV, self-consumption clearly allows them to obtain (or may obtain) more benefits than those without EV (Huang et al., 2020). However, as it is not common to consume all the generated power, the excess of energy is injected into the grid. Nevertheless, this growing trend could provoke technical issues such as voltage rising if no proper control actions over those devices are employed. Besides, if the EVs are charged out of the time of PV generation availability, the grid would have to supply extra power during the night to satisfy this new demand, which would lead to overload network assets and consequent voltage drops across its feeders.

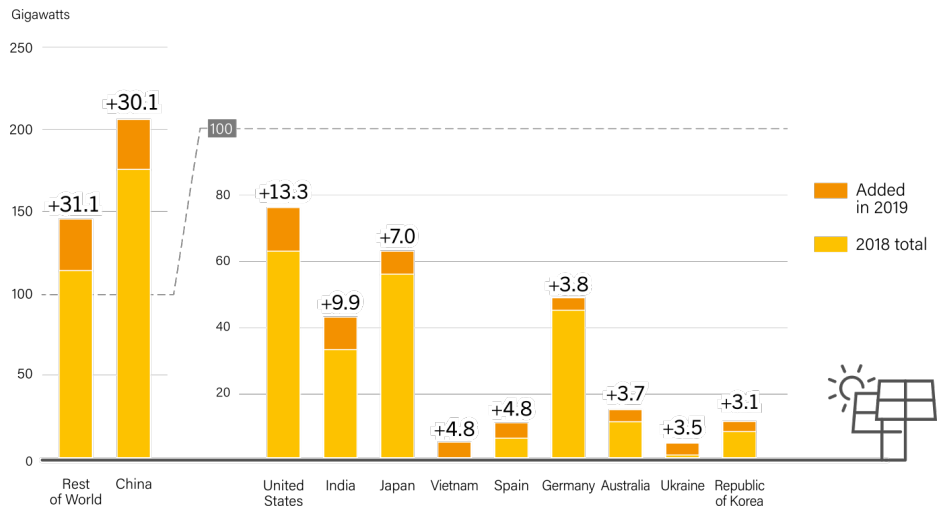


Figure 1.2: Solar PV capacity and additions in 2019 (top 10 countries for capacity added). Taken from Renewable Energy Policy Network - REN21 (2020)

Thanks to digitalisation, power systems worldwide have become more connected, smart, efficient, reliable and sustainable. This fact has enabled the interrelationship among the smart demand response, the integration of renewable energy sources, the implementation of smart charging for EVs, and the rise of small-scale DERs such as household solar photovoltaic. Besides, the recent progress obtained in the field of small-scale generation and electrical storage (e.g., for the EVs) involves thorough changes in how energy

production and distribution have been conceived for decades. In this context, the massive integration of EV and renewables can be facilitated by adopting digital technologies that provide greater visibility and controllability of these new devices in the network. Therefore, integrating these resources in sizeable quantities with smart coordination algorithms would bring some benefits to the power network, such as power management, power quality enhancement, frequency regulation, and renewable energy support (Battistelli et al., 2012, El-Zonkoly, 2014, Jia et al., 2018, Leemput et al., 2015, Zhang et al., 2018a). However, to achieve this scenario, it is necessary to investigate new approaches, strategies and agents that help to integrate these active distributed resources in large quantities into the low voltage networks.

Primarily, from the DSO perspective, the effective operation of an active distribution network can be estimated based on the general control of the resources located downstream. The term "effective operation" is considered as intended actions that modify the consumption patterns of electricity to obtain some technical or economic benefits with the help of sending price signals or consumption/generation limitations. Consequently, the expansion of such active resources results in essential challenges in the planning, investment, operation, and regulation of traditional electrical distribution systems. Additionally, these issues raise the need for new agents who can implement efficient management strategies for those devices. In this regard, the aggregator is a figure proposed by the researcher community, which has gained considerable attention because of its operational flexibility, and it is currently being implemented in legislation (European Union, 2021). In general terms, the aggregator is "an entity who acts as an intermediary between energy consumers, DER owners, and power system agents who want to manage these end-users or take advantage of the services provided by these DERs" (Burger et al., 2017).

Based on this context, this thesis proposes different management strategies as operational alternatives for the DSO and the aggregators to facilitate the integration and management of large quantities of EVs and PV units into the low voltage networks. The proposed control approaches are mainly circumscribed in the field of optimisation models, particularly employing linear and quadratic programming techniques.

## 1.2 Objectives

### 1.2.1 General

To develop a methodology that offers different approaches to the DSO (according to the available information of the network) to intelligently manage the massive penetration of EVs and PVs into the LV networks using the aggregator as the managing entity at the feeder level, *i.e.*, maximising the EV charging and the PV power generation without violating the technical limits of the LV network.

### 1.2.2 Specifics

- To define a mathematical model that accounts for the uncertainty of the PV power generation and the flexibility of EVs in order to develop more realistic scenarios for evaluating and analysing the impact of these resources on LV networks.
- To investigate the application of new analysis tools that consider the unbalanced nature and large extension of low voltage networks for its application in the coordinated management of distributed resources as part of the development of smart grids.
- To propose a conceptual scheme of coordination between the DSO and the aggregators involved in controlling the EVs and PV units in low voltage networks.
- To develop a coordination control strategy based on the application of different optimisation approaches that allow the DSO to maximise the EV charging and minimise the PV power curtailment through multiple aggregators.
- To make a proof of concept of the proposed control strategies by an experimental case study.

## 1.3 Main contributions

The main contributions of this thesis are listed below:

- A methodology to obtain the voltage and loading sensitivity matrices for unbalanced LV networks, employing the perturb-and-observe (P&O) approach. By introducing the sensitivities as a linear approximation for the network constraints, this approach reduces the complexity of the non-linear behaviour of the power flow equations.

- A mathematical model based on a simplification of a cosine function that considers the uncertainty of the PV power in order to be applied to develop more realistic scenarios in the analysis of the LV networks.

- A method based on the *Poisson* process to generate random profiles of EVs in an aggregated manner to be included in energy studies.

- A new energy-boundary model for representing the flexibility of the EVs is introduced, considering uncertainty parameters such as arrival time and travelled distance.

- A coordination scheme between DSO and aggregators was structured in a set of optimisation models named $f_1$, $f_2$, $f_3$ and $f_4$. These models categorised into three different approaches as coordination strategies at the DSO level in a decentralised manner for $f_1$ and centralised for the others, in order to assess the impact on the unbalanced LV networks when different aggregators manage several EVs and PVs. Functions $f_1$ and $f_3$ linearise network constraints throughout the sensitivity coefficients of the grid, whereas network constraints in $f_4$ are formulated as an optimal power flow linearised through the Wirtinger calculus.

## 1.4 List of publications

The following publications were developed as a result of this thesis:

### Journal papers

- **Cortés, A.**, Mazón, J., Merino, J. "Strategy of management of storage systems integrated with photovoltaic systems for mitigating the impact on LV distribution network". International Journal of Electrical Power & Energy Systems. 2018, Vol. 103, p. 470–482, ISSN 0142-0615.

- **Cortés Borray, A.F.**, Merino, J., Torres, E., Mazón, J., "A review of the population-based and individual-based approaches for electric

vehicles in network energy studies". Electric Power Systems Research. 2020, Vol. 189, p. 106785, ISSN 0378-7796.

- **Cortés Borray, A.F.**, Merino, J., Torres, E., Mazón, J. "Optimal Coordination of PV Active Power Curtailment and EVs Charging among Aggregators". Applied Sciences. 2020, Vol. 10, p. 7176.

- **Cortés Borray, A.F.**, Garcés, A., Merino, J., Torres, E., Mazón, J. "New Energy Bound-Based Model for Optimal Charging of Electric Vehicles with Solar Photovoltaic Considering Low-Voltage Network's Constraints". International Journal of Electrical Power & Energy Systems. 2021, Vol. 129, p. 106862, ISSN 0142-0615.

- **Cortés Borray, A.F.**, Merino, J., Torres, E., Garcés, A., Mazón, J. "Centralised Coordination of EVs Charging and PV Active Power Curtailment Over Multiple Aggregators in Low Voltage Networks". Sustainable Energy, Grids and Networks. 2021, Vol. 27, p. 100470, ISSN 2352-4677.

- **Cortés Borray, A.F.**, Rauma, K., Torres, E., Rodríguez-Seco, J.E., Mazón, J. "Optimal coordination of EV charging and PV power curtailment in unbalanced low voltage networks: An experimental case". in preparation to be submitted to the IET Smart Grid.

- **Cortés Borray, A.F.**, Ramirez Loaiza D.A., Garcés, A., Torres, E., Rodríguez-Seco, J.E., Mazón, J. "AC OPF for the Coordination of Multiple Aggregators for EV Charging and PV Power Curtailment in Unbalanced Low Voltage Networks". in preparation to be submitted to the International Journal of Electrical Power & Energy Systems.

**Conference proceedings**

- **Cortés, A.**, Merino, J., Torres, E. "Stochastic Generation of Aggregated Charging Profiles of PEVs for the Operation Analysis of Low Voltage Networks". The 25th International Conference And Exhibition On Electricity Distribution (CIRED)., Madrid, Spain, 3-6 June 2019.

- Sainz, J., **Cortés, A.**, Merino, J., Torres, E. "A voltage sensitivity-based method for assessment of distributed energy resources impact in unbalanced low-voltage grids". 2020 IEEE International Conference on Environment and Electrical Engineering and 2020 IEEE Industrial

and Commercial Power Systems Europe (EEEIC / I&CPS Europe), Madrid, Spain, 2020, p. 1-6.

**Book chapters**

- Merino, J., Gómez I., Fraile-Ardanuy, J., Santos M., **Cortés, A.**, et al. "Fostering DER integration in the electricity markets". in "Distributed Energy Resources in local integrated energy systems: Optimal operation and planning", Amsterdam, Elsevier, 2021, Chapter 6, p. 175–205.

## 1.5 Layout of the thesis

This document is organised as follows:

Chapter 2 presents an overview of the aggregator concept, its role under different market strategies, and the provision of grid services to the DSO. The mathematical approaches proposed in the literature for the aggregation of EVs are also reviewed and classified into three groups: individual-based, population-based, and hybrid approaches, depending on the aggregator objective.

Chapter 3 outlines the mathematical modelling of PVs and EVs. A detailed formulation for modelling the PV output power based on two approaches: the Araujo-Green model and the proposed approximation to model the PV power uncertainty. Besides, some relevant databases for extracting the necessary information to characterise the EVs demand in electrical studies are also presented. A stochastic approach based on the Poisson process is proposed to generate different sets of aggregated EVs profiles to be easily introduced in energy studies.Finally, a new energy boundary model for the EVs is introduced to represent in a simplified way the flexibility that a single vehicle or a group of vehicles can provide in an aggregated way.

Chapter 4 introduces the particular characteristics of low voltage networks and some of the proposed approaches in the literature for their analysis. The main characteristics of the low voltage network used in this thesis to analyse large penetration levels of EVs and PVs based on the analysis of different benchmark networks are described. The optimal power flow linearization based on the Wirtinger calculus and the sensitivity analysis for the unbalanced networks as mathematical approaches for assessing the low voltage grids are also introduced. The former is further expanded in Chapter 5

to the proposed convex problem.

Chapter 5 describes the mathematical formulation of the proposed four models to analyse the EV charging and the PV power curtailment at the device and aggregator level, considering the DSO as the entity that dictates the control actions to all aggregators involved. A first convex optimisation model for charging the EVs considering the PV availability for one aggregator is proposed employing a linear programming approach. This problem exemplifies the individual-based approach. Two additional convex models based on the sensitivity coefficient matrices of the network and the optimal power flow linearised through the Wintirger calculus were proposed as quadratic programming problems. These control strategies seek to define an optimal net power profile at the aggregator level under a particular DSO by managing the power of the EVs and PVs connected to the low voltage network. These problems exemplify the population-based and hybrid approaches. Different case studies are evaluated to demonstrate the robustness of the proposed methodologies.

Chapter 6 presents the experimental setup employed to test the linear programming model proposed in the Individual-based approach and the quadratic formulation at the device level in the Hybrid approaches for the optimal PV power curtailment. Three scenarios with two commercial EVs were evaluated to analyse the robustness of the algorithm in the first approach. For the second approach, one scenario was used to verify the optimal control signals in a real PV inveter operated under a PHiL simulation.

Chapter 7 outlines the main conclusions of this thesis and the future research opportunities.

Five appendices complement the thesis as follows.

- Appendix A shows the parameters for the Araujo-Green model and the proposed approximation to model the uncertainty of PV power.
- Appendix B presents in detail the proposed algorithm to compute the sensitivity matrices of an unbalanced low voltage network, which are later used in the formulation of network constraints.
- Appendix C presents the location of the EVs and PVs to simulate the proposed control charging strategy in Section 5.3 under different penetration levels.
- Appendix D briefly introduces the concept of the Wirtinger calculus and its application for linearizing the power flow equations.

- Finally, Appendix E introduces a general background of the convex optimisation problems and a brief description of the special ordered sets.

# Chapter 2

# Aggregation approaches of EVs

## 2.1 Concept and benefits of EVs aggregation

According to the European Directive 2019/944 (Council Directive, 2019), aggregation means a "function performed by a natural or legal person who combines multiple customer loads or generated electricity for sale, purchase or auction in any electricity market". This allows DERs to have greater visibility for all the techno-economic agents involved in the power system, including the flexibility they can provide. The main objective of the aggregator is to efficiently collect a certain number of DERs into a single entity, which can act either as a generation/storage system capable of supplying capacity and energy services required by the grid or as a controllable load with maximum benefit to the network (Guille and Gross, 2009). By doing so, this entity seeks the lowest costs to satisfy its portfolio's demand taking into account the costs for capacity usage (Olivella-Rosell et al., 2018a).

EV fleets can be a suitable candidate for aggregators that can exploit their flexibility by using either the vehicle-to-grid capability for load balancing or the grid-to-vehicle scheme to control the EVs charging power. In Battistelli et al. (2012), Guille and Gross (2009), Mwasilu et al. (2014), the aggregator of EVs is defined as an entity that creates a group of EVs capable of exploiting their unidirectional and bidirectional power capability to act as a distributed energy resource that can impact the grid positively. To achieve this objective, the aggregator must know the characteristic parameters (driving patterns, state of charge (SOC), or total capacity) of the EVs fleet in real-time as a response to network management during the charging period to provide, for instance, voltage regulation or other grid services (*e.g.*, congestion management, grid capacity management, control island-

ing, redundancy *n-1* support, and power quality support). Additionally, the EVs can be aggregated and controlled individually or jointly into a virtual power plant (VPP) model (Mwasilu et al., 2014). In this approach, the EVs are clustered and controlled as a single distributed energy resource, which is made visible to the transmission system operator (TSO), DSO, or the energy service provider (ESP) by the aggregator. Under this architecture, the aggregated EVs can be used to balance the demand and consumption forecast deviations of the electric power system. For all these cases, the aggregator is linked upstream to various network entities, such as the ESP, the DSO, or the TSO, through a communication interface, which allows the aggregator to inform them of its capability to provide power and energy services.

Particularly, in the VPP framework with vehicle-to-grid (V2G) technology, different control schemes can be considered depending on the EVs aggregation type within the grid. As per Mwasilu et al. (2014), the control approach in the VPP can be centralised, distributed, or hierarchical. The first scheme is based on a unique VPP control centre for decision making and information exchange, as observed in Morais et al. (2014). In contrast, in the second approach, the decisions and flow of information are entirely executed in a distributed manner. Finally, the hierarchical scheme is the intermediate between central and distributed control with some level of decision making capability distributed in the VPP.

However, such implementation requires the application of a scheme that provides the aggregator with the appropriate incentives to attract and retain enough EV owners, whose energy capacity can be of interest to a DSO or ESP. Therefore, along with meeting the EVs demand, the services provided by the EVs can be an additional source of income to the aggregator, and some of this income can be used to improve the preferential rates to the EV owners, as proposed by Honarmand et al. (2014a). Similarly, the aggregated EVs may be plugged in at locations served by different ESPs; thus, the aggregator may negotiate with more than one ESP for purchasing energy at discounted rates (Guille and Gross, 2009). Another possible solution is to integrate a large EV fleet, wherein each EV owner is dedicated to managing the queries from the DSO, TSO, or energy service providers with the help of two-way communication and control systems. However, this integration scheme might not be reliable to some extent, because dealing with each EV owner would increase the complexity of energy planning, security, and control processes (Mwasilu et al., 2014).

## 2.2 Market-based approaches for EV aggregators

Since the aggregator is an entity able to participate in both the technical and economic scenarios for managing a particular number of EVs and/or other DERs, in the literature, there are some market approaches in which the aggregator participates actively along with other stakeholders such as DSO or TSO to achieve this task. In this sense, the role and purpose of aggregation may differ depending on the market strategy, *e.g.*, transactive energy (TE) systems, local flexibility markets (LFM), or price-based strategies. Hence, to observe the participation of EV aggregators within these market-based approaches, some relevant research works in the literature are presented in Table 2.1. Note that these market-based approaches can be centralised or decentralised, depending on the design and formulation of the control methods to offer grid services or satisfy the power/energy needs of the end-users.

### 2.2.1 Transactive energy (TE)

According to The GridWise Architecture Council (2019), TE can be defined as "a set of economic and control mechanisms that allows the dynamic balance of generation and demand across the entire electrical infrastructure using value as a key operational parameter". This means making use of economic or market-based structures while considering network reliability constraints. TE methods are usually employed to manage a certain section of the power system, e.g., residential demand response. However, Jin et al. (2020) mention that TE could be less attractive for DSOs since there is no central entity responsible for satisfying their needs, leading to multiple negotiations. Nonetheless, some interesting works have been proposed in the literature. For example, Masood et al. (2020) proposed a framework where aggregators interact with a TE agent and the DSO to solve operational network problems. In order to achieve this, a bidding model is formulated as a linear programming problem that minimises the total cost of DSO for obtaining flexibility services from EVs. The work described by Hu et al. (2017a) proposes a TE approach to optimise the operational cost of EVs aggregator and network congestions for the DSO. Besides, a retailer entity settles the congestion price to reflect the violations. For a detailed discussion of TE's main features, it can be referred to the work in (Hu et al., 2017b).

Table 2.1: Comparison of different market approaches for EV aggregators

| TE | Price-based | LFM | Objective | Method | Network constraints | Ref. |
|---|---|---|---|---|---|---|
| √ | | √ | Minimise the cost and system peak load of the DSO by buying flexibility services from the aggregator of EVs | Centralised optimisation | √ | Masood et al. (2020) |
| | | √ | Maximise the profit of the EVs aggregator while the DSO obtains the lowest price of reserve services | Multi-agent management, game theory | √ | Khanekehdani et al. (2013) |
| | √ | | Minimise peak demand and operational cost of the EVs aggregator | Two-stage robust optimisation | | Xu et al. (2018) |
| | √ | | Minimise total energy cost of aggregators, system peak load, and meet charging requirements of EVs | Centralised optimisation | √ | Xu et al. (2014) |
| | | √ | Framework for a DSO to manage local load constraints by acquiring flexibility from aggregators | Multi-agent management | √ | Morstyn et al. (2019) |
| √ | | | Minimise the EVs aggregator charging cost and DSO's technical losses | Centralised optimisation | √ | Hu et al. (2017a) |

### 2.2.2 Local flexibility market (LFM)

A local flexibility market can be defined as series of trading actions where participants can be aggregated to supply flexibility services in the short or long term for a particular geographical location, DSO, TSO, and electrical network (Ramos et al., 2016). Several studies in the literature have presented different methods where the aggregator participates in a LFM. An overview of the objectives, roles, and responsibilities of LFMs that directly involve the aggregator are presented by Olivella-Rosell et al. (2018b). Khanekehdani et al. (2013) maximise the profit of an EVs aggregator who participates in the reserve services market at the distribution level using a heuristic optimisation method. A clearing price algorithm using game theory is also developed. This model also considers the DSO power restrictions in order to reduce its operational cost. The work introduced by Morstyn et al. (2019) presents an LFM based on multiple agents that allows the DSO to manage local power constraints by acquiring flexibility from competing aggregators in a decentralised manner.

### 2.2.3 Price-based schemes

In price-based schemes, the DSO predicts potential congestions on their networks at certain periods and sends the congestion price centrally to the aggregators, which schedule their resources. However, the price-based approach can lead to significant uncertainty in the load profile because the aggregators do not verify their schedules with the DSO (Parhizi et al., 2018). For example, in Xu et al. (2018), the DSO manages an LFM with multiple demand response aggregators, including EVs, in order to minimise its peak demand and to maximise its revenues. To do so, the aggregators compute their optimal energy consumption profile, which is bounded by their power and energy limits, and then, the DSO offers electricity price incentives for each aggregator by using a two-stage robust optimisation model. In Xu et al. (2014), a coordination scheme between the DSO and the EVs aggregators is presented to minimise the aggregator's operational cost and system peak load. Every aggregator buys electricity at time-of-use (TOU) rates and sells it to the EVs owners at retail prices to make profits.

## 2.3 Provision of distribution grid services by aggregators

The figure of the aggregator makes it possible for DERs to participate in providing network support services. The services that the aggregator can provide to the DSO through the EVs and other DERs will depend on the current and future network requirements. Therefore, as discussed by Quiros-Tortos et al. (2018), it is necessary to know the interaction between the EVs/DERs management schemes to address the problems at the distribution level and the availability of such resources to provide services.

Based on the literature review, there are multiple algorithms based on different control architectures to provide a single or a combination of services. For instance, Quirós-Tortós et al. (2016) developed a centralised control algorithm for mitigating the overloading and voltage issues in unbalanced LV networks because of the charging of EVs at different penetration levels. Moreover, Alam et al. (2015, 2016) designed a control strategy to optimise the use of the EV battery capacity for mitigating voltage issues in LV networks and to perform peak shaving. In work described by Farahani (2017), the voltage unbalance reduction through EVs charging/discharging optimisation was assessed.

By referring to ancillary services provided by EVs fleets, Amamra and Marco (2019) presented an intelligent scheduling strategy based on a nonlinear programming (NLP) model to supply frequency and voltage regulation services through the aggregation of EVs with V2G capability. Here, the aggregator seeks to maximise the profit of EVs owners and minimise the charging and degradation costs of their batteries when participating in both grid services. Peng et al. (2017) also proposed an optimal dispatching strategy for V2G aggregators in order to maximise their profit and satisfy the requirements of EV owners when they participate in supplementary frequency regulation. This is done by a regulation power calculation model that optimises the aggregator's profit and the tracking performance of load frequency control signal from the DSO. In addition, a multi-level methodological approach based on an extensive statistical assessment of the potential of EVs fleets to provide ancillary services at different levels of the distribution network was developed by Sarabi et al. (2016). This was performed by considering the available V2G power of the fleet, its uncertainty and impact on the reliability of bidding capacities, the flexibility of the available power interval under bidding capacity contracts, and the local limitation of different services in the distribution network. The analysed grid services in the above-mentioned

works are summarised in Table 2.2.

Hence, these facts highlight the technical potential that manages these resources, if their operation is within a regulatory framework of incentives for both the primary agents involved (TSO, DSO, aggregator, or ESP) and the end-users. A further discussion supporting active EV involvement in distribution grids, such as smart metering, EV technology, DSO-TSO regulation, trading flexibility and consumers, is presented by Knezović et al. (2017).

Table 2.2: Common grid services by Aggregators

| Ref. | Voltage regulation | Frequency regulation | Load balancing and peak power | Support to renewable energy resources | Power quality |
|---|---|---|---|---|---|
| Habib et al. (2015) | √ | √ | √ | √ | |
| Yong et al. (2015) | √ | √ | √ | √ | √ |
| Sarabi et al. (2016) | √ | √ | √ | | √ |
| Quirós-Tortós et al. (2016) | √ | | √ | | |
| Alam et al. (2015) | √ | | √ | | |
| Alam et al. (2016) | √ | | √ | √ | |
| Farahani (2017) | | | | | √ |
| Amamra and Marco (2019) | √ | √ | | | |
| Peng et al. (2017) | | √ | | | |

## 2.4 Aggregated EVs modelling

When modelling the aggregation of EVs, it is essential to consider that this set can demand or provide a certain power level to the network, which depends on the number of vehicles, its availability, battery type, and storage capacity. Other additional factors, such as energy consumption rate (ECR[1]), arrival and departure times, travelled distance, initial SOC, battery degradation, and the charge/discharge power rate, need to be considered as well. However, a difficulty of modelling the aggregation of EV is that most of these aspects are linked to the uncertainty of EV owners behaviour.

For simplicity, some researchers (Battistelli et al., 2012, Shokrzadeh et al., 2017, Zhang et al., 2017) consider that all EVs have the same battery capacity and efficiency, ignoring losses and keeping a constant charging or discharging rate. However, in other studies (Chukwu and Mahajan, 2014, Drude et al., 2014, Honarmand et al., 2014b, Mozafar et al., 2017), more detailed models where those parameters vary within a particular range were considered. For large-scale situations, some researchers use aggregated mod-

[1]The *ECR* is defined as the estimated average ratio of the electrical energy used per kilometre travelled for In-city, Highway, or Combined driving modes, expressed in kWh/km.

els to evaluate the penetration level of EVs; these models do not require individual EV charging demand forecasting or capacity evaluation (Zhang et al., 2017). For such considerations, the given approach to the aggregator model and its complexity will depend on the influence zone in the network (at HV, MV, or LV level), wherein it is evaluated to determine its efficiency. For instance, Pieltain Fernandez et al. (2011) analysed the aggregation of large-scale EVs in real distribution networks, as a planning model, for different penetration levels and simultaneity factors to assess the behaviour of investment and maintenance costs along with the incremental energy losses in the HV, MV, and LV networks. As a result, the researchers highlighted that if charging simultaneity factors decrease (smart charging strategies), up to 60–70% of the required investment to upgrade the network can be avoided. Therefore, for the TSOs and DSOs to integrate the effect of the aggregation of large quantities of EVs in grid planning, more simple models that can be integrated into their current planning programs need to be designed.

Accordingly, various schemas have been proposed in the literature to model the EVs aggregation which can be categorised into three approaches (Labeeuw and Deconinck, 2013, Oliveira and Padilha-Feltrin, 2009, Škugor and Deur, 2015a): individual-based (bottom-up), population-based (top-down), and hybrid approaches. The general equations of the most relevant methods that evaluate the aggregated EV demand are summarised in Table 2.3. Figure 2.1 shows an overview of each approach considering the basic aggregation model for the population-based scheme and the particularisation of the individual-based approach.

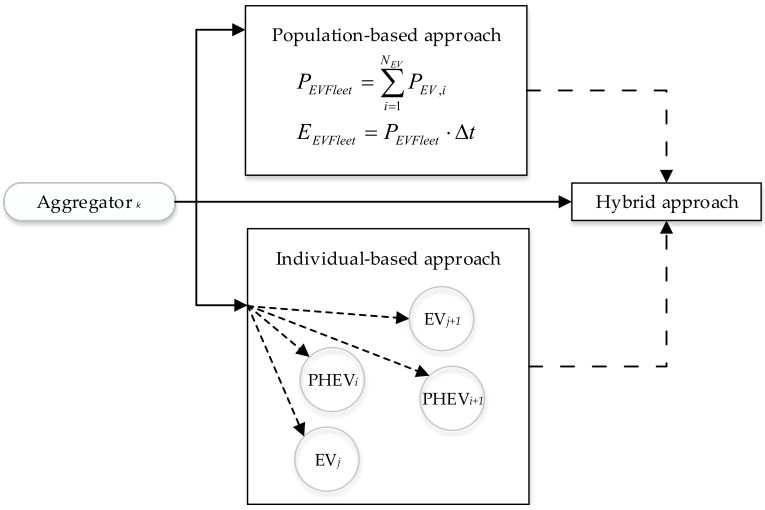


Figure 2.1: Aggregation approaches to manage the EV fleets

### 2.4.1 Population-based

When the network data scarcity becomes a limitation, a population-based approach is a suitable option to implement because it requires a lower modelling detail; there is no need to model every element individually, which reduces the intensity of modelling reasonably. Therefore, using aggregated data is not an issue if the focus is on aggregated results. However, this approach is much less encountered in the literature, and its application is sometimes limited to the estimation of energy losses and demand profiles. For instance, Oliveira and Padilha-Feltrin (2009) proposed a population-based approach for evaluating technical losses in distribution systems based on the load curve and some additional data of a given feeder or substation. This method considers the load factor and loss factor as key parameters to obtain the losses in MV and LV networks. Additionally, Labeeuw and Deconinck (2013) applied a population-based approach using Markov chains and expectation maximisation clustering models to generate a set of non-aggregated synthetic load profiles by transforming a large dataset of measured residential power.

However, regarding EVs, this approach can be encountered when modelling fleets as a single large equivalent battery with a variable energy level (Lund and Kempton, 2008, Mozafar et al., 2018), operating within an optimised boundary, as discussed by Sundstrom and Binding (2012), and Zhang et al. (2017). This approximation makes the population-based model suitable for energy planning studies, as shown by Sundstrom and Binding (2012) and Škugor and Deur (2015a,b).

The main methods to analyse the aggregation of EVs following a population-based approach are:

- The method by Battistelli et al. (2012) defines the aggregated power of a predefined number of EVs as a function of the charge/discharge, and self-discharge rates, as well as each vehicle SOC at time $t$ for a given parking of a small electric energy system. To simplify the model, the same battery specifications are considered for all the EVs. The uncertainty regarding the power profile of a parking lot is represented as a standard deviation from the expected value of the parking charging/discharging power. Thus, from the population-based approach, this parking lot can also be seen as the grouping of different EVs of residential users in an LV network, where the aggregator (under a specific DSO) needs to optimally distribute the charging power to each EV without knowing the grid in detail.

- The method of Škugor and Deur (2015a) is an energy-based approach for modelling EV fleets in electrical planning studies. It is based on the equations proposed by Lund and Kempton (2008) but adding new variables related to the SOC of the vehicles. This allows to evaluate the EV fleet energy demand by means of an average SOC of the vehicles that arrive, get connected or depart from the charging destination within some discrete-time step $k$. However, the method strongly depends on the battery and mechanical model of each vehicle, mainly from the driving power demand and the regenerative braking power. Therefore, the application of this model on a large fleet of vehicles requires taking into account several detailed parameters of every EV, which would increase the computational burden and execution time of the algorithm.

- The method of Xu et al. (2014, 2016) seeks the DSOs to schedule to different EV aggregators through their power- and energy-boundaries by minimising the energy purchase cost of all of them and load deviation of the DSOs. This is done in three steps: first, the energy and power boundaries of each aggregator are computed based on the requirements of every EV owner that is managed by this aggregator. Second, every aggregator sends that information to its DSO to compute the load profile to be optimised. Finally, every aggregator allocates to each EV the charging power profile defined by the DSO, using a heuristic optimisation algorithm.

### 2.4.2 Individual-based

The individual-based approach considers an extensively available dataset of consumers and EVs demand, photovoltaic generation, and/or local battery systems installed for use. This approach allows calculations with more accuracy, starting from individual elements in the network model, going through the feeder up to the distribution transformer. Especially, in EV grid integration studies (Liu et al., 2015, Paterakis and Gibescu, 2016, Zheng et al., 2013), this approach considers the particular vehicle battery model and the interaction between them to evaluate its aggregation. This scheme has been implemented in various studies (Marra et al., 2013, Mozafar et al., 2017, Saxena et al., 2018, van der Kam and van Sark, 2015) to evaluate the effect of the DERs mentioned above to reduce power losses, voltage fluctuations, supplying costs of EV charging demand, as well as to assess the EV battery degradation, self-consumption and load levelling. Nevertheless, the drawback of this approach is the modelling detail and the significant amount

of data required, which makes its application, computationally more time-consuming.

The more relevant methods to analyse the aggregation of EVs following an individual-based approach are:

- The method by Sundstrom and Binding (2012) is a charging energy planning approach that evaluates the EV aggregation based on the energy and power boundaries concept, similar to Zhang et al. (2017) without considering the discharging mode. However, the EVs fleet initial energy conditions are defined by a non-linear battery model for each vehicle, implemented by the authors in Sundström and Binding (2010) and partially used by Honarmand et al. (2014b). Additionally, this approach makes use of the sequential quadratic programming to obtain the reference power, which is the desired aggregated charging power time series for the DSO.

- The method by Zheng et al. (2013) considers the dynamic battery model developed by Tremblay and Dessaint (2009) as reference to evaluate the charging process of an EV with lead acid, nickel-hydrogen, or Li-ion batteries, given the initial SOC, storage capacity, and nominal voltage. The aggregation model is based on a Poisson process for the arriving vehicles to a residential parking lot. It divides the day into two time periods for both a peak and lower arrival density. A genetic algorithm is implemented to estimate the aggregation charging parameters from multiple charging curves. Moreover, an updatable optimisation method is introduced to reduce the power fluctuation level of the EVs. However, the authors do not consider the strategy over a distribution system to estimate its effect over the losses, voltage or power unbalance. Furthermore, the results of the optimisation method and the charging strategy strongly depended on the accuracy of the aggregation charging model.

- The method by Paterakis and Gibescu (2016) outlines the aggregation of EVs load profiles, mainly from the parking lots owners perspective. This approach requires the statistical evaluation of the data collected regarding arrival times, travelled distance and the EVs market share. The density functions obtained using the kernel density estimation describes the arrival time and the energy consumed in commuting, defining the EVs cluster to be charged or discharged. However, the demanded/supplied power depends on the market price signal.

- The method by Zhang et al. (2017) considers the energy and power

boundaries summation of a certain number of EVs to develop a smart charging strategy for an EV fleet with V2G capability. For avoiding individual load curve forecasting, the aggregate energy and power boundaries of the fleet are predicted every quarter-hourly. Moreover, the authors modify the least laxity first (LLF) algorithm by introducing the SOC, planning that the EVs in groups with lower indices can discharge to the grid, and vice-versa.

### 2.4.3 Hybrid

As an alternative to the pure individual- and population-based approaches, a hybrid approach can be considered, which is a combination of the above-mentioned approaches. Its application is remarkable when there is only detailed data of a specific part of the network and partial data of other zones. This is a particular approach because it consumes less time than the individual-based approach and is more accurate than the population-based approach. This approach allows obtaining a balance between data requirement and accuracy of the results. Dortolina and Nadira (2005) employes this method for estimating technical losses in distribution networks when a complete set of modelling data is not available. As this approach is less encountered in the literature for analysing the integration of DERs, this thesis proposes a suitable method that exploits the capability of this approach for the DSO to analyse the LV networks involving the aggregators as external agents in charge of managing several quantities of EVs and PVs.

Table 2.3: Relevant equations for different EV fleet modelling approaches

| Equations | Complementary expressions | Approach | Ref. |
|---|---|---|---|
| $P_{agg\ j,t} = -P_{ch,t} \cdot n_t^{ch} + P_{dch,t} \cdot n_t^{dch} + P_{Self-dch,t} \cdot n_t^{Self-dch}$ | - | Population based | Battistelli et al. (2012) |
| $SOC_{agg}(t+1) = SOC_{agg}(t) + SOC_{in,avg}(t) \cdot \frac{\Delta n_{arr}(t)}{N_{EV}} - SOC_{out,avg} \cdot \frac{\Delta n_{dep}(t)}{N_{EV}} + \eta_{ch} \cdot \frac{P_{ch,agg}(t) \cdot \Delta T}{e_{agg}^{\max}}$<br>$P_{agg} = \sum_{i=1}^{N_{EV}} P_{EV,i}(t)$ | Aggregation at time $k$<br>$SOC_{agg}(t) = E_{agg}/E_{\max,agg}$<br>$\Delta T = t_{k+1} - t_k$<br>Individual battery model<br>$SOC_j(t+1) = SOC_j(t) + \eta_{ch} \cdot \frac{P_{ch,j}(t) \cdot \Delta T}{e_j^{\max}} - \Delta SOC_j(t)$<br>$SOC_j(t) = \frac{1}{3600 \cdot e_j^{\max}} \cdot (\eta_{ch} \cdot P_{reg,j}(t) - P_{dem,j}(t)/\eta_{dch})$<br>$\Delta SOC_j(t) = \frac{P_{dem,j}(t) \cdot \Delta T}{\eta_{dch} \cdot e_j^{\max}} - \eta_{ch} \cdot \frac{P_{reg,j}(t) \cdot \Delta T}{e_j^{\max}}$ | Population based* | Škugor and Deur (2015a) |
| $E_{(t+j)}^{\max\,/\,\min} = \sum_i e_{i(t+j)}^{\max\,/\,\min}$<br>$P_{(t+j)}^{\max} = \sum_i p_{i(t+j)}^{\max}$ | Energy boundary calculation<br>$e_{i(t)}^{\max} = SOC_i^a \cdot BC_i$<br>$e_i^{\max} = (SOC_i^{\max} - SOC_i^a) \cdot BC_i$<br>$e_i^{\min} = (SOC_i^{\min} - SOC_i^a) \cdot BC_i$<br>Power boundary calculation<br>$p_{(t+j)}^{\max} = \begin{cases} 0 & j = t_i^d \dots \max\left(\Omega t_i^d\right) \\ P_{ch,i} \cdot \eta_{ch} & j = 0 \dots t_i^d - 1 \end{cases}$ | Population based | Xu et al. (2014, 2016) |
| $P_{agg} = \sum_{i=1}^{N_{EV}} P_{EVi,t}$ | Kernel density estimation-based method<br>$N_{EV} = \hat{f}_h(x)$<br>EVs power profile.<br>$P_{EVi,t} = \begin{cases} P_{ch,t} & t' < t + T_{ch,R} - 1 \\ P_{ch,t} \cdot \frac{(T_{ch,R} - T_{ch,E})}{\Delta T} & t' = t + T_{ch,R} - 1 \end{cases}$ | Individual based | Paterakis and Gibescu (2016) |

| Equations | Complementary expressions | Approach | Ref. |
|---|---|---|---|
| $P_i(t) = \begin{cases} 0 & \mathrm{t} < T_{start-ch,i} \\ P_{EV,i} & \mathrm{t} \geq T_{start-ch,i} \end{cases}$<br>$P_{agg} = \sum_{i=1}^{N_{chEV}} P_{EV,i}(t)$ | Battery model parameters<br>$E_0 = 1.0834 \cdot U_n, \quad \mathrm{K} = 0.005645 \cdot U_n/Q$<br>$A = 0.08496 \cdot U_n, \quad B = 60.0619/Q,$<br>$R = 0.01 \cdot U_n/Q, \quad \mathrm{SOC}_0 \approx N(\mu = 0.3, \sigma = 0.1)$<br>Charging battery power<br>$\mathrm{V_{batt}} = E_0 + \frac{K \cdot Q}{0.1 \cdot Q + I_t} \cdot i - \frac{K \cdot Q}{Q - I_t} \cdot I_t + A \cdot e^{-B \cdot I_t} + R \cdot i$<br>$I_t = [1 - SOC_0] \cdot Q - \int_0^t i \ \mathrm{dt}, \quad 0 \leq I_t \leq Q$<br>$P_{EV} = V_{batt} \cdot I_t$<br>EV fleet characterisation<br>$N_{EV} = [Poisson\ (\lambda_1),\ Poisson\ (\lambda_2)]$<br>$L = \frac{T_1}{\Delta T}, \quad M = \frac{T_2}{\Delta T}$<br>$N_{EV} = \sum_{i=1}^{L} n_{1i} + \sum_{i=1}^{M} n_{2i}$ | Individual based | Zheng et al. (2013) |
| $E^{+/-}(t) = \sum_i e_i^{+/-}(t)$<br>$P^{+/-}(t) = \sum_i p_i^{+/-}(t)$ | Energy boundary calculation<br>$e_i^{\max} = (SOC_i^{\max} - SOC_i^a) \cdot BC_i$<br>$e_i^{need} = (SOC_i^d - SOC_i^a) \cdot BC_i$<br>$e_i^{\min} = (SOC_i^{\min} - SOC_i^a) \cdot BC_i$<br>$e_i^+ = \begin{cases} e_i^+(t_i^d) & t > t_i^d \\ \min\ (e_i^+(t-1) + P_{ch,i} \cdot \eta_{ch} \cdot \Delta T,\ e_i^{\max}) & t_i^a < t \leq t_i^d \\ 0 & t \leq t_i^a \end{cases}$<br>$e_i^- = \begin{cases} e_i^{need} & t > t_i^d \\ \max\ (e_i^-(t-1) + P_{dch,i} \cdot \Delta T/\eta_{dch},\ e_i^{\min}, & \\ e_i^{need} - P_{ch,i} \cdot \eta_{ch} \cdot (t_i^d - t) \cdot \Delta T) & t_i^a < t \leq t_i^d \\ 0 & t \leq t_i^a \end{cases}$ | Individual based | Zhang et al. (2017) |

| Equations | Complementary expressions | Approach | Ref. |
|---|---|---|---|
| | Power boundary calculation<br>$p_i^+(t) = \begin{cases} 0 & t > t_i^d \text{ or } t \le t_i^a \\ P_{ch,i} \cdot \eta_{ch} & t_i^a < t \le t_i^d \end{cases}$<br>$p_i^-(t) = \begin{cases} 0 & t > t_i^d \text{ or } t \le t_i^a \\ P_{dch,i}/\eta_{dch} & t_i^a < t \le t_i^d \end{cases}$ | | |
| | Power boundary calculation<br>$p_i^+(t) = \sum_{i=1}^{N_{EV}} P_{\max,i,t}$<br>$p_i^-(t) = \sum_{i=1}^{N_{EV}} P_{\min,i,t}$ | | |
| $P_{ref} =$ Sequential quadratic programming-based method.<br>$E_{ref} = E_0 + \sum_{\tau=1}^{t} t_s \cdot P_{ref,\tau}$ | Energy boundary calculation<br>$e_{i,t}^{\max} = \min(e_{i,t-1}^{\max} + t_s \cdot P_{\max,i,t} - t_s \cdot P_{dem,i,t}, SOC_{\max,i} \cdot BC_i)$<br>$e_{i,t}^{\min} = \max(e_{i,t+1}^{\min} - t_s \cdot P_{\max,i,t} + t_s \cdot P_{dem,i,t}, SOC_{\min,i} \cdot BC_i)$<br>$e_t^+ = \sum_{i=1}^{N_{EV}} \left[ e_{i,t}^{\max} + \sum_{\tau=1}^{t} t_s \cdot P_{dem,i,\tau} - SOC_{\min,i} \cdot BC_i \right]$<br>$e_t^- = \sum_{i=1}^{N_{EV}} \left[ e_{i,t}^{\min} + \sum_{\tau=1}^{t} t_s \cdot P_{dem,i,\tau} - SOC_{\min,i} \cdot BC_i \right]$<br>$E_0 = \sum_{i=0}^{N_{EV}} SOC_{0,i} \cdot BC_i - SOC_{\min,i} \cdot BC_i$ | Individual based | Sundstrom and Binding (2012) |

# Chapter 3

# Mathematical modelling of PVs and EVs

## 3.1 Model of PVs

The energy provided by a PV system is given by the information about its configuration (*i.e.*, the number of strings and arrays), the geographical site, and the local weather, and it can be calculated using both indirect and direct methods. The indirect methods compute the PV power at every period and then integrate these values in a defined interval to obtain the generated energy (Rus-casas et al., 2014). This approach is mainly based on the irradiance values. On the other hand, the direct approaches calculate the supplied energy using directly the irradiation values and several parameters that define the behaviour of the PV system, such as the efficiency or the performance ratio (Rus-casas et al., 2014). Instead of using a model based on an equivalent circuit model, which requires employing numerical methods to obtain its parameters, a simple but accurate approach based on the existing relationship between the fill factor ($FF$) and the open-circuit voltage per solar cell ($V_{oc}$) can be implemented. This relation was described by Araujo and Sánchez (1982), Green (1982) in an empirical expression, as given in Equation (3.1). Note that the PV modules are commonly rated under the so-called Standard Test Conditions (STC), *i.e.*, irradiance ($G_{STC}$): 1000 $W/m^2$; Air Mass (AM): 1.5; and cell temperature ($T_c$): 25°$C$.

$$FF = \frac{V_{mpp} \cdot I_{mpp}}{V_{oc} \cdot I_{sc}} = FF_0 \cdot (1 - r_s) \tag{3.1}$$

where

$$FF_0 = \frac{\upsilon_{oc} - \ln(\upsilon_{oc} + 0.72)}{\upsilon_{oc} + 1} \tag{3.2}$$

and $I_{sc}$ is the short-circuit current at $STC$, $V_{mpp}$ and $I_{mpp}$ are the voltage and current at the maximum-power operation point at $STC$, and both define the maximum output power of the cell. These three parameters, along with the $V_{oc}$, can be found in the manufacturer's datasheets. Moreover, $r_s = 1 - {}^{FF}/_{FF_0}$ and $\upsilon_{oc} = {}^{V_{OC}}/_{V_T}$ are the normalised resistance and voltage, respectively. The last term depends on the thermal junction voltage $V_T = k \cdot T_K/q$, where $T_K$ is the Kelvin temperature. Besides, $V_T \approx 0.025\ V$ at $300\ K$ (Lorenzo, 2003), and hence, it must be corrected at $25°C$, *i.e.*, $V_T = 0.025\ V \cdot (273.15°C\ +\ 25°C)\,/300\ K$. This set of equations is valid for $\upsilon_{oc} > 15$ and $r_s < 0.4$ (Araujo and Sánchez, 1982), giving an overall accuracy better than 1%. The application of the above formulation to a PV system is immediate if all cells in the modules are assumed to be alike, and if the voltage drops across the cables connecting the system are negligible.

In order to maintain a good balance between simplicity and accuracy in the model, some assumptions are made. First, the performance of the solar cell is directly affected by the ambient temperature $T_a$ and the effective irradiance on the plane $G_{eff}$ according to Equation (3.3). Note that $G_{eff}$ can be estimated from the irradiance on the horizontal plane using the methods described by Almeida et al. (2017). Second, the short-circuit current of the solar cell depends linearly on the irradiance according to Equation (3.4). Third, the open-circuit voltage of the solar cell decreases linearly with increasing temperature on the solar cells, as given in Equation (3.5).

$$T_c = T_a + \frac{NOCT - 20^{\circ}}{800\ W/m^2} \cdot G_{eff} \tag{3.3}$$

$$I_{sc(new)} = I_{sc} \cdot \frac{G_{eff}}{G_{STC}} \tag{3.4}$$

$$Voc_{(Tc)} = Voc - \beta \cdot (T_c - 25^{\circ}) \tag{3.5}$$

where $NOCT$ is the nominal operating cell temperature, and $\beta$ is the voltage temperature coefficient, which typically equals to $0.0023°C^{-1}$ for mono and polycrystalline solar cells. In order to evaluate the maximum power of the PV system ($p_{DC} = V_{mpp(Tc)} \cdot I_{mpp(new)}$), the values of $V_{mpp(Tc)}$ and $I_{mpp(new)}$ need to be modified by $\upsilon_{oc}$ and $r_s$ according to Equations (3.6) and (3.7) (Araujo and Sánchez, 1982).

$$V_{mpp(Tc)} = N_{cell} \cdot N_s \cdot Voc_{(Tc)} \cdot \left(1 - \frac{b}{\upsilon_{oc}} \cdot \ln(a) - r_s \cdot \left(1 - a^{-b}\right)\right) \quad (3.6)$$

$$I_{mpp(new)} = N_p \cdot Isc_{(new)} \cdot \left(1 - a^{-b}\right) \quad (3.7)$$

where

$$a = \upsilon_{oc} + 1 - 2 \cdot \upsilon_{oc} \cdot r_s \quad (3.8)$$

$$b = \frac{a}{1+a} \quad (3.9)$$

and $N_{cell}$ is the number of solar cells of the PV module; $N_s$ and $N_p$, are the number of PV modules connected in series and parallel, respectively.

Since a grid-connected PV system for residential installations is generally composed of a PV array, and a power inverter, it is necessary to account for the efficiency of the latter asset in order to evaluate the output power injected into the point of connection. Therefore, the efficiency of the power inverter ($\eta_{inv}$) can be computed based on Equation (3.10) (Almeida et al., 2017, Muñoz and Perpiñán, 2016), which depends on the ratio between the actual power injected to the grid ($p_{AC}$), and its AC rated power ($p_{AC}^{rated}$).

$$\eta_{inv} = \frac{p_{AC}}{p_{AC}^{rated}} = \frac{p_{out}}{p_{out} + k_0 + k_1 \cdot p_{oout} + k_2 \cdot p_{out}^2} \quad (3.10)$$

where $p_{out} = P_{AC}/P_{AC}^{rated}$, and parameters $k_0$, $k_1$, and $k_2$ define the electrical behaviour of the inverter, *i.e.*, self-consumption, voltage drops, and power losses. These factors vary depending on the inverter's quality, and they can be obtained by fitting them from the inverter efficiency curve. Typical values are $k_0 = 0.013$, $k_1 = 0.02$ and $k_2 = 0.05$ (Silvestre, 2018), leading to 92% efficiency. An example by using synthetic data is shown in Figure 3.1.

Once Equations (3.1) to (3.10) are computed, the output power of the PV unit $i$ at time $t$, $p_{i,t}^{PV}$, is calculated according to Equation (3.11); where $p_{DC_{i,t}} = V_{\text{mpp(Tc)}} \cdot I_{\text{mpp(new)}}$.

$$p_{i,t}^{PV} = p_{DC_{i,t}} \cdot \eta_{inv} \quad (3.11)$$

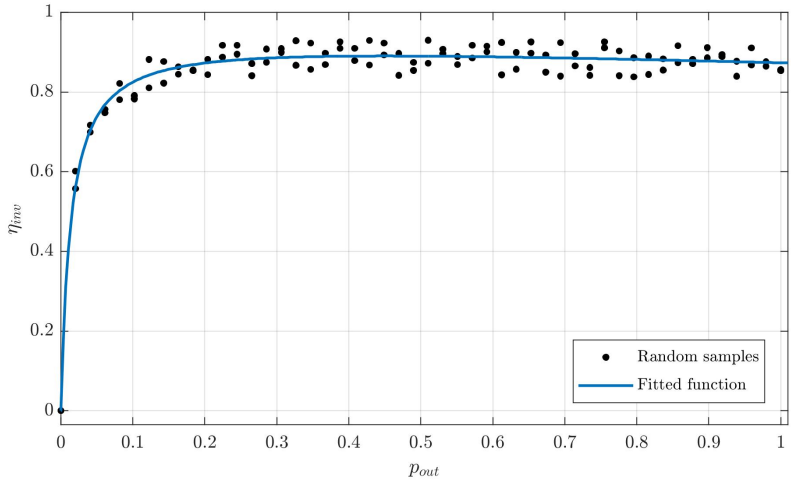


Figure 3.1: Inverter efficiency as a function of the normalised output power

### 3.1.1 Uncertainty of the PV power

A realistic representation of PV power systems requires taking into account the uncertainty of generation. In order to model the uncertainty of the PV power, first, it is necessary to analyse the behaviour of some variables such as irradiance and temperature (due to their inter-relationship). Second, include them in a model that allows calculating the output power of a PV unit, such as in the previous section. Third, forecast in a simple manner the range of variation of such power given a standard deviation value of the data.

In this sense, the yearly solar irradiance and ambient temperature data were collected from Open Data Euskadi (2018) for modelling the uncertainty of PV generation. The box-plot [1] of Figure 3.2 represents the estimated daily power production of a single-phase PV system by using the above data in the model described in Section 3.1.

Based on the PV power forecast in Figure 3.2, a math approximation for modelling the output power of PV inverters is proposed in this thesis for the summer and winter seasons. Power is represented as a shifted cosine wave squared to smooth its edges with the peak at noon, as given in Equa-

[1] Box-plot: The line that splits the box into two parts indicates the median of the data. The box represents the distance between the upper and lower quartiles, which is known as the interquartile range (IQR). The upper and lower lines are known as whiskers, which mark the data extremes. The whiskers also provide information about symmetry in the tails of the distribution. Any points lying outside the 1.5 × IQR around the box are known as "outliers" and are denoted by + symbols.

tion (3.12). This fitting function describes the uncertainty of PV power by considering the standard deviation value $\sigma$ from the data used above.

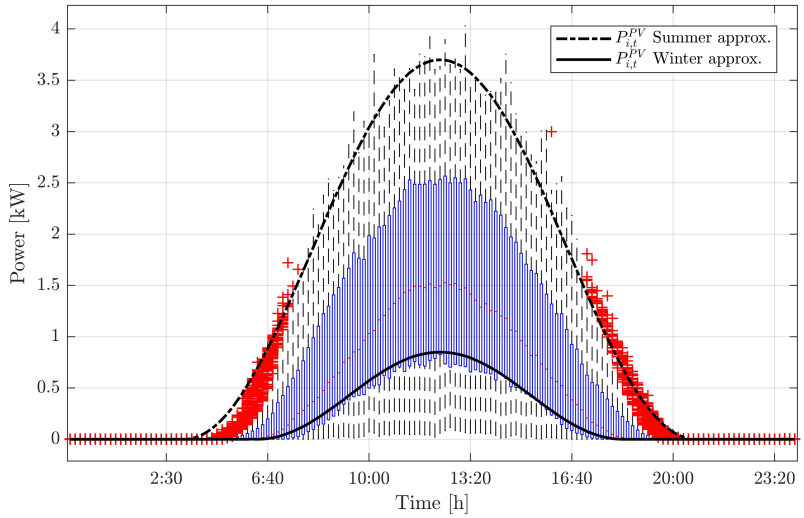


Figure 3.2: Boxplot for the PV inverter power derived from yearly meteorological data by using the model in Section 3.1. Fitted approximations of PV inverter power for summer (dashed line) and winter (continuous line) seasons.

Therefore, it is possible to generate synthetic series of PV power for a given period.

$$P_{i,t}^{PV} = P_i \cdot \cos\left(a \cdot \frac{2\pi}{N_{slots}}\left(t - \frac{N_{slots}}{2} - b\right)\right)^2 \pm \sigma \;\; \forall i \in H_{PV},\; t = 0, \ldots, N_{slots} \tag{3.12}$$

where coefficients $a$, $b$ define the period and wave shifting, and parameters $c$, $d$, allow truncating to zero the signal from $t = 0$ to $N_{slots}/c$ and from $t = \left(N_{slots} - N_{slots}/c - d\right)$ to $N_{slots}$ in order to represent the absence of solar radiation. Moreover, $P_i$ is a power set point of the inverter connected at the household $i$, $P_{i,t}^{PV}$ is the output power of the inverter hooked up at the household $i$ at time $t$, and $N_{slots}$ is the number of time slots for evaluating the model. For any evaluation period $T$, $N_{slots} = T/\Delta t$ . All model parameters are given in Appendix A.

### 3.1.2 Aggregation model of PVs

The aggregation of the available PV power generation ($P_k^{PV}$) at time $t$ is defined by Equation (3.13) as the summation of the estimated power from the individual PV unit ($p_{k,i}^{PV}$) connected at household $i$.

$$P_k^{PV}(t) = \sum_{i \in H_k^{PV}} p_{k,i}^{PV}(t), \quad \forall k \in K,\ t = 0, \ldots, N_{slots} \tag{3.13}$$

where $H_k^{PV}$ is the set of households under aggregator $k$ with a grid-connected PV system.

## 3.2 Model of EVs parking and charging behaviour

The integration of significant quantities of EVs into the LV networks, especially in residential areas, faces some limitations that restrict the network hosting capacity, primarily related to the maximum allowable voltage and currents levels. Therefore, in such local situations, network overloads can result in the accelerated ageing of the distribution grid infrastructure and eventually cause service interruptions, which could require investments for upgrading lines and transformers. So, it is becoming necessary to investigate new approaches on how to evaluate the EVs demand in an aggregated manner to prevent those undesirable effects. However, the lack of a representative sample of real EV charging profiles represents a drawback for the DSOs or for any stakeholder who wants to perform network studies evaluating the massive impact of EVs. Especially, considering the variety of manufacturers that exist in the market, the development of the lithium-ion batteries allows the globally leading automakers to present new EVs and PHEVs models with improved capabilities and broader electric ranges, which are expected to be the preferable options for the next decade (International Energy Agency (IEA), 2018).

Modelling the EV to carry out integration studies does not only imply having information on the technical characteristics of the vehicle but also on aspects related to the behaviour of the user and the recharging of the vehicle. Realistic modelling of EV aggregation requires considering a proper dataset from a reliable data source. Nowadays, researchers have access to an increasing number of databases of real data of purely electric or plug-in hybrid vehicles. This development has reduced the uncertainty in the behaviour of the owners with this type of transport, thereby expanding the

range of solutions to develop more realistic electrical studies involving these technologies. However, the data are still less for a large-scale assessment as compared to those recorded in surveys of transport authorities for ICE vehicles. Consequently, researchers are pushed to use probability distributions or in some cases to conduct surveys with a set of vehicles to evaluate various variables, such as the travelled distance, trip time, arrival and departure times, and parking time. Some relevant databases and surveys made by researchers related to ICE vehicles and EVs are described below. The main characteristics of these are summarised in Table 3.1.

### 3.2.1 Mobility surveys and databases

#### National Household Travel Survey (NHTS)

The NHTS data is the most comprehensive transportation information for the U.S. because it contains personal travel behaviour, trends in travel over time, and trip generation rates of thousands of vehicles. Therefore, it has been used in different research studies involving trips conducted by private ICE vehicles as electrifiable vehicles (Alhazmi et al., 2017, Bin Humayd and Bhattacharya, 2017, Gray and Morsi, 2017, Morais et al., 2014, Tuffner et al., 2012, Tulpule et al., 2013, Zhang et al., 2017). Darabi and Ferdowsi (2011) performed a more in-depth analysis for the vehicles daily mileage and arrival time from the 2001 NHTS data. Similarly, in (Alhazmi et al., 2017), a similar analysis was performed for the 2009 NHTS data, thereby defining a set of probability distribution functions by using the maximum-likelihood method. A recent version in 2017 (U.S. Department of Transportation) updated the information gathered in the 2001 and 2009 NHTS, and included the variable *HFUEL* to identify hybrid, plug-in hybrid, or EVs. This consideration brings new opportunities to conduct more realistic electrical studies with specific data corresponding to these technologies.

#### California Vehicle Survey

The survey conducted by the California Energy Commission from 2015 to 2017 for the residential and commercial light-duty vehicle sector collected a dataset of 3614 residential responses (including 315 EV owners) and 1712 commercial responses (including 285 EVs). According to the results reported by Mark et al. (2018), the charging behaviour is similar among residential and commercial EV owners; however, a more significant percentage of commercial PHEV owners recharge their PHEVs at work, as compared to the

residential PHEV owners. The residential EVs data of this survey was used to develop a more in-depth statistical study (Cortés et al., 2019). In this study, a methodology dependent on the Poisson process and the Monte Carlo method was proposed to generate a random series of aggregated charging profiles, which can be used for conducting electrical network studies in case of unavailability of real data. Additionally, this survey provides access to spatial data (latitude and longitude) for conducting more detailed studies by applying for approval to connect to the Transportation Secure Data Center portal in (National Renewable Energy Laboratory, 2017).

### UK National Travel Survey (NTS)

The National Travel Survey is a compendium of statistical data from 2002 to 2017 of personal travel by residents of England travelling within Great Britain. This survey gathers the results of the evaluated variables into a set of tables in ten categories, such as the average distance travelled, number of trips, start time of a journey, and the rural or urban location where the vehicle was parked overnight. The last version dataset of the NTS is available in UK Department for Transport (2018). For instance, in Bishop et al. (2013), the speed, distance travelled, and trip duration of the vehicles from the 2010 NTS were analysed to perform a distribution which provides the probability that a vehicle might be driven in any hour of the day. This evaluation allowed studying the battery degradation from the V2G technology interactions to provide either bulk energy or ancillary services to the power system.

### Zurich vehicle trace

This synthetic dataset is based on the multi-agent microscopic traffic simulator developed by the Swiss Federal Institute of Technology (ETH Zurich), which contains a detailed simulation of the Canton of Zurich in a 65000 $km^2$ area, covering 24 h information of 260000 different ICE vehicles. In Kuran et al. (2015), the vehicle arrival and departure patterns of the top five places of the database was analysed, related to the number of visits during the day, with the aim of developing an intelligent schedule to charge the EVs in a parking lot.

Table 3.1: Comparison overview of mobility databases

| Description | Source type | | Geographical data | Data type | | EV included | PHEV included | Availability | | |
|---|---|---|---|---|---|---|---|---|---|---|
| | Survey | Real measurements | | Mobility data | Charging power data | | | Open source | Request by form | Confidential |
| 2017 NHTS | √ | - | - | √ | - | √ | √ | √ | - | - |
| California Vehicle Survey | √ | - | √* | √ | √ | √ | √ | √ | - | - |
| UK National Travel Survey | √ | - | - | √ | - | - | - | √ | - | - |
| Zurich vehicle trace | √ | - | √ | √ | - | - | - | - | √ | - |
| Canadian Vehicle Use Study | √ | - | √ | √ | - | - | - | - | - | √ |
| Pecan Street Inc. | - | √ | - | - | √ | √ | √ | - | √ | - |
| ElaadNL | - | √ | √** | - | √ | √ | √ | - | √ | - |
| My Electric Avenue | - | √ | - | - | √ | √ | - | √ | - | - |
| Surveys made by researchers | √ | √ | - | √ | √ | √ | √ | √ | √ | - |

* Upon request
** Charging stations location

### Canadian Vehicle Use Study

The Canadian Vehicle Use Study is a survey conducted by Transport Canada in alliance with Environment Canada, Natural Resources Canada and different provinces (Allie, 2014). Various driving data from light, medium and heavy vehicles are collected from an onboard data-logger on the vehicle, which also records the trip purpose. These are only available by request to Transport Canada because of the sampled data amount. For instance, Shokrzadeh et al. (2017) performed driving data processing of 2840 vehicles from the Ontario province. This analysis defined the travelled distance and parking characteristics of vehicles to assess the MV/LV transformers overloading reduction by certain penetration level and by implementing V2G technology.

### Pecan Street Inc.

The Pecan Street Smart Grid Demonstration Project is a program launched in 2009 in Austin, Texas that provides an experimental measuring platform of electricity, gas, and water in 1115 residential and commercial properties, including 250 solar homes and 65 EV owners. The household consumption, EV charging demand, and PV generation are measured with a resolution ranging from 1 s to 1 min to be sent to an off-site database (PostgreSQL), which is accessible through the pgAdmin platform. It is possible to download all related data by filling a form in (Pecan Street Inc., 2019) as an academic user, whereas commercial users have access to only specific data. For instance, based on the vehicle trip data of the NHTS conducted in 2009, Harris and Webber (2014) used the Monte Carlo approach to simulate the charging demand of 10000 EVs, thereby validating the outcomes through the Pecan Street database.

### ElaadNL

The ElaadNL is a Dutch research centre specialised in smart charging infrastructure and its interoperability with the grid, whose database contains nearly one million records about the usage of charging stations installed in the Netherlands. The EV charging data is available upon request only for research purposes. Flammini et al. (2019) developed a statistical characterisation of these energy transactions historical data of 1750 public charging stations (three phase @ 12 kW) to evaluate the EV usage in terms of connected, charging, and idle times, from January 2012 to March 2016. A

clustering analysis by seasons of the EVs arrival and departure time was performed by Sadeghianpourhamami et al. (2018), which also focused on evaluating the EV flexibility exploitation by load balancing and flattening.

### My Electric Avenue

My Electric Avenue is a project conducted from 2013 to 2015 in the UK to understand the effect of EVs aggregation on LV feeders, by testing a demand control technology named Esprit, to reduce network overload. More than 76000 charging events were recorded for a year since December 2013 for 220 Nissan Leaf spread across the UK. For each EV charging event, the onboard monitoring system registered the start and end times, as well as the initial and final SOCs. Additionally, the distance, trip time, and power consumption of each EV travel were also recorded. The data is available for downloading only by filling a simple form in (EA Technology and Scottish and Southern Electricity Networks Limited, 2015). Quiros-Tortos et al. (2015) conducted a statistical study of the gathered data to assess the EVs charging behaviour, generating stochastic charging profiles to be used in smart-grid studies. Furthermore, it was observed that approximately 70% of the EVs are charged once per day, and more than 65% of those vehicles are charged until the battery full capacity is reached. It was observed that charging more likely occurred before and after work during weekdays, whereas it was more likely to occur between 10 am and 6 pm during weekends. Further, in Quirós-Tortós et al. (2016), the same authors developed a centralised control algorithm based on the obtained data to manage EVs charging points, thereby mitigating thermal and voltage issues in LV networks.

### Surveys by researchers

Some researchers (El-Zonkoly, 2014, El-Zonkoly and Dos Santos Coelho, 2015, Moradijoz et al., 2013, Sortomme et al., 2011) assumed certain penetration levels of EVs arbitrarily (such as 10%, 20%, 50%, and 100%) or according to the charging power level and node power capacity where they connect. Especially, Akhavan-Rezai et al. (2015) assumed a penetration level of 21% according to the thermal limits of the feeders; however, they made use of the Toronto Parking Authority vehicle dataset. Other researchers consider a specific number of available parking spaces for such vehicles as in Amini and Islam (2014), Battistelli et al. (2012) and Fazelpour et al. (2014) to test the developed algorithms. In Pashajavid and Golkar (2012) and Honarmand et al. (2014b) and Honarmand et al. (2014a), a survey was

conducted in Tehran city in some parking lots to obtain the daily travelled distance, and arrival and departure times from a set of ICE vehicle owners during weekdays to evaluate how to integrate the EVs into the network. Similarly, Rahbari et al. (2017) presented a survey with 300 EVs assessing the arrival and departure times, along with the initial SOC. This dataset is available to download as supplementary material from the referenced article.

A dataset with hourly records, for the year 2014, of the number of arrivals and departures from the commuter parking lot in the train station Pragal in Almada city, Portugal was presented by Figueiredo et al. (2017). Similarly, in Guner and Ozdemir (2017), the arrival and departure time records of a representative set of ICE vehicles in a parking lot was provided by the Istanbul Car Parking Corporation (ISPARK) to perform the statistical analysis of the data, using the results to evaluate the storage capacity of an EV parking lot model. Moreover, in Muratori (2017), there are two data files available to download with a 10 min resolution of 348 residential EVs related to charging Levels 1 and 2, which are linked to 200 households randomly selected from the 2009 Residential Energy Consumption Survey. The vehicle fleet consisted of 60% EVs with 321.8 km range and 40% PHEVs with 64.4 km AER.

### 3.2.2 Statistical model of EV aggregation

In this section, a methodology that allows generating a random series of aggregated charging profiles of EVs is proposed. The purpose is to provide an alternative solution to create initial input information in case of EV-real data are not available to analyse different network operational conditions. In this case, the *Poisson process* was used to formulate the aggregated power demand for a particular set of vehicles. The Monte Carlo method is used to statistically analyse the generated set of aggregated charging profiles of EVs. The proposed formulation works as a probabilistic evaluation tool that can be used by the DSO or any stakeholder in the operation and planning analysis of the LV networks.

In practice, the arrival or departure time of a set of vehicles can be described as a discrete stochastic process, where the number of events $N_t$ in a finite interval of length $t$ with independent increments obeys to the Poisson distribution. Thus, the parameter $\lambda t$ in Equation (3.14) represents the times that the random event occurs per unit time, which determines the

frequency of arrival or departure of EVs.

$$P\{N_t = n\} = \frac{(\lambda t)^n}{n!} \cdot e^{-\lambda t}, \quad n = 0, 1, 2, \ldots \tag{3.14}$$

The number of EVs that arrive ($N_{arr}^{EV}$) and depart ($N_{dep}^{EV}$) from home with a rate $\lambda_{arr}$ and $\lambda_{dep}$ for each time interval $t_i$ is described by Equations (3.15) and (3.16).

$$N_{arr}^{EV} = Poisson\ (\lambda_{arr} t_i) \tag{3.15}$$

$$N_{dep}^{EV} = Poisson\ (\lambda_{dep} t_i) \tag{3.16}$$

The aggregation of charging power ($P_t^{EV}$) at $t_1$ is given by the charging level ($P_{ch}$), the charger efficiency ($\eta_{ch}$), and the number of EVs connected to the network, as given in Equation (3.17).

$$P_{t_1}^{EV} = P_{ch} \cdot \eta_{ch} \cdot (N_{arr}^{EV}(t_1) - N_{dep}^{EV}(t_1)) \tag{3.17}$$

In the subsequent time intervals, the load curve would vary proportionally with the power demanded by the new connected vehicles and the remaining ones in $t_{i-1}$, as in (3.18). However, if at some instant $t_i$, the current load is less than zero due to the randomness of the *Poisson* distribution ($N_{dep}^{EV}(t_i) > N_{arr}^{EV}(t_i)$), the load and the number of EVs departing will be updated as shown in Equation (3.19).

$$P_{t_i}^{EV} = P_{t_{i-1}}^{EV} + P_{ch} \cdot \eta_{ch} \cdot (N_{arr}^{EV}(t_i) - N_{dep}^{EV}(t_i)) \tag{3.18}$$

$$\text{if} \quad P_{t_i}^{EV} < 0 \implies \begin{cases} N_{dep}^{EV}(t_i) = \frac{P_{t_{i-1}}^{EV}}{P_{ch} \cdot \eta_{ch}} \\ P_{t_i}^{EV} = P_{ch} \cdot \eta_{ch} \cdot N_{arr}^{EV}(t_i) \end{cases} \tag{3.19}$$

Based on the above analysis, the Monte Carlo simulation is used to perform independent random experiments (Monte Carlo trials, $n_{Tr}$) to evaluate how the aggregation of charging power is distributed employing the algorithm depicted in Algorithm 1, which significant steps are introduced as follows:

1. Obtain the required parameters from the available database of EVs
2. Define the charging power level, the efficiency, and the number of trials to generate random samples using the *Poisson* distribution

3. Compute the aggregation of load at $t_1$ and consecutive time intervals for the $jth$ Monte Carlo evaluation

4. Verify that the charging power is greater than zero

5. Obtain the matrix $P^{EV} \in \mathbb{R}^{N_{slots} \times n}$

**Algorithm 1** Random charging profile of the EVs aggregation

Compute the number of time slots $N_{slots} \leftarrow T/\Delta t$
Compute $\lambda_{arr}$ and $\lambda_{dep}$ $\forall\ t \in N_{slots}$
Define $P_{ch}$, and $\eta_{ch}$
Define the number of Monte Carlo trials ($n_{Tr}$)
$P^{EV} \in \mathbb{R}^{N_{slots} \times n} \leftarrow 0$
**for** $j \leftarrow 1, n_{Tr}$ **do**
    Compute (3.14) to (3.16)
    **for** $i \leftarrow 1, N_{slots}$ **do**
        **if** $i = 1$ **then**
            $P^{EV}_{t_i,j} \leftarrow$ Compute (3.17)
        **else**
            $P^{EV}_{t_i,j} \leftarrow$ Compute (3.18)
            **if** $P^{EV}_{t_i,j} < 0$ **then**
                Use (3.19)
            **end if**
        **end if**
    **end for**
**end for**
**return** $P^{EV} \in \mathbb{R}^{N_{slots} \times n}$

### 3.2.3 Data analysis and model evaluation

To assess the proposed formulation in Section 3.2.2, a statistical analysis was carried out using the dataset of the residential PHEVs and EVs from the 2017 California Vehicle Survey (National Renewable Energy Laboratory, 2017). Such analysis allowed to identify their commuting and charging patterns, the number of connections by charging level and the charging frequency per week. For example, in Figure 3.3, it can be observed that both the EVs and the PHEVs mostly remain connected during the early morning until 5:00 hours and in the afternoon after 17:00 hours (related to the arrival and departure rate per hour). However, in a lower percentage, some of these vehicles remain connected at noon. In more detail, the data show that 57% of the times, the vehicle owners make use of two AC charging levels at home, and only 26% of the time charge in a fast charging station in DC level (Table 3.2), as presented in Figure 3.4.

Table 3.2: Charging levels of EV/PHEV based on the SAE J1772 standard

| Type | | Power range |
|---|---|---|
| Level 1: | 120 V | 1.2–2.0 kW |
| Level 2 (low): | 240 V | 2.8–3.8 kW |
| Level 2 (high): | 240 V | 6.0–15.0 kW |
| DC level 1: | 200–450 $V_{DC}$ | 36 kW |

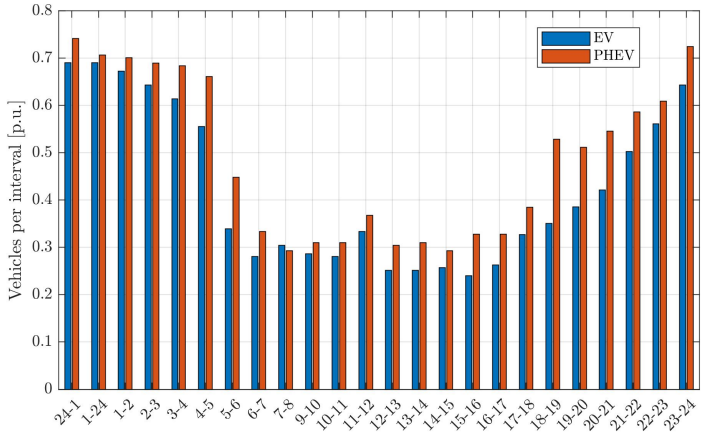


Figure 3.3: Number of EVs and PHEVs per hour

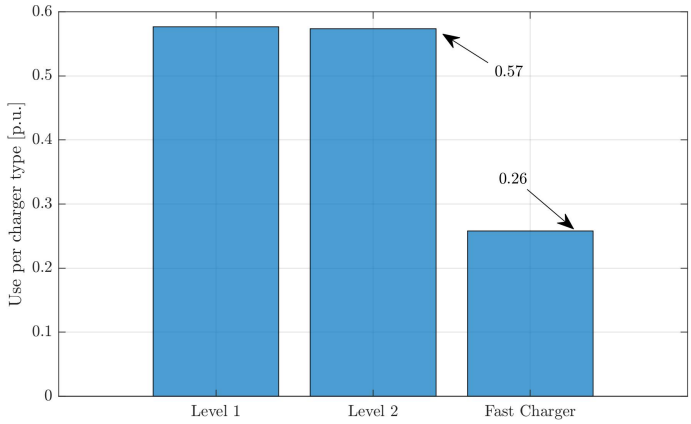


Figure 3.4: Using per charging level according to the analysed patterns of EVs and PHEVs

On the other hand, the box-plot in Figure 3.5 displays that the median of the parking time for both EVs and PHEVs using the AC Level 1 is 6-h with an inter-quartile range variation of 5-h, with a slight difference of 1-h for the PHEVs. Besides, the median of the charging time of the EVs employing AC Level 2 is lower than that of the PHEVs because the first ones charge at a higher power level, as shown in Table 3.2. Higher charging times for the EVs are also noted due to some unexpected trips (*e.g.*, to hospital, police station, and so on) or short non-regular journeys during the day (*e.g.*, theatre, mall, leisure, and so on).

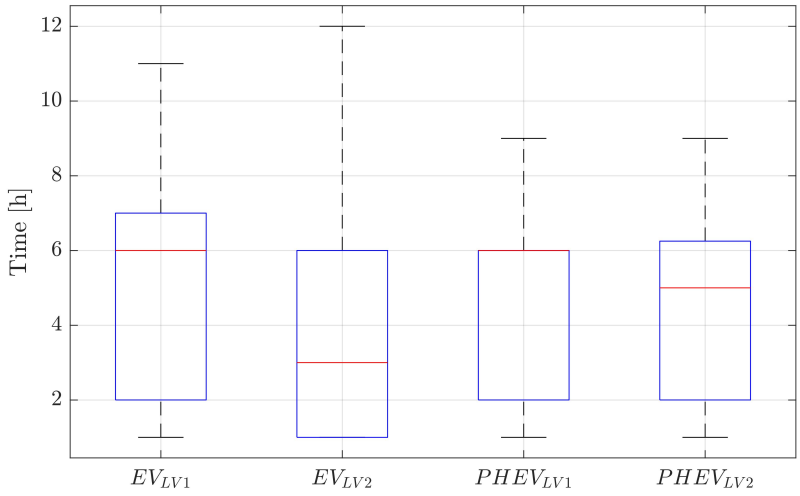


Figure 3.5: Parking time statistics per charging level and vehicle type

Due to there are numerous EVs and PHEVs models available on the market with different charging rates, and battery sizes, the owner ideally will desire to have the vehicle battery fully charged by the time it departs (range anxiety). Consequently, as atypical values, it was found that the EVs perform up to four connections per day for both charging levels as seen in Figure 3.6 (a) and (b), whereas the PHEVs display up to eight connections for the AC Level 1 and six for AC Level 2 as depicted in Figure 3.6 (c) and (d). Nevertheless, more frequently, both types of vehicles perform two connections, no matter the charging level. Furthermore, the discrete distribution which best fits the analysed data was the Poisson distribution considering the criterion of the Negative Log-Likelihood (NLL). The red curves in Figure 3.6 confirm the frequency of connection with a rate $\lambda$ close to 2 for both charging levels.

Figure 3.7 and Figure 3.8 show the relation found between the charging frequency per week and the travelled distance for both the EVs and PHEVs.

Both figures highlight that the commuting obeys the behaviour of a lognormal distribution. The mean ($\mu$) and standard deviation ($\sigma$) for both vehicle types are shown in Table 3.3. Furthermore, most EVs owners charge daily, and such frequency decreases as the days without charging increase for some owners, especially for the PHEVs. It is also noted that most of the data are concentrated in the range from 0 to 50 km with some outliers.

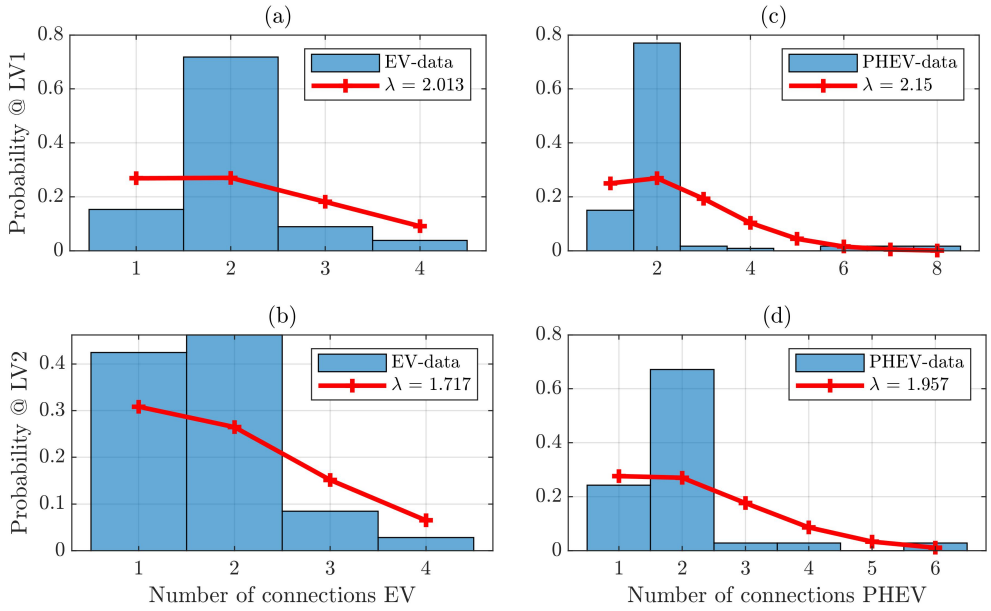


Figure 3.6: Histogram and probability density for the number of connections per day at charging level 1 and 2 for the EVs; a) and b) and the PHEVs; c) and d)

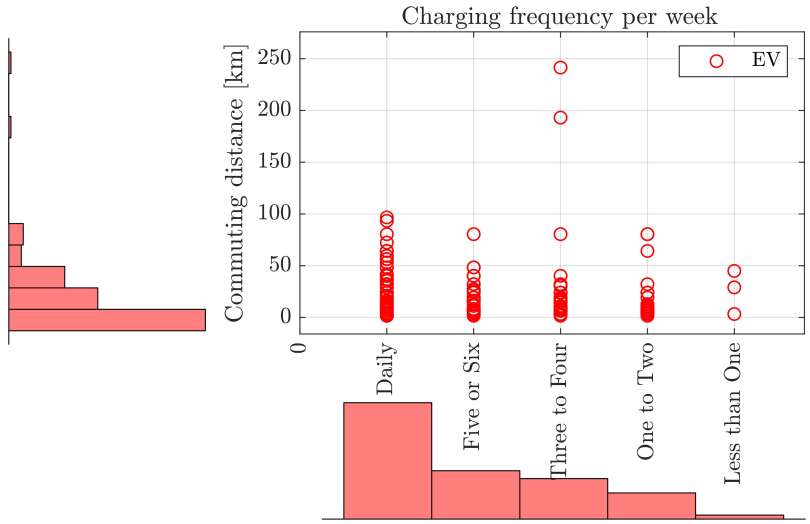


Figure 3.7: Relationship between EVs charging frequency per week and commuting distance

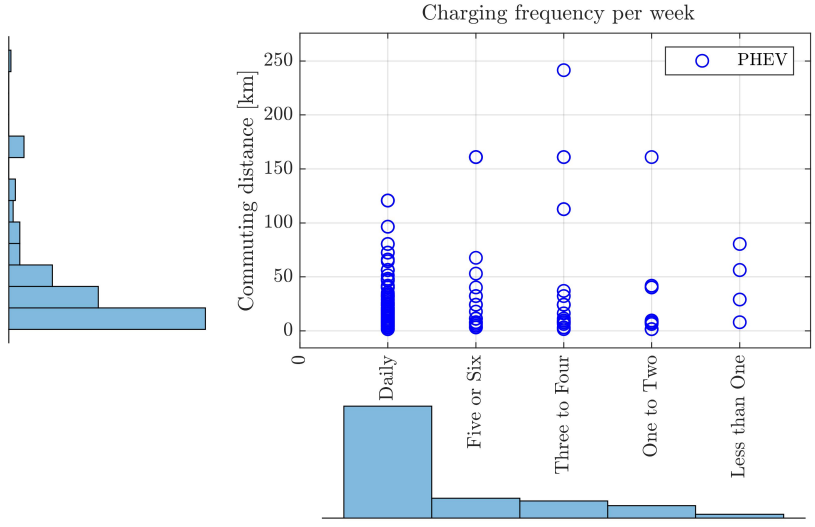


Figure 3.8: Relationship between PHEVs charging frequency per week and commuting distance

Table 3.3: Parameters of the Lognormal distribution for the commuting distance

| Vehicle type | $\mu$ | $\sigma$ |
|---|---|---|
| EV | 2.831 | 1.016 |
| PHEV | 2.938 | 1.071 |

On the other hand, Tables 3.4 and 3.5 show that the battery sizes found today in EVs and PHEVs vary considerably. For light-duty EVs and PHEVs, the range is about 16–90 kWh and 6–20 kWh, respectively. It can also be observed an average charging time of 8.3 h with a 3.7 kW onboard charger, 5.2 h and 4 h with a 7.2 kW and 11 kW off-board chargers, respectively. The last charging time is influenced by the battery capacity of Tesla S. The first charger corresponds to AC Level 1 and the other two to AC Level 2 of the standard SAE J1772 described in Mwasilu et al. (2014), Nunes et al. (2016). The ECR is computed to compare the efficiency of several EVs and PHEVs.

There are some commercial models of EVs and PHEVs, such as the Nissan Leaf (Chukwu and Mahajan, 2014), Tesla S (Paterakis and Gibescu, 2016), Mitsubishi i-MiEV (García-Villalobos et al., 2014), Chevrolet Volt (Mozafar et al., 2017), or the Toyota Prius (Tulpule et al., 2013), which are most frequently considered by researchers because of their evolution within the market; this aspect is further discussed by Mahmoudzadeh Andwari et al. (2017). Particularly, National Renewable Energy Laboratory (2017) conducted a statistical study to determine the commuting behaviour of the owners who have these vehicle types in the U.S. Based on these data, the information was classified to present the variation in travelled distance of users with cars from different automakers, as shown in the box-plot of Figure 3.9. For instance, the average commuting for Mercedes-Benz is 160 km with a high inter-quartile range variation as compared to Tesla, which doubles its electric range. It is also observed that most people perform a daily trip of less than 50 km on an average. Moreover, some outliers appear that represent the passengers who travel to rural areas or between cities with various vehicles, such as Tesla S, Ford Focus Electric, or Fiat 500e.

Moreover, the ECR for some EVs and PHEVs in the order of most efficient to least is shown in Figures 3.10 and 3.11, respectively. Thus, among the analysed vehicles, Mitsubishi i-MiEV and Hyundai IONIQ are some of the most efficient cars in the market, whereas the Toyota RAV4 EV and Cadillac ELR are the most energy consuming cars per trip.

Table 3.4: EV specifications per automaker

| Vehicle | Year | Battery capacity [kWh] | All-electric range (AER) [km] | Battery type | Charging time [h@Pch] | Pmax [kW] | ECR [kW/km] |
|---|---|---|---|---|---|---|---|
| Nissan Leaf | 2013 | 24 | 135 | Li-ion | 7.0 @ 3.3 kW<br>4.0 @ 6.6 kW | 80 | 0.1778 |
| Tesla S | 2014 | 85 | 426.5 | Li-ion | 6.7 @ 11 kW* | 270 | 0.1993 |
| Honda Fit EV | 2014 | 20 | 132 | Li-ion | 3.0 @ 6.6 kW<br>5.0 @ 9.6 kW | 100 | 0.1515 |
| Toyota RAV4 EV | 2014 | 41.8 | 165.8 | Li-ion | 6.5 @ 7.2 kW<br>12. @ 3.8 kW | 115 | 0.2521 |
| Mitsubishi i-MiEV | 2015 | 16 | 160 | Li-ion | 6.0 @ 3.8 kW<br>7.5 @ 3.7 kW | 49 | 0.1 |
| Mercedes-Benz B-Class electric | 2015 | 28 | 200 | Li-ion | 4.7 @ 7.2 kW<br>2.5 @ 11 kW* | 132 | 0.14 |
| Kia Soul EV | 2015 | 27 | 150 | Li-ion | 4.0 @ 6.6 kW | 80.5 | 0.1679 |
| Smart Cabrio | 2016 | 17.6 | 145 | Li-ion | 6.0 @ 3.3 kW | 55 | 0.1214 |
| Volkswagen e-Golf | 2016 | 24.2 | 133.6 | Li-ion | 4.0 @ 7.2 kW<br>2.7 @ 11 kW* | 85 | 0.1811 |
| BMW i3 | 2016 | 27.2 | 200 | Li-ion | 3.7 @ 7.4 kW<br>7.5 @ 3.7 kW | 125 | 0.136 |
| Volkswagen e-Golf | 2017 | 35.8 | 201 | Li-ion | 4.0 @ 7.2 kW | 100 | 0.1781 |
| Fiat 500e | 2017 | 24 | 135 | Li-ion | 4.0 @ 7.2 kW | 83 | 0.1778 |
| Chevrolet Bolt EV | 2017 | 60 | 383 | Li-ion | 9.3 @ 7.2 kW | 150 | 0.1565 |
| Ford Focus Electric | 2018 | 33.5 | 185 | Li-ion | 5.5 @ 6.6 kW | 107 | 0.1811 |
| Nissan Leaf | 2018 | 40 | 242 | Li-ion | 7.5 @ 6.6 kW | 110 | 0.1653 |
| Kia Soul EV | 2018 | 30 | 178.7 | Li-ion | 5.2 @ 6.6 kW | 81.4 | 0.1679 |

* Three-phase connection

Table 3.5: PHEV specifications per automaker

| Vehicle | Year | Battery capacity [kW] | AER [km] | Battery type | Charging time [hours@Pch] | Pmax [kW] | ECR [kWh/kW] |
|---|---|---|---|---|---|---|---|
| BMW 330e | 2015 | 7.6 | 40 | Li-ion | 2.0 @ 3.7 kW | 65 | 0.19 |
| Mercedes-Benz E 350e | 2016 | 6.2 | 33 | Li-ion | 1.7 @ 3.7 kW | 60 | 0.1878 |
| Cadillac ELR | 2016 | 17.1 | 60 | Li-ion | 5.0 @ 3.7 kW | 160** | 0.285 |
| Chevrolet Volt | 2016 | 18.4 | 85 | Li-ion | 4.5 @ 3.6 kW | 111 | 0.2164 |
| Toyota Prius Prime | 2017 | 8.8 | 35.4 | Li-ion | 5.5 @ 1.6 kW<br>2.5 @ 3.3 kW | 53 | 0.2486 |
| Kia Optima PHEV EX | 2017 | 9.8 | 46.7 | Li-poly | 2.5 @ 3.7 kW | 50 | 0.2098 |
| Audi A3 Sportback e-tron | 2017 | 8.8 | 50 | Li-ion | 2.3 @ 3.7 kW | 75 | 0.176 |
| Hyundai IONIQ | 2017 | 8.9 | 63 | Li-ion | 2.3 @ 3.7 kW | 44 | 0.1413 |
| Ford Fusion Hybrid SE | 2018 | 7.6 | 32 | Li-ion | 2.5 @ 3.6 kW | 88 | 0.2375 |

** Two motors, front-drive

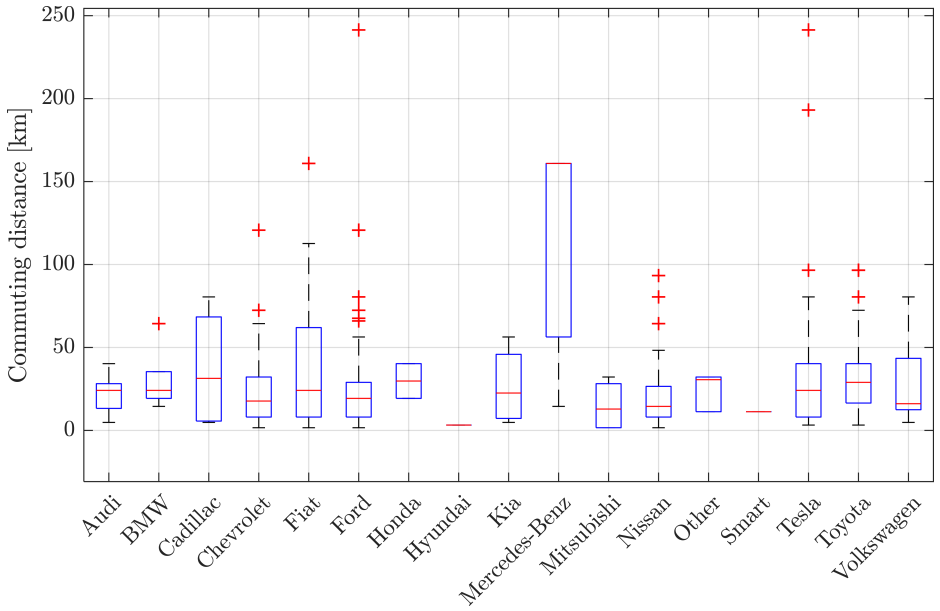


Figure 3.9: Statistical commuting distance analysis for different EV automakers computed from real data in the 2017 California Vehicle Survey

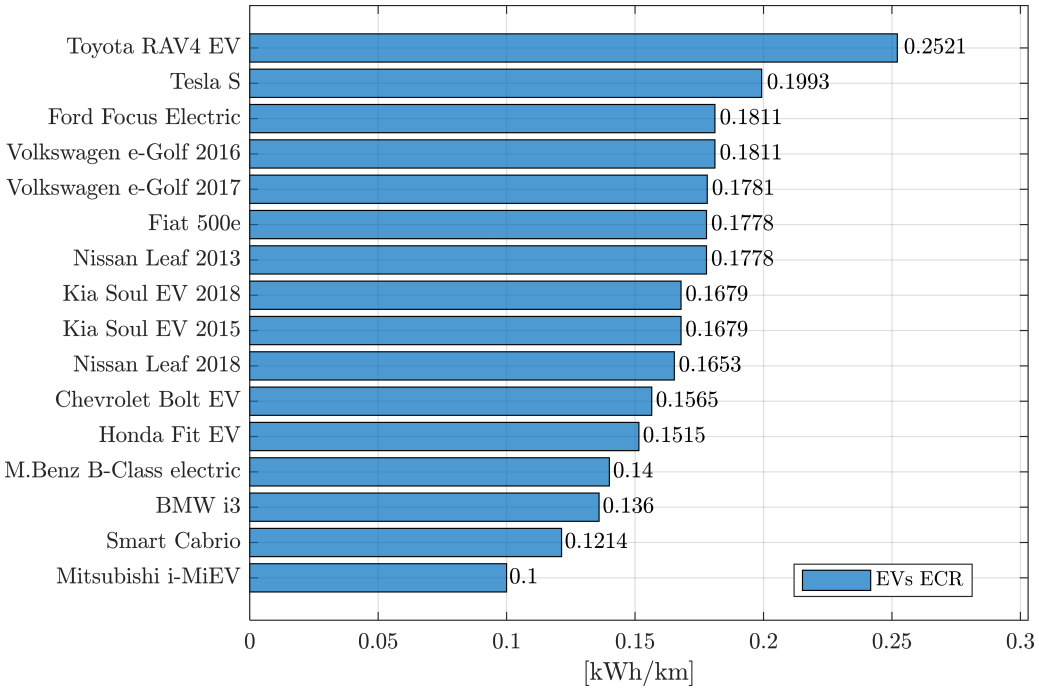


Figure 3.10: ECR computed for different EV brands registered in the 2017 California Vehicle Survey

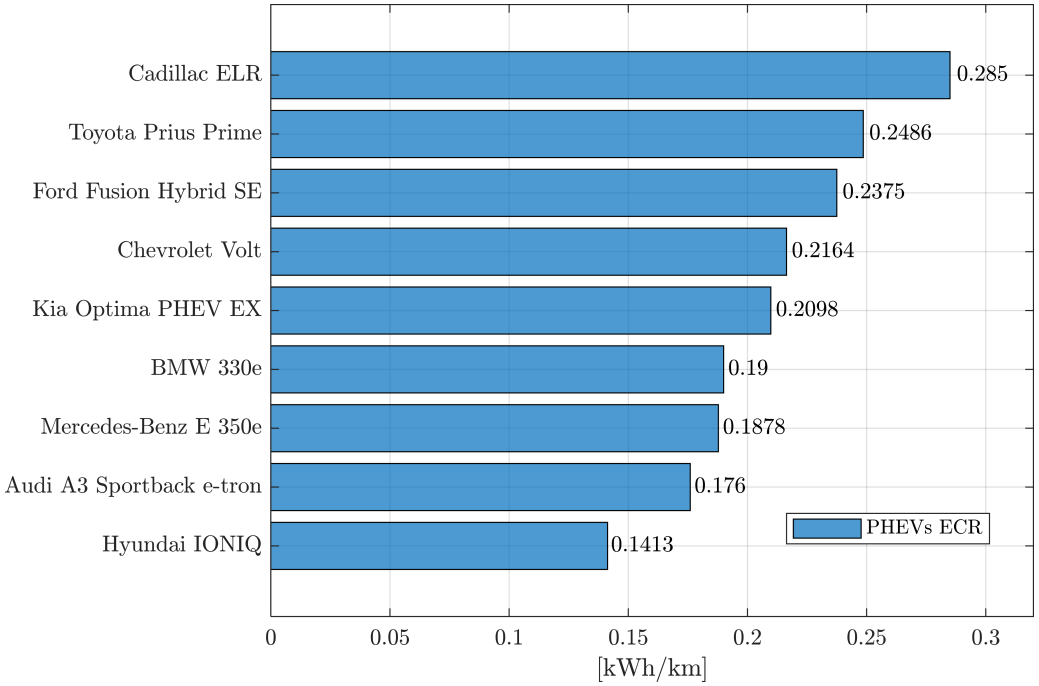


Figure 3.11: ECR computed for different PHEV brands registered in the 2017 California Vehicle Survey

From the analysed data, 367 vehicles as EVs were selected to model the load aggregation based on those drivers who start charging immediately after arriving at home and wait until they need to leave. From the total number of vehicles, 191 are EVs charging at AC Level 1 with a $P_{ch} = 1.92$ kW. The other 176 users have installed an AC Level 2 charger with a $P_{ch} = 7.2$ kW. The number of Monte Carlo trials defined to the simulation to evidence the data tendency was 10000.

The smoothing benefit arising from aggregation is of vital importance to the DSO because the more uncorrelated the demand among consumers, the more effective the overall smoothing (Freris and Infield, 2008). For that reason, as a result of using Algorithm 1 for both charging levels, the data evaluation was conducted by using a box-plot representation to show the hourly variation of the EVs charging power. Hence, in Figure 3.12 and Figure 3.14 it can be seen that the peak value of the median charging power occurs in the early morning (300 kW; 870 kW) and the maximum observed charging power take place at midnight (430 kW; 1260 kW). Besides, those peak values may vary depending on the number of Monte Carlo evaluations.

Figure 3.13 and Figure 3.15 show an example of the data dispersion due to the random assessment by the Monte Carlo method of the aggregated

charging power for a given hour from each charging level. According to the Central Limit Theorem, the sum of a large number of independent quantities tends to reach a Gaussian distribution, independent of the probability distribution function of the individual measurements (Peacock et al., 2012). This property confirms that the data distribution of Figure 3.13 fits a normal distribution with a $\mu$ of 259 kW and $\sigma$ of 25 kW along with some atypical values out of the 95% of the confidence interval (CI). Nevertheless, because of the correction effect in Algorithm 1 (in Line 14), where the foreseen power must be within the interval $[0, \infty)$, the data presented in Figure 3.15 describe an exponential distribution with $\mu = 85$ kW.

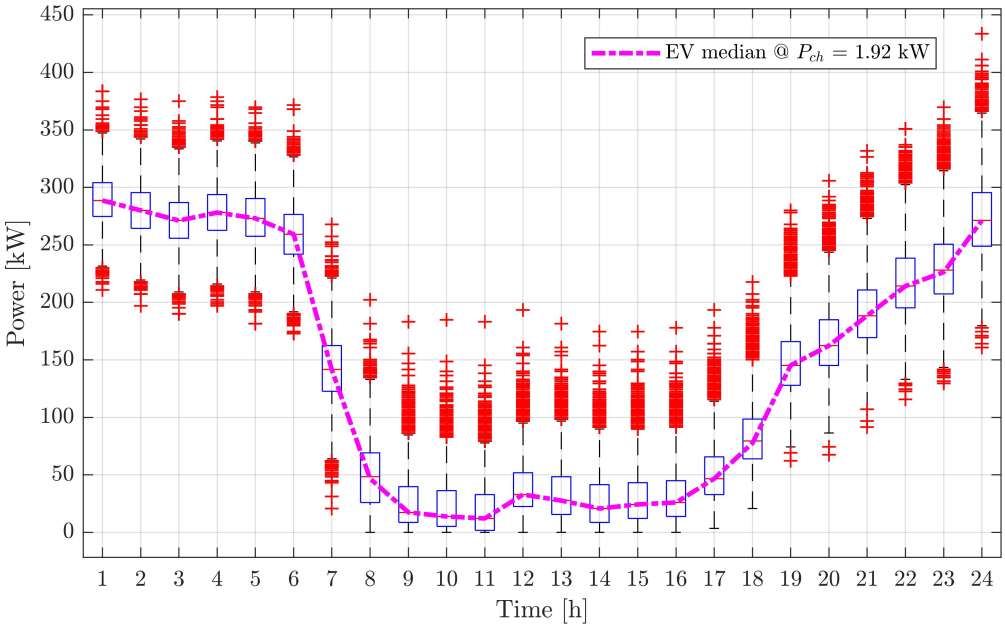


Figure 3.12: Statistical behaviour for the aggregation of EV at $P_{ch}$ = 1.92 kW

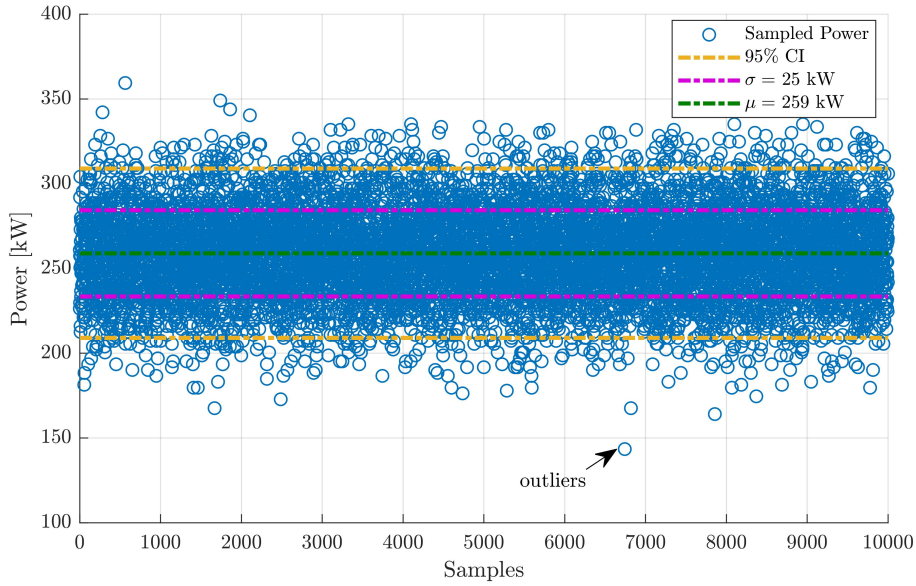


Figure 3.13: Aggregated random charging demand at 6:00 h by using the AC Level 1

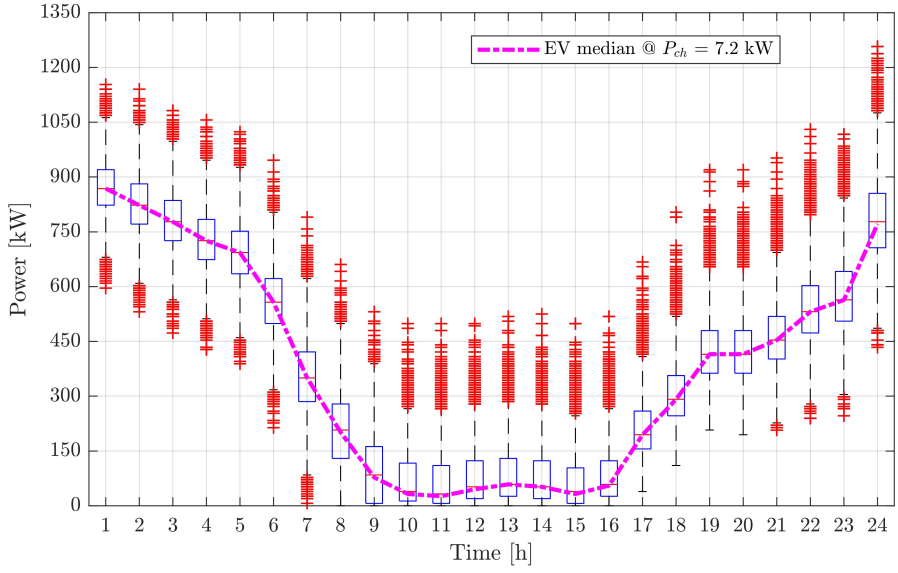


Figure 3.14: Statistical behaviour for the aggregation of EV at $P_{ch} = 7.2$ kW

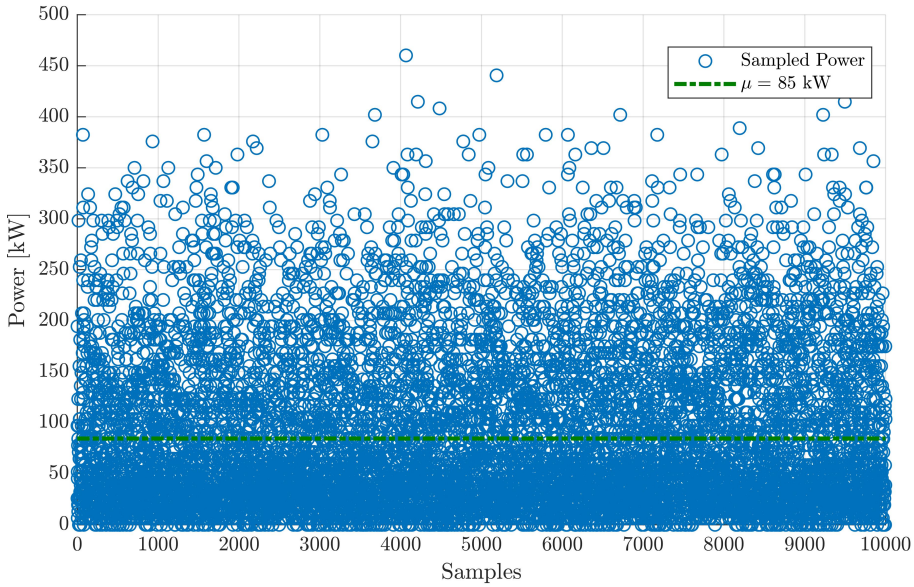


Figure 3.15: Aggregated random charging demand at 13:00 h by using the AC Level 2 (high)

## 3.3 EVs energy and power model

This section introduces a new EV model based on the lower and upper power and energy boundaries of the EV battery, which is later aggregated to be managed by a particular aggregator $k$. This approach considers as main input parameters the EV arrival/departure time, the energy characteristics of the battery and the energy requirements of the users. The V2G capability is not considered, although it can be included by introducing the discharging power and by modifying the lower limit of the battery.

The batteries of the $jth$ EV under aggregator $k$ are evaluated as a black box. This means that the charging efficiency of the batteries does not depend on the charge power $P_{k,j}^{ch}$, which can take any positive value within a certain range of nominal battery performance. Therefore, this approach simplifies the model by only considering the energy and power of the battery as input parameters in comparison with the nonlinear representation used by Hajforoosh et al. (2016), which considers charging efficiency as significant dependant on the charging rate due to the internal battery resistance.

In order to quantify the desired energy level of an EV's battery ($e_{k,j}^{obj}$) when it is connected, first, it is necessary to compute another set of energy

levels such as the arrival energy state and the rated capacity of the battery. Thus, the arrival energy level ($e_{k,j}^{arr}$) of the $jth$ EV under aggregator $k$ is determined based on its maximum battery capacity ($e_{k,j}^{Bmax}$), which is derived from the maximum state-of-charge ($SOC_{max}$) and the rated battery capacity ($BC_{k,j}$) in kWh from (3.20), as well as the energy consumption rate ($ECR_{k,j}$) and the daily travelled distance ($d_{k,j}$) in km, as given in (3.21).

$$e_{k,j}^{Bmax} = SOC_{\max} \cdot BC_{k,j} \tag{3.20}$$

$$e_{k,j}^{arr} = e_{k,j}^{\mathrm{Bmax}} - ECR_{k,j} \cdot d_{k,j} \tag{3.21}$$

Based on the arrival energy level, the desired energy level of the battery ($e_{k,j}^{obj}$) and the required energy level ($e_{k,j}^{req}$) can be obtained by Equations (3.22) and (3.23).

$$e_{k,j}^{obj} = SOC_{\mathrm{obj}} \cdot BC_{k,j} \tag{3.22}$$

$$e_{k,j}^{req} = \frac{e_{k,j}^{obj} - e_{k,j}^{arr}}{\eta_{ch}} \tag{3.23}$$

where $\eta_{ch}$ is the charger efficiency and $SOC_{obj}$ is the desired state-of-charge. The latter can be set by the owner to a specific value lower than or equal to the $SOC_{max}$. Additionally, the minimum energy level of the $jth$ EV's battery ($e_{k,j}^{Bmin}$) in (3.24) is used to verify that initial levels of $e_{k,j}^{arr}$ and $e_{k,j}^{obj}$ are feasible to be assessed. This is calculated iteratively for each EV throughout an embedded For-While loop, according to Algorithm 2. Note that for a real application of the proposed method, $e_{k,j}^{arr}$ can be directly obtained from the energy management system (EMS) of the EVs when they are connected. Therefore, it is not necessary to consider both the Equation (3.21) and the Algorithm 2. However, for energy planning studies, the whole method should be followed, as stated in this thesis.

$$e_{k,j}^{Bmin} = SOC_{\min} \cdot BC_{k,j} \tag{3.24}$$

**Algorithm 2** Correction of the energy levels per EV based on the samples of driven distance

```
for k ← 1, K do
    for j ← 1, N_k^EV do
        while (e_{k,j}^arr > e_{k,j}^obj or e_{k,j}^arr < e_{k,j}^Bmin) do
            Generate a new value of d_{k,j}, then calculate again e_{k,j}^arr and e_{k,j}^req
            as stated in (3.21) and (3.23)
        end while
    end for
end for
```

By considering the charger efficiency within the required energy level in Equation (3.23), the expected parking time ($t^{p}_{k,j}$) of the $jth$ EV under aggregator $k$ in Equation (3.25) is obtained based on the maximum charging power at the AC side of the charger ($p^{\max}_{ch}$). Note that the power level may vary due to the type of connection (single- or three-phase) and the charging standard (Cortés et al., 2019), *e.g.*, a three-phase charger with $p^{\max}_{ch} = 22$ kW and $\eta_{ch} = 0.92$ will result in a $p^{\mathrm{DC}}_{ch} = 20.24$ kW. Besides, the number of discrete-time intervals ($t^{int}_{k,j}$) for an EV $j$ parked at home, considering a time step $t_s$ and an interval length $\Delta t = t_s/60\ min$, are defined by Equation (3.26).

$$t^{p}_{k,j} = \left\lceil \frac{e^{req}_{k,j}}{p^{max}_{ch}} \right\rceil \tag{3.25}$$

$$t^{int}_{k,j} = \frac{t^{p}_{k,j}}{\Delta t} \tag{3.26}$$

Therefore, the expected disconnection time ($t^{dis}_{k,j}$) for vehicle $j$ under the $kth$ aggregator is determined by Equation (3.27), as the summation of its arrival time ($t^{arr}_{k,j}$) and parking time ($t^{p}_{k,j}$).

$$t^{dis}_{k,j} = t^{arr}_{k,j} + t^{p}_{k,j} \tag{3.27}$$

As it was discussed in Section 3.2, the arrival/departure time and the daily travelled distance of the EVs are all uncertain. However, these variables follow known probability distributions whose parameters can be predicted based on historical records. Table 3.6 summarises the use of different probability distributions by several authors to model the mobility/parking patterns of EVs. It is observed that the Gaussian and the Truncated Gaussian distributions are commonly used to model the arrival/departure time of vehicles, whereas the log-normal distribution is mostly employed to model the daily distance. Although some authors utilise a particular probability distribution to define the parking time of every vehicle, it is often determined based on arrival and departure time of the EV.

### 3.3.1 Energy and power boundaries of EVs

Under the control of an aggregator $k$, an EV $j$ with a scheduled parking time has flexible charging capacity through its energy and power boundaries, which define a possible set of charging paths (Van Roy et al., 2014). Thereby, the upper energy boundary ($e^{upper}_{k,j}$) obeys to an immediate charging process

Table 3.6: Commonly used probability distributions to describe the behaviour of the EVs

| Ref. | Time of arrival | Time of departure | Travelled distance | Parking time |
|---|---|---|---|---|
| (Hung et al., 2016) | Gaussian | | Log-normal | |
| (Yazdani-Damavandi et al., 2016) | | | Log-normal | |
| (Jhala et al., 2017) | Exponential | | | Gamma |
| (Alhazmi et al., 2017) | | | Log-normal | |
| (Shafie-Khah et al., 2016) | Truncated Gaussian | Truncated Gaussian | | |
| (Zhang and Li, 2015) | Poisson | Poisson | | |
| (Kazemi et al., 2016) | Gaussian | Gaussian | Log-normal | |
| (Aghaebrahimi et al., 2014) | Truncated Gaussian | Truncated Gaussian | Truncated Gaussian | Truncated Gaussian |
| (Mohamed et al., 2014) | Gaussian | Gaussian | | |
| (Guner and Ozdemir, 2017) | Weibull | Weibull | | |
| | Gaussian | Gaussian | | |
| | Exponential | | | |
| (Eldeeb et al., 2018) | Truncated Gaussian | Truncated Gaussian | | |

up to reach the desired energy level, which can be lower than or equal to the maximum battery capacity. In contrast, the lower energy boundary ($e_{k,j}^{lower}$) represents the curve with the maximum time delay ($t_{k,j}^{delay}$) of the charging process. Conversely, the power boundaries ($p_{k,j}^{upper/lower}$) refer to the instantaneous rated charging and discharging power at each time slot while the EV remains connected.

Based on $t_{k,j}^{arr}$ and $t_{k,j}^{dis}$, the energy boundaries for vehicle $j$ under the $kth$ aggregator are determined using the proposed recursive discrete-time equations in (3.28) to (3.30). In this model, the upper energy limit is quantified starting from the arrival energy level of the $jth$ EV under aggregator $k$ up to the number of intervals of the evaluation period ($N_{slots}$), *i.e.*, it goes from a present state up to a future one. Conversely, the lower energy boundary is computed from the required energy level of the EV $j$ under the $kth$ aggregator up to zero, i.e., it goes from a future condition up to a present one. These expressions ensure that the EV charging follows a bounded trajectory in order to provide flexibility, helping to the operation of the network and other distributed resources.

$$e_{k,j}^{upper}(t_{k,j}^{arr}+t) = min\{e_{k,j}^{upper}(t_{k,j}^{arr}+t-1) + p_{ch}^{max}\cdot\eta_{ch}\cdot\Delta t,\ e_{k,j}^{req}\}, \quad \forall k\in K, \forall j\in N_k^{EV},\ t=0,\ldots,N_{slots}-t_{k,j}^{arr} \tag{3.28}$$

$$e_{k,j}^{lower}(t_{k,j}^{dis}+t) = e_{k,j}^{req}, \quad \forall k\in K, \forall j\in N_k^{EV},\ t=t_{k,j}^{dis},\ldots,N_{slots}-t_{k,j}^{dis} \tag{3.29}$$

$$e_{k,j}^{lower}(t_{k,j}^{dis}-t) = max\{e_{k,j}^{lower}(t_{k,j}^{dis}-t+1) - p_{ch}^{max}\cdot\eta_{ch}\cdot\Delta t,\ 0\} \quad \forall k\in K, \forall j\in N_k^{EV},\ t=1,\ldots,t_{max_k}^{dis}-t_{k,j}^{arr} \tag{3.30}$$

In detail, Equation (3.28) ensures that the upper energy state of the EV $j$ in later periods ($t_{k,j}^{arr}+t$) could only be at most $P_{ch}^{max}\cdot\eta_{ch}\cdot\Delta t$ greater than

the energy remaining from the previous period ($t_{k,j}^{arr} + t - 1$). Moreover, it should also be no larger than the required energy level. Equations (3.29) and (3.30) foresee that the lower energy state of each EV at time $t_{k,j}^{dis}$ must match with the required energy level and in previous periods ($t_{k,j}^{dis} - t$) could be at most $P_{ch}^{max} \cdot \eta_{ch} \cdot \Delta t$ lower than its value at ($t_{k,j}^{arr} + t - 1$) but cannot be lower than zero. Figure 3.16 exemplifies the energy boundaries of an EV $j$ under aggregator $k$, which energy level would follow an optimal charging trajectory up to reach either the required energy state or the difference between the maximum and minimum energy level of the battery. This depends on the defined set-point for the objective energy level ($e_{k,j}^{obj}$).

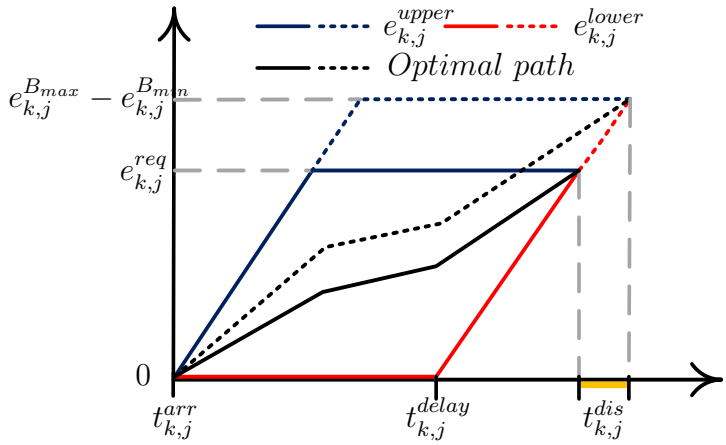


Figure 3.16: Energy boundaries of a scheduled EV under aggregator $k$

The same approach can be applied from the aggregator perspective. For example, for a unique aggregator, Equations (3.28)–(3.30) can be rewritten based on the arrival- and -objective energy level of every EV $j$ (Equations (3.32) to (3.34)) in order to know how its charging trajectory evolves between these two energy states.

$$e_j^{upper}(t) = e_j^{lower}(t) = e_j^{arr} \quad \forall j \in N_{EV},\ t = 0, \ldots, t_j^{arr} + 1 \tag{3.31}$$

$$e_j^{upper}(t_j^{arr} + t) = min\{e_j^{upper}(t_j^{arr} + t - 1) + p_{ch}^{max} \cdot \eta_{ch} \cdot \Delta t,\ e_j^{obj}\} \quad \forall j \in N_{EV},\ t = 1, \ldots, N_{slots} - t_j^{arr} \tag{3.32}$$

$$e_j^{lower}(t_j^{dis} + t) = e_j^{obj} \quad \forall j \in N_{EV},\ t = t_j^{dis}, \ldots, N_{slots} - t_j^{dis} \tag{3.33}$$

$$e_j^{lower}(t_j^{dis} - t) = max\{e_j^{lower}(t_j^{dis} - t + 1) - p_{ch}^{max} \cdot \eta_{ch} \cdot \Delta t,\ e_j^{arr}\}$$
$$\forall j \in N_{EV},\ t = 1, \ldots, t_j^{int} + 1 \quad (3.34)$$

Equation (3.31) constraints the energy state of an EV before its connection to its arrival energy level for both the upper and lower energy boundaries, as the energy state previous to this event is unknown for the aggregator. As in (3.28), Equation (3.32) seeks to define the upper energy boundary of an EV $j$, but in this case, the higher limit is no longer $e_j^{req}$ but $e_j^{obj}$. A similar change in energy limits occurs in Equation (3.33). In both Equations (3.30) and (3.34) the lower energy boundary of an EV $j$ is defined, but in the latter, the nether limit is set by $e_j^{arr}$ instead of zero. Figure 3.17 exemplifies the optimal charging trajectory of an EV $j$ between its energy boundaries, either starting from *a)* $e_j^{arr} \geq e_j^{B_{min}}$ or *b)* $e_j^{arr} = e_j^{B_{min}}$ up to reach the objective energy state as long as the set-point does not change.

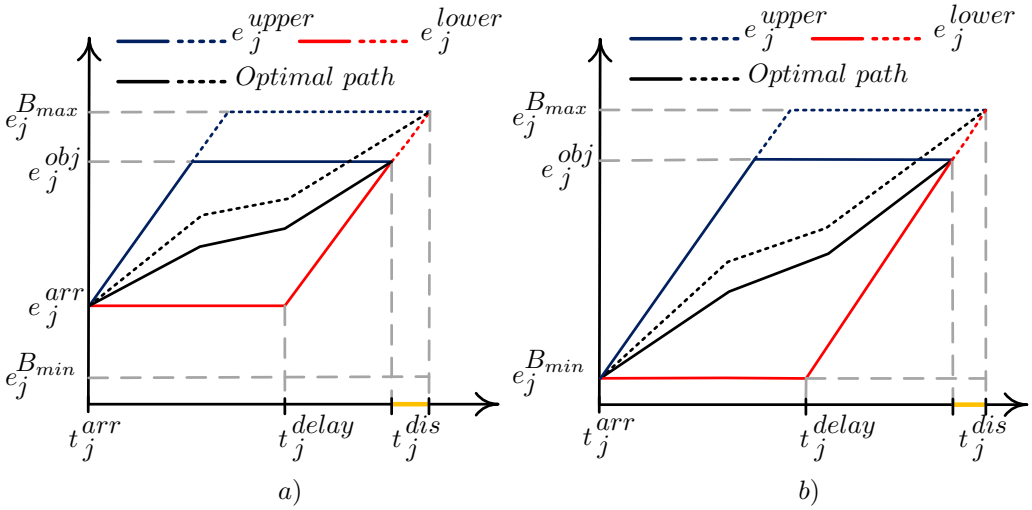


Figure 3.17: Energy boundaries of a scheduled EV under a single aggregator for *a)* $e_j^{arr} \geq e_j^{B_{min}}$ or *b)* $e_j^{arr} = e_j^{B_{min}}$

As the maximum charging power of a vehicle depends on the rated power of its charger, its upper power boundary ($p_{k,j}^{upper}$) in time slot $t$ is defined by Equation (3.35). Notice that the maximum discharging power ($p_{dch}^{max}$) of vehicle $j$ is set to zero because of the V2G capability is not considered. Hence, its lower power boundary ($p_{k,j}^{lower}$) is also zero. However, if such capability is available, $p_{k,j}^{lower}$ can be computed by Equation (3.36).

$$p_{k,j}^{upper}(t) = \begin{cases} p_{ch}^{max} \cdot \eta_{ch}, & t = t_{k,j}^{arr}, \ldots, t_{k,j}^{dis} \\ 0 & otherwise \end{cases} \qquad \forall k \in K, \forall j \in N_k^{EV} \quad (3.35)$$

$$p_{k,j}^{lower}(t) = \begin{cases} \frac{p_{dch}^{max}}{\eta_{ch}}, & t = t_{k,j}^{arr}, \ldots, t_{k,j}^{dis} \\ 0 & otherwise \end{cases} \qquad \forall k \in K, \forall j \in N_k^{EV} \quad (3.36)$$

where ($\eta_{ch}$) is the efficiency of the discharging process.

### 3.3.2 Aggregation model of EVs

The flexibility of a sizeable fleet of EVs is defined by aggregating the flexibility of each vehicle $j$ under aggregator $k$. Therefore, the total energy- and -power boundaries of the $kth$ aggregator are given by Equations (3.37) and (3.38). Once the aggregator has gathered this information, it is sent to the DSO to optimise the aggregated charging pattern without concerning of the charging requirements of each EV. This avoids disclosing private information of the aggregator's customers with the DSO. An example of the aggregation of individual flexibility of EVs is shown in Figure 3.18. In Figure 3.18a), the dashed line between $E_k^{upper}$ and $E_k^{lower}$ depicts a possible charging trajectory of the EV fleet, whereas in Figure 3.18b), the solid line between $P_k^{upper}$ and $P_k^{lower}$ represents the above trajectory in terms of charging power.

$$E_k^{upper/lower}(t) = \sum_{j \in N_k^{EV}} e_{k,j}^{upper/lower}(t), \quad \forall k \in K,\ t = 0, \ldots, N_{slots} \quad (3.37)$$

$$P_k^{upper/lower}(t) = \sum_{j \in N_k^{EV}} p_{k,j}^{upper/lower}(t), \quad \forall k \in K,\ t = 0, \ldots, N_{slots} \quad (3.38)$$

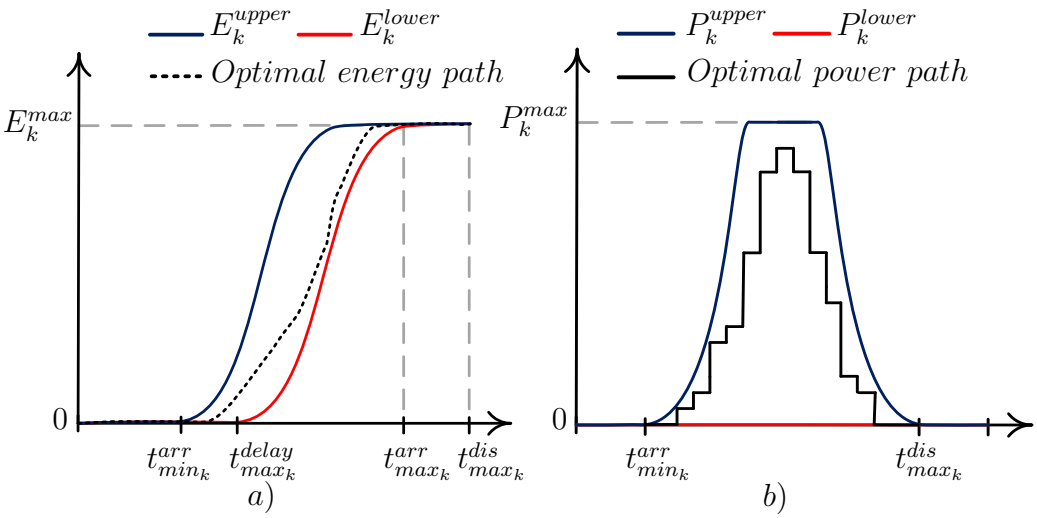


Figure 3.18: Aggregation of the flexibility of a fleet of EVs under aggregator $k$. *a*) energy boundaries, *b*) power boundaries

# Chapter 4

# Modelling of the LV network for integrating EVs and PVs

## 4.1 LV network model

Modern LV networks face a high presence of electric vehicles and renewable energy, motivated by the increasing concern about air quality and oil dependency. This trend is expected to continue in the coming years. Despite the clear advantages from the environmental point of view, these technologies present new challenges for their massive integration in the grid that require to be addressed with new operation methods, e.g., for optimising the charging of EVs and PV power generation. However, as a first instance, it is necessary to know in good detail the network in which all these devices will be integrated.

Hence, for understanding the characteristics, behaviour, and future needs of the LV distribution networks, it is necessary to account for a reference network model that can be used as a representation for actual grids to analyse their capability to host new technologies such as EVs or PVs. This would allow proposing new strategies to increase the penetration level of such technologies, minimising the impact on LV networks. The distribution network modelling can be done with different levels of detail depending on the goal to be achieved, e.g., voltage regulation, loading levels, short-circuit analysis, time-domain simulations, etc. In general, DSOs do not develop network models at secondary voltage level mainly because of the conventional passive nature of LV circuits and the assumption that demand (size and behaviour) does not change suddenly over the time (Espinosa and Ochoa, 2015).

In the literature, most of the benchmark networks are three-phase and balanced, especially for high voltage (HV) and medium voltage (MV) levels. The IEEE test feeders (Kersting, 2001) are the most common topologies used by researchers to test the performance of their algorithms. Other sets of reference networks were also released by CIGRE (Strunz et al., 2014), Pacific Northwest National Laboratory (PNNL) (Schneider et al., 2008), and Texas A&M University (2020). Note that all of these feeders represent U.S. networks. Some other networks in Mateo et al. (2018), Strbac and McDonald (2015), Strunz et al. (2014) represent typical European transmission and distribution systems.

However, it is much harder to find reference networks at the LV level which include the unbalanced nature of the loads based on their demand patterns. To surpass this limitation, especially related to confidentiality and intellectual property, some academic institutions have released LV networks which are based on real data for mimicking portions of the European distribution system. Mateo et al. (2018) have built several representative LV networks based on real technical data provided by 79 large European DSOs. Additionally, in Electriciy North West (2019), Espinosa and Ochoa (2015), there is available a comprehensive 25 set of LV networks with a series of real LV feeders in the UK to be used in quasi-dynamic state simulations. From the latter, the IEEE European Low Voltage Test Feeder was included as a reference circuit in IEEE Test Feeder Working Group (2020).

In this research, in order to obtain a good balance between simplicity and exactness in modelling the LV network, two feeders have been extracted from one of the LV networks in (Electriciy North West, 2019) to investigate the applicability of the coordination schemes proposed in Chapter 5. These radial distribution feeders supply power to 55 and 75 single-phase households unevenly distributed per phase through 1.431 km and 2.569 km of cables, respectively. The unbalanced condition in both feeders is mainly given by the loads connected to phase $a$, as summarised in Table 4.1. Feeders are connected to an 11 kV medium-voltage network through an 800 kVA distribution transformer with a delta/grounded-wye connection. The rated phase-to-phase voltage at the secondary is 400 V $\pm$10%. It is assumed that the cross-section of the neutral conductor equals to phase conductor for both the three- and single-phase service cables. The one-line diagram of the feeders is shown in Figure 4.1. These feeders were modelled, firstly, in PowerFactory using DGS (DIgSILENT interface for GIS and SCADA), and then employing Python. The latter was used to test a linear approximation of the power flow on the complex plane, which is discussed in Section 5.8.

Table 4.1: Number of households connected per phase

| Number of Households per Feeder | 1 | 2 |
|---|---|---|
| Phase $a$ | 21 | 28 |
| Phase $b$ | 19 | 26 |
| Phase $c$ | 15 | 21 |
| Total | 55 | 75 |

The load curve for each household was obtained from a pool of 100 load profiles given in Electriciy North West (2019), Espinosa and Ochoa (2015), which were assigned in ascending order to each home. These time series reproduce real patterns of domestic power consumption for a day with a time resolution of one minute. However, in this thesis, load profiles are subsequently downsampled to a time series with a 10-minute time step. The loads are modelled as constant power ($P$) with a lagging power factor of 0.95.

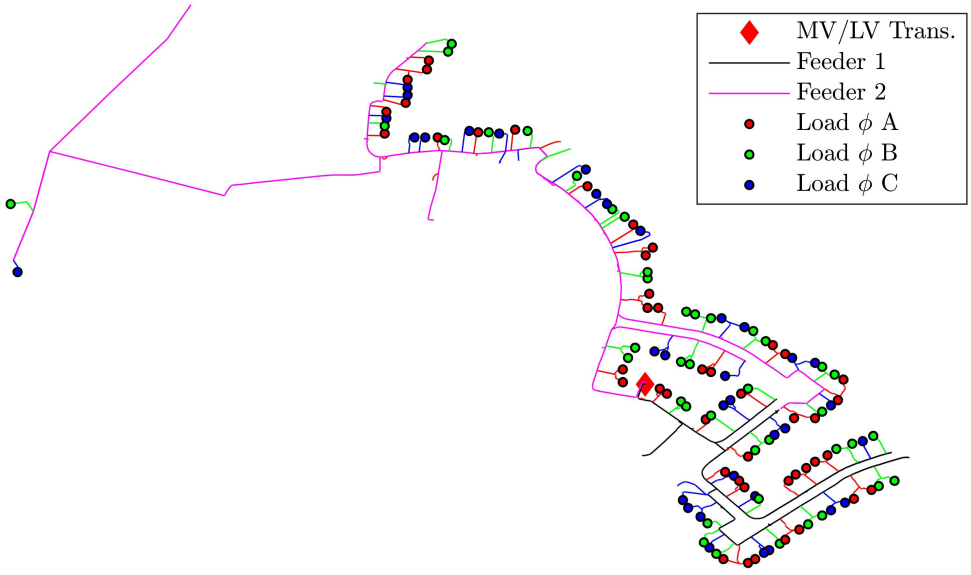


Figure 4.1: LV network diagram

## 4.2 LV network analysis

The load flow analysis is a relevant tool for the planning and design of electric power systems, as it helps to assess the network under different operating conditions. In the literature, there are several well-known methods to perform this task in transmission systems, such as Newton-Raphson, Fast Decoupled and DC power flow, while the Backward/Forward Sweep (Eminoglu and Hocaoglu, 2008, Sarmiento et al., 2019) is one of the most extensively employed methods for distribution systems. The application of these methods is highly dependent on the physical and electrical characteristics of the network. For example, distribution systems differ from the transmission systems by displaying higher $R/X$ ratios, shorter line lengths, mixed underground-overhead line sections, an extensive number of branches and nodes, phase unbalances, and usually radial arrangement and unique point of supply. Due to the complexity of the distribution systems, a balanced case is usually considered to perform different analysis on network planning studies considering the non-convex and nonlinear nature of the conventional power flow. As most of these studies are carried out in a steady state of the network, the computation time is not a relevant factor. However, when it comes to a quasi-dynamic analysis, where optimising in several time steps is required, the computational burden and robustness become binding factors. Thus, the use of the sensitivity coefficients of the network and the linearization of the power flow equations are introduced in this thesis as analysis tools to assess the optimal status of the LV network and the integration of distributed resources.

### 4.2.1 Load flow linearization

The linearization of the power flow equations is an effective approach for simplifying and speeding up the calculation of the control, operation, and optimisation of the power system. Particularly, to assess the optimal state of the power system, the Optimal Power Flow (OPF) approach is one of the most practically relevant and well-researched subfields of constrained nonlinear optimisation because it seeks to optimise the operation of the power system subject to the power flow constraints and other operational restrictions (*e.g.*, limits on switching equipment, voltage and currents limits, transmission stability and minimum output power of generators). A detailed introduction to the OPF problem from the operations research perspective can be read in Frank and Rebennack (2016). As the power flow equations are nonlinear and non-convex, this type of optimisation problems are in gen-

eral much harder to solve, and therefore, global solution and convergence are not guaranteed in those models. However, diverse convex approximations have been proposed in the literature to deal with this problem. For example, Garces (2016b) presents a convex quadratic approximation for the solution of the OPF in power distribution systems which is based on the linear formulation developed in Garces (2016a). Other analytical approaches are presented in Farivar and Low (2013), and Franco et al. (2018).

As the study of the power flow equations requires the use of a general theory for functions of several complex variables, Wirtinger calculus [1] (Bouboulis, 2010, Fischer, 2005) emerges as a suitable alternative in this aspect for calculating linearisations in non-analytical complex functions (*i.e.*, when these do not fulfil the Cauchy-Riemann conditions) such as power flow equations. For instance, Dzafic et al. (2019) and Sarmiento et al. (2019) used this approach to expand the power flow equations in terms of the phasor voltages and their conjugates to be implemented in the Newton-Raphson algorithm. This means that the complex-valued formulation is solved without the need to split it into two real-valued equations. A similar approach is employed by Jabr et al. (2018) to analyse microgrids operating in island mode, with the difference that the proposed method does not require computing and factorising the Jacobian matrix at every iteration. On the contrary, Ramirez et al. (2019) present a linear formulation of the power flow, also using the Wirtinger calculus, for grid-connected microgrids and unbalanced distribution networks without imposing constraints related to radiality or $X/R$ ratio. This method can be computed either in real or in per-unit values. Given that the latter approach guarantees an affine separation between voltages and powers, a modification of the power balance has been introduced in this thesis to be employed in an OPF model, which will be further discussed in Chapter 5.

For explaining this approach, first, let us consider a three-phase distribution system modelled by means of the nodal admittance matrix ($Y_{bus}$), where all the nodes are ordered according to the phase of the system, as shown in Equation (4.1).

[1] See Appendix D for a brief introduction.

$$\begin{pmatrix} \mathbb{I}_0^a \\ \mathbb{I}_N^a \\ \mathbb{I}_0^b \\ \mathbb{I}_N^b \\ \mathbb{I}_0^c \\ \mathbb{I}_N^c \end{pmatrix} = \overbrace{\begin{pmatrix} \mathbb{Y}_{00}^{aa} & \mathbb{Y}_{0N}^{aa} & \mathbb{Y}_{00}^{ab} & \mathbb{Y}_{0N}^{ab} & \mathbb{Y}_{00}^{ac} & \mathbb{Y}_{0N}^{ac} \\ \mathbb{Y}_{N0}^{aa} & \mathbb{Y}_{NN}^{aa} & \mathbb{Y}_{N0}^{ab} & \mathbb{Y}_{NN}^{ab} & \mathbb{Y}_{N0}^{ac} & \mathbb{Y}_{NN}^{ac} \\ \mathbb{Y}_{00}^{ba} & \mathbb{Y}_{0N}^{aa} & \mathbb{Y}_{00}^{bb} & \mathbb{Y}_{0N}^{bb} & \mathbb{Y}_{00}^{bc} & \mathbb{Y}_{0N}^{bc} \\ \mathbb{Y}_{N0}^{ba} & \mathbb{Y}_{NN}^{ba} & \mathbb{Y}_{N0}^{bb} & \mathbb{Y}_{NN}^{bb} & \mathbb{Y}_{N0}^{bc} & \mathbb{Y}_{NN}^{bc} \\ \mathbb{Y}_{00}^{ca} & \mathbb{Y}_{0N}^{ca} & \mathbb{Y}_{00}^{cb} & \mathbb{Y}_{0N}^{cb} & \mathbb{Y}_{00}^{cc} & \mathbb{Y}_{0N}^{cc} \\ \mathbb{Y}_{N0}^{ca} & \mathbb{Y}_{NN}^{ca} & \mathbb{Y}_{N0}^{cb} & \mathbb{Y}_{NN}^{cb} & \mathbb{Y}_{N0}^{cc} & \mathbb{Y}_{NN}^{bc} \end{pmatrix}}^{Y_{bus}} \cdot \begin{pmatrix} \mathbb{V}_0^a \\ \mathbb{V}_N^a \\ \mathbb{V}_0^b \\ \mathbb{V}_N^b \\ \mathbb{V}_0^c \\ \mathbb{V}_N^c \end{pmatrix} \tag{4.1}$$

However, this equation can be rewritten in a more compact form by grouping the phases, as shown in Equation (4.2).

$$\begin{pmatrix} \mathbb{I}_0^{abc} \\ \mathbb{I}_N^{abc} \end{pmatrix} = \begin{pmatrix} \mathbb{Y}_{00}^{abc} & \mathbb{Y}_{0N}^{abc} \\ \mathbb{Y}_{N0}^{abc} & \mathbb{Y}_{NN}^{abc} \end{pmatrix} \cdot \begin{pmatrix} \mathbb{V}_0^{abc} \\ \mathbb{V}_N^{abc} \end{pmatrix} \tag{4.2}$$

where 0 represents the slack node (substation) and $N = \{1, 2, \dots n\}$ are the remaining nodes, *i.e.*, those single-, bi-, or three-phase nodes that physically exist in the network. Hence, $N$ will be less than the number of three-phase lines $3 \times L$. As the voltage at the substation is a priori known, serving as a reference, the nodal angle of the phases takes values in the set $\{0, -2\pi/3, 2\pi/3\}$ for wye connected loads. Hence, the three-phase voltages can be expressed in a complex exponential form according to Equation (4.3).

$$V_0 = \mathbb{V}_0^{abc} \circ \begin{pmatrix} 1 \\ e^{-j2\pi/3} \\ e^{j2\pi/3} \end{pmatrix} \tag{4.3}$$

where $(\circ)$ is the Hadamard[2] product or element-wise product.

Once the three-phase voltage at the slack node has been defined, a new vector $V_T$ is generated by employing the Kronecker[3] product $V_0 \otimes \mathbf{1}$, where

[2]The Hadamard product is an operator that takes two matrices (or vectors) of equal dimension and generates a new matrix (or vector) by multiplying them term by term. This means that if $A = (a_{ij}) \in \mathbb{R}^{N \times M}$ and $B = (b_{ij}) \in \mathbb{R}^{N \times M}$ then $C = A \circ B = (a_{ij} \cdot b_{ij}) \in \mathbb{R}^{N \times M}$. In Python, the Hadamard product is obtained by the * command, so the methodology's implementation is straightforward. An important property is that this product is associative, distributive and commutative.

[3]The Kronecker product is an operation on two matrices (or vectors) of arbitrary size resulting in a block matrix. This means that if $A$ is an $M \times N$ matrix and $B$ is a $P \times Q$ matrix, then the Kronecker product $A \otimes B$ is the $PM \times QN$ block matrix. In Python, this operation can be carried out through the *Numpy* library, employing the command np.kron(a,b).

**1** is a vector of ones of length equal to the total number of lines $L$. Later, the resultant vector is indexed by $N$ in order to obtain the voltage in all existing network nodes, *i.e.*, $V_N = V_T(N)$.

In this sense, according to Ramirez Loaiza (2020), by applying the Wirtinger linearisation (see Appendix D) on the conventional power flow equation (4.4), the approximated representation of the three-phase power flow in an unbalanced LV network can be expressed by Equation (4.5).

$$S_i^* = \sum_{n=1}^{3} V_i^* Y_{n,i} V_n + \sum_{\substack{j=1 \\ j \neq i}}^{N} V_i^* Y_{i,j} V_j \tag{4.4}$$

$$S_{net}^* = H \cdot V_N^* + M \cdot V_N + J \tag{4.5}$$

where $^*$ represents the complex conjugate; $H$, $M$ and $J$ are constant matrices defined as follows.

$$H = diag\{Y_{N0} \cdot V_0\} + diag\{Y_{NN} \cdot V_N\} \tag{4.6}$$

$$M = diag\{V_N^*\} \cdot Y_{NN} \tag{4.7}$$

$$J = -diag\{V_N\} \cdot (Y_{NN} \cdot V_N^*) \tag{4.8}$$

where $Y_{NN}$ is an $N \times N$ matrix composed of the set of admittances that are not related to the slack node; however, $Y_{N0}$ does consider those admittances in a $N \times 3$ matrix, and $V_N$ are the resultant voltages after solving the OPF model. To evaluate the model in per-unit values, matrices $Y_{NN}$ and $Y_{N0}$ must be multiplied by $(V_{nom}/\sqrt{3})^2/S_{base}$, and therefore, the net power must be divided by $S_{base}$.

Additionally, the maximum voltage drop across the network can be defined by Equation (4.9), where $\|\cdot\|$ represents the absolute-value norm or Euclidean norm of the complex voltage. This equation defines a circular region in which the voltages are feasible. Therefore, the parameter $\delta_{\max} \in [0, 1]$ is assigned based on the grid code of the DSO to operate the network. Since this approximation is defined for a balanced case, the slack node's angle equals 0°. However, for the unbalanced three-phase case, the angular rotation described before is required. Therefore, this constraint will be expanded for the unbalanced case in Section 5.8.

$$\|V_0 - V_N\| \leq \delta_{\max} \tag{4.9}$$

The performance of the above linearisation is demonstrated by using the LV network in Figure 4.1. First, an unbalanced three-phase analysis

in steady-state was performed through PowerFactory. Then, by solving the linear problem in Equation (4.5) by means of DOcplex in Python, differences between the absolute value of voltages in PowerFactory and the Wirtinger linearisation are depicted in the boxplot of Figure 4.2. Notice that the error's median is greater for phase $a$ because this is the most loaded phase for both feeders. Besides, it can be seen that the maximum error for both feeders was less than $4.5 \times 10^{-3}$ $p.u.$ and $1.5 \times 10^{-3}$ $p.u.$, respectively, considering that this a non-iterative method. Therefore, those error values can be considered when a close-to-the-optimal solution is admissible.

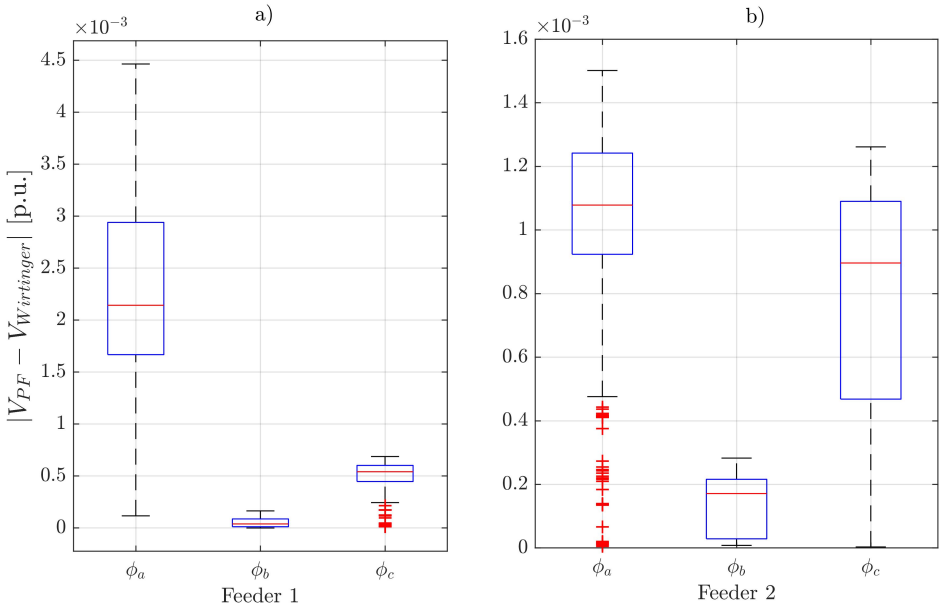


Figure 4.2: Error derived between the unbalanced load flow in PF and the linearisation using Wirtinger calculus

### 4.2.2 Sensitivity analysis

Sensitivity analyses in power systems allow assessing the impact on their performance when varying one or a set of electrical parameters. This tool is applied in both the planning and operation of power systems when it is required to foresee the changes of specific variables (*e.g.*, $\partial V/\partial P$, $\partial I/\partial P$, $\partial P_{loss}/\partial P$) produced by variations in load and generation. In particular, voltage sensitivity analysis is the base for solving different power system optimisation problems, such as voltage regulation, loss reduction, network expansion planning, and optimal placement of reactive sources, DERs, FACTS,

and generators (Conti et al., 2010).

In the literature, there exist three main approaches to perform the voltage sensitivity analysis on an electrical system. The first method (Barcelo and Lemmon, 1988) uses the submatrices of the inverse Jacobian Matrix by employing the Newton-Raphson algorithm in the load flow computation. The second approach (Christakou et al., 2013) is known as the perturb-and-observe (P&O) method, which performs a small change to an input control variable and registers the effect over the whole network. The third technique (Gurram and Subramanyam, 1999) employs Tellegen's theorem and the notion of adjoint networks. This approach needs an initial load flow solution to create a particular adjoint network to be solved and get the required sensitivities. All these methods have been widely employed for three-phase balanced systems at high- and medium-voltage levels (Aghatehrani and Kavasseri, 2011, Tamp and Ciufo, 2014) and only in a few cases for unbalanced LV networks (Di Fazio et al., 2018, Esmaili and Goldoust, 2015, Farahani, 2017, O'Connell et al., 2014, Yan and Saha, 2012). According to Ni et al. (2018), the methods mentioned before are based on local sensitivity analysis (LSA), as these study how a single input affects the output while treating the other inputs as deterministic values. This means that these techniques locally estimate each sensitivity in the vicinity of a nominal value of the selected input.

Additionally, the approach for getting the voltage sensitivity matrices varies according to the network topology and voltage level. For instance, Mendonca and Green (2019) proposed an active network management scheme for the DERs installed in radial distribution networks based on the local computation of the voltage sensitivities. Zhang et al. (2018b) presented a decentralised control for HV networks to manage voltage rise problems in nodes with distributed generation (DG) based on multiple power flow calculations from planning data to produce a non-linear function representing the dependencies between the voltage of a particular node and the power injections from the DG. A three-phase balanced network was considered in both cases, so those approaches are not suitable for LV networks due to their unbalanced nature. In contrast, Richardson et al. (2012a) and O'Connell et al. (2014) applied the voltage sensitivity coefficients in a centralised charging strategy for electric vehicles in an unbalanced LV network, which were obtained by employing the P&O method and the inverse Jacobian Matrix to obtain the sensitivity of voltage, respectively. Besides, Sainz et al. (2020) developed an algorithm based on the P&O method to assess different control strategies over DERs installed in unbalanced LV networks using the voltage sensitivity coefficients derived from the active and reactive power variations. Though

voltages in LV networks are less sensitive to reactive power variations than to active power changes, the authors outline that maximum absolute values of voltage sensitivity due to reactive power variations do not occur in load nodes of the same phase; these belong to load nodes from other phases. The algorithm can be implemented in different power flow simulation software as long as the modelling of unbalanced systems is supported. In addition, Yan and Saha (2012) proposed a method to analyse the voltage sensitivity due to PV power variations in unbalanced networks with different line configurations, phase sequences, and phase loading levels in order to define a suitable network reconfiguration to solve the voltage problems. The authors highlight that significant voltage variation may be observed for a more asymmetrical line geometry with a higher $R/X$ ratio. Moreover, the phase physical positions also determine the voltage variation sensitivity.

Most of the works described above calculate the sensitivity coefficients for a balanced case and considering the fact that commercial software packages like PowerFactory ('DIgSILENT GmbH Germany, 2019) compute the sensitivity values in terms of the sequence components for the unbalanced case, which result in an impractical way to handle the information of the network, in this thesis, a methodology to get the matrices of sensitivity coefficients for unbalanced LV networks with DERs based on the P&O approach is proposed. According to Di Fazio et al. (2018), high accuracy values of the sensitivity coefficients can be obtained by performing the load flow calculation rather than measurements on the network, taking into account that the computational efficiency decreases if many DERs have to be considered. So, in this thesis, the calculation of the sensitivity coefficients is performed by taking advantage of the embedded power flow tool in PowerFactory and its ability to automate simulation-related tasks through Python (Python Software Foundation, 2018).

Unbalanced three-phase load flows are used to generate the network sensitivity coefficients, which will be subsequently used in the definition of network constraints in Chapter 5. In order to get the sensitivity values due to the addition of load and generation, a steady load of 1 kW is initially assigned to each household, which is the maximum average demand from all power profiles used. Then a load flow is solved to record the loading levels per phase of lines and distribution transformers, as well as the voltage at each household. Subsequently, the load is increased to 2 kW at the first household, then the load flow is executed again, and the new results from the specified points on the network are stored. This data is then used to compute the sensitivities of voltage and loading due to the addition of load. For example, the volt-

age sensitivity is calculated as $\partial V/\partial P = (V_i^{\text{new}} - V_i^{\text{base}})/(P_{Load_i}^{\text{new}} - P_{Load_i}^{\text{base}})$[4], where $V_i^{\text{base}}$ and $V_i^{\text{new}}$ represent the initial and new voltage level from the load flow due to the change in the steady-state power at every load $i$. A similar approach is considered for computing the loading sensitivities. To reflect the addition of generation, the initial load changes to 0 kW. Voltage and loading sensitivities for the components of interest of the network are obtained by means of the application of the same procedure. Note that before varying a new household load, the previous one is restored to its original power level. This routine is repeated for the whole set of households, lines and distribution transformers to obtain the sensitivity coefficients of the network. Full insight into the working principle of the methodology is provided in Appendix B.

Figure 4.3 to Figure 4.5 show the sensitivity coefficients obtained for the LV network in Figure 4.1 by employing the previous approach. Figure 4.3 shows how voltage drops rise as the distance from the substation increases, concentrating on connections close to the location where a particular load is modified. The diagonal elements $\partial V_i/\partial P_i$ of the matrix represent the voltage variation at bus $i$ due to a variation of active power at the same point. The non-diagonal elements $\partial V_h/\partial P_i$ describe the voltage variation at node $h$ due to the variation in active power at busbar $i$. The magnitude of voltage deviations ranges from $-1.07$ V/kW to 0.012 V/kW, and it is more noticeable when the household is connected to the same phase as the point of load variation. On the contrary, when the generation varies in the same load node, the above sensitivity values become positive with a difference of $10^{-4}$ order of magnitude. Notice that high sensitivity means that even small changes in active power cause large changes in the voltage magnitude. As mentioned before, this effect can be observed at the load nodes located far from the main transformer.

Due to the single-phase connection of the loads, it was found that increasing the load in phase $a$ causes the voltage sensitivities to become positive in phase $b$ and negative in phase $c$. When this is done in phase $b$, the sensitivities are positive in phase $c$ and negative in phase $a$. Finally, when this occurs in phase $c$, the sensitivities come to be positive in phase $a$ and negative en phase $b$. Note that this effect is opposite when generation is added, as shown in Figure 4.4.

On the other hand, the sensitivity of the distribution transformer loading depicted in Figure 4.5 is limited to each feeder phase at which the load is

[4]The sensitivities expressions for the loading level in lines and transformers can be found in lines 22-26 from the algorithm in Appendix B.

modified, *i.e.*, all positive data. Note that the sensitivity values are opposite when the generation is included in the same load node. Due to voltage drops and losses along each feeder, a slight increase in power sensitivities can be noted with increasing distance from the substation. The sensitivity coefficients of each feeder are not presented because those are similar to the above ones but including the effect between each other, which is $10^{-4}$ order of magnitude.

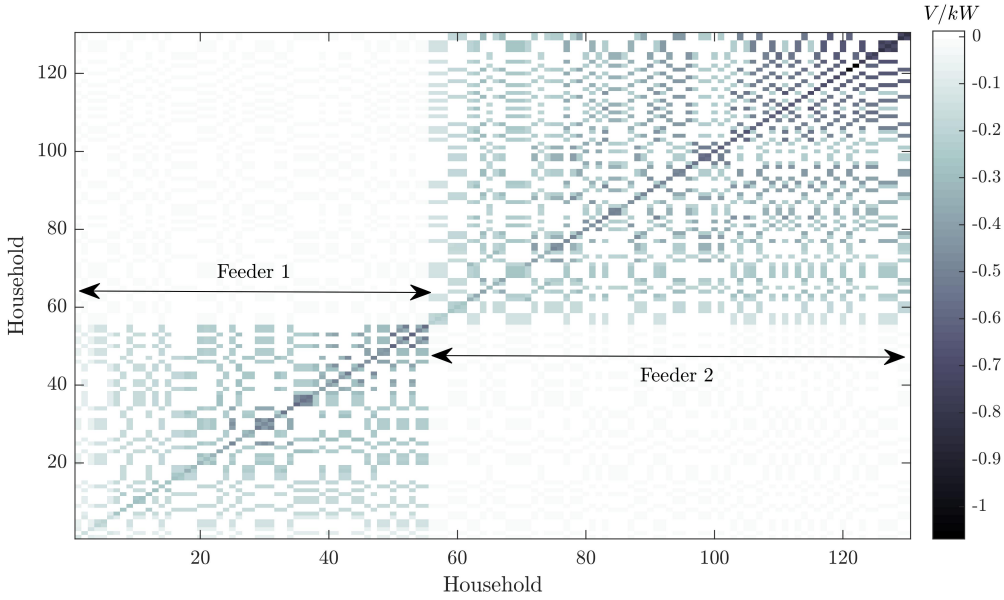


Figure 4.3: Voltage sensitivity matrix due to the addition of load

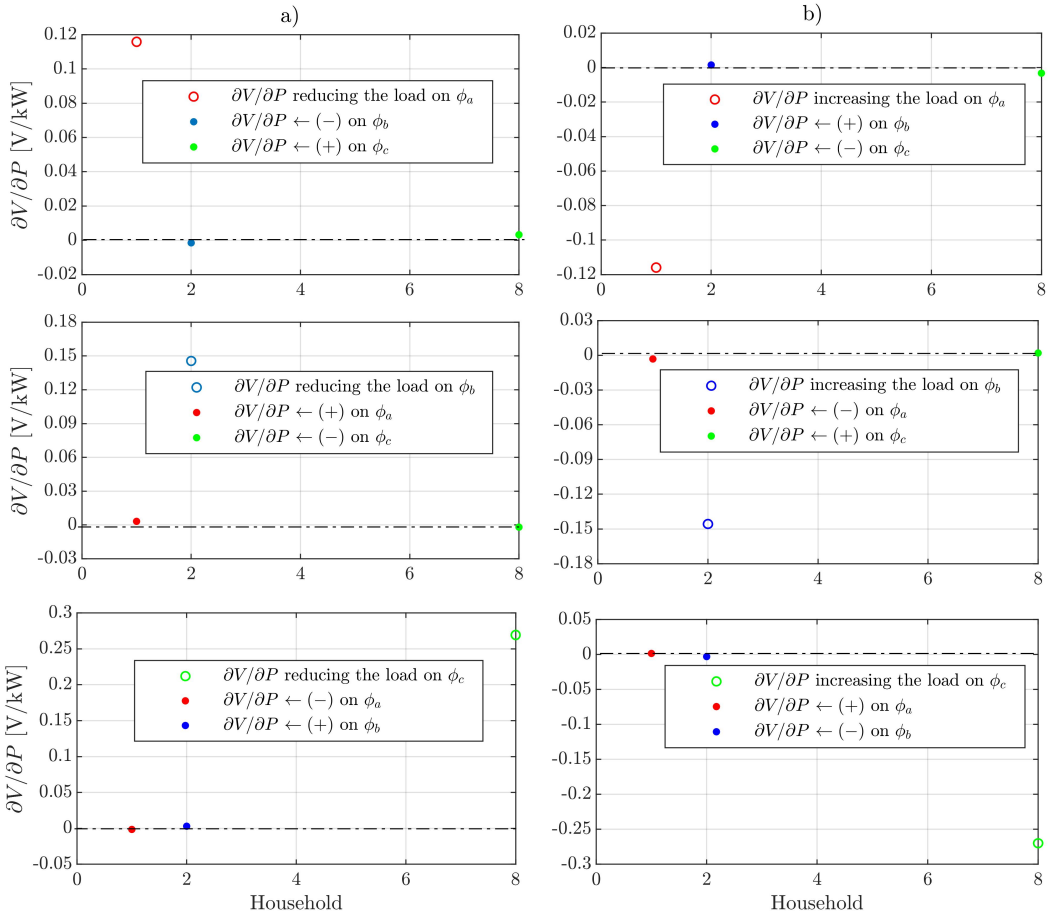


Figure 4.4: The effect on voltage sensitivity on different phases by *a*) adding or *b*) decreasing load like a generator on a particular phase

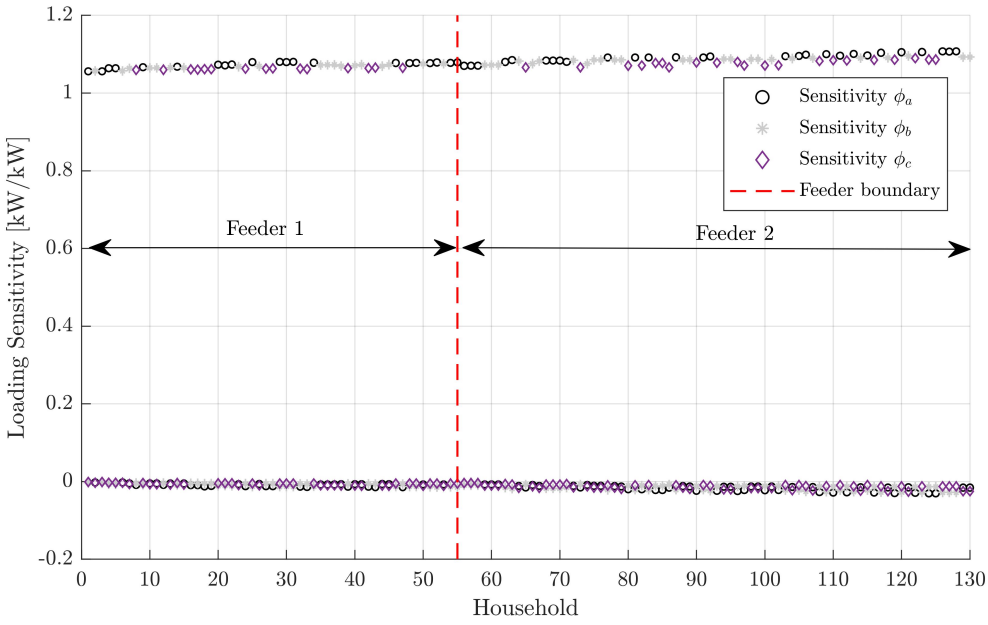


Figure 4.5: Loading sensitivities of the distribution transformer

# Chapter 5

# New proposed smart charging and PV power curtailment methodology

## 5.1 Generalities and background

Drawbacks of the uncontrolled EVs charging process in LV networks have been widely studied by several researchers like García-Villalobos et al. (2014), Hajforoosh et al. (2016), Mwasilu et al. (2014), Richardson et al. (2012a). All these studies conclude that this passive strategy causes significant voltage drops and overloads on LV feeders. Moreover, with an increasing level of PV penetration in the distribution networks, reverse power flow and voltage rise would also be expected (Alam et al., 2016). Therefore, these effects can lead to an expensive investment and time-consuming tasks to reinforce network capacity.

In order to deal with these problems, there would be a need to stimulate the self-consumption of PV power for charging the EV battery when possible. This means taking advantage of the correlation between both distributed energy resources, which mainly depends on the driver's mobility uses, the PV power forecast and the implementation of an effective smart control strategy. For instance, a user with several daily trips near to its household could benefit from almost 70% of PV power generation during the charging process, whereas a user with a long-range trip would take less advantage of that power availability (Hoarau and Perez, 2018). Thereby, this highlights the potential to further redistribute the EV charging process to better match with PV power generation. Besides, this aspect is also influenced by the

weather conditions, *i.e.*, the EV owners will tend to charge their batteries early on a sunny day, reducing the electric power demand at peak hours. However, it is required to devise new controlled charging schemes that can be implemented in a centralised, distributed or decentralised mode, as classified by Antoniadou-Plytaria et al. (2017). Since centralised methods require full network visibility and handling a significant amount of information to be transmitted and processed, the decentralised and distributed schemes are more attractive because they can be gradually implemented and use local communications (García-Villalobos et al., 2014, Mendonca and Green, 2019).

In regard to new control strategies, multiple solutions for solving technical problems on distribution networks with EVs and PVs have been proposed and assessed in the literature to provide to the DSO a set of practical alternatives for solving network congestion with respect to the traditional network reinforcement. Thus, different researchers like Esmaili and Goldoust (2015), Farahani (2017), O'Connell et al. (2014), Richardson et al. (2012a,b) have studied the use of network sensitivity coefficients to approximate the voltage, loading level or both in unbalanced LV networks when adding new loads such as EVs. As the use of the sensitivity coefficients allows linearizing the LV network at a particular operation point, reducing the complexity of including the power flow equations in the definition of the optimisation problem, these studies have used them within different optimisation techniques (*e.g.*, linear (Esmaili and Goldoust, 2015, Richardson et al., 2012a,b), nonlinear (O'Connell et al., 2014) and heuristic (Farahani, 2017)) to coordinate in a centralised manner the charging process of EVs. For example, in the work described by Richardson et al. (2012b), the load level increase for both the network's transformer and lines due to power demanded by the EVs is evaluated based on their sensitivity coefficients expressed in kVA/kW. This criterion is also used by Esmaili and Goldoust (2015) for assessing the loading level on the distribution transformer. Likewise, in work carried out by Richardson et al. (2012a), the load variation on the main cable is evaluated by these sensitivities expressed in A/kW. However, it is worth mentioning that apparent power and current are complex values, and therefore, the modulus is always positive. Hence, the way of expressing these sensitivities is valid only if load addition is considered (e.g., the EVs). Besides, representing the sensitivities values in that form is no longer valid if the power flow changes its direction because of excess intermittent renewable electricity. This means that the reverse power flow in the network cannot be computed through those magnitudes within the linearization. Hence, if considering PV generation, the loading sensitivity coefficients for lines and distribution transformers must be calculated in terms of the active power

(*i.e.*, kW/kW) to evidence the power flow direction.

On the other hand, in conjunction with the charging strategy for the EVs, some authors include EV flexibility through their energy/power boundaries. Thus, Zhang et al. (2017) proposed an aggregate power- and energy-boundary model for EVs with vehicle-to-grid capacity to provide power reserve services to the grid. The model is included as a constraint in a day-ahead scheduling problem formulated as a mixed-integer nonlinear programming (MINLP) model. In work developed by Chen et al. (2017), an energy-boundary model for V2G along with a charging power allocation algorithm to offer power reserve services is introduced. Here, the upper and lower energy boundaries of EVs are computed in real-time as a function of the battery voltage, current, charging/discharging rate, and the state-of-charge. As this model requires extensive information about the EV, for a large number of EVs, it will be computationally more intense. Additionally, other energy models are used only for charging EVs as part of different charging strategies based on quadratic programming (QP) (Sundstrom and Binding, 2012) and linear programming (LP) techniques (Sundstrom and Binding, 2012, Xu et al., 2014, 2016). For example, in work described by Sundstrom and Binding (2012), the upper and lower energy limits are obtained by considering the electrical power demand during driving with the maximum and minimum energy capacity of the battery, respectively. These last two constants are also used by Zhang et al. (2017). Moreover, both authors use of a nonlinear battery model to compute the initial energy of EVs using an extensive set of parameters. In work performed by Xu et al. (2014) and Xu et al. (2016) similar equations to compute the energy boundaries of the EVs are used. Both studies define the arrival energy state as zero, which then increases up to the required energy level of each EV. Besides, these studies, excluding the one by Sundstrom and Binding (2012), do not consider any network topology or related technical constraints.

In regard to the aggregators into the EV charging strategies, in Luo et al. (2013), a two-stage optimisation model to identify the optimal charging states of EVs in a given day employing a MILP technique is proposed. The first stage seeks to minimise the peak load with the EVs charging demand, and in the second stage, the load fluctuation is minimised considering the fixed value of peak load from the previous stage. The work presented in Amamra and Marco (2019) proposed a control system through a nonlinear programming (NLP) model to support the V2G operation of EV fleets in the day-ahead scheduling. This approach allows the aggregator to provide frequency and voltage regulation services to the grid while minimising the EVs charging cost and the level of battery degradation. Based on the inverse

optimisation technique, which directly tries to infer the information on how the aggregators define their power consumption, the authors in (Xu et al., 2018) developed an estimation method to obtain the energy requirements of the aggregators via historical observations of price-consumption data. Another price-based mechanism is presented in (Hu et al., 2017a). Here, the authors present a transactive control method based on a linear and quadratic programming formulation to optimise the operational cost of EVs and power losses of the LV network by considering power transformer congestion and voltage violations.

Besides, other authors analyse the influence of the PVs on the LV networks, e.g., Ricciardi et al. (2019) employed an OPF approach based on a QP formulation to minimise the PV power curtailment on the unbalanced LV networks. In Su et al. (2014), an unbalanced three-phase case is also analysed using a multiobjective OPF problem to minimise network losses and the cost of PV power curtailment, as well as the improvement of voltage magnitude and balance profiles. An optimal power threshold per aggregator to limit the aggregated excess of PV energy injected into the LV network during periods of high generation and low demand was formulated as a MILP model by Cortés Borray et al. (2020). On the contrary, Marra et al. (2014) proposed through a linear programming approach a common PV power threshold that triggers the storage systems in the LV feeder in order to store the excess of energy that could lead to overvoltage situations. This means that the output power of PV inverters is not curtailed during high PV generation periods. It is worth mentioning that the above-mentioned works set the limit of PV power to be injected into the grid as a percentage value of the inverter rated power. Nonetheless, this limit can also be expressed using a reference signal, such as the voltage at the point of common coupling (PCC) (Ghosh et al., 2017, Hashemi and Østergaard, 2017).

Nonetheless, the above-mentioned studies do not analyse in conjunction the addition of PVs and EVs an aggregated manner to assess their impact on the LV network. Only a few cases like Marra et al. (2013) analyse both devices in a simple unbalanced LV network using the voltage sensitivity coefficients in a network constraint within a mixed-integer linear programming (MILP) model that minimises the energy storage systems (ESSs) charging power in EV stations for providing voltage support in those feeders with PVs. The above-mentioned research works are summarised in Table 5.1.

Based on the above-mentioned, this chapter aims to fill the existing gap in the literature by proposing a methodology that offers different approaches to the DSO (according to the amount of available information) to optimise the massive penetration of EVs and PVs into the LV networks using the

aggregator as manager entity at feeder level.

## 5.2 Overview of the proposed methodology

Taking into account that most of the network services presented in Table 2.2 are usually provided at the transmission level, this thesis adds to the state-of-the-art a new interaction schema among aggregators and the DSO to offer the latter several grid services at low-voltage level, as shown in Figure 5.1. Given the flexibility of DERs and the purpose of satisfying the grid technical targets, the services provided by the aggregators can be divided into those for load support and voltage management. These services, in turn, can also be split into several functions. The provision of these services can be based on a suitable division of the network by zones (*i.e.*, a group of end-users served by an electrical substation in a specific geographical location) with their corresponding aggregators, which should operate their zone according to the optimal load profile to derive signals provided by the DSO to the EVs owners and other installed DERs. This scheme requires a sequential communication link between the DSO and the aggregators to verify the effectuated control actions.

To exemplify the interaction between the DSO and an aggregator $k$, Figure 5.2 shows a detailed structure including PV inverters, EVs chargers, demand profiles of the users, and the embedded control unit. The unit with the embedded controller can manage and communicate with the power inverters, chargers, and EVs' battery management systems. Based on the received information from these devices, the aggregator sends its needs to the DSO, which optimises the aggregated loading profile for that aggregator, also considering the operational constraints of the LV network. Afterwards, the aggregator dictates the optimal power to each EV and PV. Note that different optimisation techniques can be employed to achieve this task.

Based on the described framework, four models named $f_1$, $f_2$, $f_3$ and $f_4$ were proposed into three different approaches when multiple aggregators under a single DSO manage significant levels of EVs and PVs in the LV networks. Model $f_1$, which is part of the Individual-based approach, is considered a coordination strategy operated in a decentralised manner at the aggregator level. Model $f_2$ is part of the Population-based approach and is also considered a coordination strategy but operated in a centralised manner at the DSO level.

Table 5.1: Research works related to the analysis of EVs and PVs in unbalanced networks.

| Ref. | Drawbacks Uncontrolled EV Charging | EV Charging Analysis | EV Power and Energy Boundaries | EV Aggregator | PV Analysis | PV Active Power Curtailment |
|---|---|---|---|---|---|---|
| García-Villalobos et al. (2014) | √ | | | | | |
| Hajforoosh et al. (2016) | √ | √ | | | | |
| Mwasilu et al. (2014) | √ | | | | | |
| Richardson et al. (2012a) | √ | √ | | | | |
| Richardson et al. (2012b) | √ | √ | | | | |
| Alam et al. (2016) | | √ | | | √ | |
| Hoarau and Perez (2018) | | √ | | | √ | |
| Esmaili and Goldoust (2015) | | √ | | | | |
| Farahani (2017) | | √ | | | | |
| O'Connell et al. (2014) | | √ | | | | |
| Zhang et al. (2017) | | √ | √ | | | |
| Chen et al. (2017) | | √ | √ | | | |
| Sundstrom and Binding (2012) | | √ | √ | | | |
| Xu et al. (2014) | | √ | √ | √ | | |
| Xu et al. (2016) | | √ | √ | √ | | |
| Luo et al. (2013) | | √ | | √ | | |
| Amamra and Marco (2019) | | √ | | √ | | |
| Xu et al. (2018) | | √ | √ | √ | | |
| Hu et al. (2017a) | | √ | | √ | | |
| Ricciardi et al. (2019) | | | | | √ | √ |
| Su et al. (2014) | | | | | √ | √ |
| Cortés Borray et al. (2020) | | | | √ | √ | √ |
| Marra et al. (2014) | | | | | √ | √ |
| Ghosh et al. (2017) | | | | | √ | √ |
| Hashemi and Østergaard (2017) | | | | | √ | √ |

| Ref. | Voltage Sensitivity ($\Delta V/\Delta P$) | Current Sensitivity ($\Delta I/\Delta P$) | Aparent Power Sensitivity ($\Delta S/\Delta P$) | Losses Sensitivity ($\Delta P_{loss}/\Delta P$) | Unbalanced Network | OPF | Optimisation Technique |
|---|---|---|---|---|---|---|---|
| García-Villalobos et al. (2014) | | | | | | | |
| Hajforoosh et al. (2016) | | | | | | | CAPSO |
| Mwasilu et al. (2014) | | | | | | | |
| Richardson et al. (2012a) | √ | √ | | | √ | | LP |
| Richardson et al. (2012b) | √ | √ | √ | | √ | | LP |
| Alam et al. (2016) | | | | | √ | | |
| Hoarau and Perez (2018) | | | | | | | |
| Esmaili and Goldoust (2015) | √ | | √ | √ | √ | | LP |
| Farahani (2017) | √ | | | √ | √ | | PSO |
| O'Connell et al. (2014) | √ | | | | √ | | SQP |
| Zhang et al. (2017) | | | | | | | MINLP |
| Chen et al. (2017) | | | | | | | |
| Sundstrom and Binding (2012) | | | | | | | QP and LP |
| Xu et al. (2014) | | | | | | | LP |
| Xu et al. (2016) | | | | | | | QP |
| Luo et al. (2013) | | | | | | | MILP |
| Amamra and Marco (2019) | | | | | | | NLP |
| Xu et al. (2018) | | | | | | | HPSOM |
| Hu et al. (2017a) | | | | | | √ | QP and LP |
| Ricciardi et al. (2019) | | | | | √ | √ | QP and MILP |
| Su et al. (2014) | | | | | √ | √ | SQP |
| Cortés Borray et al. (2020) | | | | | √ | | MILP |
| Marra et al. (2014) | √ | | | | √ | | MILP |
| Ghosh et al. (2017) | | | | | | | |
| Hashemi and Østergaard (2017) | | | | | | | |

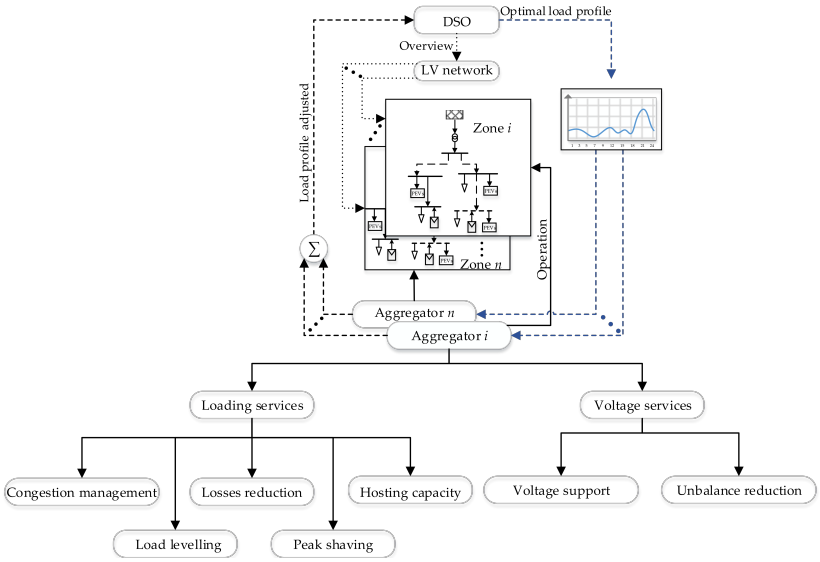


Figure 5.1: Proposed structure of potential services from the aggregator to the DSO by an operational zone of the LV network

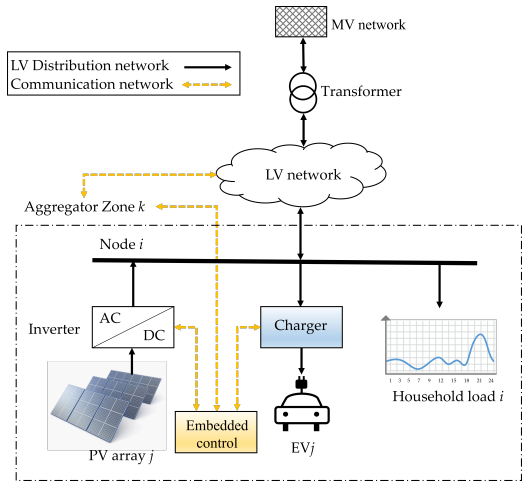


Figure 5.2: Interaction of the DSO-Aggregator border

Finally, models $f_3$ and $f_4$ are included in the Hybrid approach as centralised coordination strategies at the DSO level. Formulations $f_1$ and $f_3$ linearise network constraints throughout the sensitivity coefficients of the grid by using the P&O method presented in Section 4.2.2, whereas $f_4$ treats network constraints in an optimal power flow problem, which is linearised through the Wirtinger calculus, as described in Section 4.2.1. Because $f_2$

only consider the loading level of the network assets, none of the above linearization approaches is needed.

A simplified schema of the proposed coordination strategies is depicted in Figure 5.3. For the Individual-based approach, the aggregator has a double way communication channel with the EVs, and only the PVs send to it their current output power. Here, the aggregator seeks to charge all the EVs considering the PV availability and the technical constraints of the LV network. The Population-based approach gathers all the aggregators involved in the LV network managed by the DSO, which dictates the optimal loading level profile to each of them based on the provided information from the Aggregators. In this approach, only the loading level of the grid is considered as the technical restriction. Finally, the Hybrid approach encloses the other two methods, and the optimisation is carried out at the DSO level. Here, the PVs have a double-way communication channel with the aggregator because it needs to send them the optimal power curtailment value for not causing excessive voltage levels and overloading the grid. The following sections describe in detail each of the introduced models and prove them through different case studies.

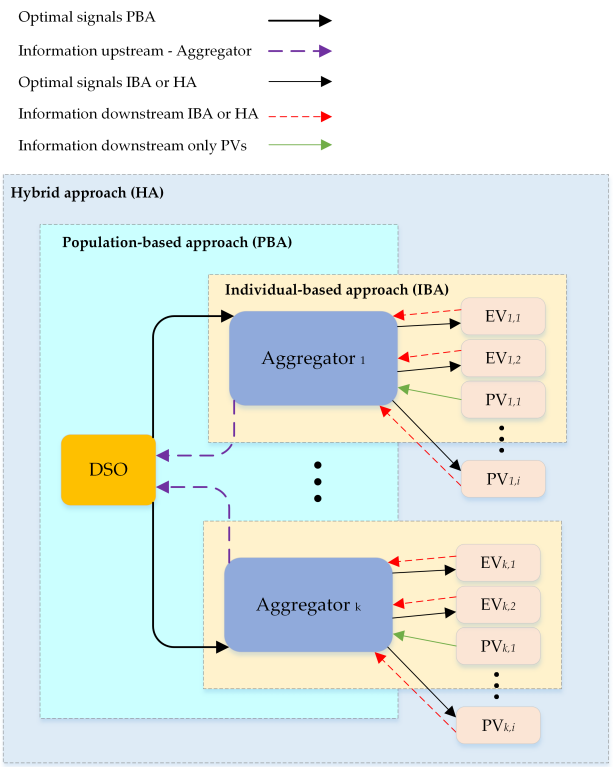


Figure 5.3: Simplified flowchart of the proposed methodology

## 5.3 Optimisation of EVs charging via individual-based approach

### 5.3.1 Objective function

With the energy boundaries of the EVs, the aggregator seeks to coordinate the charging of all EVs to maximise customer satisfaction taking advantage of the available PV power without violating grid technical limits. Thereby, during the daytime charging of EVs, the proposed optimisation problem aims to improve the self-consumption of PV power and reduce the dependence on the network. This means maximising power delivered to all EVs for a given period by optimising the charging rate of each EV connected. The optimised charging profile is centrally calculated by the aggregator based on an LP model which assures an even distribution of the power at each time slot for all EVs. Mathematically, the optimisation problem to be solved by the aggregator at $t$ is given by Equation (5.1).

$$\underset{\forall i \neq \emptyset}{\text{maximise}}\ f_1 = \sum_{i \in H} \sum_{t \in N_{slots}} (P_{i,t}^{EV} - \Delta_{i,t}^{P_{inc}}) \cdot x_{i,t} \tag{5.1}$$

where $H$ denotes the number of households being supplied by the DSO, $x_{i,t}$ is a binary matrix $[x]_{H \times N_{slots}}$ such that $x_{i,t} = 1$ if the EV $j$ is connected to the household $i$ at time $t$, and 0 otherwise. It should be noted that $t_j^{int}$ (Equation (3.26)) settles the availability span for vehicle $j$ when it is connected to the household $i$. Additionally, $P_{i,t}^{EV} = p_{i,t}^{ch} \cdot \eta_{ch}$ is the charging power in kW for the vehicle connected to the household $i$ at time $t$, which can vary from zero up to the rated power of the charger. $\Delta_{i,t}^{P_{inc}}$ is the increase in the rate of charge in kW for the vehicle connected to the household $i$ at time $t$. This term is introduced as a penalty deviation variable to handle conditions in which a fixed rate of charge ($\Delta_P$) cannot be satisfied due to the lower energy boundary from constraint (5.5).

Notice that the optimisation problem discards the households without a PV, an EV or both, *i.e.*, $i \neq \emptyset$; which reduces the number of variables and constraints, and therefore, the computational burden. However, the non-evaluated households are included in the post-optimisation process based on the optimisation outcomes.

In order to ensure a proper network operation with the embedded PV generation while supplying households and EVs demand, the objective function in (5.1) must be subject to a series of constraints related to the power/energy of the EVs and PVs, the voltage and loading levels of the network

at each time slot.

### 5.3.2 EVs constraints

Based on the energy level of EV batteries, its charging rate is dynamically adjusted without violating grid technical limits as follows:

$$0 \leq P_{i,t}^{EV} \leq P_{ch}^{max} \cdot \eta_{ch},\ \forall i \neq \emptyset \in H, \forall t \tag{5.2}$$

$$P_{i,t-1}^{EV} - (\Delta_P + \Delta_{i,t}^{P_{inc}}) \leq P_{i,t}^{EV} \leq P_{i,t-1}^{EV} + (\Delta_P + \Delta_{i,t}^{P_{inc}}), \quad \forall i \neq \emptyset \in H, \forall t \quad \text{if} \quad x_{i,t} \neq 0 \tag{5.3}$$

$$0 \leq \Delta_{i,t}^{P_{inc}} \leq \Delta_{max}^{P},\ \forall i \neq \emptyset \in H, \forall t \tag{5.4}$$

$$e_i^{lower}(t_j^{arr} + t) \leq e_i^{EV}(t_j^{arr} + t) \leq e_i^{upper}(t_j^{arr} + t), \quad \forall i \neq \emptyset \in H, \forall j \in N_{EV}, t = 0, \ldots, t_j^{int} + 1 \tag{5.5}$$

Following the linear objective function in (5.1), constraint (5.2) imposes that the charging power for the vehicle connected to the household $i$ cannot exceed its power boundaries at any time step. Constraint (5.3) limits significant variations in the charging rate for consecutive time slots through a fixed set-point of $\Delta_P$ that can be relaxed only when necessary using the penalty deviation variable $\Delta_{i,t}^{P_{inc}}$ . This occurs in vehicles with narrow energy boundaries where a power boost is needed in the next time step for not violating the lower energy bound. Constraint (5.4) ensures that an increase in the charging rate of the EV connected to the household $i$ should be no larger than the remaining capacity of the charger ($\Delta_{max}^{P} = p_{ch}^{max} \cdot \eta_{ch} - \Delta_P$). Constraint (5.5) states that the energy level for vehicle $j$, which is connected to household $i$, at every time $t$ is within its energy boundaries. This energy state is detailed in Equation (5.6) for the arrival time interval ($t_j^{arr}$) of vehicle $j$ and later periods by considering the energy remaining from the previous period ($t_j^{arr} + t - 1$) and the charging power at time $t$. Notice that the index $i$ for the energy boundaries in restriction (5.5) differs from index $j$ in Equations (3.31)–(3.34), as they are used here to denote the household $i$ to which the EV $j$ is connected.

$$e_i^{EV}(t_j^{arr}+t) = \begin{cases} e_j^{arr} + P_i^{EV}(t_j^{arr} + t) \cdot \Delta t, & t = 0,\ \forall i \neq \emptyset \in H, \forall j \in N_{EV} \\ e_i^{EV}(t_j^{arr} + t - 1) + P_i^{EV}(t_j^{arr} + t) \cdot \Delta t,\ t = 1, \ldots, t_j^{int} + 1, \end{cases} \quad \forall i \neq \emptyset \in H, \forall j \in N_{EV} \tag{5.6}$$

### 5.3.3 Network constraints

The addition of EVs and PVs alongside the network may cause a significant drop or rise in voltage magnitude at every load node. This depends on several factors, which includes the charging rate of the EV, the injected power by the PV system and their location in the network. To ensure that voltage magnitude is within the operating limits defined by the DSO, the following constraint is defined:

$$V_{min} \leq V_{i,t}^{fc} + \alpha_{i,i} \cdot P_{i,t}^{EV} + \beta_{i,i} \cdot P_{i,t}^{PV} + \sum_{\substack{h \in H \\ i \neq h}} (\alpha_{h,i} \cdot P_{h,t}^{EV} + \beta_{h,i} \cdot P_{h,t}^{PV}) \leq V_{max},$$

$$\forall i \neq \emptyset \in H, \forall t \in N_{slots} \quad (5.7)$$

where $V_{i,t}^{fc}$ is the forecasted voltage at the $ith$ household node; $\alpha_{i,i}$ and $\beta_{i,i}$ represent the voltage sensitivity ($\partial V/\partial P$) at household node $i$ due to the supplied power to the EV $i$ and the generated power by the PV unit $i$; $\alpha_{h,i}$ and $\beta_{h,i}$ are the voltage sensitivity for household $i$ as a result of the demanded power by the EV $h$ and the produced power by the PV unit $h$. Note that a negative sensitivity value in $\alpha$ represents a voltage drop in such node, while in $\beta$ that value will be positive, which indicates a voltage rise. Additionally, $V_{min}$ and $V_{max}$ define the minimum and maximum permissible network voltage levels. It should also be noted that $\alpha$ and $\beta$ are two square matrices of $H \times H$, and the term $i \neq h$ in constraint (5.7) means that $i$ remains fixed while $h$ varies.

In addition to voltage levels, further constraints for maintaining the active power flow within the operational limits of the network assets are evaluated. This means that it is necessary to consider how the active power variation from the PVs and EVs affects the loading level of the entire network by making use of the sensitivity coefficients. The proposed linearisation for power flowing through the cables and distribution transformers of the LV-network is presented as follows:

$$P_{Line_{l,\phi,t}}^{fc} + \sum_{\substack{h \in H \\ h \neq \emptyset}} (\mu_{h,\phi,l} \cdot P_{h,t}^{EV} + \lambda_{h,\phi,l} \cdot P_{h,t}^{PV}) \leq S_{Line_{l,\phi}}^{rated} \cdot \cos(\varphi),$$

$$\forall l \in L, \phi = 1, 2, 3, \forall t \in N_{slots} \quad (5.8)$$

$$P_{Trans_{j,\phi,t}}^{fc} + \sum_{\substack{h \in H \\ h \neq \emptyset}} (\delta_{h,\phi,j} \cdot P_{h,t}^{EV} + \epsilon_{h,\phi,j} \cdot P_{h,t}^{PV}) \leq S_{Trans_{j,\phi}}^{rated} \cdot \cos(\varphi),$$

$$\forall j \in Trans, \phi = 1, 2, 3, \forall t \in N_{slots} \quad (5.9)$$

where $P^{fc}_{Line_{l,\phi,t}}$ and $P^{fc}_{Trans_{j,\phi,t}}$ are the forecasted loading levels in kW for the supplying cable $l$ and distribution transformer $j$ per phase $\phi$ at time $t$. Moreover $\mu_{h,\phi,l}$, $\delta_{h,\phi,j}$, and $\lambda_{h,\phi,l}$, $\epsilon_{h,\phi,j}$ are the loading sensitivity coefficients for each phase $\phi$ of the service cable $l$ and transformer $j$ due to the demanded power by vehicle $h$, and the generated power by PV unit $h$, both in kW. Note that a positive sensitivity value in $\mu$ and $\delta$ represents an increase of the loading level on the main cable, whereas, in $\lambda$ and $\epsilon$ , those values will be negative, which indicates a reduction in the loading level. All these coefficients are three-dimensional matrices of $[H \times \phi \times (Line \text{ or } Trans)]$. Lastly, $S^{rated}_{Line_{l,\phi}} \cdot \cos(\varphi)$ and $S^{rated}_{Trans_{j,\phi}} \cdot \cos(\varphi)$ represent the rated capacity per phase in kW for both the service cable $l$ and the distribution transformer $j$. The initial voltage magnitude at the household nodes and the base loading level on the main cable and the distribution transformer are calculated beforehand as parameters considering their forecasting through the unbalanced quasi-dynamic power flow for the whole test period $T$ in PowerFactory.

Besides, only one set of sensitivities is calculated along the test period, as this approach reduces the computational burden and execution time of the algorithm. These sensitivity values cannot be expected to match those in which the load continually varies on the feeder but allow quantifying the impact that multiple EVs and PVs, charging and injecting power simultaneously, can have on a particular node, service cable and distribution transformer on the network.

In this approach, only the computed charging power for the time interval $[t^{arr}_j, t^{dis}_j]$ is sent to each charging spot once the optimisation problem has been solved. Therefore, at the end of the charging process, it is expected that each EV has reached its desired energy level. To summarise, Figure 5.4 outlines the simplified procedure of the proposed centralised control method.

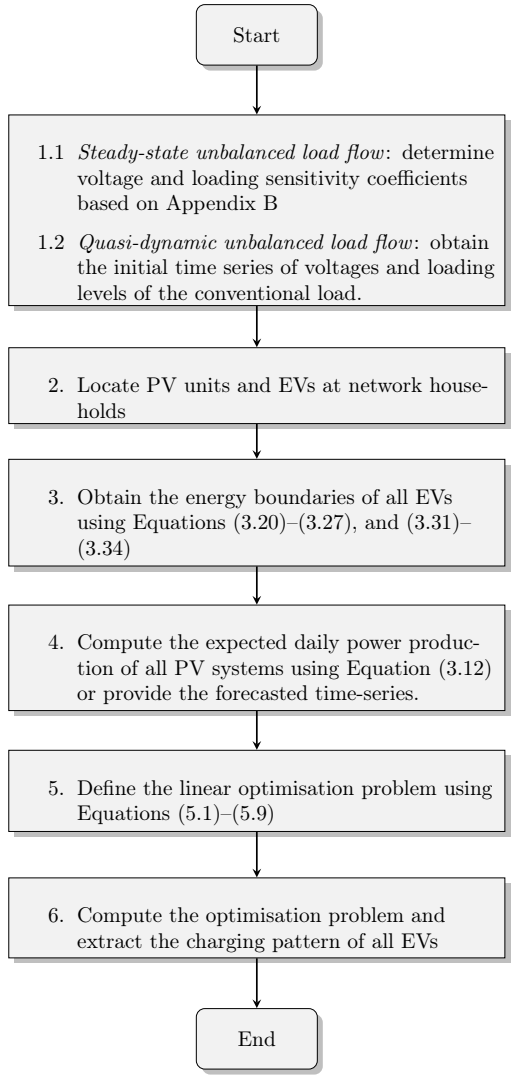


Figure 5.4: Simplified flowchart of the proposed individual-based methodology

## 5.4 Description of the test cases used for problem (5.1)

The proposed optimisation problem $f_1$ has been applied to the feeder model described in Section 4.1.Initially, a penetration level of 60% for both the EVs and PVs in the feeder shown in Figure 5.5($a$) was considered. This means that 33 of the 55 households have both a PV and EV operating at certain time slots of the test period. This penetration level was deemed appropriate

to assess the robustness of the proposed control charging strategy. However, in a scenario with a higher penetration level of EVs and PVs, without a proper control action, the required charging power would increase significantly in hours of high demand, decreasing the correlation with the PV output power. Therefore, this may cause an undesired operating condition in the LV network. Thereby, to demonstrate the need to use network restrictions under these conditions, a second case with a penetration level of 90% of PV units and 80% of EVs for the winter case was evaluated, as shown in Figure 5.5($b$). In this scenario, the method described in Section 5.3 was employed with and without network constraints (*i.e.*, Equations (5.7)–(5.9)). Both the EVs and PVs were randomly assigned among the households using a discrete uniform distribution $\mathcal{U}\{1, 55\}$. The number of EVs and PVs connected per phase are presented in Table 5.2. The location of each EV and PV for both cases is detailed in Appendix C.

Table 5.2: Number of EVs and PVs connected per phase and penetration level

| | Case | 1 | | 2 | |
|---|---|---|---|---|---|
| Phase $\phi$ | Number of Households | EVs | PVs | EVs | PVs |
| A | 21 | 11 | 11 | 12 | 16 |
| B | 19 | 11 | 11 | 19 | 19 |
| C | 15 | 11 | 11 | 13 | 14 |
| Total | 55 | 33 | 33 | 44 | 49 |

Households with EVs are equipped with a single-phase charging spot of 3.7 kW via a standard AC connection. The charger efficiency is assumed to be $\eta_{ch} = 0.92$ (Xu et al., 2014). The fixed variation for the rate of charge ($\Delta_P$) in constraint (5.3) is set at 0.5 kW. The daily travelled distance $d_{k,j}$ is evaluated from real data (National Renewable Energy Laboratory, 2017) by a lognormal distribution function with parameters $\mathcal{N}(\mu_{\ln} = 2.89257, \sigma_{\ln} = 0.91779)$. A truncated normal distribution is adopted from Shafie-Khah et al. (2016) to represent the arrival time of each EV as $\mathcal{N}(\mu = 16:00, \sigma = 3h, t_{\min} = 11:00, t_{\max} = 23:00)$, where $t_{\min}$ and $t_{\max}$ denote the arrival time range of EVs with mean $\mu$ and standard deviation $\sigma$.

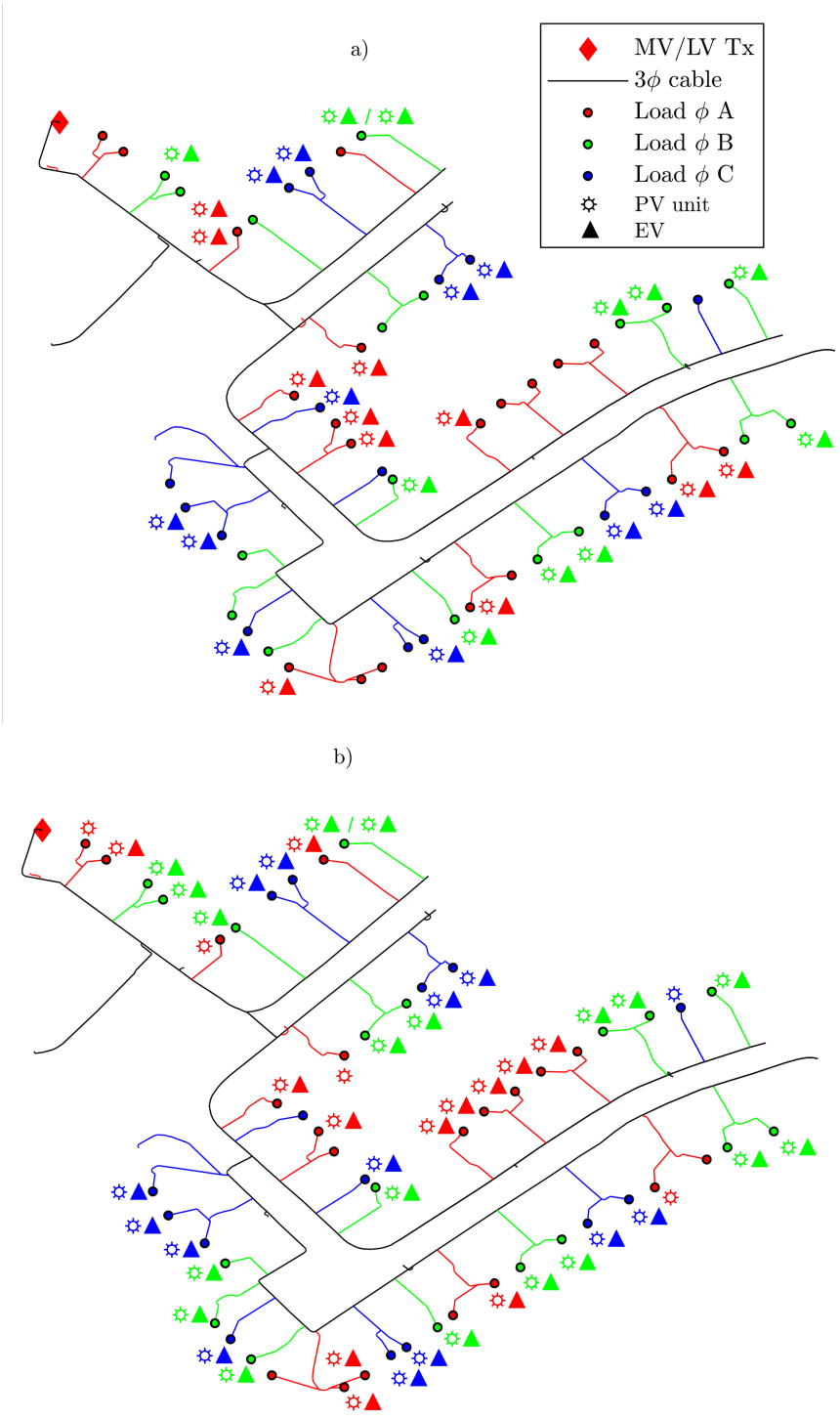


Figure 5.5: Low voltage test feeder for a) 60% of PV and EVs, b) 90% for PVs and 80% for EVs

In Case 1, all EVs are simulated based on the specifications for a Nissan Leaf (U.S. Department of Energy, 2015): BC = 24 kWh and ECR = 0.1778 kWh/km. In Case 2, for simulating an EV with a higher energy requirement, the electric Kia Soul (KIA, 2018) (BC = 30 kWh and ECR = 0.1679 kWh/km) was considered. For both cases, the battery energy levels are constrained to a $SOC_{\min} = 0.2$ and $SOC_{\max} = 0.95$ to avoid permanent battery damage or early ageing. Although the desired state-of-charge $SOC_{\text{obj}}$ depends on the user's driving needs, for simulation purpose, this was set to reach the $SOC_{\max}$.

Considering that residential PV systems can vary in a range from 2 to 5 kW (Santos et al., 2017), the PV units size at the evaluated households was limited to $P_i = 3.7$ kW, which is the maximum power for summer, with a unity power factor. However, for the winter season, a maximum power $P_i = 0.8$ kW was defined, as shown in Figure 3.2. Additionally, the maximum and minimum allowable voltage at each time step is set to 0.9 p.u. and 1.1 p.u., considering the European standard EN 50160 (UNE-EN-50160, 2011). The rated capacity of the main cable is 215 A (*i.e.*, $S^{\text{rated}}_{Line_{l,\phi}} \cdot \cos(\varphi) = 47.17$ kW per phase, assuming a lagging power factor of 0.95).

By considering that the initial penetration level is the most likely occurrence condition in the near future, one hundred series of simulations were carried out using the LV feeder in Figure 5.5*a*) for both the winter and summer seasons to prove the effectiveness of the proposed method. The first simulation was executed following the flowchart in Figure 5.4, and the remaining ones were performed starting from step 3 to 6. As the second case is a critical situation with less probability of occurrence, only a single simulation was carried out to assess the need for the proposed network constraints. Simulations were run for a test period $T = 30$ hours (*i.e.*, starting from 00:00 to 06:00 the next day) with a 10-minute interval (*i.e.*, 180 slots of time). The proposed model in (5.1)–(5.9) is solved by CPLEX 12.9 under its API in Python (DOcplex) (IBM, 2020).

### 5.4.1 Results of the individual-based approach

Figures 5.6*a*) and 5.6*b*) show the uncertainty of the EVs arrival time for both winter and summer when running 100 simulations per season, respectively. In both figures, the mean value of the number of EVs arriving at home per hour during a winter and summer day is represented by the green and magenta lines, respectively. For those EVs that arrive late, it is expected that these would charge up to the early morning.

Under the premise that the aggregator can manage the embedded control unit of each EV charger and monitoring the PV inverters from a remote location, Figures 5.7-–5.9 show how such control actions limit the loading level on the main service cable when connecting the EVs and PVs for winter and summer, respectively. Due to the lower number of solar radiation hours during winter, PV generation is much lower compared to the summer case, and hence, the reverse power flow on the main cable. In Figures 5.7 and 5.8, although phase $A$ displays an initial higher loading level from 16:00 hours to 21:00 hours, the average loading level in all phases for that time range is always below the rated capacity of the main cable. Even with some charging outliers, the proposed control strategy limits the loading level on the main cable to its nominal value while ensuring the desired charging level of all EVs. The outliers from midnight to the early morning occur because some EVs arrive with a low energy level or come late for charging.

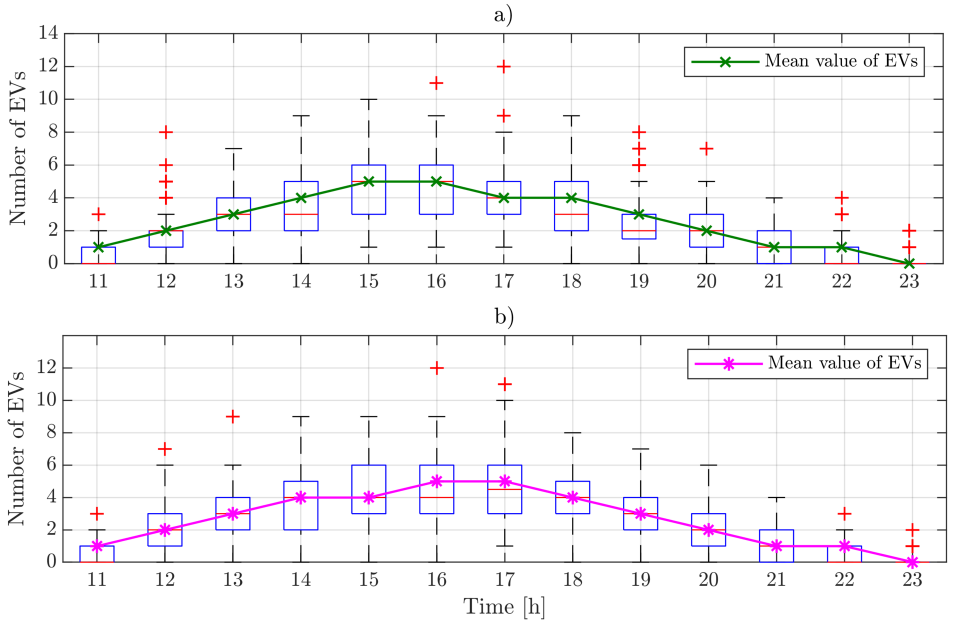


Figure 5.6: Boxplot and mean value of EV arrival time during $a$) winter day and $b$) summer day in Case 1

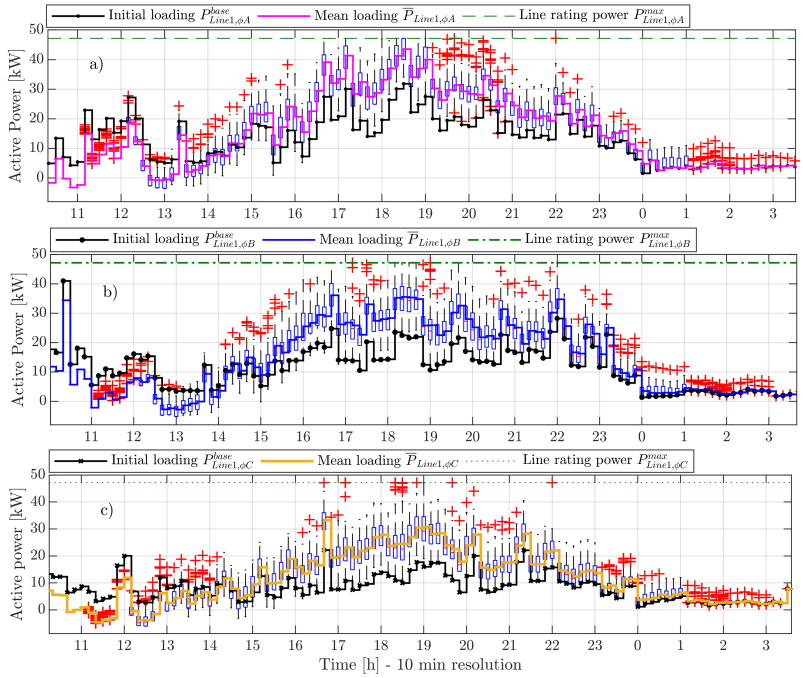


Figure 5.7: Boxplot of loading level per phase on the feeder's main cable based on 100 optimisation scenarios for winter in Case 1

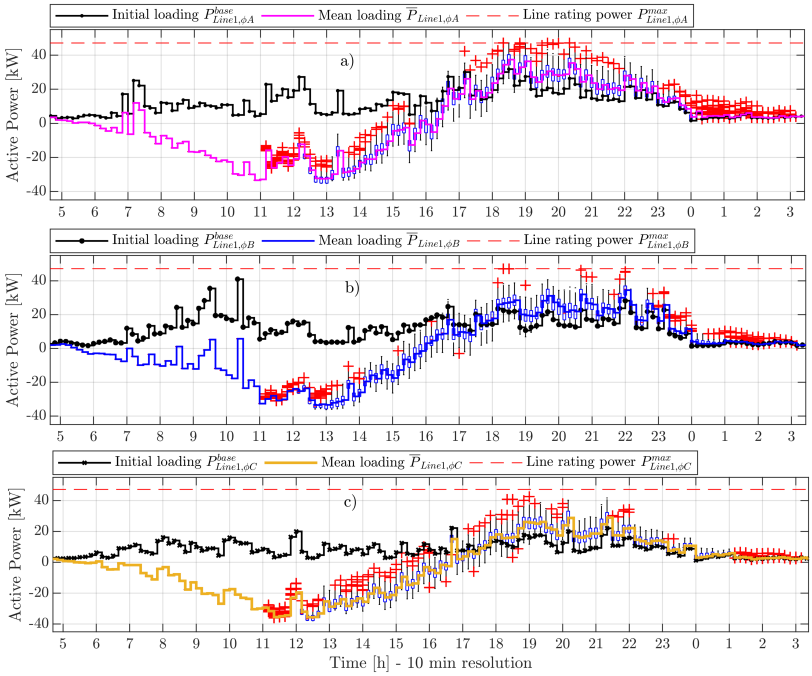


Figure 5.8: Boxplot of loading level per phase on the feeder's main cable based on 100 optimisation scenarios for summer in Case 1

On the other hand, the three-phase average loading level is below 83 kW from 16:30 hours to 20:00 hours during summer compared to winter thanks to the remaining PV energy downstream, which is used by the household loads and the EVs, as shown in Figure 5.9. Since no control actions over PV generation are considered, it is assumed that the surplus power is injected into the network, and it can be either sold or not to the DSO.

For comparison, Figure 5.10 shows the aggregated charging power for the winter scenario in Case 2 if an uncontrolled charging event would occur, along with the aggregated charging profiles using the proposed control method with and without network constraints. As the PV generation is low during the winter, the self-consumption for charging the EVs tends to be reduced, which increases the loading level of the main cable, as seen in Figure 5.11. In this figure, the improvement of the loading level per phase on the main cable is achieved by considering network constraints. On the other hand, if only constraints for power- and energy-boundaries of EVs are considered, this can produce overload events at any phase during the simultaneous charging process, as shown in Figure 5.11. Therefore, if the optimisation problem does not consider the proposed network constraints, a safe operative condition for the LV network cannot be guaranteed.

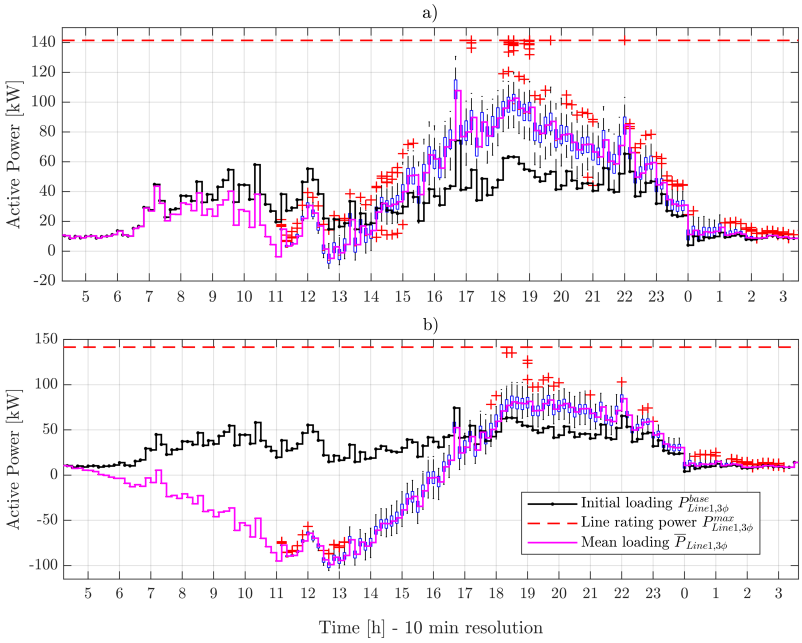


Figure 5.9: Boxplot of loading level for the three-phase main cable based on 100 optimisation scenarios for *a*) winter and *b*) summer in Case 1

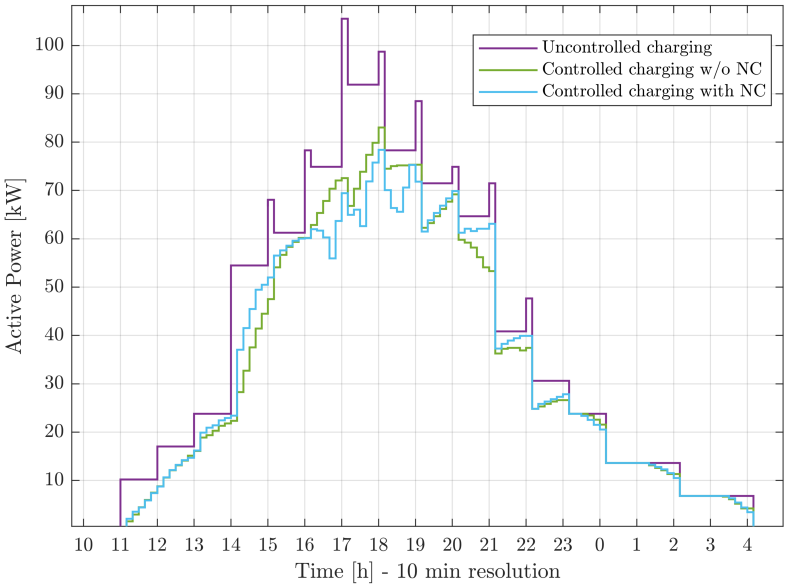


Figure 5.10: Comparison between uncontrolled- and controlled charging with and without network constraints (NC) in Case 2

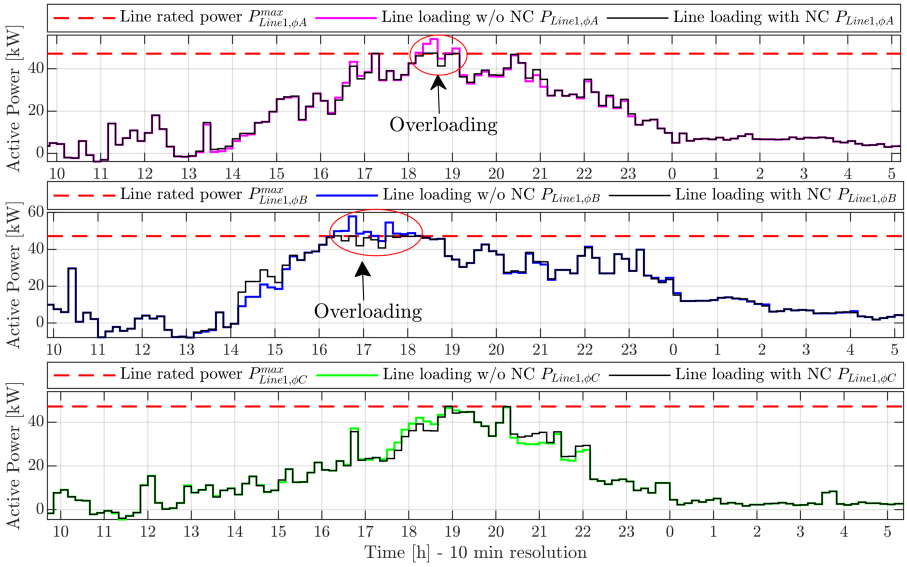


Figure 5.11: Comparison of the loading level per phase with and without network constraints (NC) in Case 2

Due to the rated power of the distribution transformer is much higher than that of the main cable, for this particular feeder, constraint (5.9) would

not be violated. Therefore, by applying the optimisation method, the power level on the LV side of the distribution transformer will be equal to the one on the service cable.

As an example to demonstrate that the proposed voltage approximation in constraint (5.7) is valid, two scenarios from Case 1 were analysed, *i.e.*, scenarios 97 (winter) and 51 (summer). Figures 5.12 and 5.13 show how voltage at household 53, which is located at the end of the feeder, is affected by the charging process and generation from other EVs and PVs. Both figures compare three voltage profiles; the initial voltage profile of the households, the voltage profile computed from the optimisation model and the voltage profile obtained using the quasi-dynamic load flow in PowerFactory. The second voltage profile relies on utilising the sensitivity coefficients (SC), the optimised charging profiles of EVs and the expected PV power. The latter voltage profile is obtained from uploading the optimised charging profiles of EVs in PowerFactory. For both scenarios, all voltage values are within the operational limits of the network, which indicates that the voltage level is not the binding constraint for this particular feeder, and therefore, the focus for the results will be on the loading levels, as shown in Figures 5.7–5.8 and 5.11.

The accuracy of the optimisation method was proved through the error in voltage computation from the results for both cases, as shown in Figures 5.14 and 5.15. Voltage error along the test period was less than 0.2% and 2% for winter and summer, respectively. These values differ from one season to another due to there is a higher level of PV generation which increases the losses on the feeder, and only one set of SC along the test period is used. Now, if we compare the winter scenario of Case 1 with Case 2 (Figures 5.14($a$) and 5.15), it is observed that the addition of new EVs and PVs will increase the voltage error due to just one set of sensitivity coefficients is following all changes in load during the test period. However, the error is still less than 1%, and hence, this exemplifies that the proposed linearization is still valid for a massive penetration level.

Note that depending on the irradiance level, temperature and the load demand, the reverse power flow and its impact on voltage rise due to PV power will be at the most severe state at noon. This is when PV output power is at its maximum level, and power demand is the lowest. However, this condition can be mitigated by charging the EVs, taking advantage of the correlation that exists between them and the PVs. Therefore, thanks to the sensitivity coefficients for PV units in both loading and voltage level within the network restrictions, it is possible to reproduce such operative condition, as seen in Figures 5.7– 5.8 and Figures 5.11-–5.15.

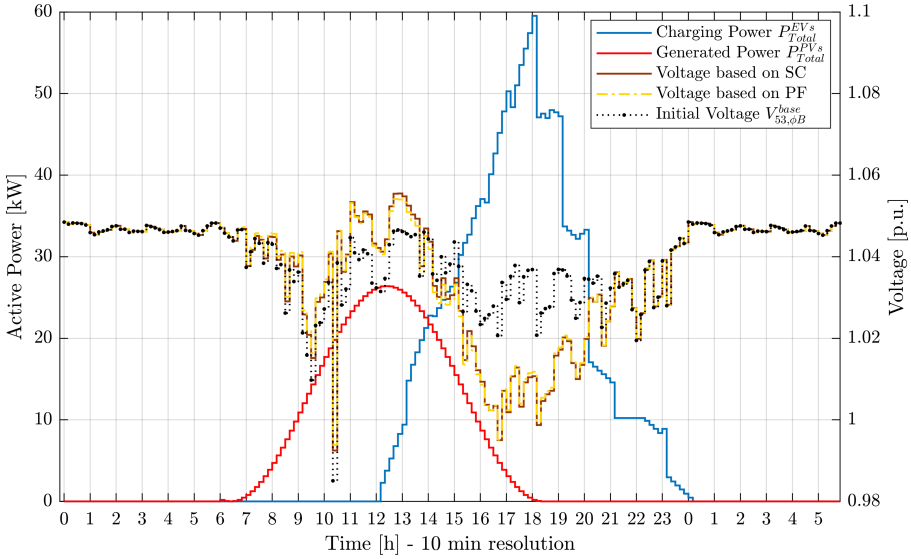


Figure 5.12: Voltage profile at Load 53 due to the effect of total charging power and the PV power during winter (Case 1, scenario 97)

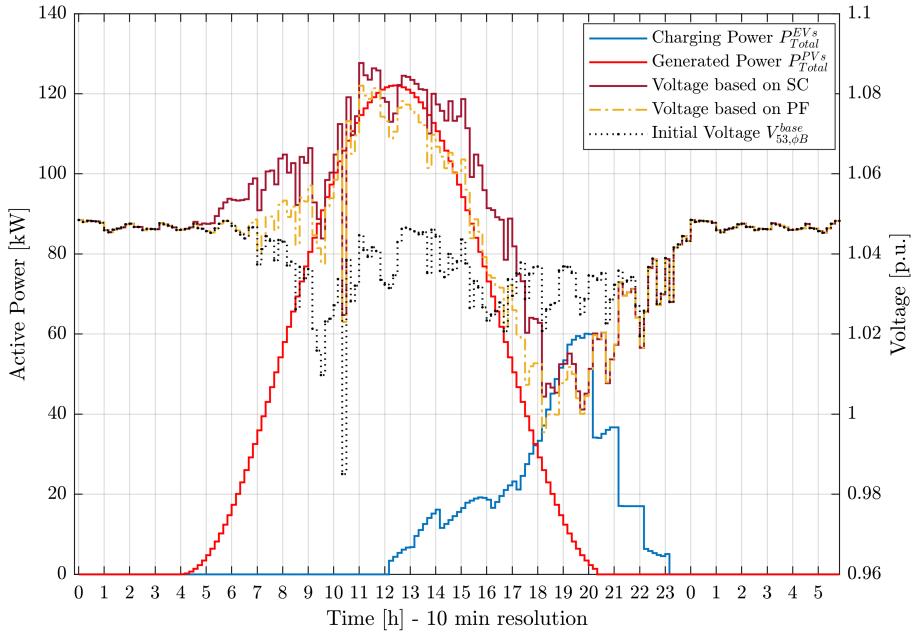


Figure 5.13: Voltage profile at household 53 due to the effect of total charging power and the PV power during summer (Case 1, scenario 51)

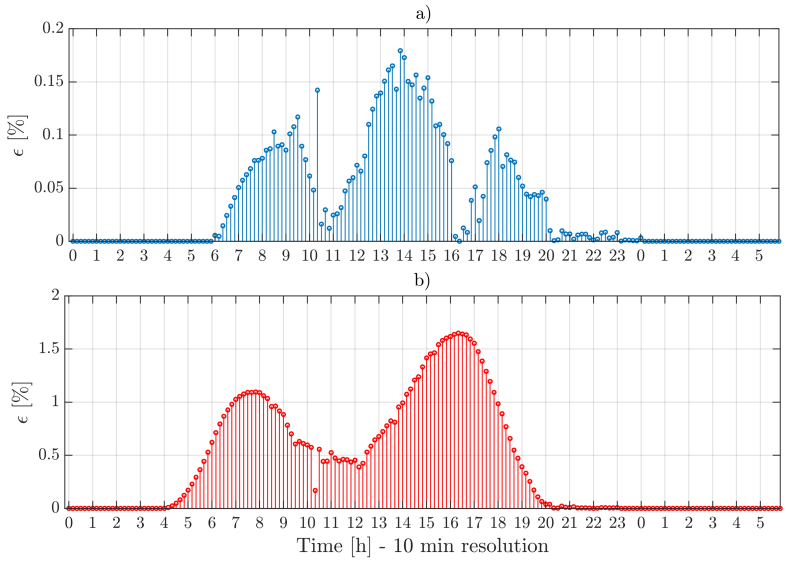


Figure 5.14: Voltage error at Load 53 by using the sensitivity coefficients for *a*) winter and *b*) summer in Case 1

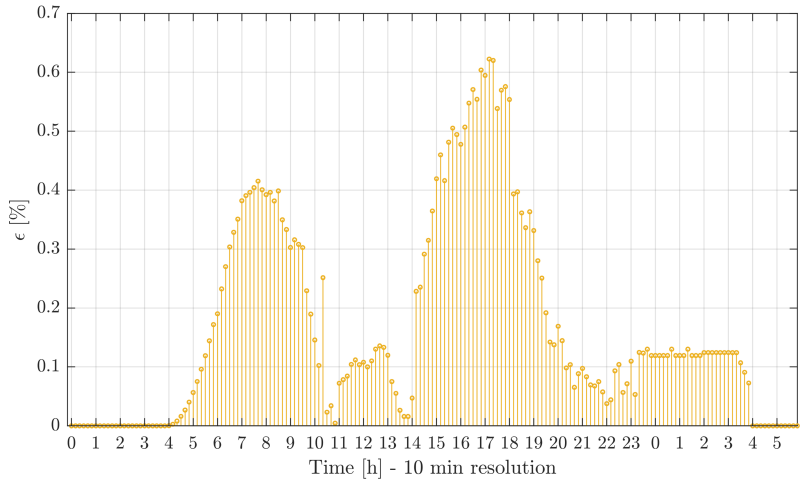


Figure 5.15: Voltage error at Load 53 by using the sensitivity coefficients in a higher penetration level of PVs and EVs in winter (Case 2)

### 5.4.2 Electric vehicles energy requirement

In order to show the effectiveness of the proposed centralised charging strategy, four cases of EVs with different charging patterns and energy trajectories

have has been extracted from scenario 51 (Case 1), as given in Figures 5.16 and 5.17, respectively. These results come out of the parameters defined in Section 5.4 and a daily travelled distance $d_{k,j} = \{34, 78, 61, 41\}$ in km for EVs located at households 4, 20, 45 and 54, respectively.

Figure 5.16 shows the optimal charging pattern, time availability and power generated for the selected EVs and PVs. It is observed that the charging profiles satisfy both the objective function and EVs constraints (5.2)–(5.4). For comparison, in Figure 5.16($a$), the pre-set value of $\Delta_P$ is kept during the charging process, whereas in Figure 5.16($d$), *e.g.*, the penalty deviation variable was used at time interval 92 (15:20 h) to reach the required energy level faster due to its shorter time window in comparison to the one in other EVs. It is also noted that the proposed charging strategy automatically delays the charging process, when it is necessary, to meet the charging demand of all EVs. Besides, it can be seen that the EVs with an early arrival take advantage of PV output power to be charged. This significantly reduces the load level on the main service cable.

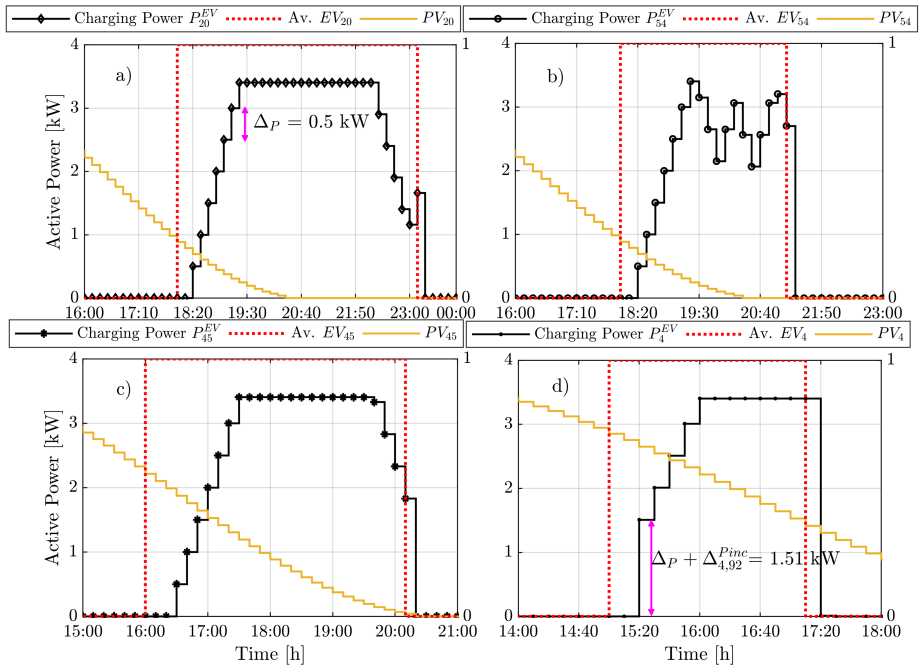


Figure 5.16: Optimal charging profiles for the EVs located at households $a$) 20, $b$) 54, $c$) 45 and $d$) 4 in Case 1

Figure 5.17 displays the energy paths from the selected EVs, which were obtained using the proposed control strategy. These energy trajectories cor-

respond to the charging profiles in Figure 5.16. To exemplify the energy requirements of EVs, in Figure 5.17*a*), for the EV at household 20 the arrival energy is $e^{\text{arr}}_{1,20} = (24\text{ kWh} \times 0.95) - (0.1778\text{ kWh/km} \times 78\text{ km}) = 8.93$ kWh while the objective energy level is $e^{\text{req}}_{1,20} = ((24\text{ kWh} \times 0.95)/0.92) = 15.07$ kWh for a parking time of $t^{\text{p}}_{1,20} = ceil\{15.07\text{ kWh}/3.7\text{ kW}\} = 5$ hours, which is equivalent to $t^{\text{int}}_{1,20} = 5\text{ h}/(10\text{ min}/60\text{ min}) = 30$ intervals of 10 minutes. These calculations were carried out in all simulations according to step three from Figure 5.4.

When the energy boundaries are too narrow, or the charging process is delayed, the energy trajectory tends to move towards the lower energy boundary, as shown in Figures 5.17*c*) and 5.17*d*). However, for EVs with a longer charging time and a slight delay, the energy path would go through the middle of the energy boundaries, as given in Figure 5.17*a*). On the other hand, if charging power varies once its rated capacity has been reached (Figure 5.16*b*)), the energy trajectory would vary accordingly to these changes until meeting the required energy state, as depicted in Figure 5.17*b*). Therefore, these results confirm the effectiveness of the proposed method.

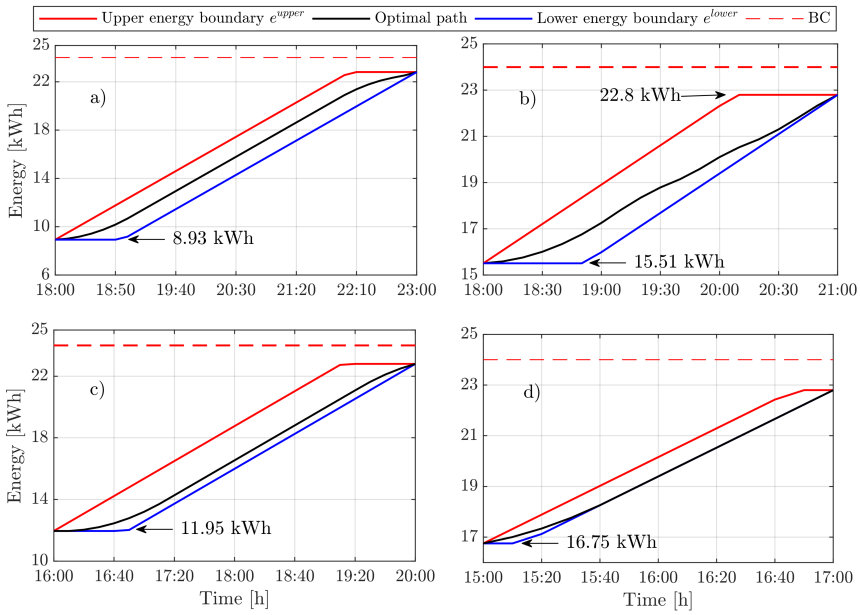


Figure 5.17: Optimal energy trajectories for the EVs located at households *a*) 20, *b*) 54, *c*) 45 and *d*) 4 in Case 1

## 5.5 Centralised optimisation of aggregators at the DSO's level

### 5.5.1 Objective function

With the aggregation of the individual energy- and power-boundaries of the EVs and the aggregation of the available PV power generation, the DSO attempts to coordinate for all aggregators the aggregated EVs charging and minimise the aggregated PV power curtailment to maximise the operational performance of its network. For the aggregators, this means maximising the energy and power needs of their end-users. Both the export limit of the aggregated PV power and the charging profile for each aggregator are calculated in a centralised manner based on a quadratic optimisation model which takes as input information: 1) the requirements of each aggregator, 2) its forecasted load profile, and 3) the loading limits of the network assets. The optimisation problem to be solved at every time step at the DSO level is formulated as follows.

$$\begin{aligned}\text{maximise } f_2 = &\sum_{k\in K}\sum_{t\in N_{slots}}\left(\left(1-\frac{P^{PV}_{k,t}\cdot\zeta_{k,t}}{\sum_{i\in H_{PV}} p^{rated}_{PV_{k,i}}}\right)\cdot P^{PV}_{k,t}\cdot\zeta_{k,t}\right)\\ &+\sum_{k\in K}\sum_{t\in N_{slots}} P^{EV}_{k,t} - \omega\cdot\sum_{k\in K}\sum_{t\in N_{slots}} O_{k,t} - \gamma\cdot\sum_{k\in K}\sum_{t\in N_{slots}}\Delta^{P}_{k,t} \quad (5.10)\end{aligned}$$

The first term of the above objective function seeks to achieve an even distribution of the PV power curtailment of all aggregators by dynamically adjusting their export limit $\zeta$ between zero and one in order to maintain the loading limits of the LV network. This is done by applying a weighting according to the available PV power (Equation (3.13)) of aggregator $k$ at the previous time step. Notice that weighting mainly depends on the summation of the PV units' rated capacity ($p^{\text{rated}}_{PV_{k,i}}$) managed by the aggregator $k$. The second term quantifies the optimal charging power ($P^{EV}_{k,t}$) for aggregator $k$ at time $t$. In the third term, excessive overloading conditions of the feeders from the distribution transformer at each time interval, which are represented by a penalty deviation variable $O_{k,t}$ which in turn helps to ensure the problem feasibility, are penalised by means of a large positive weight $\omega$. The last term penalises significant variations in the charging rate ($\Delta^{P}_{k,t}$) for the $kth$ aggregator by using a large positive factor $\gamma$.

### 5.5.2 Aggregators constraints

Following the above quadratic objective function, constraint (5.11) ensures that the absolute value of the net power of all aggregators does not exceed the rated capacity of the distribution transformer ($S^{\text{rated}}_{\text{Trans}_j} \cdot \cos(\varphi)$). However, the distribution transformer could be subjected to overload conditions in case of an extensive charging demand or reverse power flow. Similarly, constraint (5.12) imposes the absolute value of the maximum power flow through the main cable of the feeder managed by the $kth$ aggregator, which can also be subjected to temporary overloads. In order to handle these situations, those constraints are relaxed by introducing the penalty deviation variable $O_{k,t}$. By adding the above two nonlinear constraints (because of the absolute value function), the quadratic programming problem becomes a mixed-integer quadratic programming (MIQP) model when such restrictions are linearized by using the special ordered sets (SOS) (see Appendix E).

$$| \sum_{k \in K} (P^{PV}_{k,t} \cdot \zeta_{k,t} - (P^{EV}_{k,t} + P^{fc}_{\text{Line}_{k,t}})) | \leq S^{\text{rated}}_{\text{Trans}_j} \cdot \cos(\varphi) + \sum_{k \in K} O_{k,t}, \quad \forall t, \forall j \in \text{Trans} \tag{5.11}$$

$$| P^{PV}_{k,t} \cdot \zeta_{k,t} - (P^{EV}_{k,t} + P^{fc}_{\text{Line}_{k,t}}) | \leq S^{\text{rated}}_{\text{Line}_k} \cdot \cos(\varphi) + O_{k,t}, \ \forall k \in K, \forall t \tag{5.12}$$

In constraint (5.13), the aggregated charging power should not give rise to overload the main service cable of the feeder, which is represented by $P^{\max}_{k,t} = \min\{P^{\text{upper}}_{k,t}, P^{\text{rated}}_{\text{Line}_k} - P^{fc}_{\text{Line}_{k,t}}\}$, where $P^{\text{rated}}_{\text{Line}_k} = S^{\text{rated}}_{\text{Line}_k} \cdot \cos(\varphi)$ is the rated capacity of the main service cable and $P^{fc}_{\text{Line}_{k,t}}$ is the forecasted power demand on the feeder. Note that the forecasted baseload profile per aggregator at the feeder level ($P^{fc}_{\text{Line}_{k,t}}$) can be easily solved by current techniques such as time series, least squares, probabilistic forecasting, among others (Essallah and Khedher, 2019, Gönen, 2007). However, this restriction is relaxed to support temporary overload conditions because of using $O_{k,t}$.

$$P^{EV}_{k,t} \leq P^{\max}_{k,t} + O_{k,t}, \ \forall k \in K, \forall t \tag{5.13}$$

Besides, constraint (5.14) imposes that the aggregated rate of charge ($\Delta^{P}_{k,t}$) of the aggregator $k$ should not display significant variations in power over consecutive time steps in order to limit the thermal stress in the main cable of its feeder. As the current charging level is compared to the one at the previous time step, this constraint is defined for all intervals where $P^{\text{upper}}_{k,t}$ is different from zero.

$$P^{\text{EV}}_{k,t-1} - \Delta^{P}_{k,t} \leq P^{\text{EV}}_{k,t} \leq P^{EV}_{k,t-1} + \Delta^{P}_{k,t}, \ \forall k \in K, \forall t \quad \text{if} \quad P^{\text{upper}}_{k,t} \neq 0 \tag{5.14}$$

Finally, constraint (5.15) ensures the optimal charging power of each aggregator satisfies their forecasted cumulative energy boundaries by employing the recursive equation in (5.16).

$$E^{\text{lower}}_{(k,t^{\text{arr}}_{\min_k}+t)} \leq E_{(k,t^{\text{arr}}_{\min_k}+t)} \leq E^{\text{upper}}_{(k,t^{\text{arr}}_{\min_k}+t)},\ \forall k \in K, t = 0, \ldots, N_k^{p_{int}} \quad (5.15)$$

$$E_{(k,t^{\text{arr}}_{\min_k}+t)} = E_{(k,t^{\text{arr}}_{\min_k}+t)} + P^{EV}_{(k,t^{\text{arr}}_{\min_k}+t)} \cdot \Delta t,\ \forall k \in K, t = 0, \ldots, N_k^{p_{\text{int}}} \quad (5.16)$$

Note that the complexity of this optimisation problem is mainly given by the number of aggregators and the length of the evaluation period ($N_{\text{slots}} = T/\Delta t$), which makes the proposed problem be easily solved. After solving this convex optimisation model, the DSO can send the optimal charging profile to each aggregator for further intelligent dispatching. To summarise, Figure 5.18 outlines the simplified procedure of the proposed centralised control strategy.

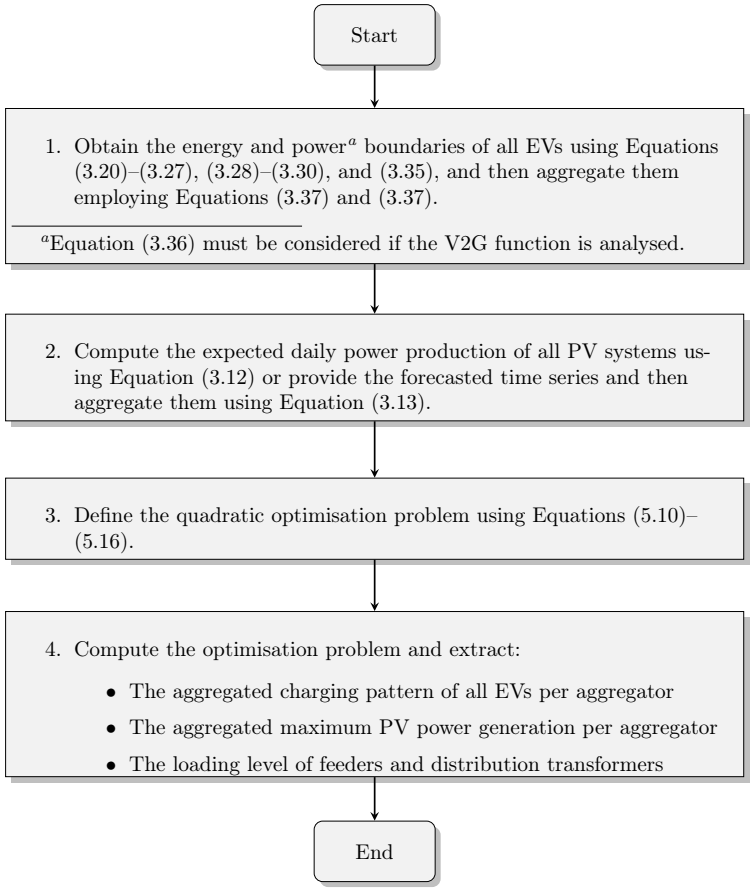


Figure 5.18: Simplified flowchart of the proposed methodology based on the population approach

## 5.6 Centralised optimisation of aggregators at the DSO's level with voltage constraints

### 5.6.1 Objective function

In the above optimisation problem, the DSO only can evaluate the performance of the LV network by tracking and regulating the net power of each agregator based on the loading constraints in the transformer and main cables of the feeders. However, if the DSO requires to assess the voltage limitations in the LV network, it is necessary to include additional constraints for each aggregator in order to avoid any undesirable operational situation. Hence, to assess how the voltage level is affected by introducing a large number of PVs and EVs in the LV network, first, the DSO must fully know its network, *i.e.*, the characteristics of their assets, the size and location of the EVs and PVs, along with the end-users demand. To protect end-user privacy, the aggregator is the only entity who knows their energy needs in detail. Second, it is needed to consider the introduction of smart meters with load and generation control capability in residential housing so that the aggregators can manage these devices in a coordinated manner. Under this assumption, and by taking the objective function in (5.10), three additional terms are included on it to define the new objective function as follows.

$$\begin{aligned}\text{maximise } f_3 = f_2 + \sum_{k\in K}\sum_{i\in H_k^{PV}}\sum_{t\in N_{\text{slots}}}\left(\left(1-\frac{p_{k,i,t}^{PV}\cdot\zeta_{k,i,t}}{p_{PV_{k,i,t}}^{\text{rated}}}\right)\cdot P_{k,i,t}^{PV}\cdot\zeta_{k,i,t}\right)\\ +\sum_{k\in K}\sum_{i\in H_k^{\text{EV}}}\sum_{t\in N_{\text{slots}}}(P_{k,i,t}^{EV}-\Delta_{k,i,t}^{P_{\text{inc}}})\cdot x_{k,i,t}-\lambda\cdot\sum_{k\in K}\sum_{\phi\in p}\sum_{t\in N_{\text{slots}}}O_{k,\phi,t}^{ph}\end{aligned} \tag{5.17}$$

As the PV systems can provide local voltage support by using an active power curtailment method in order to keep the voltage profile within a predefined upper threshold, it is assumed that the end-user $i$ under aggregator $k$ can export its exceeding energy to the grid. To do so, the PV inverter will need to check the demand continuously and its power production to regulate the PV generation through the limit factor $\zeta_{k,i,t}$ for each time step. Note that the export limit of each PV unit highly depends on the voltage sensitivity coefficients (constraint (5.30)) of the network to keep the voltage within its operational range. Hence, the second term in Equation (5.17) seeks to maximise the generated PV power of the $i$th end-user (right-hand term of Equation (3.13)), limiting it when occurring an overvoltage or overload condition. Notice that the curtailed PV power ($p_{k,i,t}^{PV}\cdot\zeta_{k,i,t}$) is evenly distributed

among all users by weighting, as all the PV units are likely to contribute to the aggregated reverse power flow. The third term intends to maximise the charging power of every EV owner by dynamically adjusting the rate of power of its charger, avoiding voltage violations across the network caused by excessive loading conditions on the feeder.

For an unbalanced LV network, loads are unevenly distributed across the network. Hence, each phase of the system may experience different loading conditions when the EVs and PVs are connected. With a high penetration level of these devices, it is likely to observe an overload situation in any phase ($O^{ph}_{k,\phi,t}$). Therefore, the last term of Equation (5.17) seeks to penalise this condition by a large positive factor $\lambda$.

In order to guarantee a proper network operation at each time step, the objective function in (5.17) must be subject to a series of constraints related to the power/energy of the EVs, PVs and aggregators, as well as the voltage levels of the network.

### 5.6.2 Aggregators constraints

For the new optimisation problem, constraints (5.11)–(5.16), which are related with the power and energy at aggregator level are still valid.

### 5.6.3 EVs and PVs constraints

In order to satisfy the voltage limits through the aggregator's feeder, it is necessary to account for additional restrictions that assure a feasible solution to the problem. Thus, constraint (5.18) states that the charging power of the EV connected at household $i$ under aggregator $k$ should not exceed the rated capacity of its charger at any time. Notice that $P^{\text{EV}}_{k,i,t} = 0$ when the EV is not hooked up at household $i$.

$$0 \leq P^{\text{EV}}_{k,i,t} \leq P^{\max}_{ch} \cdot \eta_{ch},\ \forall k \in K, \forall i \in H^{\text{EV}}_k, \forall t \tag{5.18}$$

Constraint (5.19) ensures that $P^{\text{EV}}_{k,i,t}$ should not drastically vary over consecutive time steps, unless the EV gets disconnected, by dynamically adjusting the charging rate of the EV under aggregator $k$. Note that $\Delta^{P_{\text{inc}}}_{k,i,t}$ is a penalty deviation variable which should be no larger than the rated capacity of the EV charger, as stated in constraint (5.20).

$$P^{\text{EV}}_{k,i,t-1} - \Delta^{P_{inc}}_{k,i,t} \leq P^{\text{EV}}_{k,i,t} \leq P^{EV}_{k,i,t-1} + \Delta^{P_{\text{inc}}}_{k,i,t},\ \forall k \in K, \forall i \in H^{\text{EV}}_k, \quad \forall t \quad \text{if} \quad x_{k,i,t} \neq 0 \tag{5.19}$$

$$0 \leq \Delta_{k,i,t}^{P_{\text{inc}}} \leq P_{ch}^{\max} \cdot \eta_{ch},\ \forall k \in K, \forall i \in H_k^{\text{EV}}, \forall t \tag{5.20}$$

Constraint (5.21) imposes that the individual energy requirements of EVs under aggregator $k$ should always be fulfilled while these remain connected ($t_{k,j}^{\text{int}}$). Notice that the energy state of EV $j$ under the $kth$ aggregator is computed by Equation (5.22) at $t_{k,j}^{\text{arr}}$ and later periods by considering the energy remaining from the previous period ($t_{k,j}^{\text{arr}} + t - 1$) and the charging power at time $t$.

$$e_{k,i}^{\text{lower}}(t_{k,j}^{\text{arr}} + t) \leq e_{k,i}^{\text{EV}}(t_{k,j}^{\text{arr}} + t) \leq e_{k,i}^{\text{upper}}(t_{k,j}^{\text{arr}} + t), \\ \forall k \in K, \forall i \in H_k^{\text{EV}}, \forall j \in N_k^{EV}, t = 0, \ldots, t_{k,j}^{\text{int}} + 1 \tag{5.21}$$

$$e_{k,i}^{\text{EV}}(t_{k,j}^{\text{arr}} + t) = e_{k,i}^{\text{EV}}(t_{k,j}^{\text{arr}} + t - 1) + P_{k,i}^{\text{EV}}(t_{k,j}^{\text{arr}} + t) \cdot \Delta t, \\ \forall k \in K, \forall i \in H_k^{\text{EV}}, \forall j \in N_k^{\text{EV}}, t = 0, \ldots, t_{k,j}^{int} + 1 \tag{5.22}$$

Constraint (5.23) enforces that the summation of the maximum injected power from the PV unit connected at household $i$ under aggregator $k$ must be equal to the aggregated maximum PV power of such aggregator. Besides, constraint (5.24) ensures that the total PV power generation per phase should not exceed the rated capacity of each phase of the main cable ($p_{\text{Line}_{k,\phi}}^{\text{rated}}$), where $H_{k,\phi}^{PV}$ is number households connected at phase $\phi$ which have a PV unit managed by the aggregator $k$.

$$\sum_{i \in H_k^{PV}} (p_{k,i,t}^{PV} \cdot \zeta_{k,i,t}) = P_{k,t}^{PV} \cdot \zeta_{k,t},\ \forall k \in K, \forall t \tag{5.23}$$

$$\sum_{i \in H_{k,\phi}^{PV}} (p_{k,i,t}^{PV} \cdot \zeta_{k,i,t}) <= p_{Line_{k,\phi}}^{\text{rated}},\ \forall k \in K, \forall \phi \in p, \forall t \tag{5.24}$$

Constraints (5.25) and (5.26) impose that the summation of the optimal charging power and the dynamic charging rate of the connected EV at household $i$ under aggregator $k$ have to be equal to the aggregated optimal charging demand and the aggregated charging rate of such aggregator, respectively.

$$\sum_{i \in H_k^{\text{EV}}} P_{k,i,t}^{\text{EV}} = P_{k,t}^{EV},\ \forall k \in K, \forall t \tag{5.25}$$

$$\sum_{i \in H_k^{\text{EV}}} \Delta_{k,i,t}^{P_{inc}} = \Delta_{k,t}^{P},\ \forall k \in K, \forall t \quad \text{if} \quad P_{EV_{k,t}}^{\text{upper}} \neq 0 \tag{5.26}$$

Constraint (5.27) defines that the sum of the overloading in all phases must be equal to the overloading condition at the level of the $kth$ aggregator to maintain the power balance.

$$\sum_{\phi \in p} O^{ph}_{k,\phi,t} = O_{k,t}, \ \forall k \in K, \forall t \tag{5.27}$$

Finally, constraint (5.28) states that the total charging power of the EVs connected at phase $\phi$ should not be larger than the available capacity on such phase of the feeder, but it could be overloaded if the power requirements of the EVs are not met. Note that this restriction is similar to (5.13), but at phase level.

$$\sum_{i \in H^{\text{EV}}_{k,\phi}} P^{EV}_{k,i,t} \leq P^{\max}_{k,\phi,t} + O^{ph}_{k,\phi,t}, \ \forall k \in K, \forall \phi \in p, \forall t \tag{5.28}$$

where $P^{\max}_{k,\phi,t} = \min\{p^{\text{upper,ph}}_{k,\phi,t}, p^{\text{rated}}_{\text{Line}_{k,\phi}} - p^{fc}_{\text{Line}_{k,\phi,t}}\}$, $H^{EV}_{k,\phi}$ is is number households connected at phase $\phi$ which have a EV managed by the aggregator $k$, $p^{fc}_{\text{Line}_{k,\phi,t}}$ is the forecasted power per phase of the $kth$ aggregator, and $p^{\text{upper,ph}}_{k,\phi,t}$ is the aggregated upper power boundary of all EVs connected at phase $\phi$, which is defined by Equation (5.29). As the $kth$ aggregator has already computed the individual power boundary of the $jth$ EV using Equation (3.35), and as it knows the location of such vehicle at household $i$, a such individual limit is represented per phase by $p^{\text{upper,ph}}_{k,\phi,i}(t)$.

$$p^{\text{upper,ph}}_{k,\phi}(t) = \sum_{i \in H^{\text{EV}}_{k,\phi}} p^{\text{up,ph}}_{k,\phi,i}(t), \ \forall k \in K, \forall \phi \in p, \forall t \tag{5.29}$$

### 5.6.4 Voltage constraints

As the addition of EVs and PV units alongside the LV network may cause a significant drop or rise in voltage magnitude at every load node, constraint (5.7) has been modified by including the individual adjustment of PV export limit $\zeta$, as shown in constraint (5.30).

$$\begin{aligned} V_{\min} \leq V^{\text{ini}}_{i,t} + \alpha_{i,i} \cdot P^{EV}_{k,i,t} + \beta_{i,i} \cdot p^{PV}_{k,i,t} \cdot \zeta_{k,i,t} + \\ \sum_{\substack{h \in H \\ i \neq h}} (\alpha_{h,i} \cdot P^{\text{EV}}_{k,h,t} + \beta_{h,i} \cdot p^{PV}_{k,h,t} \cdot \zeta_{k,h,t}) \leq V_{\max}, \\ \forall k \in K, \forall i \neq \emptyset \in H, \forall t \end{aligned} \tag{5.30}$$

Once solved the proposed convex model, the DSO can send different signals to each aggregator such as the individual and aggregate charging pattern of all EVs per aggregator, the individual and aggregate maximum PV power generation per aggregator, the voltage profiles of all network users, and the loading level of feeders and distribution transformers. To summarise, Figure 5.19 outlines the simplified procedure of the proposed centralised control method.

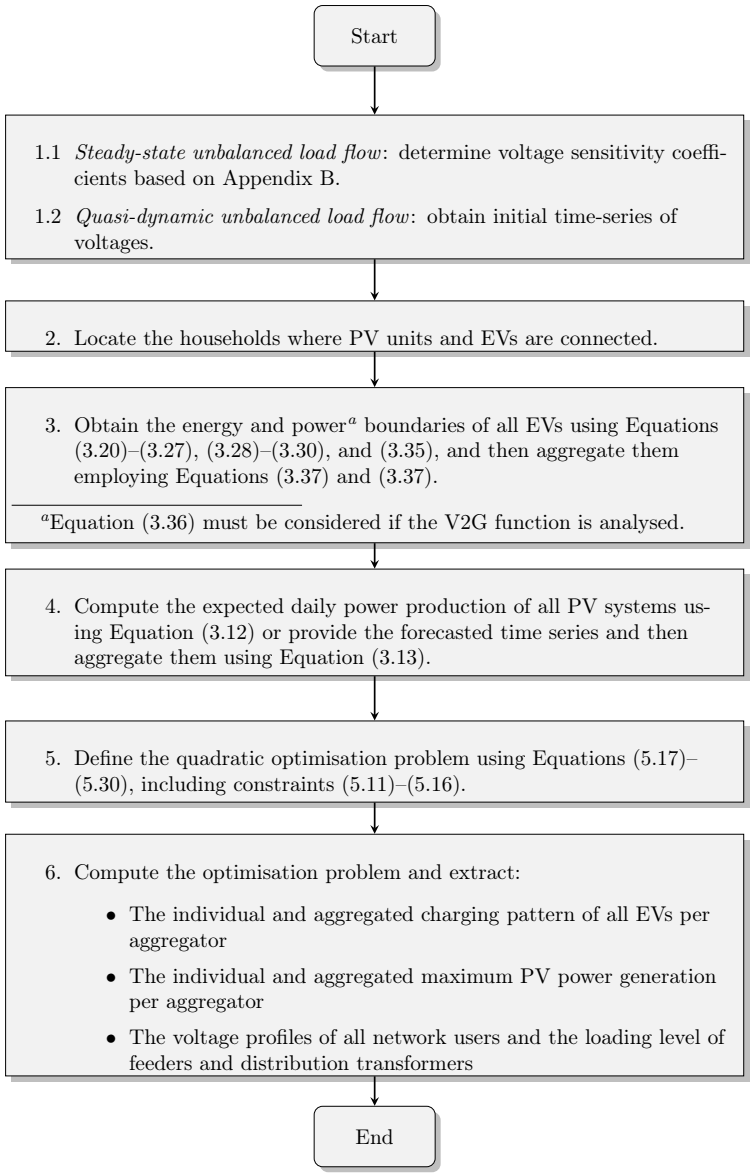


Figure 5.19: Simplified flowchart of the proposed methodology based on the hybrid approach using the voltage sensitivity coefficients

## 5.7 Description of the test cases used for problems (5.10) and (5.17)

In order to validate the proposed coordination strategy, two case studies have been undertaken.

- Case 1: In this case, the convex optimisation model in (5.10)–(5.16) is analysed. This means that the DSO only considers the loading capacity of the main service cables and distribution transformer as the reference parameter. Detailed topological configuration of the LV network is not needed. The aggregators report their energy and power requirements in an aggregated manner.

- Case 2: The convex optimisation problem in (5.17)–(5.30), including restrictions (5.11)–(5.16) is evaluated. The information of the LV network is considered as the DSO knows in detail the grid. A residential LV network (Figure 4.1) with two feeders which supply power to 55 and 75 households with a lagging power factor of 0.95, respectively, has been considered. The aggregators inform the voltage and loading levels per user node as additional information with respect to Case 1.

The rated capacity of each service cable is 215 $A$, *i.e.*, $p^{\text{rated}}_{\text{Line}_{k,\phi}} = 47.17$ kW per phase, taking into account also a lagging power factor of 0.95. Both feeders are derived from a 350 kVA distribution transformer with a rated phase-to-phase voltage at the secondary of 400 $V$ with $\pm 10\%$ allowable variation. It is assumed that each feeder is managed by an aggregator, *i.e.*, $K = 2$. Data of residential load and network parameters were collected from (Electriciy North West, 2019).

A critical penetration level of 100% for both the EVs and PVs in each feeder was considered. It means that all households (see Table 4.1) in both feeders have both a PV and EV operating at certain time slots of the test period. EVs and PVs are simulated using the specifications given in Table 5.3. EVs travelled distance and arrival time are modelled using log-normal (National Renewable Energy Laboratory, 2017) and truncated Gaussian (Shafie-Khah et al., 2016) distribution functions, respectively.

Simulations are executed for 30 hours with 10-minute time intervals, *i.e.*, $N_{\text{slots}} = 180$. Weight parameters $\omega$, $\gamma$, and $\lambda$ were adjusted to 1000. It is used CPLEX 12.9 under its API in Python (DOcplex) (IBM, 2020) to solve the two proposed optimisation models on a laptop with a four cores Intel Core i7 processor and 12 GB memory. It takes less than 1 second to

solve the proposed optimisation problem in (5.10)–(5.16) and 5 s to solve the presented optimisation model in (5.17)–(5.30), including restrictions in (5.11)–(5.16).

Table 5.3: EV and PV data used for simulation

| Description | Parameter |
|---|---|
| EV model | Nissan Leaf |
| Battery Capacity | 24 kWh |
| ECR | 0.1778 kWh/km |
| Rated Charger Power | 3.7 kW |
| Charger efficiency | 0.92 |
| Daily driven distance | $\mathcal{N}(\mu_{\ln} = 2.89257, \sigma_{\ln} = 0.91779)$ |
| Arrival time | $\mathcal{N}(\mu = 16:00, \sigma = 3\ h, t_{\min} = 11:00, t_{\max} = 23:00)$ |
| $SOC_{obj}$ | 0.95 |
| Rated PV Inverter Power | 5 kW |
| Inverter Power Factor | 1 |

### 5.7.1 Results of the population-based and hybrid approach

This section presents and analyses the results obtained by employing the proposed coordination strategy among two aggregators considering a 100% penetration level of PVs and EVs. Figure 5.20 shows the statistical daily power generation for a 5 kW single-phase PV system with a 10 min resolution interval as a result of the model in Section 3.1. Based on this result, the PV power output of each household within the *kth* aggregator is randomly generated based on the mean and standard deviation value at each time step from the above figure. Then, the resulting PV power profiles are aggregated using Equation (3.13).

On the other hand, Figure 5.21 exemplifies the behaviour of the PV power curtailment factor $\zeta$ for a PV unit installed in a household at the beginning and the end of both feeders if a linear approach were used instead of a quadratic formulation like in (5.17). Figures 5.21($a$) and $c$), show that the households along the feeder may experience an uneven distribution of the value of $\zeta$ if a linear approximation for the power curtailment is employed. This means that some users will be more penalised than others, depending on their location across the network. However, as all the PV units will contribute to the aggregated reverse power flow, these should be evenly penalised regardless of their location in the feeder, as shown in Figures 5.21($b$) and ($d$).

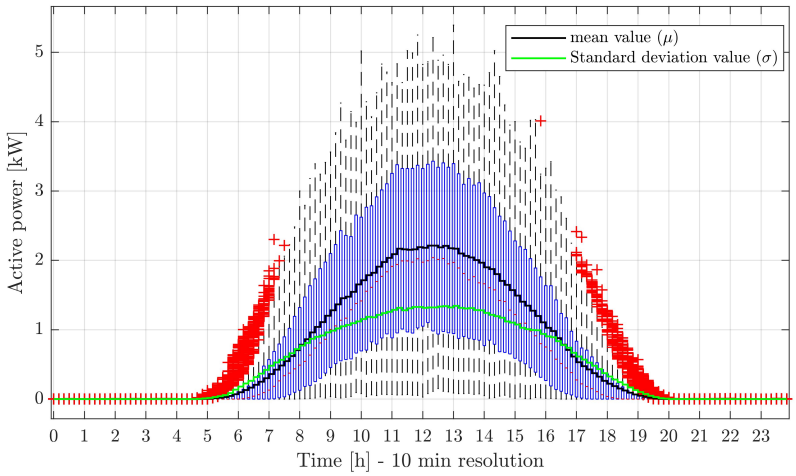


Figure 5.20: Boxplot for the PV inverter power derived from yearly meteorological data by using the model in Section 3.1.

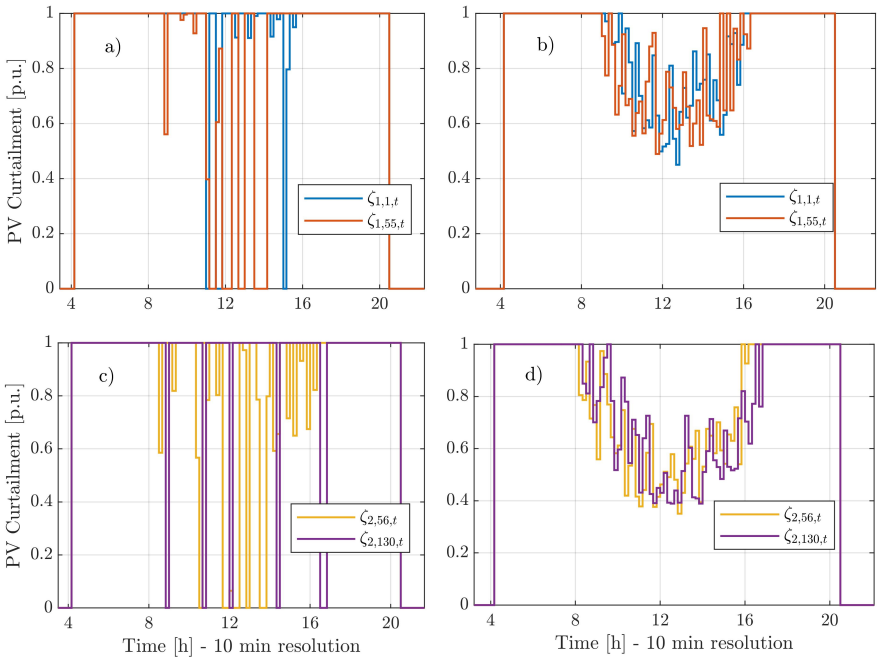


Figure 5.21: Comparison between the linear ((*a*) and (*c*)) and quadratic ((*b*) and (*d*)) approaches for the PV power curtailment factor $\zeta$ for aggregator 1 and 2. (*a*) Household 1 in feeder 1, (*b*) Household 55 in feeder 1, (*c*) Household 56 in feeder 2, (*d*) Household 130 in feeder 2.

### Charging behaviour at Aggregator level

As a result of the proposed optimisation problem in (5.10)–(5.16) (Case 1), Figure 5.22 compares the upper power boundaries, the optimal charging power ($P_k^{\text{EV}}$), the maximum charging power ($P_{ch}^{\max}$), and the overloading levels ($OL_k$) for both aggregators. Figure 5.22*a*) shows that power needs from both aggregators are met thanks to the delay in the charging process and the dynamic adjustment of $\Delta_k^P$. However, in Figure 5.22*b*), it can be seen that the aggregator two exceeds the remaining capacity of its feeder in order to fulfil its charging requirements. Although it seems to occur for an extended period (16:00 to 21:00), in fact, the overloading condition only occurs in a shorter period because this situation is analysed from the point of view of the net power on the feeder, as shown in Figure 5.27.

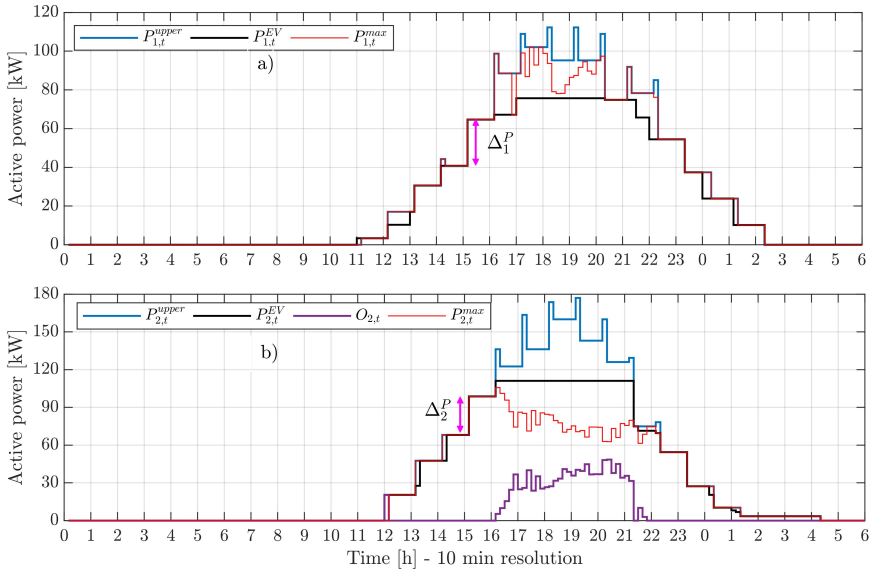


Figure 5.22: Case 1: Upper power boundary (blue), maximum power on the feeder (red), overloading on the feeder (purple), and the optimal charging power profile (black) for *a*) the first aggregator and *b*) second aggregator.

On the other hand, Figures 5.23 and 5.24 depict the behaviour of the variables described above, but this time, per phase and aggregator, respectively, after solving the convex problem in (5.17)–(5.30), *i.e.*, Case 2. Due to the granularity of the input information, the aggregator is able to evaluate if there is an overload condition per phase, contrary to Case 1. By comparing Figures 5.23 and 5.24, it can be seen that both aggregators require a power level further to the capacity of the feeder for charging the EVs connected to

phase $a$. This effect also occurs in phases $b$ and $c$ for the second aggregator because of the number of households on the feeder (Table 4.1). Nonetheless, the total overloading effect is seen reduced by evaluated it through the net power per phase on the feeder due to the contribution of the PV power. Serving the EVs locally reduces the power flow from the upstream network and enhances network voltage.

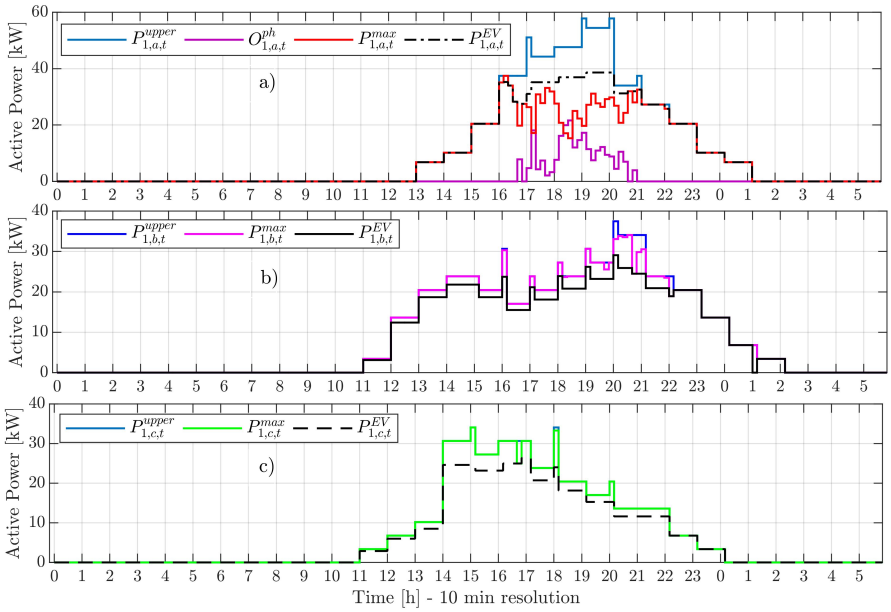


Figure 5.23: Case 2: Upper power boundary, maximum power, overloading, and optimal charging power profile per phase for the first aggregator.

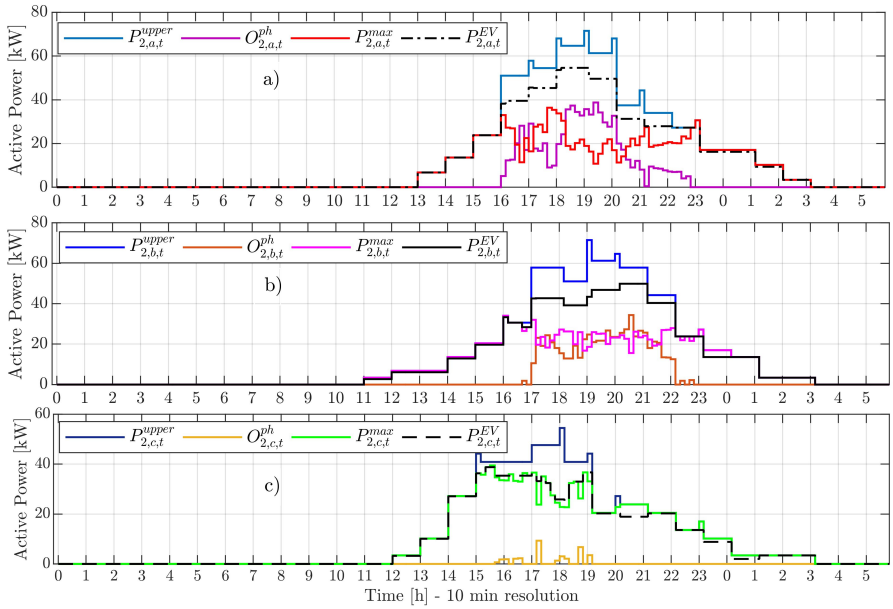


Figure 5.24: Case 2: Upper power boundary, maximum power, overloading, and optimal charging power profile per phase for the second aggregator.

For comparison, Figures 5.25 and 5.26 depict for each case and aggregator how the supplied energy to their EVs evolves between their aggregated energy boundaries as a result of the obtained optimal charging profile. It can be seen that, in both cases, the energy trajectory starts close to the upper boundary, which means that all EVs are charging at the rated capacity of their chargers. Then, during the charging period, power is modified according to constraints in (5.14) and (5.18)–(5.20) for Case 1 and 2, respectively, up to reach the lower boundary, *i.e.*, the charging power is slightly delayed for some EVs.

Note that, in both cases, the amount of energy supplied to the EVs of each aggregator at the end of their charging periods is almost the same for the first aggregator and slightly different for the second. This means that a total of 717 kWh and 974 kWh in Case 1, and 713 kWh and 1009 kWh in Case 2, respectively, were delivered by combining the network and the aggregated PV power. This small difference is generally given by factors (vehicle usage, personal habits, and working schedules) which are relatively steady and which could change slowly, *i.e.*, the characteristics of the charging will not suddenly change with the same trajectory.

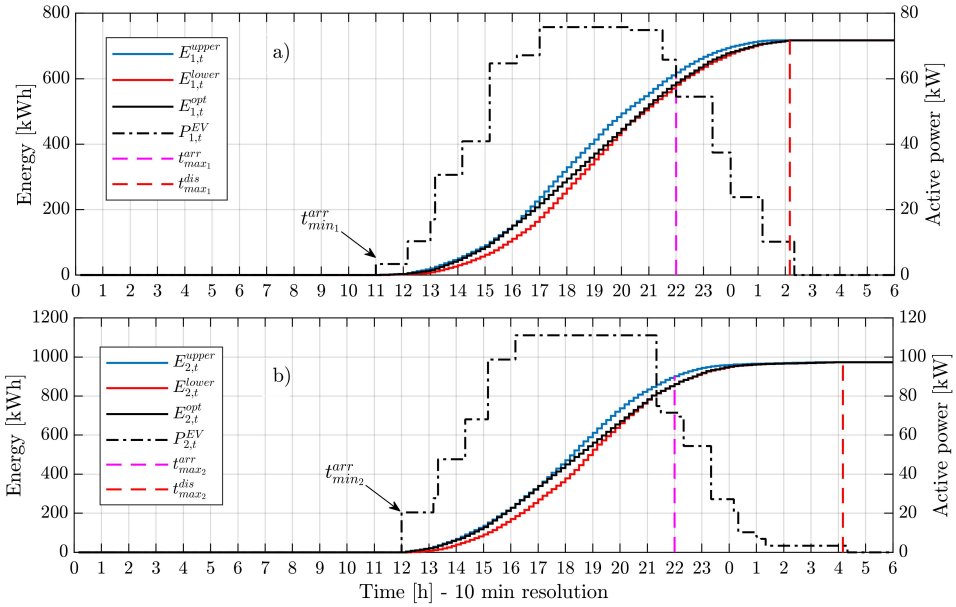


Figure 5.25: Optimal charging trajectory and charging profile for *a*) the first aggregator and *b*) second aggregator

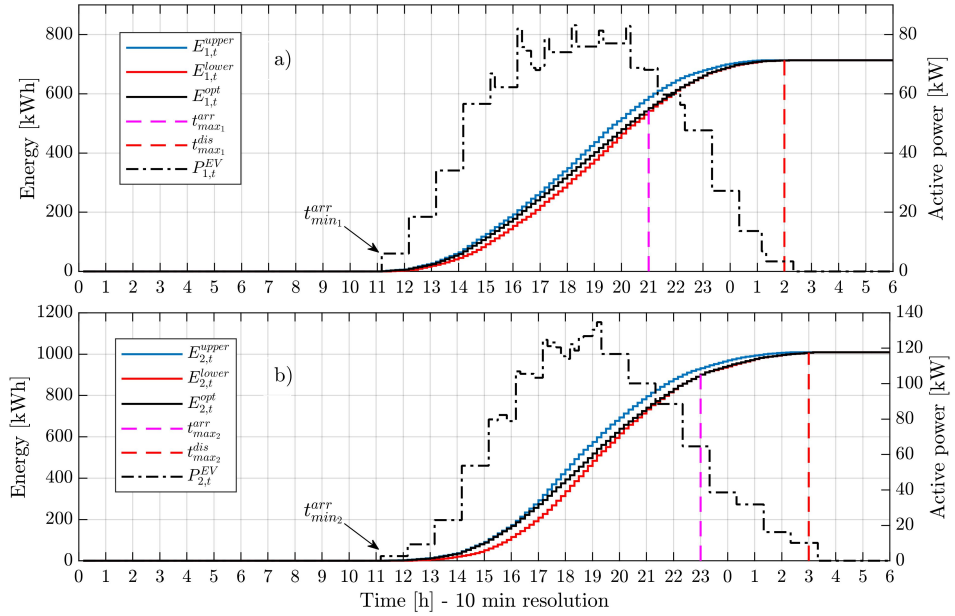


Figure 5.26: Optimal charging trajectory and charging profile with voltage constraints for *a*) the first aggregator and *b*) second aggregator

### Feeders loading level

In Figure 5.27, several operational curves are compared for both aggregators in order to exemplify the obtained results after solving the proposed optimisation problem in (5.10)–(5.16). First, the aggregated PV power of each aggregator is in average reduced 22.5% and 24.7%, respectively, with respect to the estimated PV generation (curve with red dots) due to the weighting term in (5.10). This can be seen in terms of the total net power (dash-dotted line) through the main service cables of the feeders. In Figure 5.27*b*), the second aggregator, during the maximum PV power generation, limits the reverse power flow to the rated capacity of their feeders ($P^{\text{rated}}_{\text{Line}_k} = 141.5$ kW) because of the operating constraint in (5.12). Second, during the evening peak demand period, it experiences an overloading event for approximately 2.25 hours, which overpasses the rated capacity of its feeder in 32%. This occurs because the objective function in (5.10) is penalised by simultaneously charging a large number of EVs during that time. Despite this operational condition, the loading level on the main transformer is maintained below its rated capacity, as shown in Figure 5.29. Besides, it is also presented the self-consumed PV power by the EVs and the users' demand.

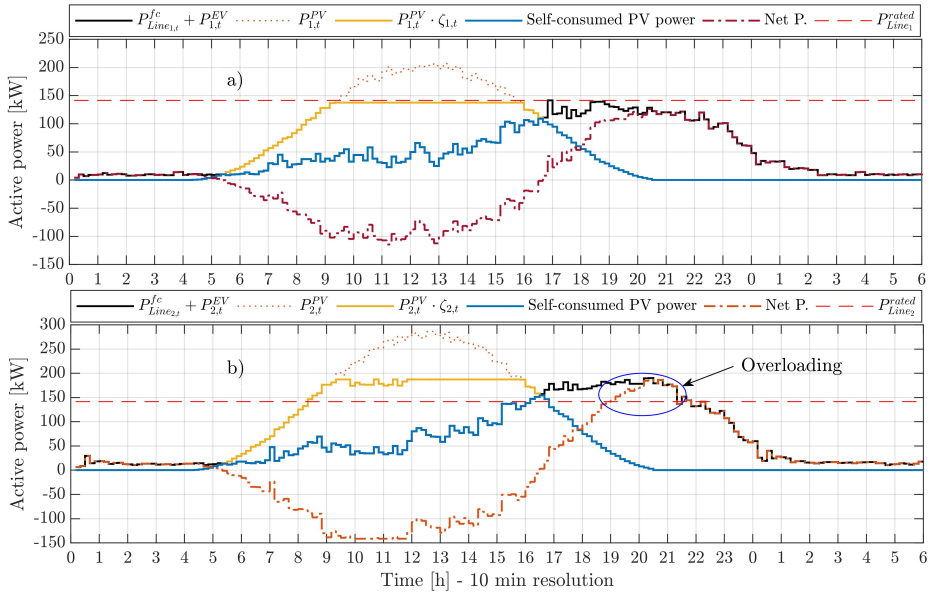


Figure 5.27: Net power on the feeder's main cable without VC for the *a*) first aggregator and *b*) second aggregator

Figure 5.28 shows the three- and single-phase net power on each feeder as a result of solving the optimisation problem from Section 5.6. The reverse

power flow in all phases of both feeders is limited to the single-phase capacity of the service cable due to constraint in (5.24). However, for the first feeder (Figure 5.28*a*), the impact of the EVs located in phase $a$ is evident, with the loading level above the rated capacity of the phase, while phase $b$ and phase $c$ loading levels are below this limit. Similar overloading events occur at the second feeder (Figure 5.28*b*) but in phases $a$ and $b$, as these supply power to more households than phase $c$, which is also be reflected in the total net power at the aggregator level. Thus, by adding the new constraints and variables to the coordination schema in (5.10), the DSO can identify overload events in any phase of the aggregator's feeder due to the unbalanced nature of the loads. This result also highlights the significance of modelling unbalanced networks, as a balanced representation would not have captured the impact in any phase of the system, suggesting incorrectly that additional EV load or PV generation could be introduced without breaching limits.

Notice that evaluating this critical penetration level on this particular network and assuming that the EVs owners are not flexible in changing their expected energy level, there would be two feasible solutions: reinforcement of the main service cable of each feeder or the installation of centralised BESSs, which could store the surplus PV power and give it back when necessary to reduce the loading level on the feeders.

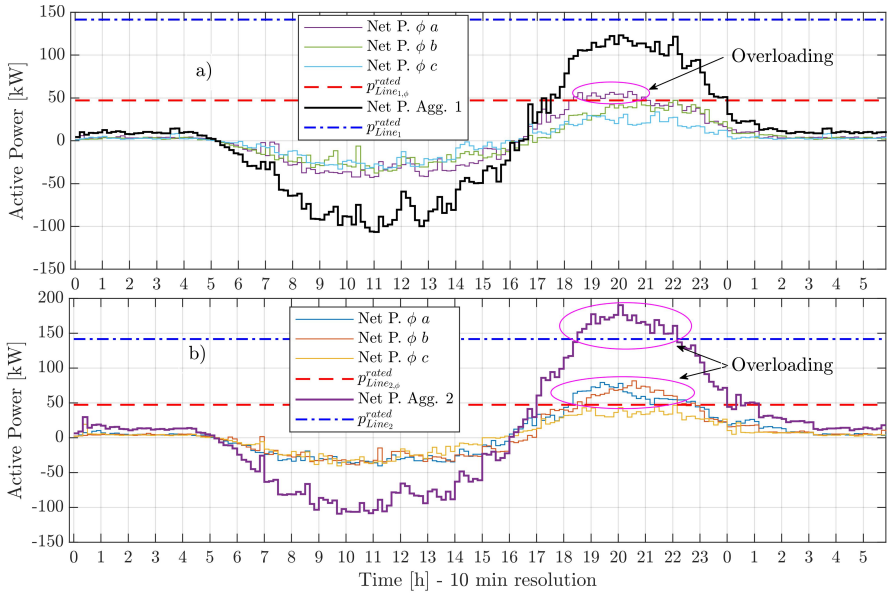


Figure 5.28: Three- and single-phase net power on the feeder's main cable of the $a$) first aggregator and $b$) second aggregator.

Note also that each aggregator could experience higher overloading events if a proper control strategy is not considered, *i.e.*, the maximum expected charging power value ($P_{ch}^{\max}$) would be equal to the upper power boundary of each aggregator. In addition, for a higher charging mode (according to the IEC 61851 (Martínez-Lao et al., 2017)) and a larger PV rated capacity, the penetration level would be much lower. However, if it is required to maintain the same penetration level, it would be necessary to reinforce both the transformer and the main cables.

**Transformer loading level**

For comparison, the total net power through the main distribution transformer with and without voltage constraints is presented in Figure 5.29. It is evident that for both cases, the transformer capacity is high enough for accommodating both the additional charging demand and local generation; taking into account the parameters in Section 5.7. It can also be seen that the reverse power flow level is lower when considering the voltage constraints in conjunction with the PV power curtailment restrictions in (5.23) and (5.24). Moreover, the aggregated charging power is slightly delayed without accounting for the voltage constraints because only the loading criteria is evaluated by the control strategy. Notice that the results from this critical scenario would provide to the DSO the input data for planning the reinforcement of their assets.

**LV network voltages**

As a result of implementing the proposed coordination model in Section 5.6, the single-phase voltage distribution of all household nodes in both feeders is shown in Figures 5.30*a*) and *b*). The impact of active power injection in both feeders during midday on voltages is clearly visible, as these high values are induced by the simultaneous power generation of multiple PVs. However, it can be seen that the whiskers in Figure 5.30*a*) are limited to 1.1 *p.u.* due to voltage constraint in (5.30). It also shows that even though the loading levels in some phases for both aggregators are exceeded during the charging of the EVs, as depicted in Figure 5.28, the voltage drops within acceptable limits. Therefore, it is important to consider the voltage effect in the simulated network.

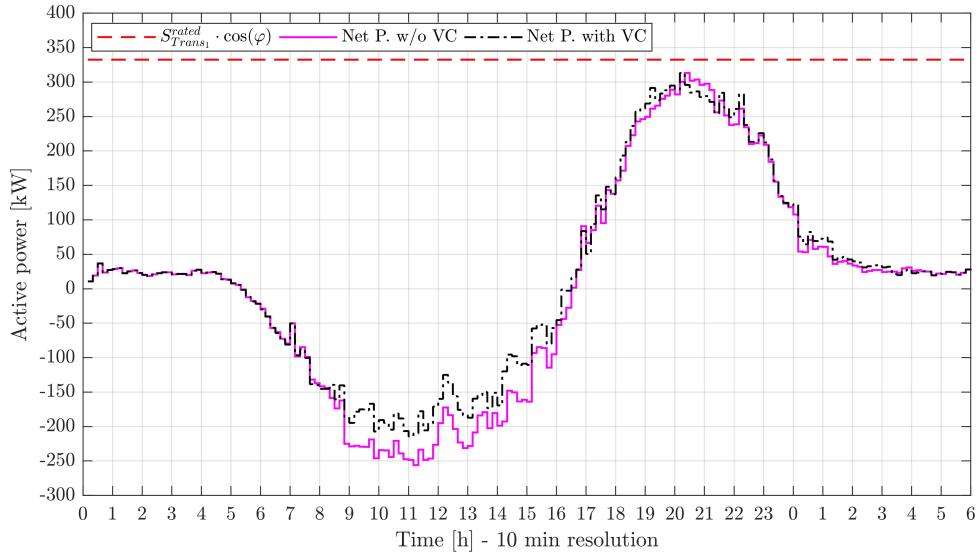


Figure 5.29: Net power on the distribution transformer with and without voltage constraints (VC)

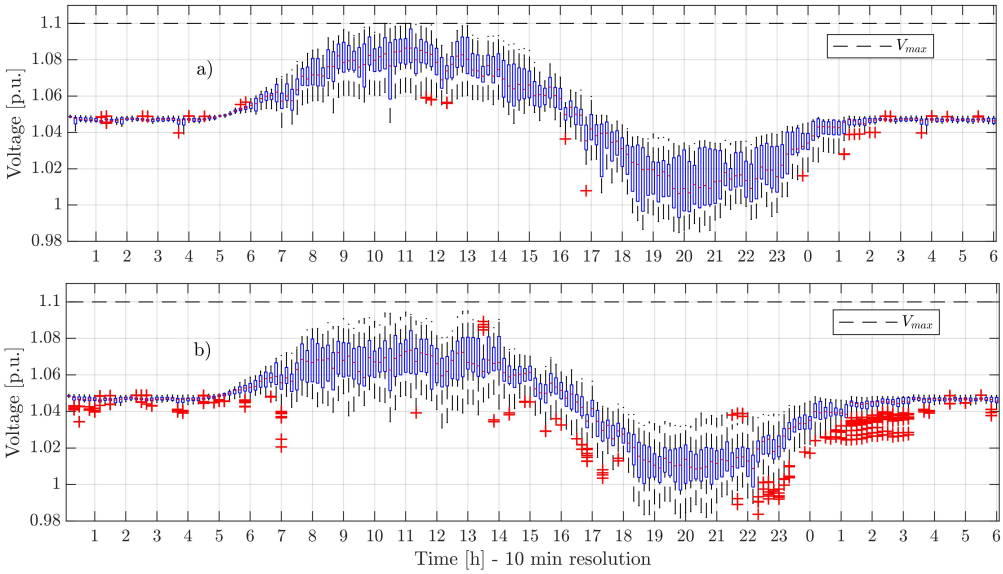


Figure 5.30: Boxplot of voltage profile for the households managed by *a*) the first aggregator and *b*) second aggregator.

## 5.8 Centralised optimisation using the linearisation for the unbalanced power flow

In this section, the proposed objective function in (5.17) is rewritten based on the network nodes in order to include the new linear approximation of the power flow described in Section 4.2.1. Note two things, the functionality description of each term given in Sections 5.6.1 and 5.5.1 remains equal for this optimisation problem, and only those variables without the subindex $t$ are updated at every timestep.

$$\begin{aligned}\text{maximise } f_4 = &\sum_{k\in K}\sum_{t\in N_{slots}}\left(\left(1-\frac{P_k^{PV}\cdot\zeta_{k,t}}{\sum_{i\in H_{PV}}P_{PV_{k,i}}^{rated}}\right)\cdot P_k^{PV}\cdot\zeta_{k,t}\right)\\ &+\sum_{k\in K}\sum_{t\in N_{slots}}P_{k,t}^{EV}-\omega\cdot\sum_{k\in K}\sum_{t\in N_{slots}}O_{k,t}-\gamma\cdot\sum_{k\in K}\sum_{t\in N_{slots}}\Delta_{k,t}^{P}\\ &+\sum_{t\in N_{\text{slots}}}\sum_{\substack{i\in N\\ S_{PV_i}^{\text{re}}\neq 0}}\left(\left(1-\frac{S_{PV_i}^{\text{re}}\cdot\zeta_{i,t}}{P_{PV_{i,t}}^{\text{rated}}}\right)\cdot S_{PV_i}^{\text{re}}\cdot\zeta_{i,t}\right)+\sum_{t\in N_{\text{slots}}}\sum_{\substack{i\in N\\ x_i\neq 0}}(P_{i,t}^{EV}-\Delta_{i,t}^{P_{\text{inc}}})\cdot x_i\end{aligned} \tag{5.31}$$

### 5.8.1 Network constraints

Equation (4.5), which represents the linearized power flow, is rewritten into its real and imaginary parts in order to introduce the proposed control variables for the optimal PV power curtailment and smart charging of EVs per aggregator. First, the product of matrices $H\cdot V_N^*$ and $M\cdot V_N$ is operated according to Equations (5.32) and (5.33), respectively. Since most of the terms of $H$ and $M$ are zero, the resulting matrices can be handled as a set of compressed sparse [1] row matrices in order to reduce the computational burden. Hence, a new set of matrices can be defined as a function of the set of nodes and time, as shown in Equations (5.34)–(5.37).

[1] A matrix is said to be sparse if a large proportion of its entries are zero. Hence, memory usage and computational complexity can be enhanced by using a sparse matrix coding. A simple but effective sparse coding is to store a matrix $A\in\mathbb{R}^{N\times P}$ as a collection of triples $\{(i,j,A_{i,j}:1\leq i\leq N,1\leq j\leq P,A_{i,j}\neq 0)\}$. In Python, this is managed as a dictionary with indices as keys and matrix entries as values.

$$(H^{\text{re}}_{i,k} + jH^{\text{im}}_{i,k}) \cdot (V^{\text{re}}_{N_{k,t}} - jV^{\text{im}}_{N_{k,t}}) = (H^{\text{re}}_{i,k} \cdot V^{\text{re}}_{N_{k,t}} + H^{\text{im}}_{i,k} \cdot V^{\text{im}}_{N_{k,t}}) + j(V^{\text{re}}_{N_{k,t}} \cdot H^{\text{im}}_{i,k} - H^{\text{re}}_{i,k} \cdot V^{\text{im}}_{N_{k,t}}) \quad (5.32)$$

$$(M^{\text{re}}_{i,k} + jM^{\text{im}}_{i,k}) \cdot (V^{\text{re}}_{N_{k,t}} + jV^{\text{im}}_{N_{k,t}}) = (M^{\text{re}}_{i,k} \cdot V^{\text{re}}_{N_{k,t}} - M^{\text{im}}_{i,k} \cdot V^{\text{im}}_{N_{k,t}}) + j(V^{\text{im}}_{N_{k,t}} \cdot M^{\text{re}}_{i,k} + M^{\text{im}}_{i,k} \cdot V^{\text{re}}_{N_{k,t}}) \quad (5.33)$$

$$A_{i,t} = A_{i,t} + (H^{\text{re}}_{i,k} \cdot V^{\text{re}}_{N_{k,t}} + H^{\text{im}}_{i,k} \cdot V^{\text{im}}_{N_{k,t}}) \; \forall (i,k) \in \text{sparse}\{H^{\text{re}}_{i,k}\}, \; \forall t \quad (5.34)$$

$$B_{i,t} = B_{i,t} + (V^{\text{re}}_{N_{k,t}} \cdot H^{\text{im}}_{i,k} - H^{\text{re}}_{i,k} \cdot V^{\text{im}}_{N_{k,t}}) \; \forall (i,k) \in \text{sparse}\{H^{\text{im}}_{i,k}\}, \; \forall t \quad (5.35)$$

$$C_{i,t} = C_{i,t} + (M^{\text{re}}_{i,k} \cdot V^{\text{re}}_{N_{k,t}} - M^{\text{im}}_{i,k} \cdot V^{\text{im}}_{N_{k,t}}) \; \forall (i,k) \in \text{sparse}\{M^{\text{re}}_{i,k}\}, \; \forall t \quad (5.36)$$

$$D_{i,t} = D_{i,t} + (V^{\text{im}}_{N_{k,t}} \cdot M^{\text{re}}_{i,k} + M^{\text{im}}_{i,k} \cdot V^{\text{re}}_{N_{k,t}}) \; \forall (i,k) \in \text{sparse}\{M^{\text{im}}_{i,k}\}, \; \forall t \quad (5.37)$$

As a result, the power flow can be expressed as a function of the above matrices, as shown in Equations (5.38) and (5.39). As $J$ is a vector, its real and imaginary parts are straightly employed.

$$Re\{S^{*}_{net}\} = A_{i,t} + C_{i,t} + J^{\text{re}}_{i} \quad (5.38)$$

$$Im\{S^{*}_{net}\} = B_{i,t} + D_{i,t} + J^{\text{im}}_{i} \quad (5.39)$$

Besides, the left-side terms of the above equations can be expanded by introducing the balance of active and reactive power between the PV generation, the conventional load and the EV charging at node $i$. Notice that Equation (5.41) considers that the PV inverter can operate with a different power factor than unity. Note also that $x_i$ represents the availability of the EV at node $i$ for a given time $t$. It is also considered that each EV charger operates with a unity power factor.

$$\zeta_{i,t} \cdot S^{\text{re}}_{PV_i} - (S^{\text{re}}_{Load_i} + x_i \cdot P_{EV_{i,t}}) = \text{Re}\{S^{*}_{net}\} \quad (5.40)$$

$$-(S^{\text{im}}_{PV_i} - S^{\text{im}}_{Load_i}) = \text{Im}\{S^{*}_{net}\} \quad (5.41)$$

Therefore, the power flow constraints are obtained by replacing Equation (5.38) into (5.40), and Equation (5.39) into (5.41), resulting in Equations (5.42) and (5.43), respectively. Notice that these equations define an affine space, even when those are separated into real and imaginary parts, since $H$, $M$, or $J$ do not depend on power.

$$\zeta_{i,t} \cdot S^{\text{re}}_{PV_i} - (S^{\text{re}}_{Load_i} + x_i \cdot P_{EV_{i,t}}) = A_{i,t} + C_{i,t} + J^{\text{re}}_{i} \quad \forall i \in N, \forall t \quad (5.42)$$

$$-(S^{\text{im}}_{PV_i} - S^{\text{im}}_{Load_i}) = B_{i,t} + D_{i,t} + J^{\text{im}}_{i} \quad \forall i \in N, \forall t \quad (5.43)$$

On the other hand, if maximum drop constraint (4.9) is relaxed (*i.e.*, after separate it in its real and imaginary parts, as shown in Equation (5.44)), then the model becomes a quadratic optimisation with a quadratic constraint that can be easily handled by solvers such as DOcplex in Python. Nonetheless, Equation (5.44) must be verified after the optimisation because the load flow's accuracy depends highly on the value of this constraint.

$$(V_{0_i}^{\text{re}} - V_{N_{i,t}}^{\text{re}})^2 + (V_{0_i}^{\text{im}} - V_{N_{i,t}}^{\text{im}})^2 \leq \delta_{\max}^2 \quad \forall i \in N, \forall t \tag{5.44}$$

Note that the addition of the above constraint makes that the QP in (5.31) becomes a quadratically constrained quadratic problem (QCQP).

### 5.8.2 Aggregators constraints

Constraints (5.13)–(5.16) are still valid for this approach, as these restrictions only depend on the aggregator itself.

### 5.8.3 EVs and PVs constraints

To assure a feasible solution to the problem, the following set of restrictions are included[2]. Constraint (5.45) states that the charging power of the EV connected at household node $i$ should not exceed the rated capacity of its charger at any time. Notice that $P_{i,t}^{\text{EV}} = 0$ when the EV is not connected.

$$0 \leq P_{i,t}^{\text{EV}} \leq P_{ch}^{\max} \cdot \eta_{ch}, \ \forall t, \forall i \in N \text{ if } x_i \neq 0 \tag{5.45}$$

Constraint (5.46) limits sudden changes of $P_{i,t}^{\text{EV}}$ over consecutive time steps by dynamically tuning the charging rate of the EV at node $i$. Further, constraint (5.47) states that the penalty deviation variable $\Delta_{i,t}^{P_{\text{inc}}}$ should be no larger than the rated capacity of the EV charger.

$$P_{i,t-1}^{\text{EV}} - \Delta_{i,t}^{P_{inc}} \leq P_{i,t}^{\text{EV}} \leq P_{i,t-1}^{EV} + \Delta_{i,t}^{P_{\text{inc}}}, \ \forall t, \forall i \in N \text{ if } x_i \neq 0 \tag{5.46}$$

$$0 \leq \Delta_{i,t}^{P_{\text{inc}}} \leq P_{ch}^{\max} \cdot \eta_{ch}, \ \forall t, \forall i \in N \text{ if } x_i \neq 0 \tag{5.47}$$

The energy boundary constraints (5.21) and (5.22) are also included in this optimisation problem, as they depend on the energy state of each EV. Constraints (5.48) and (5.49) impose that the summation of the optimal charging

[2]Notice that subindex $k$ for the EVs and PVs from problem $f_3$ is no longer used in this optimisation problem. Constraints are formulated for all the connected devices into the LV network. The number of EVs and PVs for a particular aggregator is later categorised using a sparse matrix based on the node where each device is connected.

power and the dynamic charging rate of the connected EV at household node $i$ under aggregator $k$ have to be equal to the aggregated optimal charging demand and the aggregated charging rate of such aggregator, respectively.

$$\sum_{(k,i)\in \text{ sparse}\{N_{k,i}^{EV}\}} (P_{i,t}^{\text{EV}} \cdot x_i) = P_{k,t}^{EV},\ \forall t, \forall k \in K \tag{5.48}$$

$$\sum_{(k,i)\in \text{ sparse}\{N_{k,i}^{EV}\}} (\Delta_{i,t}^{P_{inc}} \cdot x_i) = \Delta_{k,t}^{P},\ \forall t, \forall k \in K \text{ if } P_{EV_{k,t}}^{\text{upper}} \neq 0 \tag{5.49}$$

Constraint (5.50) enforces that the summation of the maximum injected power from the PV unit connected at the household node $i$ under aggregator $k$ must be equal to the aggregated maximum PV power of such aggregator. $N_{k,i}^{PV}$ is denoted as a sparse row matrix of the households nodes with a PV unit managed by the aggregator $k$.

$$\sum_{(k,i)\in \text{ sparse}\{N_{k,i}^{PV}\}} (S_{PV_i}^{\text{re}} \cdot \zeta_{i,t}) = P_k^{PV} \cdot \zeta_{k,t},\ \forall t, \forall k \in K \text{ if } P_k^{PV} \neq 0 \tag{5.50}$$

Once solved the proposed convex model, the DSO can send different signals to each aggregator such as the individual and aggregate charging pattern of all EVs per aggregator, the individual and aggregate maximum PV power generation per aggregator, the voltage profiles of all network users, and the loading level of feeders and distribution transformers. To summarise, Figure 5.31 outlines the simplified procedure of the proposed centralised control method.

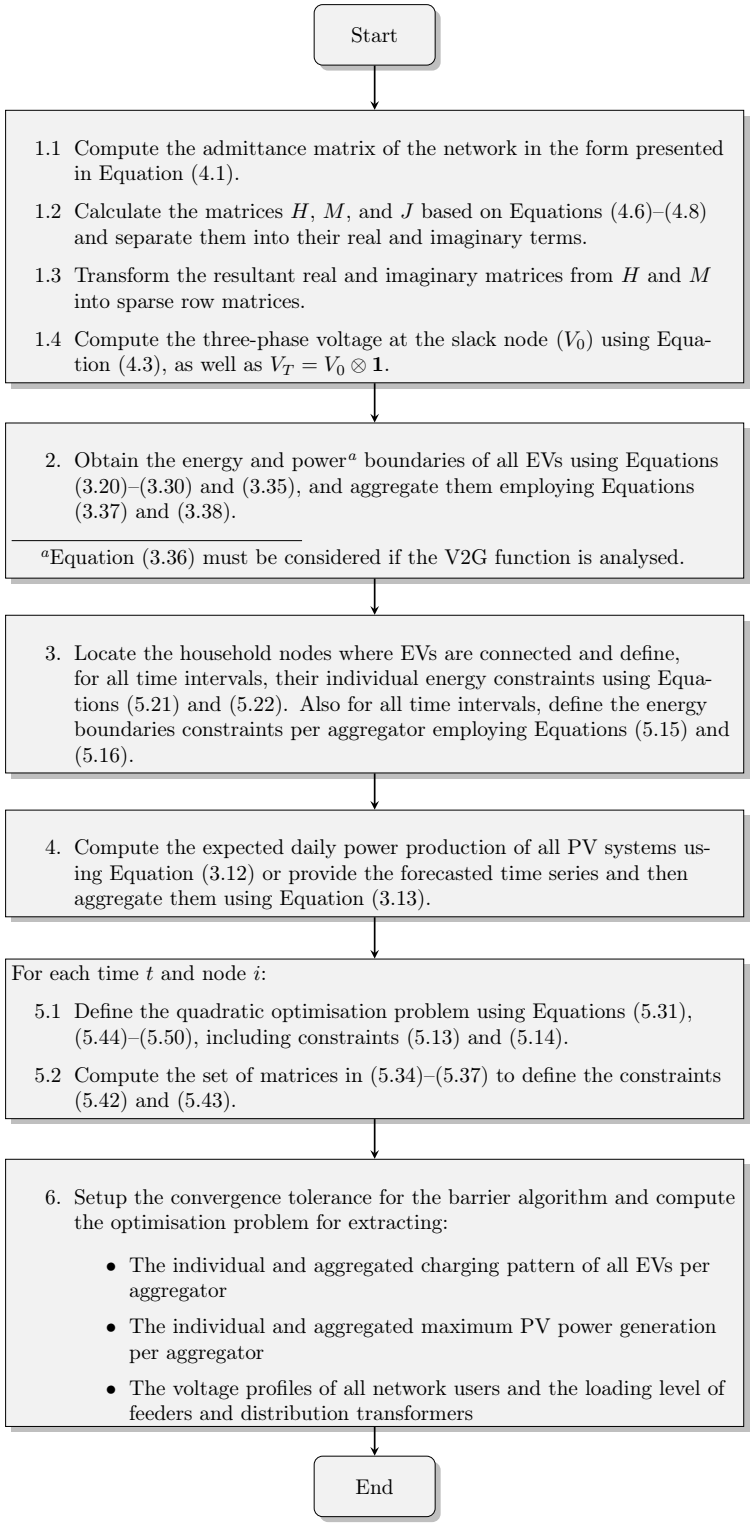


Figure 5.31: Simplified flowchart of the proposed methodology based on the hybrid approach using a linear OPF approach

## 5.9 Description of the test cases used for problem (5.31)

The performance and robustness of the convex optimisation model in (5.31) are verified by considering an 80% and 90% penetration level for EVs and PVs, respectively, in the LV network depicted in Figure 4.1. Both insertion levels are computed based on the total number of users, *i.e.*, 130. The number of EVs and PVs per phase and feeder are summarised in Tables 5.4 and 5.5. These devices are simulated using the specifications given in Table 5.3. From Figure 5.20, a unique PV power output profile with a maximum value of 5 kW has been assigned to those users with a PV unit. Weight parameters $\omega$, $\gamma$, and $\lambda$ are also adjusted to 1000.

Table 5.4: Number of EVs and PVs connected per phase in Feeder 1

| Phase $\phi$ | Number of Households | EVs | PVs |
|---|---|---|---|
| $a$ | 21 | 19 | 19 |
| $b$ | 19 | 13 | 15 |
| $c$ | 15 | 11 | 13 |
| Total | 55 | 43 | 47 |

Table 5.5: Number of EVs and PVs connected per phase in Feeder 2

| Phase $\phi$ | Number of Households | EVs | PVs |
|---|---|---|---|
| $a$ | 28 | 20 | 24 |
| $b$ | 26 | 23 | 25 |
| $c$ | 21 | 19 | 21 |
| Total | 75 | 62 | 70 |

It is known the test network has 2135 nodes, but most of these work as junction nodes for drawing the path of the feeders up to the end-users. However, these nodes can be reduced by calculating an equivalent line segment from the load node up the derived branch from the main service cable. Since this method considers the admittance matrix of the grid, the computational burden for compiling the convex problem with the original number of network nodes (*i.e.*, a $[6405 \times 6405]$ matrix) would be a time-consuming task,

especially when computing equations (5.34)–(5.37) to be later inserted in constraints (5.42) and (5.43). Hence, for mitigating this issue, the test network has been reduced to $N = 553$, resulting in a $[1659 \times 1659]$ admittance matrix. This simplification gives fewer variables to be evaluated, and therefore, reduces the computation time. Considering that voltage constraint (5.44) significantly influences the load flow's exactitude, convergence tolerance for the barrier algorithm internally used by CPLEX is set to $1 \times 10^{-11}$. Therefore, it takes nearly 16 minutes to solve $1.1 \times 10^6$ variables along with $673 \times 10^3$ linear restrictions and $219 \times 10^3$ quadratic constraints for the proposed optimisation problem.

### 5.9.1 Results of the linearized approach

Figure 5.32 presents the three- and single-phase net power on each feeder (similar to Figure 5.28) after solving the optimisation problem presented in Section 5.8. However, in this case, the reverse power flow through the three phases of both feeders is limited to the single-phase capacity of the service cable due to the power flow and voltage constraints (5.42) and (5.44), respectively. This effect is given because the real and imaginary parts of matrices $H$, $M$ and $J$ highly depend on the voltage of the nodes, and as it is constrained to a certain increment, then also the net power on each phase of the feeder.

In Figure 5.32*a*), the loading level (total and per phase) in the first feeder does not exceed its nominal capacity. The method has achieved this by curtailing PV generation during periods of high irradiance and delaying some EVs' charging up to the maximum waiting time of their energy boundaries. This effect can also be observed in the voltage profile of the households connected per phase of this feeder, where the voltage is below the network limit, as shown in Figure 5.33.

On the other hand, Figure 5.32*b*) shows that the exported net power per phase on the second feeder reaches its rated capacity following a similar pattern between phases because of the applied weighting formulation at the device and aggregator level in the control strategy. This behaviour is due to the voltage value on each phase has reached the operational limit of 1.1 *p.u.*, as shown in Figure 5.34. Besides, during peak hour, this feeder is slightly overloaded because of the high power demand of the EVs, mainly in phases $a$ and $b$, as depicted in Figure 5.32*b*). Due to the greater number of users-and- penetration level in the second feeder, the voltage level is a bit lower than in the first feeder but still within limits.

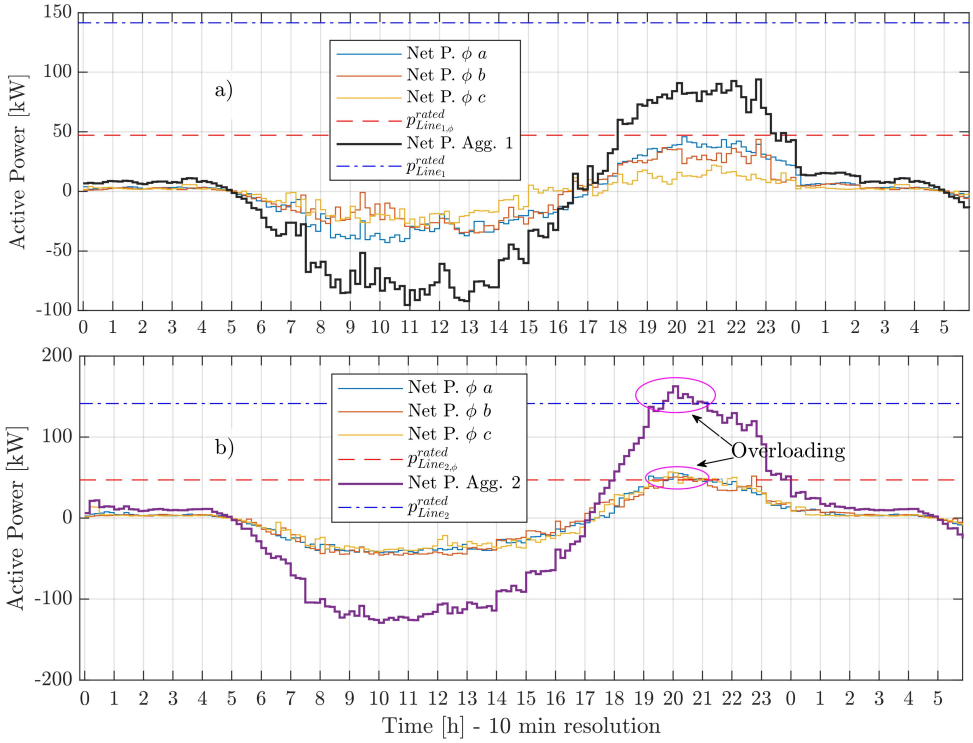


Figure 5.32: Three- and single-phase net power on the feeder's main cable of the *a*) first aggregator and *b*) second aggregator employing the Wirtinger linearisation.

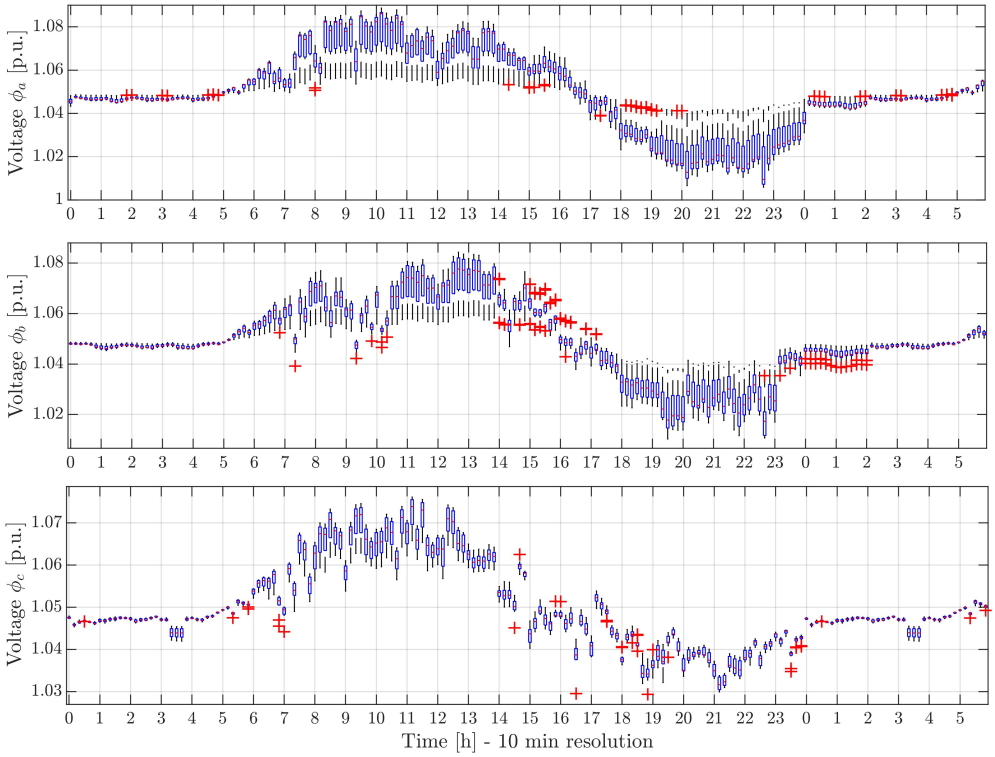


Figure 5.33: Boxplot of voltage profile per phase for the households managed by the first aggregator.

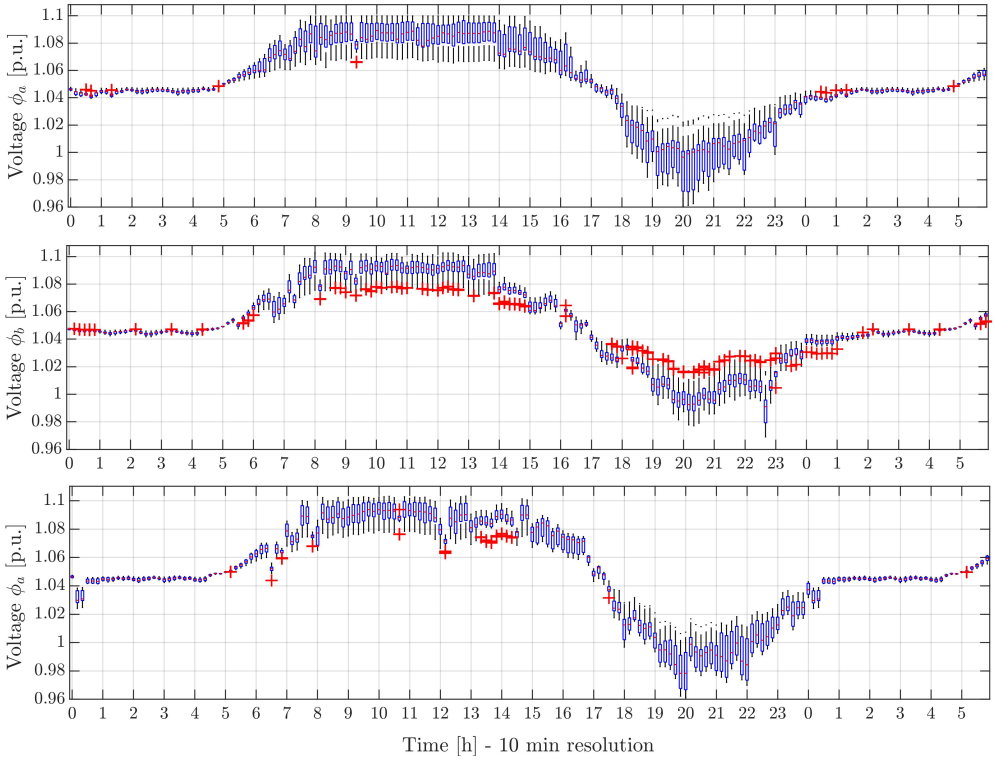


Figure 5.34: Boxplot of voltage profile per phase for the households managed by the second aggregator.

## 5.10 Summary of the proposed methodology

This section presents an overview of the different optimal coordination strategies described through the chapter. Highlighting that these strategies can be employed depending on the detail of results that the DSO needs to analyse.

In Sections 5.3, 5.5, 5.6 and 5.8, four optimisation problems named $f_1$, $f_2$, $f_3$ and $f_4$ were proposed as coordination strategies among the DSO, the aggregators and the end-users into three different approaches: individual, population, and hybrid. The first model was defined at the aggregator level, whereas the other three models were proposed at the DSO level.

The application of each model will depend on the available information of the LV network under study. For example, if the DSO or any stakeholder counts with detailed data of power profiles per user and the whole topology of the LV feeder, the Individual-based approach (model $f_1$) can be applied to optimise the charging of the EVs without controlling the PVs at the aggregator level. If only the aggregation of the load profiles and the amount of EVs and PVs at the feeder level is available along with the rated capacity of the main cables and distribution transformer, the Population-based approach (model $f_2$) will be suitable for optimising the expected charging power of the EVs, and the maximum injected PV power per aggregator to the network. However, if a combination of the above two cases is available, the Hybrid approaches (model $f_3$ and $f_4$) can be employed to obtain detailed information related to the optimal charging pattern of the EVs or the amount of PV power curtailment at the end-user, aggregator or DSO level. Additional information such as the loading level of the feeders or the voltage profile of the whole network can also be analysed. Note that it cannot be accessed to the voltage behaviour of the network for the Population-based approach because it does not consider the topology of the network. Models $f_3$ and $f_4$ differ from one another because the first uses the sensitivity coefficients of the network and the other model employs the linearised OPF to evaluate the voltage at the end-user level.

In addition, the proposed four optimisation problems have the following advantages:

- Model $f_1$ can be more relevant to analyse individual feeders because it takes into account detailed information about all the assets connected to these to deliver particular optimal control signals, exploiting the use of network sensitivity coefficients by linearizing both the loading levels and voltages of the network.

- By aggregating the individual power and energy boundaries of the EVs and the expected PV power generation per aggregator before the coordination at the DSO, the computational burden of the optimisation problems is highly reduced. The amount of data exchange between the aggregators and DSO is reduced for the convex model $f_2$.

- By comparing the three optimisation models, the convex formulation in $f_2$ reduces the problem dimension to the number of aggregators and time intervals, which enables the proposed strategy to be easily solved even with a high number of PVs and EVs per aggregator.

- For the optimisation problems $f_3$ and $f_4$, the DSO can dictate the individual and aggregated optimal power profile of the EVs and PVs managed by the aggregator $k$, respectively. Note that the aggregators are located at the LV side of the distribution transformer, which means that each aggregator manages a feeder derived from the transformer.

- Different operational scenarios in the LV network can be foreseen by the DSO to dictate to each aggregator, thanks to the less complex, smooth and stable profile from aggregating the PV generation and the power/energy boundaries of EVs.

- The DSO can determine its peak net power flexibly based on the information provided by each aggregator.

- If the DSO decides that PV curtailment and EV charging have to be driven by price, the corresponding term within $f_2$ to $f_4$ can be easily included.

Based on the above-mentioned, Table 5.6 briefly summarises the main aspects of the four proposed models for the DSO to optimally coordinate the operation of large quantities of EVs and PVs connected to the LV network by means of different aggregators.

Table 5.6: Summary of the proposed control methods for the DSO and Aggregators

| Category | Description | Model | | | |
|---|---|---|---|---|---|
| | | $f_1$ | $f_2$ | $f_3$ | $f_4$ |
| Aggregator approach | Individual-based | √ | | | |
| | Population-based | | √ | | |
| | Hybrid | | | √ | √ |
| Network constraints | Voltage Constraints | √ | | √ | √ |
| | Loading level Constraints | √ | √ | √ | √ |
| Optimisation technique | LP | √ | | | |
| | QP | | √ | √ | √ |
| Network analysis tool | Sensitivity Coefficients | √ | | √ | |
| | OPF | | | | √ |
| Apply to | Aggregator level | √ | | | |
| | DSO level | | √ | √ | √ |

# Chapter 6

# Experimental case studies

## 6.1 Description of the experimental setup for the individual-based approach

In order to verify the real performance of the proposed control strategy in Section 5.3, an experimental test case was carried out at the Smart Grid Technology Lab at TU Dortmund University. In Figure 6.1[1], it can be observed that the laboratory is equipped with different assets such as an emulator of LV cables, on-load tap changer transformers, redox-flow and Li-ion batteries, power amplifiers, controllable loads and the EV charging station used to test the control charging strategy (red square).

The proposed algorithm was implemented in Python and tested in the Phoenix Contact Advanced EV charge controller of an RWE eSTATION charging station. This device allows limiting the charging current from 6 A to 16 A through Modbus TCP/IP protocol. The charging station is equipped with two independent charging outlets up to 11 kW (400 V AC). In one of the charging outlets was installed a KoCoS EPPE CX power quality analyser to measure the voltage, current and active power from the grid. This device represents the smart meter in a real case. Two commercial EVs were tested, taking into account the technical characteristics of the charging station. A Nissan Leaf with a single-phase connection up to 3.7 kW (230 V AC) and a BMW i3 with a three-phase connection up to 11 kW. The technical characteristics of the tested EVs are presented in Table 6.1. Regarding the LV network and the households consumption, the same feeder from Section 5.4 was used to allocate the EVs and PVs. As the load and PV generation pro-

[1]The complete description of the laboratory can be found in Spina et al. (2018).

files resolution is 1 min, this was selected as the sample time for carrying out the experimental test. Only 10 households with EVs and PV units were considered, and it was assumed that all vehicles arrive at 11:00 h in order to take advantage of the available PV power in winter. A simplified schema of the employed setup topology is presented in Figure 6.2.

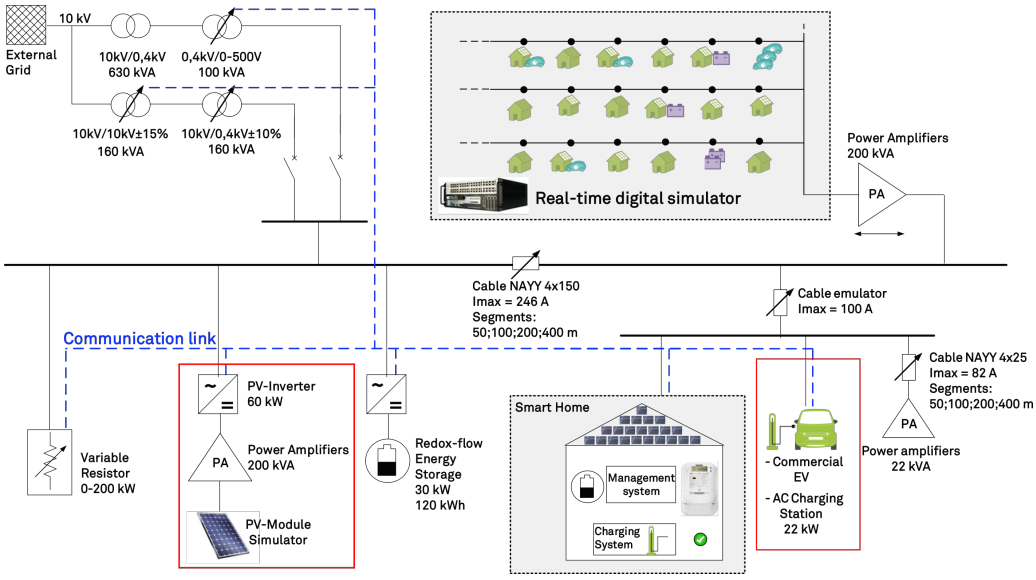


Figure 6.1: Smart Grid Technology Lab layout. Adapted from Spina et al. (2018)

Table 6.1: Technical characteristics of the tested vehicles

| Vehicle | Nissan Leaf 2014 | BMW i3 2016 |
|---|---|---|
| Battery capacity | 24.1 kWh | 33.2 kWh |
| On-board charger efficiency | 0.89 | 0.93 |
| Connector IEC 62196 | Type 1 | Type 2 |
| Max. Charging current | 16 A | 32 A (1-phase) |
| AC topology | 1-phase | 1- and 3-phase |

For this experimental setup, the yellow block in Figure 6.2 represents the aggregator for the analysed feeder. Here, the individual-based model described in Section 5.3 is computed at each time $t$. Before connecting with the charging station, the sensitivity coefficients of the network are computed in PowerFactory employing the algorithm in Appendix B. Then, from $t = 0$ to the minimum arrival time of the emulated vehicles, the optimisation runs

in simulation time, *i.e.*, in a few seconds. Afterwards, the connection with the charging station is established using the Modbus library (ModbusTcpClient) in Python for reading the electrical variables from the KoCos meter and sending the optimal setpoint of current every 1 min. This process is repeated until the calculated time of EV disconnection. From that point, the optimisation runs again in simulation time up to the end of the test period.

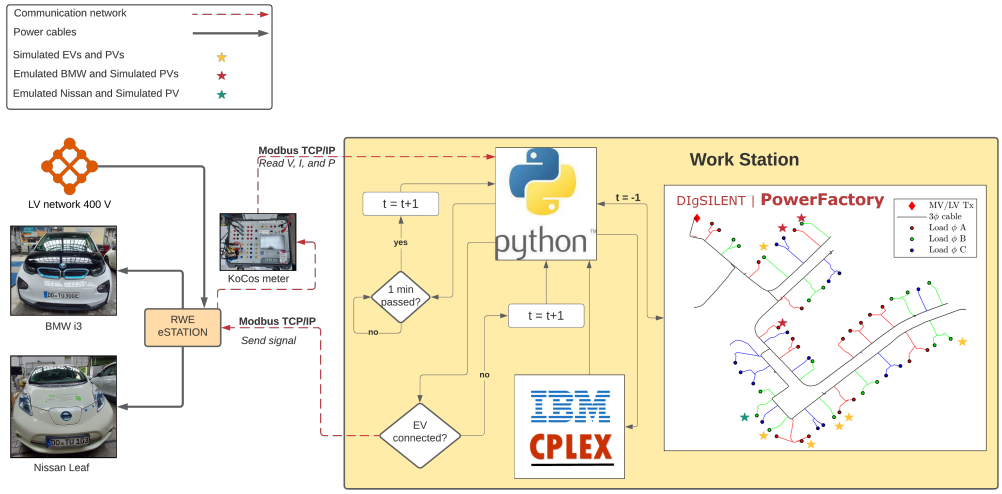


Figure 6.2: Simplified scheme of the laboratory setting

Due to the limitation of measuring one charging outlet, two scenarios were tested. One scenario with 9 simulated EVs and 1 emulated EV (the green star in Figure 6.2 depicts the Nissan Leaf), and the other scenario with 7 simulated EVs and 3 emulated EVs. The red stars represent these 3 EVs in Figure 6.2, which in turn depict the BMW i3. Due to the internal topology of the BMW i3, it can be analysed as 3 individual vehicles. Notice that the PVs were only simulated for both scenarios.

Since it is not possible to get access to the SOC of both EVs when these are connected to the charging station, it was necessary to perform the following trial before the experimental test. First, the EVs were fully charged to be driven in a round-trip of approximately 23.4 km (Figure 6.3) from the Smart Grid Technology Lab [2]. Then, these were connected again to the charging station to measure the required energy to be fully charged. By doing this test, it was found that the energy necessary to reach the rated

[2]The research team of the Lab usually employs this route as a reference journey of a user with an EV.

battery capacity of the Nissan Leaf and the BMW i3 was 3.8 kWh and 2.9 kWh, respectively. Note that these values can vary for the same route because they highly depend on the driving mode, state of the tires, average velocity, and other external factors that can modify the energy consumption rate (kWh/km) of the vehicles.

Afterwards, the same route was driven again, trying to keep the initial drive mode to carry out the experimental test in Figure 6.2. Then, with the above-found energy values, the arrival energy of both EVs was estimated by subtracting them from the nominal battery capacity of each vehicle.

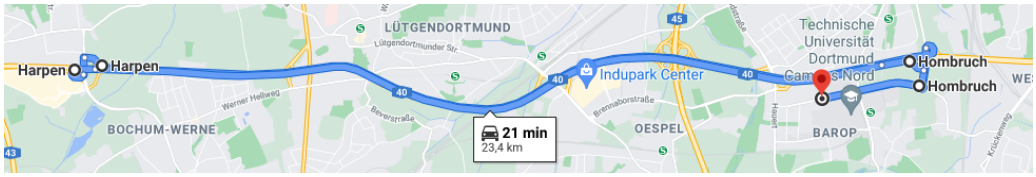


Figure 6.3: Testing route for the Nissan Leaf and BMW i3

### 6.1.1 Experimental results for the individual-based approach

As a result of employing the proposed linear programming model in the first scenario, Figures 6.4 and 6.5 compare the simulated and measured charging power/energy of the Nissan Leaf. It can be seen in both figures that the EV starts charging 1 min after being connected with a $\Delta_P = 1.38$ kW, *i.e.*, 6 A, which is the minimum current to activate the charge controller. After that, the charging power continues increasing up to reach the maximum charging power, *i.e.*, 3.7 kW. It can be noticed also that the measured power follows the optimal charging set point with small deviations associated with the instant where the measure was taken (see also Figure 6.5). Since the charging process followed the upper energy boundary, the Nissan Leaf reached its nominal battery capacity value at interval 730 (12:10 h), as shown in Figure 6.5. Therefore, the remaining availability was 40 min (blue line). Besides, during the charging stage, the 3.7 kW PV unit connected to the same household delivered a maximum power output of 0.8 kW, considering the description of the test case in Section 5.4 for the winter season.

Regarding the results of the second scenario, Figures 6.6 and 6.7 compare the simulated and measured charging power/energy of the EVs connected at households 11, 12, and 21, which are represented by the three-phase connection of the BMW i3. These users were selected because these are

connected to the phases $c$, $b$, and $a$, respectively. For all three vehicles, the charging process is delayed 2 min after being connected. As the case before, the initial charging power equals 1.38 kW and continues increasing up to reach 3.7 kW. In this case, the measured power tries to follow the optimal set point, but it keeps below the reference for EVs 12 and 21. According to the charging tests carried out in this laboratory by Caro et al. (2021), this happens because the on-board charger injects unbalanced charging currents, *i.e.*, the current through phase $a$ is greater than in phase $b$, and the current in phase $b$ is higher than in phase $c$. Due to the constant voltage stage from the constant current-constant voltage (CCCV) algorithm in the DC-DC converter of the BMW i3, the charging current starts to decrease even when the setpoint sent to the charging station is higher. This is because the traction battery is reaching its maximum $SOC$. Similar to scenario one, the PVs delivers the same amount of power.

Due to the difference between the optimal charging power and the measured power, a small amount of energy variation ($\Delta_E$) exists at the end of the charging period, as shown in Figure 6.7. It is also noted that the nominal energy value of all three EVs is reached before their maximum disconnection time because the charging process followed the upper energy boundary.

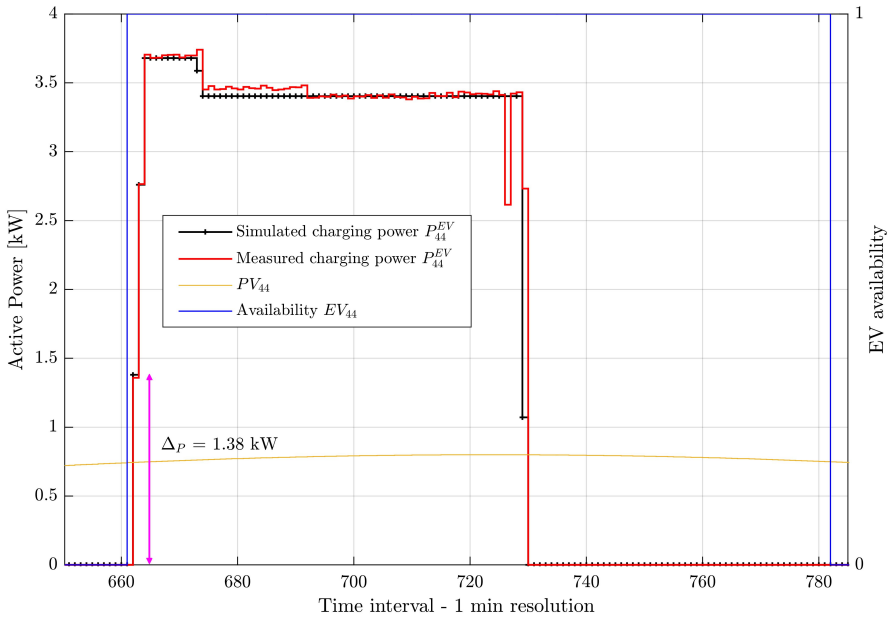


Figure 6.4: Simulated and measured optimal charging profile for the EV located at household 44

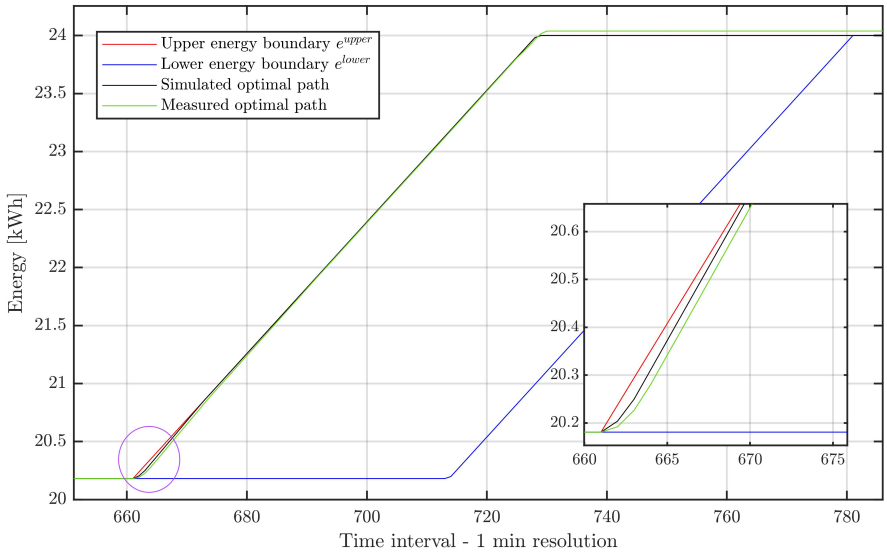


Figure 6.5: Simulated and measured optimal energy trajectories for the EV located at household 44

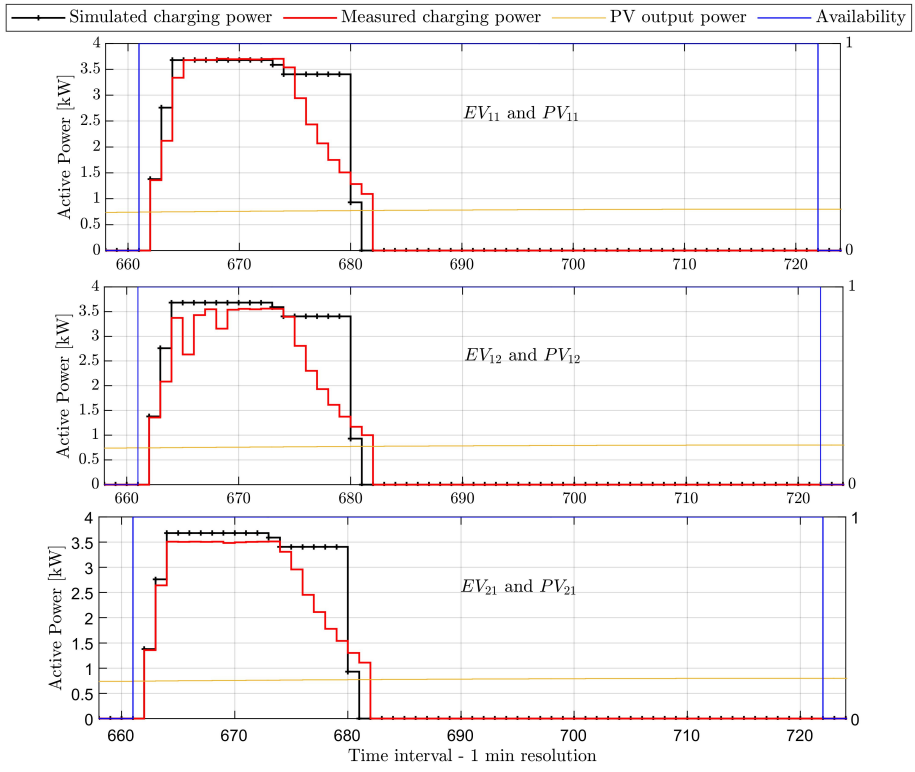


Figure 6.6: Simulated and measured optimal charging profile for the EVs located at households 11, 12 and 21

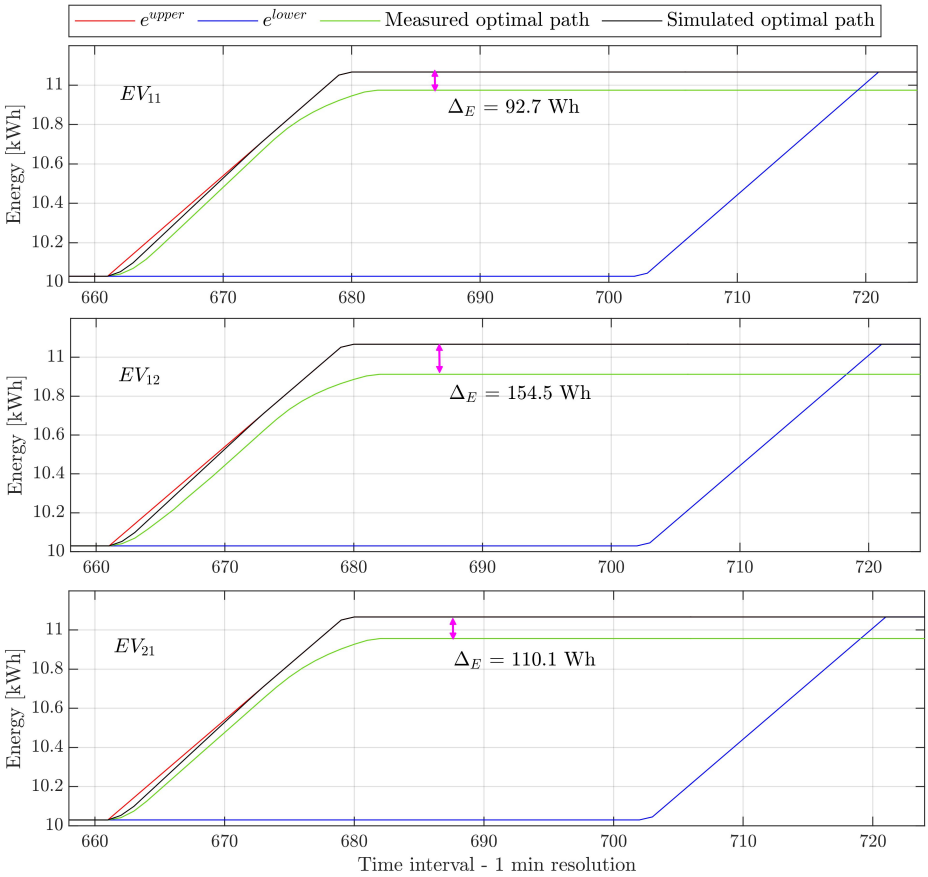


Figure 6.7: Simulated and measured optimal energy trajectories for the EVs located at households 11, 12 and 21

With the aim of testing the control strategy in the BMW i3 with a lower SOC value, an additional scenario was studied. For this case, a journey of approximately 132 km was performed, also starting with the vehicle fully charged from the Smart Grid Technology Lab to Düsseldorf centre and returning again, as shown in Figure 6.8. In this case, the arrival energy was approximately equal to 13.2 kWh (4.38 kWh per emulated vehicle), which was estimated through Equation (3.21), knowing the travelled distance, the battery capacity and an $ECR = 0.153$ kWh/km from the configuration system of the vehicle.

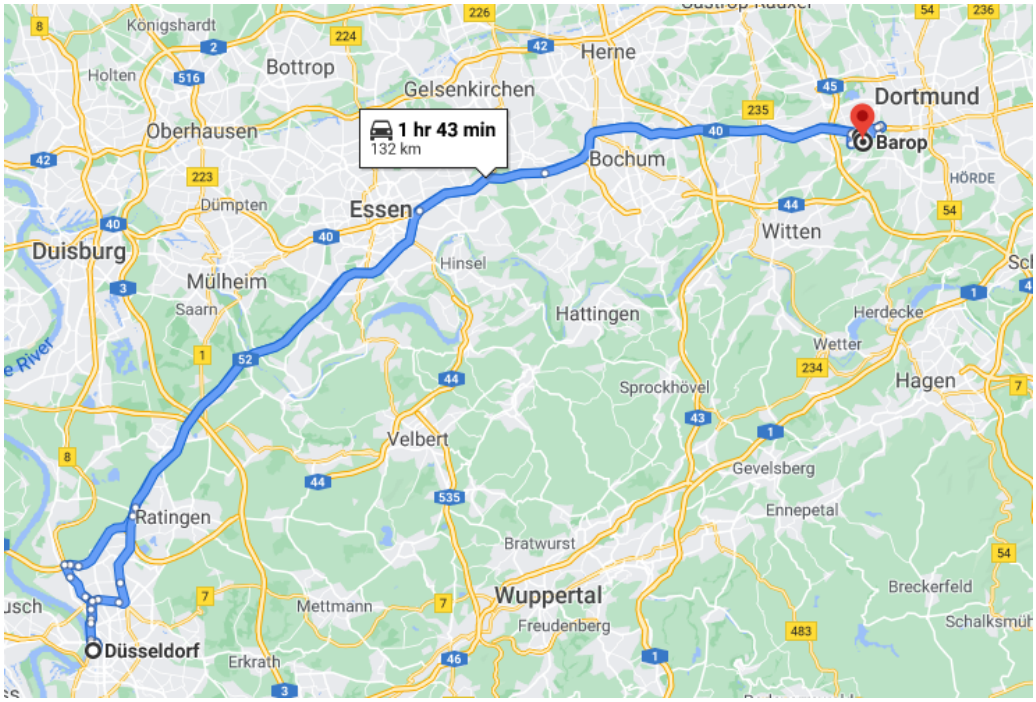


Figure 6.8: Testing route for a long trip with the BMW i3

The new test was configured and executed as in the second scenario, but this time with a lower arrival energy state. The results are depicted in Figures 6.9 and 6.10, which as before, present the simulated and measured charging power/energy of the EVs connected at households 11, 12, and 21. It can be noted in Figure 6.9 that both the measured and the optimal charging power are quite close to each other for all three EVs before interval 763 (12:43 h) when the CCCV algorithm automatically starts to decrease the value of the charging power in all phases. However, when the charging process is almost finalising, a peak power value of 2.3 kW appears in phase $a$ at interval 772 (12:52 h), which slowly decreases during approximately 8 min up to the disconnection time. Caro et al. (2021) suggested that the reason why the charging power increases in phase $a$ at the end of the charging period is because it is likely to be connected to a single-phase converter that supplies power to an auxiliary battery of the vehicle for all the visual indicators and the charging control of the BMW i3. Similar to scenario two, the PVs delivers the same amount of power.

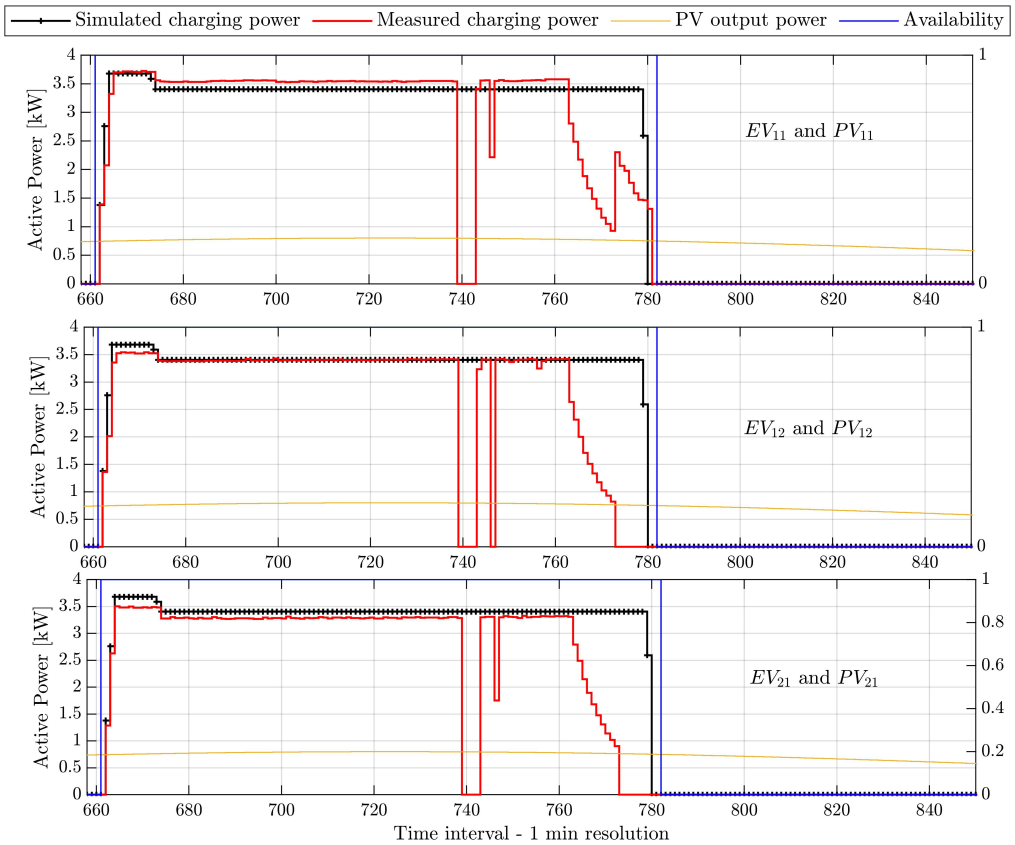


Figure 6.9: Simulated and measured optimal charging profile for the EVs located at households 11, 12 and 21 after performing a long trip

In terms of energy, the charging power profile from the above figure is depicted in Figure 6.10. For all three emulated vehicles, it can be observed that the optimal and measured charging energy paths follow a similar trajectory within their energy boundaries at the beginning of the charging process. However, the measured energy kept constant for about 3 min from interval 739 (12:19 h) because the charging station was intentionally disconnected (Figure 6.9 ) in order to test the recovering of the charging process in all three phases. By doing so, the measured energy path of all phases got out from the computed trajectory, deriving in a greater $\Delta_E$ at the of the charging process, especially for phases $b$ and $c$. This also occurs because the proposed control strategy is not operated as a closed-loop control, and therefore, it is not possible to execute the correction action under these perturbations. Besides, by comparing Figures 6.7 and 6.10, it can be observed that the longer the available range of EV connection, the narrower its energy boundaries, and therefore, the maximum time of delaying to start charging.

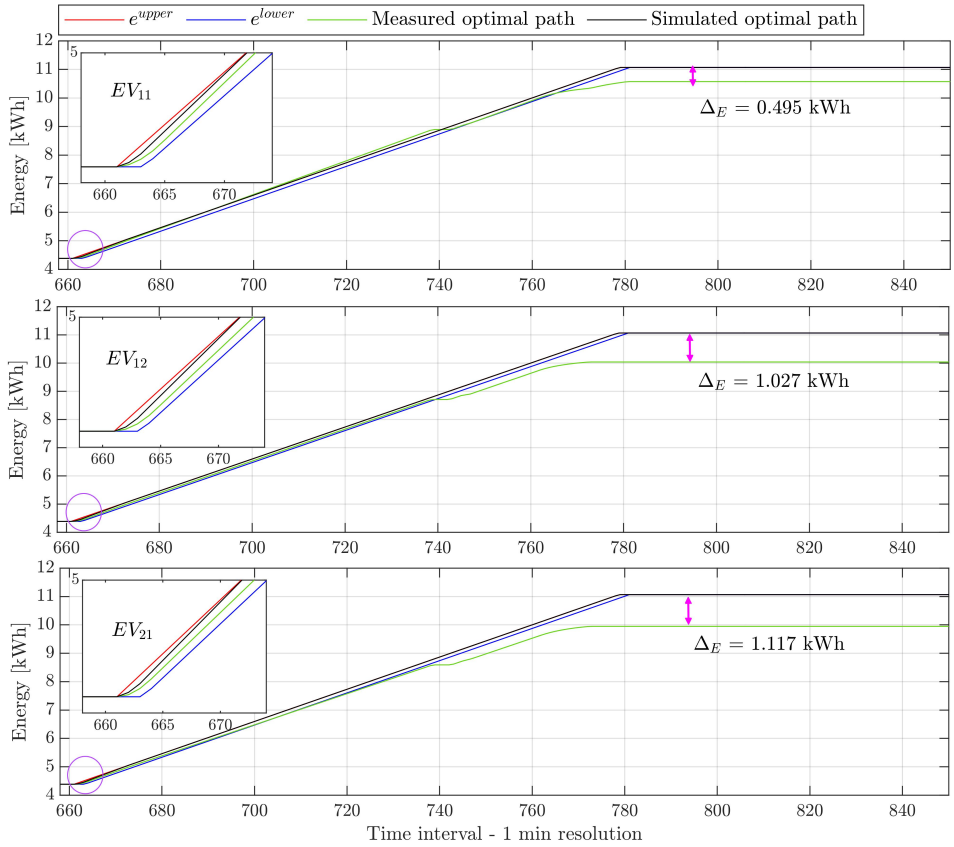


Figure 6.10: Simulated and measured optimal energy trajectories for the EVs located at households 11, 12 and 21 after performing a long trip

Finally, it was found for all the three analysed scenarios that even when all 10 EVs were connected at the same hour, the voltage level and the loading level in the main feeder's cable and the distribution transformer were within their operational limits. Hence, these are not the binding constraints due to the lower penetration level of EVs and PVs.

## 6.2 Experimental setup for the PV power curtailment

As a proof of concept of the quadratic formulation employed at the device level in models $f_3$ and $f_4$ to optimise the PV power curtailment in the LV network, an experimental test was carried out using the 60 kVA PV inverter and the 200 kVA power amplifiers group (based on the layout in Figure 6.1)

as a Power Hardware-in-the-Loop (PHiL) simulation in conjunction with Python, as shown in Figure 6.11. In this setup, the PV power at the DC side of the inverter is provided by one of the power amplifiers (configured in DC bipolar current mode) by a single cell PV model developed in RT-Lab. The PV inverter is connected along with the variable resistive load to the busbar 2 (mid cabinet). The other power amplifier is employed to emulate the AC three-phase-four-wire source connected to the same busbar. A SCADA interface controls both power amplifiers.

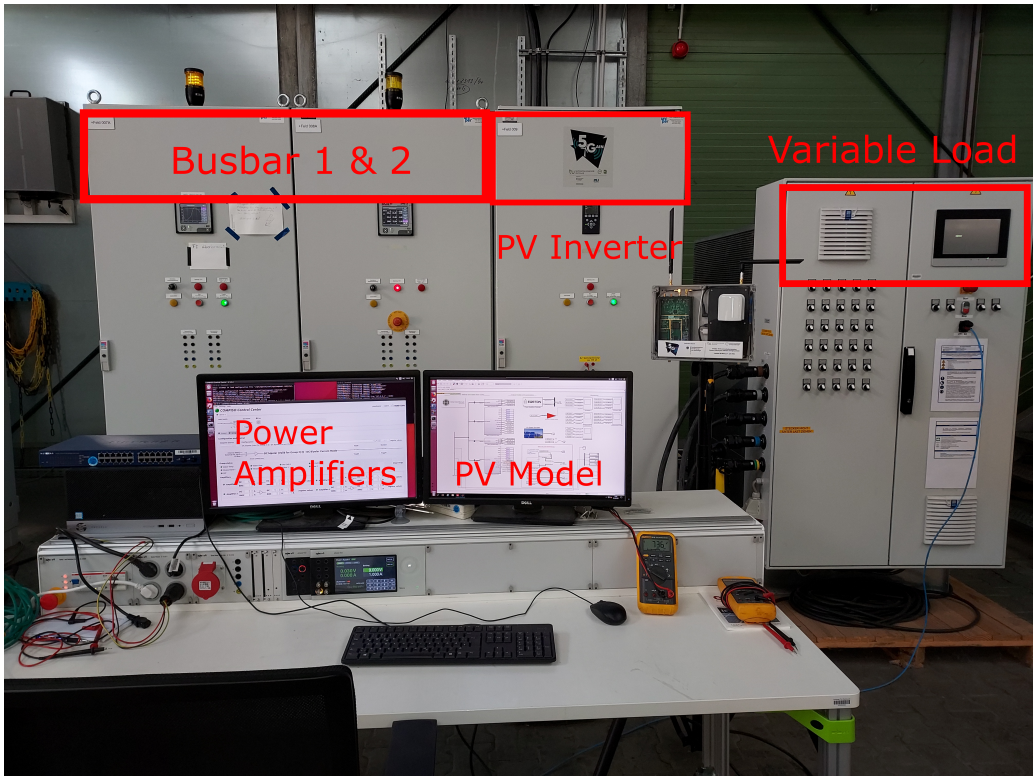


Figure 6.11: Experimental setup for the PV inverter operation

### 6.2.1 Experimental results for the PV power curtailment

Taking into account that the PV inverter assumed for a household has a rated power of 5 kVA operated with a unity power factor, the real inverter would be oversized for this purpose. For that reason, a scale factor of 10 was applied to the optimal value of the simulation in order to obtain a better output power response from the inverter, i.e., if the optimal setpoint is 2.5

kW, the inverter would operate at 25 kW.

As a result of this approach, Figure 6.12 compares three PV power profiles: one profile obtained without any control on the PV inverter, and the simulated and measured PV power profile considering the power curtailment factor $\zeta$. It can be noted that the simulated PV power curves are based on a clear day nearly to the standard test conditions. However, the output power of the real inverter presents fast variations due to its maximum power point tracker algorithm, particularly for lower power values.

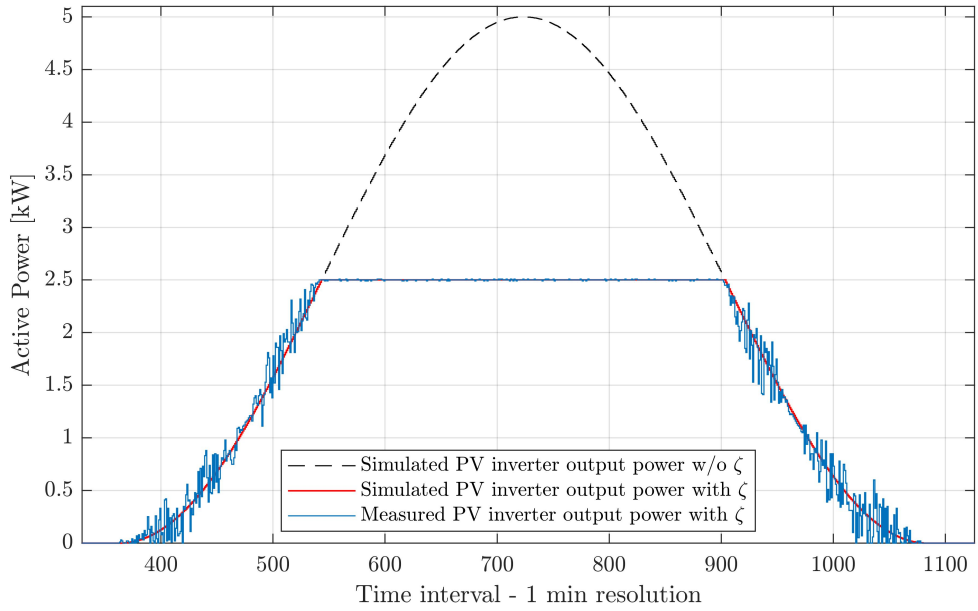


Figure 6.12: Comparison of the simulated and measured PV inverter output power at household 44 considering the power curtailment factor $\zeta$

# Chapter 7

# Conclusions

This chapter synthesises the main results of this thesis and presents some recommendations for further investigations.

Considering that an LV grid is a very local network that covers a small area and with a low number of customers (more in dense urban areas and much less in rural areas), from the approaches described in Section 2.4, it can be said that for an LV network study where the power flow depends on each load, the individual-based approach can be more relevant because it takes into account detailed information about all the assets in the network under study to deliver particular results, whereas a population-based model could be employed to large scale analysis. For example, at the MV level, this model could be used to represent all EVs behind an MV/LV transformer.

A straightforward stochastic model based on the Poisson process for generating several EV charging profiles as an alternative solution to provide initial input information in case of EV-real data is not available to analyse different network operational conditions was developed in Section 3.2.2.

A mathematical approximation for modelling the uncertainty of PV output power was proposed in Chapter 3, considering the appraisement of real data of irradiance and ambient temperature. Another contribution was developing an energy boundary model for EVs, which ensures that the proposed charging strategies in Chapter 5 find an optimal charging path by dynamically adjusting a variable charging rate in conjunction with (or not) a fixed power value to assure the technical limits of the network. This model highlights two main aspects. First, a more compact formulation seeks to compute both the upper and lower energy boundaries from zero and another formulation from the arrival energy. Second. this model can be used regardless of the number of aggregators. As the energy boundary model is based on sev-

eral constant parameters such as the daily travelled distance, arrival time, battery capacity and energy consumption rate of the vehicle, the computational burden of the model is lower compared with other detailed models of the EV.

A new charging strategy was developed in Section 5.3 to find in a decentralised fashion the best charging pattern that meets the energy requirements of each EVs connected to the LV network while taking advantage of the PV generation and maintaining the network within its operational limits. The proposed strategy exploits the use of network sensitivity coefficients by linearizing both the loading levels and voltages of the network. This coordination strategy is verified using real data from an LV feeder and load demand for winter and summer. Numerical results demonstrate that the proposed charging strategy is feasible and effective for finding the optimal charging profile of each EV while addressing network constraints. Besides, this charging strategy ensures an even distribution of charging power at each time slot for all EVs. Further, this method can also be extended to define the most suitable PV export limits if exist a tighter requirement concerning the voltage level or loading level on the assets of the DSO.

Experimental studies proved the concept of the above-described charging schema at the aggregator level by comparing the charging process of two commercial EVs. By doing so, small charging power variations with respect to the optimal power value were found for the first vehicle, whereas for the second vehicle, these variations were more significant due to the internal charging control algorithm of the EV.

In Sections 5.5, 5.6 and 5.8, three optimisation problems named $f_2$, $f_3$ and $f_4$ (based on a quadratic programming approach) were proposed as a centralised coordination strategy to optimise the EVs charging and the export limit of PV power into the LV network. The PV power curtailment is defined in a weighting fashion among multiple aggregators at the DSO level. $f_2$ considers the loading constraints of the main transformer and its feeders to be used when there is no detailed information about the LV network topology. $f_3$ was developed as an extension of $f_2$ by including the voltage constraints in terms of the sensitivity coefficients of the LV network. $f_4$ was proposed in a similar way to $f_3$ but considering network constraints as a linearised OPF. By including the voltage constraints, $f_3$ and $f_4$ can provide the required voltage support in the midday when the PV impact is most severe and during the occurrence of the maximum evening load. These two models are useful when a complete dataset of the LV network is available, and the DSO needs to verify that the voltage limits are not committed when a significant level of EVs and PVs is introduced.

Numerical examples demonstrate the effectiveness of the proposed methodology to minimise the overload level on network assets and to maintain the operational voltage levels of the network when multiple aggregators manage high penetration of PVs and EVs.

The proposed quadratic formulation at the device level in models $f_3$ and $f_4$ to optimise the PV power curtailment was tested in the laboratory using the PHiL simulation in conjunction with Python. It was found that the proposed formulation can be employed to control the optimal active power setpoint of a real PV inverter.

Even though the proposed methodology was tested in a particular LV network, it was designed to be implemented in any four-wire three-phase LV network in order to fully analyse the impact of the installed resources.

## 7.1 Future work

The study carried out during this thesis has also led to identifying potential improvements and future work, which are condensed as follows.

- Inclusion of BESSs and the V2G capability of the EVs to develop a suitable demand-side management strategy for the end-users and the aggregators.
- Extension of the proposed OPF approach in this thesis in the cases of DSO ownership of batteries. This case will need the iterative calculation of battery ageing to achieve the pursued objective (minimise losses, economic dispatch, reliable operation, congestion management, and so on).
- Extension of the proposed formulations in Sections 5.5, 5.6 and 5.8 to account for the impact on MV or HV networks when multiple aggregators at the LV level are managed for one or several DSOs.
- Modify the proposed methodology for the case when multiple aggregators exist on the same feeder, *i.e.*, the end-user can select a particular aggregator that manages its energy resources.
- Application of a Model Predictive Control schema to improve the response of the proposed convex problems in real-time applications.

# Appendix A

# PV system model parameters

Several major design parameters for the PV model are presented in Tables A.1 and A.2 as a reference.

Table A.1: Parameters of the PV module and inverter for the Araujo-Green model

| Parameter | Value | Unit |
|---|---|---|
| $I_{scn}$ | 8.83 | $A$ |
| $V_{ocn}$ | 37.4 | $V$ |
| $I_{mpp}$ | 8.31 | $A$ |
| $V_{mpp}$ | 30.1 | $V$ |
| $NOCT$ | 45 | $^{\circ}C$ |
| $Np$ | 1 | |
| $Ns$ | 15 | |
| $k$ | $1.3806503 \cdot 10^{-23}$ | $J/K$ |
| $q$ | $1.60217646 \cdot 10^{-19}$ | $C$ |
| $G_{STC}$ | 1000 | $W/m^2$ |
| $T_{ref}$ | 25 | $^{\circ}C$ |
| $\beta$ | 0.0023 | $^{\circ}C^{-1}$ |
| $\eta_{inv}$ | 0.99 | |

Table A.2: Parameters for the approximation of the PV inverter output power

| Parameter | Summer | Winter |
|---|---|---|
| $a$ | 5/7 | 1 |
| $b$ | 2 | 2 |
| $c$ | 6 | 4 |
| $d$ | *3* | 2 |

# Appendix B

# Algorithm for the sensitivity coefficient matrices

**Algorithm 3** Sensitivity coefficient matrices for unbalanced LV networks

**function** ComputeSensitivities($\Phi, V_i^{\text{base}}, P_{Line_{l,\phi}}^{base}, P_{Trans_{j,\phi}}^{base}$)
    Initialise variables for the new voltage value of the loads ($V^{\text{new}}$), feeder loading level ($P_{Line}^{new}$), and distribution transformers loading level ($P_{Trans}^{new}$)
    **for** $i \leftarrow 1, H$ **do**
        $V_i^{\text{new}} \leftarrow$ Read the initial voltage magnitude of the Household $i$
    **end for**
▷ Active power per phase on each feeder
    Initialise counter variable $l \leftarrow 0$
    **while** $l < L$ **do**
        Read individual element from PF: $Line \leftarrow Lines_l$
        **for** $\phi \leftarrow 0, \Phi$ **do**
            $P_{Line_{l,\phi}}^{new} \leftarrow$ Read the initial active power magnitude on phase $\phi$ from the object $Line$
        **end for**
        $l = l + 1$
    **end while**
▷ Active power per phase on each distribution transformer
    Initialise counter variable $j \leftarrow 0$
    **while** $j < Trans$ **do**
        Read individual element from PF: $Tx \leftarrow Trans_j$
        **for** $\phi \leftarrow 0, \Phi$ **do**
            $P_{Trans_{j,\phi}}^{new} \leftarrow$ Read the initial active power magnitude on phase $\phi$ from the object $Tx$
        **end for**
        $j = j + 1$
    **end while**

▷ Compute sensitivities
$\partial V/\partial P_{Load} \leftarrow$ `list(map(sub,` $V_i^{\text{new}}, V_i^{\text{base}}$`))`
**for** $\phi \leftarrow 0, \Phi$ **do**
$\partial P_{Line}/\partial P_{Load} \leftarrow$ `list(map(sub,` $P^{new}_{Line_{l,\phi}}, P^{base}_{Line_{l,\phi}}$`))`
$\partial P_{Trans}/\partial P_{Load} \leftarrow$ `list(map(sub,` $P^{new}_{Trans_{l,\phi}}, P^{base}_{Trans_{l,\phi}}$`))`
**end for**
**return** $\partial V/\partial P_{Load},\ \partial P_{Line}/\partial P_{Load},\ \partial P_{Trans}/\partial P_{Load}$
**end function**

Initialise variables for the voltage sensitivity $(\alpha, \beta)$, loading sensitivity on lines $(\mu, \lambda)$, and loading sensitivity on distribution transformers $(\delta, \epsilon)$
Initialise variables for the initial voltage value of the loads ($V^{\text{base}}$), feeder loading level ($P^{base}_{Line}$), and distribution transformers loading level ($P^{base}_{Trans}$)
▷ Initial voltage magnitude
**Execute** unbalanced load flow
**for** $i \leftarrow 1, H$ **do**
$V_i^{\text{base}} \in \mathbb{R}^{H\times 1} \leftarrow$ Read the initial voltage magnitude of the Household $i$
**end for**
▷ Initial active power per phase on each feeder
Initialise counter variable $l \leftarrow 0$
**while** $l < L$ **do**
Read individual element from PF: $Line \leftarrow Lines_l$
**for** $\phi \leftarrow 0, \Phi$ **do**
$P^{base}_{Line_{l,\phi}} \in \mathbb{R}^{\Phi\times L} \leftarrow$ Read the initial active power magnitude on phase $\phi$ from the object $Line$
**end for**
$l = l + 1$
**end while**
▷ Initial active power per phase on each distribution transformer
Initialise counter variable $j \leftarrow 0$
**while** $j < Trans$ **do**
Read individual element from PF: $Tx \leftarrow Trans_j$
**for** $\phi \leftarrow 0, \Phi$ **do**
$P^{base}_{Trans_{j,\phi}} \in \mathbb{R}^{\Phi\times Trans} \leftarrow$ Read the initial active power magnitude on phase $\phi$ from the object $Tx$
**end for**
$j = j + 1$
**end while**
▷ Computation of the new voltage and power levels
▷ By increasing load
**for** $i \leftarrow 1, H$ **do**
**if** $i = 0$ **then**
Read individual element from PF: $Load \leftarrow H_i$
Set active power of $Load \leftarrow 2$ kW
**else**
Read individual element from PF: $Load \leftarrow H_i$
Set active power of $Load \leftarrow 2$ kW
Read individual element from PF: $Load \leftarrow H_{i-1}$
Set active power of $Load \leftarrow 1$ kW
Set power factor of $Load \leftarrow 0.95$
**end if**

**Execute** unbalanced load flow
$(\partial V/\partial P_{Load},\ \partial P_{Line}/\partial P_{Load},\ \partial P_{Trans}/\partial P_{Load}) =$
ComputeSensitivities$(\Phi, V_i^{\text{base}}, P^{base}_{Line_{l,\phi}}, P^{base}_{Trans_{j,\phi}})$
$\alpha \in \mathbb{R}^{H\times H} \leftarrow$ `append(` $\partial V/\partial P_{Load}$`)`
$\mu \in \mathbb{R}^{H\times\Phi\times L} \leftarrow$ `append(` $\partial P_{Line}/\partial P_{Load}$`)`
$\delta \in \mathbb{R}^{H\times\Phi\times Trans} \leftarrow$ `append(` $P_{Trans}/\partial P_{Load}$`)`
▷ Load reducing (*i.e.*, generation effect)
**if** $i = 0$ **then**
    Read individual element from PF: $Load \leftarrow H_i$
    Set active power of $Load \leftarrow 0$ kW
**else**
    Read individual element from PF: $Load \leftarrow H_i$
    Set active power of $Load \leftarrow 0$ kW
    Read individual element from PF: $Load \leftarrow H_{i-1}$
    Set active power of $Load \leftarrow 1$ kW
    Set power factor of $Load \leftarrow 0.95$
**end if**
**Execute** unbalanced load flow
$(\partial V/\partial P_{Load},\ \partial P_{Line}/\partial P_{Load},\ \partial P_{Trans}/\partial P_{Load}) =$
ComputeSensitivities$(\Phi, V_i^{\text{base}}, P^{base}_{Line_{l,\phi}}, P^{base}_{Trans_{j,\phi}})$
**if** $i = H - 1$ **then** ▷ Restore last k-th load to 1 kW
    Set active power of $Load \leftarrow 1\ kW$
    Set power factor of $Load \leftarrow 0.95$
**end if**
$\beta \in \mathbb{R}^{H\times H} \leftarrow$ `append(` $\partial V/\partial P_{Load}$`)`
$\lambda \in \mathbb{R}^{H\times\Phi\times L} \leftarrow$ `append(` $\partial P_{Line}/\partial P_{Load}$`)`
$\epsilon \in \mathbb{R}^{H\times\Phi\times Trans} \leftarrow$ `append(` $P_{Trans}/\partial P_{Load}$`)`
**end for**

# Appendix C

# Detailed location of EVs and PVs in the LV feeders

In Table C.1, rows highlighted in blue represent the EVs and PVs connected to a particular household whose results were displayed in Figures 5.16 and 5.17. The red rows in Tables C.1 and C.2 depict the households chosen to exemplify the impact of charging and generation in voltage profile, as shown in Figures 5.12–5.15. These users were selected by taking into account their location and phase on the feeder in order to show the performance of the proposed decentralised charging strategy in Section 5.3

Table C.1: Location of EVs and PVs in the 906-node feeder for a penetration level of 60%

| EV & PV | Load | Node | Phase | EV & PV | Load | Node | Phase |
|---|---|---|---|---|---|---|---|
| 1 | 47 | 835 | C | 18 | 46 | 817 | A |
| 2 | 39 | 701 | C | 19 | 10 | 248 | B |
| 3 | 2 | 47 | B | 20 | 41 | 755 | B |
| 4 | 55 | 906 | A | 21 | 43 | 780 | C |
| 5 | 14 | 289 | A | 22 | 4 | 73 | A |
| 6 | 19 | 342 | C | 23 | 45 | 813 | B |
| 7 | 27 | 539 | C | 24 | 22 | 388 | A |
| 8 | 28 | 556 | C | 25 | 12 | 264 | C |
| 9 | 52 | 898 | A | 26 | 53 | 899 | B |
| 10 | 32 | 614 | C | 27 | 8 | 208 | C |
| 11 | 40 | 702 | B | 28 | 36 | 676 | B |
| 12 | 54 | 900 | A | 29 | 34 | 629 | A |
| 13 | 5 | 74 | A | 30 | 17 | 327 | C |
| 14 | 35 | 639 | B | 31 | 11 | 249 | B |
| 15 | 21 | 387 | A | 32 | 16 | 320 | C |
| 16 | 23 | 406 | B | 33 | 37 | 682 | B |
| 17 | 20 | 349 | A | | | | |

Table C.2: Location of EVs and PVs in the 906-node feeder for a penetration level of 80% for EVs and 90% for PVs

| Load | Node | Phase | PV | EV | Load | Node | Phase | PV | EV |
|---|---|---|---|---|---|---|---|---|---|
| 1 | 34 | A | 1 | 1 | 29 | 562 | A | 26 | 26 |
| 2 | 47 | B | 2 | 2 | 30 | 563 | A | 27 | 27 |
| 3 | 70 | A | 3 | - | 31 | 611 | A | 28 | 28 |
| 4 | 73 | A | 4 | - | 32 | 614 | C | 29 | 29 |
| 6 | 83 | B | 5 | 5 | 33 | 619 | C | 30 | - |
| 7 | 178 | B | 6 | 6 | 34 | 629 | A | 31 | 31 |
| 8 | 208 | C | 7 | 7 | 35 | 639 | B | 32 | 32 |
| 9 | 225 | A | 8 | 8 | 36 | 676 | B | 33 | 33 |
| 10 | 248 | B | 9 | 9 | 37 | 682 | B | 34 | 34 |
| 11 | 249 | B | 10 | 10 | 38 | 688 | B | 35 | 35 |
| 12 | 264 | C | 11 | 11 | 39 | 701 | C | 36 | 36 |
| 13 | 276 | B | 12 | 12 | 40 | 702 | B | 37 | 37 |
| 14 | 289 | A | 13 | - | 41 | 755 | B | 38 | 38 |
| 15 | 314 | B | 14 | 14 | 42 | 778 | C | 39 | 39 |
| 16 | 320 | C | 15 | 15 | 43 | 780 | C | 40 | 40 |
| 17 | 327 | C | 16 | 16 | 44 | 785 | B | 41 | 41 |
| 18 | 337 | C | 17 | 17 | 45 | 813 | B | 42 | 42 |
| 21 | 387 | A | 18 | 18 | 47 | 835 | C | 43 | 43 |
| 22 | 388 | A | 19 | 19 | 48 | 860 | A | 44 | 44 |
| 23 | 406 | B | 20 | 20 | 49 | 861 | A | 45 | 45 |
| 24 | 458 | C | 21 | 21 | 50 | 886 | B | 46 | 46 |
| 25 | 502 | A | 22 | 22 | 51 | 896 | A | 47 | 47 |
| 26 | 522 | B | 23 | 23 | 52 | 898 | A | 48 | - |
| 27 | 539 | C | 24 | 24 | 53 | 899 | B | 49 | 49 |
| 28 | 556 | C | 25 | 25 | | | | | |

# Appendix D

# Wirtinger calculus in the power flow linearisation

Some of the key concepts related to the Wirtinger calculus are briefly presented below.

The derivative and the conjugate Wirtinger derivative of a complex function $f(z) = f(x+iy) = u(x,y) + iv(x,y)$ can be defined by Equations (D.1) and (D.2) (Bouboulis, 2010, Hunger, 2007).

$$\frac{\partial f}{\partial z} = \frac{1}{2}\left(\frac{\partial u}{\partial x} + \frac{\partial v}{\partial y}\right) + \frac{i}{2}\left(\frac{\partial v}{\partial x} - \frac{\partial u}{\partial y}\right) \tag{D.1}$$

$$\frac{\partial f}{\partial z^*} = \frac{1}{2}\left(\frac{\partial u}{\partial x} - \frac{\partial v}{\partial y}\right) + \frac{i}{2}\left(\frac{\partial v}{\partial x} + \frac{\partial u}{\partial y}\right) \tag{D.2}$$

Note that $z^* = x - iy$ denotes the complex conjugate of $z = x + iy$. In particular, according to (D.3), $z^*$ can be considered as a constant when differentiating with respect to $z$ and vice-versa.

$$\frac{\partial}{\partial z} z^* = \frac{\partial}{\partial z^*} z = 0 \tag{D.3}$$

The complex differential operators in (D.1) and (D.2) allow linearising on the plane of the complex numbers for non-analytical[1] functions such as the power flow in (4.4). Therefore, a complex function can be linearised in terms of the Wirtinger's operators considering the Taylor series expansion

[1] In general, non-analytic functions do not satisfy the Cauchy-Riemann equations, that

around $z_0$, as follows:

$$f \approx f(z_0) + \frac{\partial}{\partial z}\Delta z + \frac{\partial}{\partial z^*}\Delta z^* \tag{D.4}$$

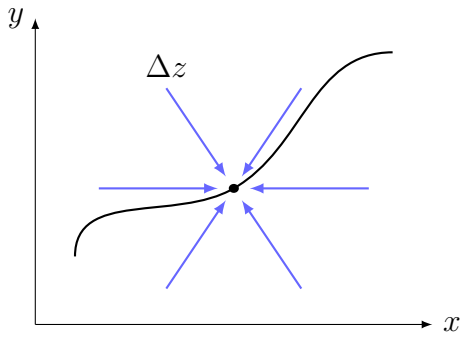


Figure D.1: Example of the geometry of the Cauchy–Riemann equations.

Based on (D.4), a function $f(x_i^*, x_j) = x_i^* x_j$ can be linearised around $(x_{i0}^*, x_{j0})$ as follows:

$$f(x_i^*, x_j) \approx x_{i0}^* x_{j0} + x_{j0}\Delta x_i^* + x_{i0}^*\Delta x_j \tag{D.5}$$

$$= x_{i0}^* x_{j0} + x_{j0}(x_i^* - x_{i0}^*) + x_{i0}^*(x_j - x_{j0}) \tag{D.6}$$

$$= x_{j0}x_i^* + x_{i0}^* x_j - x_{i0}^* x_{j0} \tag{D.7}$$

Similarly, the above example can be applied to the non-linear term $V_i^* V_j$ in (4.4), which solution derives into (D.8) (Ramirez et al., 2019).

$$f(V_i^*, V_j) = V_{j0}V_i^* + V_{i0}^* V_j - V_{i0}^* V_{j0} \tag{D.8}$$

After replacing (D.8) in (4.4) and expanding its terms, the resulting equation is algebraically manipulated to derive in Equation (4.5). In simple terms, this linearisation defines an affine equation where power is not included in the definition of the constant matrices.

---

is:

$$\frac{\partial u(x,y)}{\partial x} = \frac{\partial v(x,y)}{\partial y}$$
$$\frac{\partial v(x,y)}{\partial x} = -\frac{\partial u(x,y)}{\partial y}$$

In geometrical terms, the above equations imply that the derivative in all directions is the same (Arfken et al., 2013), as shown in Figure D.1

# Appendix E

# Convex optimisation problems

## E.1 Convex sets

In simple terms, a set is convex if one can choose any pair of points within this set so that the line segment joining them also belongs to the set. Mathematically, a set $\Omega \subseteq \mathbb{R}^n$ is convex provided that, for any $x, y \in \Omega$ and $\lambda \in [0, 1]$ it has:

$$\lambda x + (1 - \lambda)y \in \Omega \tag{E.1}$$

*i.e.*, the line segment joining $x, y$ lies entirely in $\Omega$, as shown in Figure E.1.

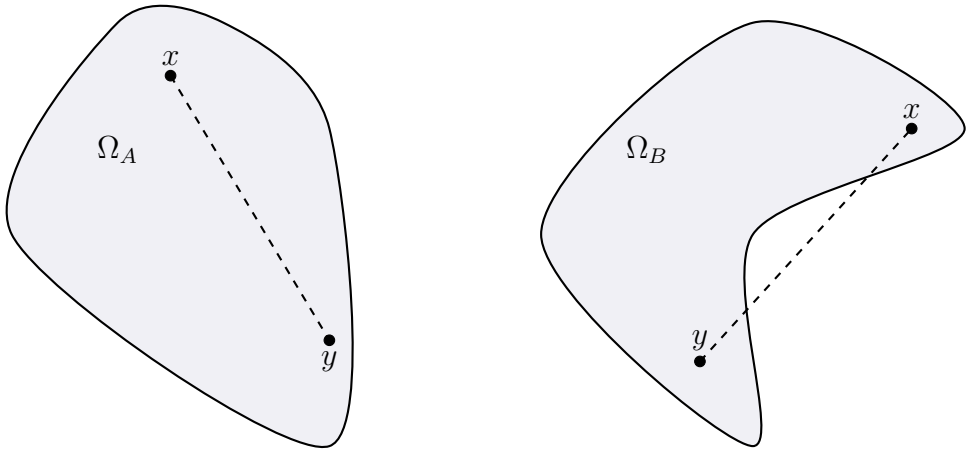


Convex set $\Omega_A$ Non-convex set $\Omega_B$

Figure E.1: Example of convex and non-convex set

## E.2 Convex function

It is said that a function $f : \mathbb{R}^n \to \mathbb{R}$ is convex if its domain is a convex set and for all $x, y$ in its domain, and all $\lambda \in [0, 1]$ it has:

$$f(\lambda x + (1 - \lambda)y) \leq \lambda f(x) + (1 - \lambda)f(y) \tag{E.2}$$

On the other hand, if $-f(x)$ is convex then it is said that $f(x)$ is concave. Besides, a convex function implies that any line segment between two points $x, y$ is above the function, as shown in Figure E.2 for the case of functions $f(x) = x^2$ and $f(x) = -\ln(x)$.

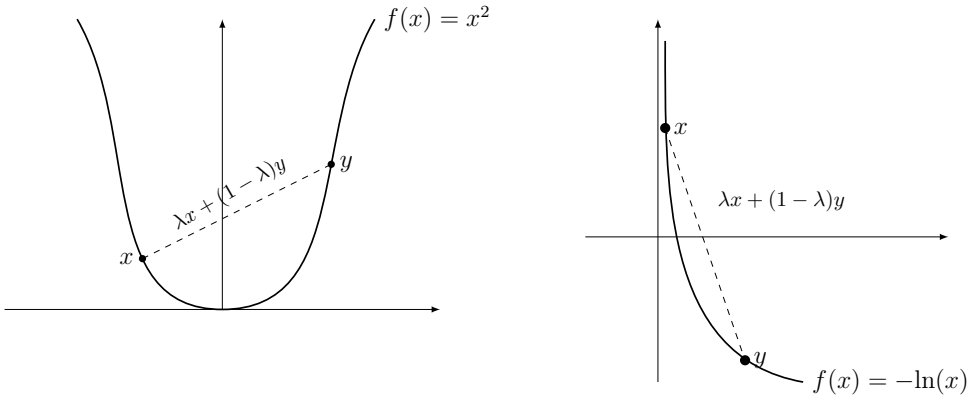


Figure E.2: Example of two convex functions

## E.3 Convex problem

Convex optimisation problems are those that can be defined in a convex solution space and are given by:

$$\begin{aligned} \text{minimise} \quad & f_0(x) \\ \text{subject to} \quad & f_i(x) \leq b_i, \qquad i = 1, \ldots, m \end{aligned} \tag{E.3}$$

where the functions $f_0, ..., f_m : \mathbb{R}^n \to \mathbb{R}$ are convex. This means that definition in Appendix E.2 is satisfied for all $x, y \in \mathbb{R}^n$ and $\lambda \in [0, 1]$. In addition, the linear programming problem, quadratic programming problem, and quadratically constrained quadratic problem are special cases of the general convex optimisation problem (E.3).

### E.3.1 Linear programming (LP)

Linear programming models are problems that contain a linear objective function and linear constraints and can be expressed in canonical form as:

$$\begin{aligned} \text{minimise} \quad & c^T x \\ \text{subject to} \quad & Ax \leq b \end{aligned} \tag{E.4}$$

### E.3.2 Quadratic programming (QP)

Quadratic programming is a special case of non-linear programming that seeks to optimise a problem with a quadratic objective function and linear constraints. Its general form is:

$$\begin{aligned} \text{minimise} \quad & \frac{1}{2} x^T H x + c^T x \\ \text{subject to} \quad & Ax \leq b \end{aligned} \tag{E.5}$$

For convex quadratic problems, $H$ must be positive semi-definite, *i.e.*, $H \succeq 0$.

### E.3.3 Quadratically constrained quadratic programming (QCQP)

Quadratically constrained quadratic programming seeks to optimise a problem with both a quadratic objective function and quadratic constraints. Its general form is:

$$\begin{aligned} \text{minimise} \quad & \frac{1}{2} x^T H x + c^T x \\ \text{subject to} \quad & x^T Q_i x + a_i^T x \leq b_i, \qquad i = 1, \ldots, m \end{aligned} \tag{E.6}$$

For convex QCQPs, $H$ and $Q$ must be positive semi-definite, *i.e.*, $H \succeq 0$ and $Q \succeq 0$.

## E.4 Special ordered set (SOS)

A special ordered set is a way to restrict the number of nonzero solution values among a specified set of variables in a model. These are classified into two types. A detailed demonstration of both SOS types can be found in Hummeltenberg (1984).

- SOS Type 1 is a set of variables where at most, one variable may be nonzero.
- SOS Type 2 is a set of variables where at most, two variables may be nonzero. If two variables are nonzero, they must be adjacent in the set.

The elements of a special ordered set individually may be continuous or discrete variables in any combination. However, even when all the elements are continuous, a model containing one or more SOSs becomes a discrete optimisation problem requiring the mixed-integer optimiser for its solution. This is the case of constraints (5.11) and (5.12) after linearising them employing SOSs Type 1 in CPLEX. For this reason, the QPs in Sections 5.5 and 5.6 becomes MIQPs.

# Bibliography

M R Aghaebrahimi, M M Ghasemipour, and A Sedghi. Probabilistic optimal placement of EV parking considering different operation strategies. In *Proceedings of the Mediterranean Electrotechnical Conference - MELECON*, number April, pages 108–114, 2014. ISBN 9781479923373. doi: 10.1109/MELCON.2014.6820516.

Rasool Aghatehrani and Rajesh Kavasseri. Reactive power management of a DFIG wind system in microgrids based on voltage sensitivity analysis. *IEEE Transactions on Sustainable Energy*, 2(4):451–458, 2011. ISSN 19493029. doi: 10.1109/TSTE.2011.2159745.

Elham Akhavan-Rezai, Mostafa F. Shaaban, E. F. El-Saadany, and Fakhri Karray. Online Intelligent Demand Management of Plug-In Electric Vehicles in Future Smart Parking Lots. *IEEE Systems Journal*, 10(2):483–494, 2015. ISSN 19379234. doi: 10.1109/JSYST.2014.2349357.

M. J.E. Alam, Kashem M. Muttaqi, and Danny Sutanto. A Controllable Local Peak-Shaving Strategy for Effective Utilization of PEV Battery Capacity for Distribution Network Support. *IEEE Transactions on Industry Applications*, 51(3):2030–2037, 2015. ISSN 00939994. doi: 10.1109/TIA.2014.2369823.

M. J.E. Alam, Kashem M. Muttaqi, and Danny Sutanto. Effective Utilization of Available PEV Battery Capacity for Mitigation of Solar PV Impact and Grid Support with Integrated V2G Functionality. *IEEE Transactions on Smart Grid*, 7(3):1562–1571, 2016. ISSN 19493053. doi: 10.1109/TSG.2015.2487514.

Yassir A Alhazmi, Haytham A Mostafa, and Magdy M.A. Salama. Optimal allocation for electric vehicle charging stations using Trip Success Ratio. *International Journal of Electrical Power and Energy Systems*, 91:101–116, 2017. ISSN 01420615. doi: 10.1016/j.ijepes.2017.03.009. URL `http://dx.doi.org/10.1016/j.ijepes.2017.03.009`.

Émile Allie. Canadian Vehicle Use Study: Electronic Data Collection. In *2014 International Methodology Symposium*, pages 1–7, Québec, 2014. Statistics Canada. URL https://www.statcan.gc.ca/eng/conferences/symposium2014/program.

Marcelo Pinho Almeida, Mikel Muñoz, Iñigo de la Parra, and Oscar Perpiñán. Comparative study of PV power forecast using parametric and nonparametric PV models. *Solar Energy*, 155:854–866, 10 2017. ISSN 0038092X. doi: 10.1016/j.solener.2017.07.032. URL http://dx.doi.org/10.1016/j.solener.2017.07.032https://linkinghub.elsevier.com/retrieve/pii/S0038092X17306175.

Sid Ali Amamra and James Marco. Vehicle-to-Grid Aggregator to Support Power Grid and Reduce Electric Vehicle Charging Cost. *IEEE Access*, 7:178528–178538, 2019. ISSN 21693536. doi: 10.1109/ACCESS.2019.2958664.

M H Amini and A Islam. Allocation of electric vehicles' parking lots in distribution network. In *2014 IEEE PES Innovative Smart Grid Technologies Conference, ISGT 2014*, pages 1–5. IEEE, 2 2014. ISBN 9781479936526. doi: 10.1109/ISGT.2014.6816429. URL http://ieeexplore.ieee.org/document/6816429/.

Kyriaki E. Antoniadou-Plytaria, Iasonas N. Kouveliotis-Lysikatos, Pavlos S. Georgilakis, and Nikos D. Hatziargyriou. Distributed and Decentralized Voltage Control of Smart Distribution Networks: Models, Methods, and Future Research. *IEEE Transactions on Smart Grid*, 8(6):2999–3008, 11 2017. ISSN 1949-3053. doi: 10.1109/TSG.2017.2679238. URL http://ieeexplore.ieee.org/document/7874216/.

G. L. Araujo and E. Sánchez. Analytical expressions for the determination of the maximum power point and the fill factor of a solar cell. *Solar Cells*, 5 (4):377–386, 4 1982. ISSN 03796787. doi: 10.1016/0379-6787(82)90008-4.

George Brown Arfken, Hans Weber, and Frank E Harris. Complex Variable Theory. In *Mathematical Methods for Physicists - A Comprehensive Guide*, chapter 11, pages 469–550. Elsevier, Waltham, MA 02451, USA, seventh edition, 2013. ISBN 9788578110796.

W.R. Barcelo and W.W. Lemmon. Standardized sensitivity coefficients for power system networks. *IEEE Transactions on Power Systems*, 3 (4):1591–1599, 1988. ISSN 08858950. doi: 10.1109/59.192969. URL http://ieeexplore.ieee.org/document/192969/.

C Battistelli, L Baringo, and A. J. Conejo. Optimal energy management of small electric energy systems including V2G facilities and renewable energy sources. *Electric Power Systems Research*, 92:50–59, 2012. ISSN 03787796. doi: 10.1016/j.epsr.2012.06.002.

Abdullah S. Bin Humayd and Kankar Bhattacharya. Distribution system planning to accommodate distributed energy resources and PEVs. *Electric Power Systems Research*, 145:1–11, 2017. ISSN 03787796. doi: 10.1016/j.epsr.2016.12.016.

Justin D.K. Bishop, Colin J Axon, David Bonilla, Martino Tran, David Banister, and Malcolm D. McCulloch. Evaluating the impact of V2G services on the degradation of batteries in PHEV and EV. *Applied Energy*, 111:206–218, 2013. ISSN 03062619. doi: 10.1016/j.apenergy.2013.04.094.

Pantelis Bouboulis. Wirtinger's Calculus in general Hilbert Spaces. Technical report, University of Athens, 2010. URL `http://users.uoa.gr/`.

Scott Burger, Jose Pablo Chaves-Ávila, Carlos Batlle, and Ignacio J. Pérez-Arriaga. A review of the value of aggregators in electricity systems. *Renewable and Sustainable Energy Reviews*, 77:395–405, 9 2017. ISSN 13640321. doi: 10.1016/j.rser.2017.04.014. URL `https://linkinghub.elsevier.com/retrieve/pii/S1364032117305191`.

Luis Manuel Caro, Gustavo Ramos, Kalle Rauma, David Felipe Celeita Rodriguez, Davis Montenegro Martinez, and Christian Rehtanz. State of Charge Influence on the Harmonic Distortion from Electric Vehicle Charging. *IEEE Transactions on Industry Applications*, 57(3):2077–2088, 5 2021. ISSN 19399367. doi: 10.1109/TIA.2021.3057350.

Qifang Chen, Nian Liu, Cungang Hu, Lingfeng Wang, and Jianhua Zhang. Autonomous Energy Management Strategy for Solid-State Transformer to Integrate PV-Assisted EV Charging Station Participating in Ancillary Service. *IEEE Transactions on Industrial Informatics*, 13(1):258–269, 2017. ISSN 15513203. doi: 10.1109/TII.2016.2626302.

Konstantina Christakou, Jean Yves Leboudec, Mario Paolone, and Dan Cristian Tomozei. Efficient computation of sensitivity coefficients of node voltages and line currents in unbalanced radial electrical distribution networks. *IEEE Transactions on Smart Grid*, 4(2):741–750, 2013. ISSN 19493053. doi: 10.1109/TSG.2012.2221751.

Uwakwe C Chukwu and Satish M Mahajan. V2G Parking Lot With PV Rooftop for Capacity Enhancement of a Distribution System. *IEEE Transactions on Sustainable Energy*, 5(1):119–127, 1 2014. ISSN 19493029. doi: 10.1109/TSTE.2013.2274601. URL http://ieeexplore.ieee.org/document/6588628/.

Celine Cluzel, Alastair Hope Morley, and Jonathan Murray. Transport Energy Infrastructure Roadmap to 2050, 2015. URL https://www.lowcvp.org.uk/assets/reports/LowCVPInfrastructureRoadmap-Methanereport.pdf.

S. Conti, S. Raiti, and G. Vagliasindi. Voltage sensitivity analysis in radial MV distribution networks using constant current models. *IEEE International Symposium on Industrial Electronics*, pages 2548–2554, 2010. doi: 10.1109/ISIE.2010.5637545.

Andrés Cortés, Julia Merino, and Esther Torres. Stochastic Generation of Aggregated Charging Profiles of PEVs for the Operation Analysis of Low Voltage Networks. In *The 25th International Conference And Exhibition On Electricity Distribution*, pages 3–6. CIRED, 2019. doi: http://dx.doi.org/10.34890/671. URL https://www.researchgate.net/publication/333673075.

Andrés Felipe Cortés Borray, Julia Merino, Esther Torres, and Javier Mazón. Optimal Coordination of PV Active Power Curtailment and EVs Charging among Aggregators. *Applied Sciences*, 10(20):7176, 10 2020. ISSN 2076-3417. doi: 10.3390/app10207176. URL https://www.mdpi.com/2076-3417/10/20/7176.

Council Directive. 2019/944 of the European Parliament and of the Council of 5 June 2019 on common rules for the internal market for electricity and amending Directive 2012/27/EU, 6 2019. URL https://eur-lex.europa.eu/legal-content/EN/TXT/?uri=OJ:L:2019:158:TOC.

Zahra Darabi and Mehdi Ferdowsi. Aggregated Impact of Plug-in Hybrid Electric Vehicles on Electricity Demand Profile. *IEEE Transactions on Sustainable Energy*, 2(4):501–508, 10 2011. doi: 10.1109/TSTE.2011.2158123. URL http://ieeexplore.ieee.org/document/5779754/.

Anna Rita Di Fazio, Mario Russo, Sara Valeri, and Michele De Santis. Linear method for steady-state analysis of radial distribution systems. *International Journal of Electrical Power and Energy Systems*, 99(January):744–755, 2018. ISSN 01420615. doi: 10.1016/j.ijepes.2018.02.001. URL https://doi.org/10.1016/j.ijepes.2018.02.001.

C.A. Dortolina and R. Nadira. The Loss That is Unknown is No Loss At All: A Top-Down/Bottom-Up Approach for Estimating Distribution Losses. *IEEE Transactions on Power Systems*, 20(2):1119–1125, 5 2005. ISSN 0885-8950. doi: 10.1109/TPWRS.2005.846104. URL `http://ieeexplore.ieee.org/document/1425611/`.

Lukas Drude, Luiz Carlos Pereira Junior, and Ricardo Rüther. Photovoltaics (PV) and electric vehicle-to-grid (V2G) strategies for peak demand reduction in urban regions in Brazil in a smart grid environment. *Renewable Energy*, 68:443–451, 2014. ISSN 09601481. doi: 10.1016/j.renene.2014.01.049.

Izudin Dzafic, Rabih A. Jabr, and Tarik Hrnjic. High Performance Distribution Network Power Flow Using Wirtinger Calculus. *IEEE Transactions on Smart Grid*, 10(3):3311–3319, 2019. ISSN 19493053. doi: 10.1109/TSG.2018.2824018.

EA Technology and Scottish and Southern Electricity Networks Limited. My Electric Avenue Report, 2015. URL `http://myelectricavenue.info/learning-outcomes`.

Amany El-Zonkoly. Intelligent energy management of optimally located renewable energy systems incorporating PHEV. *Energy Conversion and Management*, 84:427–435, 2014. ISSN 01968904. doi: 10.1016/j.enconman.2014.04.050.

Amany El-Zonkoly and Leandro Dos Santos Coelho. Optimal allocation, sizing of PHEV parking lots in distribution system. *International Journal of Electrical Power and Energy Systems*, 67:472–477, 2015. ISSN 01420615. doi: 10.1016/j.ijepes.2014.12.026. URL `http://dx.doi.org/10.1016/j.ijepes.2014.12.026`.

Hassan H Eldeeb, Samy Faddel, and Osama A Mohammed. Multi-Objective Optimization Technique for the Operation of Grid tied PV Powered EV Charging Station. *Electric Power Systems Research*, 164(July):201–211, 2018. ISSN 0378-7796. doi: 10.1016/j.epsr.2018.08.004. URL `https://doi.org/10.1016/j.epsr.2018.08.004`.

Electriciy North West. Low Voltage Network Solutions, 2019. URL `https://www.enwl.co.uk/lvns`.

U. Eminoglu and M. H. Hocaoglu. Distribution Systems Forward/Backward Sweep-based Power Flow Algorithms: A Review and Comparison Study. *Electric Power Components and Systems*, 37(1):91–110, 12

2008. ISSN 1532-5008. doi: 10.1080/15325000802322046. URL https://www.tandfonline.com/doi/full/10.1080/15325000802322046.

Ertrac, EPoSS, and ETIP SNET. European Roadmap Electrification of Road Transport, 2017. URL https://www.etip-snet.eu/wp-content/uploads/2017/09/ERTRAC_ElectrificationRoadmap2017.pdf.

Masoud Esmaili and Ali Goldoust. Multi-objective optimal charging of plug-in electric vehicles in unbalanced distribution networks. *International Journal of Electrical Power & Energy Systems*, 73:644–652, 12 2015. ISSN 01420615. doi: 10.1016/j.ijepes.2015.06.001. URL https://linkinghub.elsevier.com/retrieve/pii/S0142061515002574.

Alejandro Navarro Espinosa and Luis (Nando) Ochoa. Dissemination Document " Low Voltage Networks Models and Low Carbon Technology Profiles ". Technical Report June, The University of Manchester, 2015.

Sirine Essallah and Adel Khedher. A comparative study of long-term load forecasting techniques applied to Tunisian grid case. *Electrical Engineering*, 101(4):1235–1247, 2019. ISSN 14320487. doi: 10.1007/s00202-019-00859-w. URL https://doi.org/10.1007/s00202-019-00859-w.

European Commission. Energy Roadmap 2050 Impact assessment and scenario analysis. Technical report, Brussels, 2011. URL https://ec.europa.eu/energy/sites/ener/files/documents/roadmap2050_ia_20120430_en_0.pdf.

European Commission. Clean energy for all Europeans, 2019. URL https://ec.europa.eu/energy/en/topics/energy-strategy-and-energy-union/clean-energy-all-europeans.

European Union. Directive (EU) 2019/944 on common rules for the internal market for electricity, 2021. URL https://eur-lex.europa.eu/legal-content/EN/TXT/?uri=LEGISSUM%3A4404055.

Hassan Feshki Farahani. Improving voltage unbalance of low-voltage distribution networks using plug-in electric vehicles. *Journal of Cleaner Production*, 148:336–346, 4 2017. ISSN 09596526. doi: 10.1016/j.jclepro.2017.01.178. URL http://www.sciencedirect.com/science/article/pii/S0959652617302007http://linkinghub.elsevier.com/retrieve/pii/S0959652617302007.

Masoud Farivar and Steven H. Low. Branch flow model: Relaxations and convexification-part i. *IEEE Transactions on Power Systems*, 28(3):2554–2564, 2013. ISSN 08858950. doi: 10.1109/TPWRS.2013.2255317.

Farivar Fazelpour, Majid Vafaeipour, Omid Rahbari, and Marc A Rosen. Intelligent optimization to integrate a plug-in hybrid electric vehicle smart parking lot with renewable energy resources and enhance grid characteristics. *Energy Conversion and Management*, 77:250–261, 1 2014. ISSN 01968904. doi: 10.1016/j.enconman.2013.09.006. URL `http://linkinghub.elsevier.com/retrieve/pii/S0196890413005438`.

Raquel Figueiredo, Pedro Nunes, and Miguel C. Brito. The feasibility of solar parking lots for electric vehicles. *Energy*, 140:1182–1197, 2017. ISSN 03605442. doi: 10.1016/j.energy.2017.09.024.

Robert F. H. Fischer. Appendix A: Wirtinger Calculus. In *Precoding and Signal Shaping for Digital Transmission*, pages 405–413. John Wiley & Sons, Inc., Hoboken, NJ, USA, 1 2005. doi: 10.1002/0471439002.app1. URL `http://doi.wiley.com/10.1002/0471439002.app1`.

Marco Giacomo Flammini, Giuseppe Prettico, Andreea Julea, Gianluca Fulli, Andrea Mazza, and Gianfranco Chicco. Statistical characterisation of the real transaction data gathered from electric vehicle charging stations. *Electric Power Systems Research*, 166(September 2018): 136–150, 2019. ISSN 03787796. doi: 10.1016/j.epsr.2018.09.022. URL `https://doi.org/10.1016/j.epsr.2018.09.022`.

John F. Franco, Luis F. Ochoa, and Ruben Romero. AC OPF for smart distribution networks: An efficient and robust quadratic approach. *IEEE Transactions on Smart Grid*, 9(5):4613–4623, 9 2018. ISSN 19493053. doi: 10.1109/TSG.2017.2665559.

Stephen Frank and Steffen Rebennack. An introduction to optimal power flow: Theory, formulation, and examples. *IIE Transactions (Institute of Industrial Engineers)*, 48(12):1172–1197, 2016. ISSN 15458830. doi: 10.1080/0740817X.2016.1189626. URL `http://dx.doi.org/10.1080/0740817X.2016.1189626`.

Leon Freris and David Infield. Power Balance / Frequency Control. In *Renewable Energy in Power Systems*, page 58. John Wiley & Sons Ltd, Chichester, United Kingdom, 2008. ISBN 978-0-470-98894-7. URL `https://www.wiley.com/en-us/Renewable+Energy+in+Power+Systems-p-9780470988947`.

Alejandro Garces. A Linear Three-Phase Load Flow for Power Distribution Systems. *IEEE Transactions on Power Systems*, 31(1):827–828, 2016a. ISSN 08858950. doi: 10.1109/TPWRS.2015.2394296.

Alejandro Garces. A quadratic approximation for the optimal power flow in power distribution systems. *Electric Power Systems Research*, 130:222–229, 2016b. doi: 10.1016/j.epsr.2015.09.006. URL `http://dx.doi.org/10.1016/j.epsr.2015.09.006`.

J. García-Villalobos, I Zamora, J. I. San Martín, F J Asensio, and V Aperribay. Plug-in electric vehicles in electric distribution networks: A review of smart charging approaches, 2014. ISSN 13640321. URL `http://dx.doi.org/10.1016/j.rser.2014.07.040`.

Shibani Ghosh, Saifur Rahman, and Manisa Pipattanasomporn. Distribution Voltage Regulation Through Active Power Curtailment With PV Inverters and Solar Generation Forecasts. *IEEE Transactions on Sustainable Energy*, 8(1):13–22, 1 2017. ISSN 19493029. doi: 10.1109/TSTE.2016.2577559.

Turan Gönen. Chapter 2: Load Characteristics. In *Electric Power Distribution System Engineering*, chapter 2, pages 35–91. CRC Press, Boca Raton, FL, second edition, 2007.

M K Gray and W G Morsi. On the impact of single-phase plug-in electric vehicles charging and rooftop solar photovoltaic on distribution transformer aging. *Electric Power Systems Research*, 148:202–209, 2017. ISSN 03787796. doi: 10.1016/j.epsr.2017.03.022.

Martin Andrew Green. Efficiency limits, losess, and measurement. In *Solar Cells: Operating Principles, Technology and System Applications*, chapter 5, pages 96–97. Prentice Hall, 1982. ISBN 0138222703.

Christophe Guille and George Gross. A conceptual framework for the vehicle-to-grid (V2G) implementation. *Energy Policy*, 37(11):4379–4390, 2009. ISSN 03014215. doi: 10.1016/j.enpol.2009.05.053.

Sitki Guner and Aydogan Ozdemir. Stochastic energy storage capacity model of EV parking lots. *IET Generation, Transmission & Distribution*, 11(7):1754–1761, 2017. ISSN 1751-8687. doi: 10.1049/iet-gtd.2016.1406. URL `http://digital-library.theiet.org/content/journals/10.1049/iet-gtd.2016.1406`.

Ravindranath Gurram and B. Subramanyam. Sensitivity analysis of radial distribution network - adjoint network method. *International Journal of Electrical Power and Energy System*, 21(5):323–326, 1999. ISSN 01420615. doi: 10.1016/S0142-0615(98)00058-1.

Salman Habib, Muhammad Kamran, and Umar Rashid. Impact analysis of vehicle-to-grid technology and charging strategies of electric vehicles on distribution networks - A review, 2015. ISSN 03787753. URL http://ac.els-cdn.com/S0378775314020370/1-s2.0-S0378775314020370-main.pdf?_tid=38961f80-705b-11e7-b0e0-00000aacb360&acdnat=1500892456_34a3900aa04366d9daee1b67585bf69a.

Somayeh Hajforoosh, Mohammad A.S. Masoum, and Syed M. Islam. Online optimal variable charge-rate coordination of plug-in electric vehicles to maximize customer satisfaction and improve grid performance. *Electric Power Systems Research*, 141:407–420, 12 2016. ISSN 03787796. doi: 10.1016/j.epsr.2016.08.017. URL https://linkinghub.elsevier.com/retrieve/pii/S037877961630311X.

Chioke B Harris and Michael E Webber. An empirically-validated methodology to simulate electricity demand for electric vehicle charging. *Applied Energy*, 126:172–181, 8 2014. ISSN 03062619. doi: 10.1016/j.apenergy.2014.03.078. URL http://dx.doi.org/10.1016/j.apenergy.2014.03.078https://linkinghub.elsevier.com/retrieve/pii/S0306261914003183.

Seyedmostafa Hashemi and Jacob Østergaard. Methods and strategies for overvoltage prevention in low voltage distribution systems with PV. *IET Renewable Power Generation*, 11(2):205–214, 2017. ISSN 1752-1416. doi: 10.1049/iet-rpg.2016.0277. URL http://digital-library.theiet.org/content/journals/10.1049/iet-rpg.2016.0277.

Quentin Hoarau and Yannick Perez. Interactions between electric mobility and photovoltaic generation: A review. *Renewable and Sustainable Energy Reviews*, 94:510–522, 10 2018. ISSN 13640321. doi: 10.1016/j.rser.2018.06.039. URL https://linkinghub.elsevier.com/retrieve/pii/S1364032118304751.

Masoud Honarmand, Alireza; Zakariazadeh, and Shahram; Jadid. Integrated scheduling of renewable generation and electric vehicles parking lot in a smart microgrid. *Energy Conversion and Management*, 86:745–755, 10 2014a. ISSN 01968904. doi: 10.1016/j.enconman.2014.06.044. URL http://linkinghub.elsevier.com/retrieve/pii/S019689041400569X.

Masoud Honarmand, Alireza Zakariazadeh, and Shahram Jadid. Optimal scheduling of electric vehicles in an intelligent parking lot considering vehicle-to-grid concept and battery condition. *Energy*, 65:572–579, 2014b. ISSN 03605442. doi: 10.1016/j.energy.2013.11.045.

Junjie Hu, Guangya Yang, Henrik W. Bindner, and Yusheng Xue. Application of Network-Constrained Transactive Control to Electric Vehicle Charging for Secure Grid Operation. *IEEE Transactions on Sustainable Energy*, 8(2):505–515, 4 2017a. ISSN 1949-3029. doi: 10.1109/TSTE.2016.2608840. URL `http://ieeexplore.ieee.org/document/7565647/`.

Junjie Hu, Guangya Yang, Koen Kok, Yusheng Xue, and Henrik W. Bindner. Transactive control: a framework for operating power systems characterized by high penetration of distributed energy resources. *Journal of Modern Power Systems and Clean Energy*, 5(3):451–464, 5 2017b. ISSN 21965420. doi: 10.1007/s40565-016-0228-1.

Pei Huang, Marco Lovati, Xingxing Zhang, and Chris Bales. A coordinated control to improve performance for a building cluster with energy storage, electric vehicles, and energy sharing considered. *Applied Energy*, 268:114983, 6 2020. ISSN 03062619. doi: 10.1016/j.apenergy.2020.114983. URL `https://linkinghub.elsevier.com/retrieve/pii/S0306261920304955`.

Wilhelm Hummeltenberg. Implementations of special ordered sets in MP software. *European Journal of Operational Research*, 17(1):1–15, 1984. ISSN 03772217. doi: 10.1016/0377-2217(84)90002-X.

Duong Quoc Hung, Zhao Yang Dong, and Hieu Trinh. Determining the size of PHEV charging stations powered by commercial grid-integrated PV systems considering reactive power support. *Applied Energy*, 183:160–169, 2016. ISSN 03062619. doi: 10.1016/j.apenergy.2016.08.168.

Raphael Hunger. An Introduction to Complex Differentials and Complex Differentiability. Technical report, Technische Universitat Munchen, Munich, 2007.

IBM. DOcplex Python Modeling API, 2020. URL `https://www.ibm.com/support/knowledgecenter/SSSA5P_12.8.0/com.ibm.docplex.help/DOcplex/topics/DOcplex_home.html`.

IEEE Test Feeder Working Group. PES Test Feeder, 2020. URL `https://site.ieee.org/pes-testfeeders/resources/`.

International Energy Agency (IEA). Global EV Outlook 2018: Towards cross-modal electrification, 2018. URL https://webstore.iea.org/global-ev-outlook-2018.

Rabih A. Jabr, Izudin Dzafic, and Bikash C. Pal. Compensation in Complex Variables for Microgrid Power Flow. *IEEE Transactions on Power Systems*, 33(3):3207–3209, 5 2018. ISSN 0885-8950. doi: 10.1109/TPWRS.2018.2816809. URL http://ieeexplore.ieee.org/document/8318631/.

Kumarsinh Jhala, Balasubramaniam Natarajan, Anil Pahwa, and Larry Erickson. Coordinated Electric Vehicle Charging for Commercial Parking Lot with Renewable Energy Sources. *Electric Power Components and Systems*, 45(3):344–353, 2 2017. ISSN 1532-5008. doi: 10.1080/15325008.2016.1248253. URL https://www.tandfonline.com/doi/full/10.1080/15325008.2016.1248253.

Hongjie Jia, Xiaomeng Li, Yunfei Mu, Chen Xu, Yilang Jiang, Xiaodan Yu, Jianzhong Wu, and Chaoyu Dong. Coordinated control for EV aggregators and power plants in frequency regulation considering time-varying delays. *Applied Energy*, 210:1363–1376, 1 2018. ISSN 03062619. doi: 10.1016/j.apenergy.2017.05.174.

Xiaolong Jin, Qiuwei Wu, and Hongjie Jia. Local flexibility markets: Literature review on concepts, models and clearing methods. *Applied Energy*, 261:114387, 3 2020. ISSN 03062619. doi: 10.1016/j.apenergy.2019.114387. URL https://doi.org/10.1016/j.apenergy.2019.114387https://linkinghub.elsevier.com/retrieve/pii/S0306261919320744.

Mohammad Amin Kazemi, Mostafa Sedighizadeh, Mohammad Javad Mirzaei, and Omid Homaee. Optimal siting and sizing of distribution system operator owned EV parking lots. *Applied Energy*, 179:1176–1184, 2016. ISSN 03062619. doi: 10.1016/j.apenergy.2016.06.125. URL http://dx.doi.org/10.1016/j.apenergy.2016.06.125.

WH Kersting. Radial distribution test feeders. In *2001 IEEE Power Engineering Society Winter Meeting. Conference Proceedings (Cat. No.01CH37194)*, volume 2, pages 908–912. IEEE, 2001. ISBN 0-7803-6672-7. doi: 10.1109/PESW.2001.916993. URL http://ieeexplore.ieee.org/xpls/abs_all.jsp?arnumber=916993http://ieeexplore.ieee.org/document/916993/.

Habibalah Kh Khanekehdani, Masoud M. Tafreshi, and Marzieh Khosravi. Modeling operation of electric vehicles aggregator in reserve services market by using game theory method. *Journal of Renewable and Sustainable Energy*, 5(6):1–15, 2013. ISSN 19417012. doi: 10.1063/1.4850524.

KIA. 2018 Kia Soul EV Specifications, 2018. URL `https://www.kiamedia.com/us/en/models/soul-ev/2018/specifications`.

Katarina Knezović, Mattia Marinelli, Antonio Zecchino, Peter Bach Andersen, and Chresten Traeholt. Supporting involvement of electric vehicles in distribution grids: Lowering the barriers for a proactive integration. *Energy*, 134:458–468, 2017. ISSN 03605442. doi: 10.1016/j.energy.2017.06.075.

Mehmetkr Sukru Kuran, Aline Carneiro Viana, Luigi Iannone, Daniel Kofman, Gregory Mermoud, and Jean P Vasseur. A smart parking lot management system for scheduling the recharging of electric vehicles. *IEEE Transactions on Smart Grid*, 6(6):2942–2953, 11 2015. ISSN 19493053. doi: 10.1109/TSG.2015.2403287. URL `http://ieeexplore.ieee.org/document/7056538/`.

Wouter Labeeuw and Geert Deconinck. Residential Electrical Load Model Based on Mixture Model Clustering and Markov Models. *IEEE Transactions on Industrial Informatics*, 9(3):1561–1569, 8 2013. ISSN 1551-3203. doi: 10.1109/TII.2013.2240309. URL `http://ieeexplore.ieee.org/document/6412795/`.

Niels Leemput, Frederik Geth, Juan Van Roy, Jeroen Büscher, and Johan Driesen. Reactive power support in residential LV distribution grids through electric vehicle charging. *Sustainable Energy, Grids and Networks*, 3:24–35, 2015. ISSN 23524677. doi: 10.1016/j.segan.2015.05.002.

Nian Liu, Qifang Chen, Jie Liu, Xinyi Lu, Peng Li, Jinyong Lei, and Jianhua Zhang. A Heuristic Operation Strategy for Commercial Building Microgrids Containing EVs and PV System. *IEEE Transactions on Industrial Electronics*, 62(4):2560–2570, 4 2015. ISSN 0278-0046. doi: 10.1109/TIE.2014.2364553. URL `http://ieeexplore.ieee.org/lpdocs/epic03/wrapper.htm?arnumber=6933935`.

Eduardo Lorenzo. Energy Collected and Delivered by PV Modules. In *Handbook of Photovoltaic Science and Engineering*, chapter 20, pages 949–953. John Wiley & Sons Ltd, 2003. ISBN 0471491969. URL `www.wileyeurope.com`.

Henrik Lund and Willett Kempton. Integration of renewable energy into the transport and electricity sectors through V2G. *Energy Policy*, 36(9): 3578–3587, 9 2008. ISSN 03014215. doi: 10.1016/j.enpol.2008.06.007. URL https://www.sciencedirect.com/science/article/pii/S0301421508002838https://linkinghub.elsevier.com/retrieve/pii/S0301421508002838.

Zhuowei Luo, Zechun Hu, Yonghua Song, Zhiwei Xu, and Haiyan Lu. Optimal coordination of plug-in electric vehicles in power grids with cost-benefit analysis - Part I: Enabling techniques. *IEEE Transactions on Power Systems*, 28(4):3546–3555, 2013. ISSN 08858950. doi: 10.1109/TPWRS.2013.2262318.

Amin Mahmoudzadeh Andwari, Apostolos Pesiridis, Srithar Rajoo, Ricardo Martinez-Botas, and Vahid Esfahanian. A review of Battery Electric Vehicle technology and readiness levels. *Renewable and Sustainable Energy Reviews*, 78(October 2015):414–430, 10 2017. ISSN 13640321. doi: 10.1016/j.rser.2017.03.138. URL https://linkinghub.elsevier.com/retrieve/pii/S1364032115005961https://linkinghub.elsevier.com/retrieve/pii/S1364032117306251.

Fowler Mark, Tristan Cherry, Thomas Adler, Mark Bradley, and Alex Richard. 2015-2017 California Vehicle Survey. Technical report, California Energy Commission, RSG, 2018. URL https://www.nrel.gov/transportation/secure-transportation-data/assets/pdfs/cec_2015-2017_california_vehicle_survey_report.pdf.

Francesco Marra, Guangya Y. Yang, Chresten Traeholt, Esben Larsen, Jacob Ostergaard, Bostjan Blazic, and Wim Deprez. EV charging facilities and their application in LV feeders with photovoltaics. *IEEE Transactions on Smart Grid*, 4(3):1533–1540, 2013. ISSN 19493053. doi: 10.1109/TSG.2013.2271489.

Francesco Marra, Guangya Yang, Chresten Traeholt, Jacob Ostergaard, and Esben Larsen. A Decentralized Storage Strategy for Residential Feeders With Photovoltaics. *IEEE Transactions on Smart Grid*, 5(2):974–981, 3 2014. ISSN 1949-3053. doi: 10.1109/TSG.2013.2281175. URL http://ieeexplore.ieee.org/document/6612760/.

Juan Martínez-Lao, Francisco G. Montoya, Maria G. Montoya, and Francisco Manzano-Agugliaro. Electric vehicles in Spain: An overview of charging systems. *Renewable and Sustainable Energy Reviews*, 77:970–983, 2017. ISSN 18790690. doi: 10.1016/j.rser.2016.11.239.

Arsalan Masood, Junjie Hu, Ai Xin, Ahmed Rabee Sayed, and Guangya Yang. Transactive Energy for Aggregated Electric Vehicles to Reduce System Peak Load Considering Network Constraints. *IEEE Access*, 8: 31519–31529, 2020. ISSN 21693536. doi: 10.1109/ACCESS.2020.2973284.

Carlos Mateo, Giuseppe Prettico, Tomás Gómez, Rafael Cossent, Flavia Gangale, Pablo Frías, and Gianluca Fulli. European representative electricity distribution networks. *International Journal of Electrical Power & Energy Systems*, 99(July 2017):273–280, 7 2018. ISSN 01420615. doi: 10.1016/j.ijepes.2018.01.027. URL `https://doi.org/10.1016/j.ijepes.2018.01.027https://linkinghub.elsevier.com/retrieve/pii/S014206151731801X`.

Thiago R. F. Mendonca and Tim C. Green. Distributed Active Network Management Based on Locally Estimated Voltage Sensitivity. *IEEE Access*, 7:105173–105185, 2019. ISSN 2169-3536. doi: 10.1109/ACCESS.2019.2931955. URL `https://ieeexplore.ieee.org/document/8781767/`.

Ahmed Mohamed, Vahid Salehi, Tan Ma, and Osama Mohammed. Real-Time Energy Management Algorithm for Plug-In Hybrid Electric Vehicle Charging Parks Involving Sustainable Energy. *IEEE Transactions on Sustainable Energy*, 5(2):577–586, 4 2014. ISSN 1949-3029. doi: 10.1109/TSTE.2013.2278544. URL `http://ieeexplore.ieee.org/document/6615945/`.

M Moradijoz, M. Parsa Moghaddam, M R Haghifam, and E Alishahi. A multi-objective optimization problem for allocating parking lots in a distribution network. *International Journal of Electrical Power and Energy Systems*, 46(1):115–122, 2013. ISSN 01420615. doi: 10.1016/j.ijepes.2012.10.041. URL `http://dx.doi.org/10.1016/j.ijepes.2012.10.041`.

Hugo Morais, Tiago Sousa, Zita Vale, and Pedro Faria. Evaluation of the electric vehicle impact in the power demand curve in a smart grid environment. *Energy Conversion and Management*, 82:268–282, 6 2014. ISSN 01968904. doi: 10.1016/j.enconman.2014.03.032. URL `http://linkinghub.elsevier.com/retrieve/pii/S0196890414002246`.

Thomas Morstyn, Alexander Teytelboym, and Malcolm D. McCulloch. Designing decentralized markets for distribution system flexibility. *IEEE Transactions on Power Systems*, 34(3):1–12, 2019. ISSN 08858950. doi: 10.1109/TPWRS.2018.2886244.

Mostafa Rezaei Mozafar, Mohammad H. Moradi, and M.H. Hadi Amini. A simultaneous approach for optimal allocation of renewable energy sources and electric vehicle charging stations in smart grids based on improved GA-PSO algorithm. *Sustainable Cities and Society*, 32(November 2016): 627–637, 2017. ISSN 22106707. doi: 10.1016/j.scs.2017.05.007.

Mostafa Rezaei Mozafar, M. Hadi Amini, and M. Hasan Moradi. Innovative appraisement of smart grid operation considering large-scale integration of electric vehicles enabling V2G and G2V systems. *Electric Power Systems Research*, 154:245–256, 1 2018. ISSN 03787796. doi: 10.1016/j.epsr.2017.08.024. URL `http://linkinghub.elsevier.com/retrieve/pii/S0378779617303498`.

J. Muñoz and O. Perpiñán. A simple model for the prediction of yearly energy yields for grid-connected PV systems starting from monthly meteorological data. *Renewable Energy*, 97:680–688, 11 2016. ISSN 09601481. doi: 10.1016/j.renene.2016.06.023. URL `http://dx.doi.org/10.1016/j.renene.2016.06.023https://linkinghub.elsevier.com/retrieve/pii/S0960148116305444`.

Matteo Muratori. Impact of uncoordinated plug-in electric vehicle charging on residential power demand - supplementary data, 2017. URL `doi:10.7799/1363870`.

Francis Mwasilu, Jackson John Justo, Eun Kyung Kim, Ton Duc Do, and Jin Woo Jung. Electric vehicles and smart grid interaction: A review on vehicle to grid and renewable energy sources integration. *Renewable and Sustainable Energy Reviews*, 34:501–516, 2014. ISSN 13640321. doi: 10.1016/j.rser.2014.03.031.

National Renewable Energy Laboratory. Transportation Secure Data Center, 2017. URL `https://www.nrel.gov/transportation/secure-transportation-data/tsdc-california-vehicle-survey-2017.html`.

Fei Ni, Michiel Nijhuis, Phuong H. Nguyen, and Joseph F.G. Cobben. Variance-Based Global Sensitivity Analysis for Power Systems. *IEEE Transactions on Power Systems*, 33(2):1670–1682, 2018. ISSN 08858950. doi: 10.1109/TPWRS.2017.2719046.

Pedro Nunes, Raquel Figueiredo, and Miguel C Brito. The use of parking lots to solar-charge electric vehicles, 2016. ISSN 18790690.

Alison O'Connell, Damian Flynn, and Andrew Keane. Rolling multi-period optimization to control electric vehicle charging in distribution networks. *IEEE Transactions on Power Systems*, 29(1):340–348, 2014. ISSN 08858950. doi: 10.1109/TPWRS.2013.2279276.

M. E. Oliveira and A. Padilha-Feltrin. A top-down approach for distribution loss evaluation. *IEEE Transactions on Power Delivery*, 24(4):2117–2124, 2009. ISSN 08858977. doi: 10.1109/TPWRD.2009.2014266.

Pol Olivella-Rosell, Eduard Bullich-Massagué, Mònica Aragüés-Peñalba, Andreas Sumper, Stig Ødegaard Ottesen, Josep-Andreu Vidal-Clos, and Roberto Villafáfila-Robles. Optimization problem for meeting distribution system operator requests in local flexibility markets with distributed energy resources. *Applied Energy*, 210:881–895, 1 2018a. ISSN 03062619. doi: 10.1016/j.apenergy.2017.08.136. URL http://dx.doi.org/10.1016/j.apenergy.2017.08.136https://linkinghub.elsevier.com/retrieve/pii/S0306261917311522.

Pol Olivella-Rosell, Pau Lloret-Gallego, Íngrid Munné-Collado, Roberto Villafafila-Robles, Andreas Sumper, Stig Ottessen, Jayaprakash Rajasekharan, and Bernt Bremdal. Local Flexibility Market Design for Aggregators Providing Multiple Flexibility Services at Distribution Network Level. *Energies*, 11(4):822, 4 2018b. ISSN 1996-1073. doi: 10.3390/en11040822. URL http://www.mdpi.com/1996-1073/11/4/822.

Open Data Euskadi. Weather stations: readings collected in 2017, 2018. URL https://opendata.euskadi.eus/catalogo/-/estaciones-meteorologicas-lecturas-recogidas-en-2017/.

Sina Parhizi, Amin Khodaei, and Mohammad Shahidehpour. Market-based versus price-based microgrid optimal scheduling. *IEEE Transactions on Smart Grid*, 9(2):615–623, 2018. ISSN 19493053. doi: 10.1109/TSG.2016.2558517.

Ehsan Pashajavid and Masoud ALIAKBAR Golkar. Placing parking lot of plug-in electric vehicles within a distribution grid considering high penetration level of photovoltaic generation. In *CIRED 2012 Workshop: Integration of Renewables into the Distribution Grid*, number May, pages 386–386. IET, 2012. ISBN 978-1-84919-628-4. doi: 10.1049/cp.2012.0901. URL http://digital-library.theiet.org/content/conferences/10.1049/cp.2012.0901.

Nikolaos G Paterakis and Madeleine Gibescu. A methodology to generate power profiles of electric vehicle parking lots under different operational strategies. *Applied Energy*, 173:111–123, 2016. ISSN 03062619. doi: 10.1016/j.apenergy.2016.04.024. URL http://dx.doi.org/10.1016/j.apenergy.2016.04.024.

John Peacock, Andy Taylor, and Andy Lawrence. Astronomical Statistics. Technical report, The University of Edinburgh, 2012. URL http://www.roe.ac.uk/~jap/teaching/astrostats/.

Pecan Street Inc. Dataport, 2019. URL https://dataport.cloud/data/database.

Chao Peng, Jianxiao Zou, Lian Lian, and Liying Li. An optimal dispatching strategy for V2G aggregator participating in supplementary frequency regulation considering EV driving demand and aggregator's benefits. *Applied Energy*, 190:591–599, 2017. ISSN 03062619. doi: 10.1016/j.apenergy.2016.12.065.

Luis Pieltain Fernandez, Tomás Gomez San Roman, Rafael Cossent, Carlos Mateo Domingo, and Pablo Frias. Assessment of the Impact of Plug-in Electric Vehicles on Distribution Networks. *IEEE Transactions on Power Systems*, 26(1):206–213, 2 2011. ISSN 0885-8950. doi: 10.1109/TPWRS.2010.2049133. URL http://ieeexplore.ieee.org/document/5471115/.

Python Software Foundation. Python 3.6.6, 2018. URL https://www.python.org/downloads/release/python-366/.

Jairo Quiros-Tortos, Luis F. Ochoa, and Becky Lees. A statistical analysis of EV charging behavior in the UK. In *2015 IEEE PES Innovative Smart Grid Technologies Latin America (ISGT LATAM)*, number October, pages 445–449. IEEE, 10 2015. ISBN 978-1-4673-6605-2. doi: 10.1109/ISGT-LA.2015.7381196. URL http://ieeexplore.ieee.org/document/7381196/.

Jairo Quirós-Tortós, Luis F. Ochoa, Sahban W. Alnaser, and Tim Butler. Control of EV Charging Points for Thermal and Voltage Management of LV Networks. *IEEE Transactions on Power Systems*, 31(4):3028–3039, 2016. ISSN 08858950. doi: 10.1109/TPWRS.2015.2468062.

Jairo Quiros-Tortos, Luis Ochoa, and Timothy Butler. How Electric Vehicles and the Grid Work Together: Lessons Learned from One of the Largest Electric Vehicle Trials in the World. *IEEE Power and Energy Magazine*,

16(6):64–76, 11 2018. ISSN 1540-7977. doi: 10.1109/MPE.2018.2863060. URL https://ieeexplore.ieee.org/document/8501603/.

Omid Rahbari, Majid Vafaeipour, Noshin Omar, Marc A Rosen, Omar Hegazy, Jean Marc Timmermans, Seyedmohammadreza Heibati, and Peter Van Den Bossche. An optimal versatile control approach for plug-in electric vehicles to integrate renewable energy sources and smart grids. *Energy*, 134:1053–1067, 2017. ISSN 03605442. doi: 10.1016/j.energy.2017.06.007. URL http://dx.doi.org/10.1016/j.energy.2017.06.007.

Diego A. Ramirez, Alejandro Garces, and Juan Jose Mora-Florez. A Wirtinger Linearization for the Power Flow in Microgrids. In *IEEE Power and Energy Society General Meeting*, volume 2019-Augus. IEEE Computer Society, 8 2019. ISBN 9781728119816. doi: 10.1109/PESGM40551.2019.8973647.

Diego Alejandro Ramirez Loaiza. *Tertiary control in microgrids : an optimal power flow approach based on convex optimization and Wirtinger calculus (Master thesis).* Universidad Tecnológica de Pereira (UTP), 2020. URL https://sites.google.com/utp.edu.co/alejandro/página-principal.

Ariana Ramos, Cedric De Jonghe, Virginia Gómez, and Ronnie Belmans. Realizing the smart grid's potential: Defining local markets for flexibility. *Utilities Policy*, 40:26–35, 2016. ISSN 09571787. doi: 10.1016/j.jup.2016.03.006.

Renewable Energy Policy Network - REN21. Renewables 2018 Global Status Report, 2018. URL http://www.ren21.net/gsr-2018/.

Renewable Energy Policy Network - REN21. Renewables 2020 Global Status Report, 2020. URL https://www.ren21.net/gsr-2020/chapters/chapter_01/chapter_01/#sub_2.

Tiago R. Ricciardi, Kyriacos Petrou, John F. Franco, and Luis F. Ochoa. Defining Customer Export Limits in PV-Rich Low Voltage Networks. *IEEE Transactions on Power Systems*, 34(1):87–97, 2019. ISSN 08858950. doi: 10.1109/TPWRS.2018.2853740.

Peter Richardson, Damian Flynn, and Andrew Keane. Local versus centralized charging strategies for electric vehicles in low voltage distribution systems. *IEEE Transactions on Smart Grid*, 3(2):1020–1028, 2012a. ISSN 19493053. doi: 10.1109/TSG.2012.2185523.

Peter Richardson, Damian Flynn, and Andrew Keane. Optimal charging of electric vehicles in low-voltage distribution systems. *IEEE Transactions on Power Systems*, 27(1):268–279, 2012b. ISSN 08858950. doi: 10.1109/TPWRS.2011.2158247.

C Rus-casas, J D Aguilar, P Rodrigo, F Almonacid, and P J Pérez-higueras. Classification of methods for annual energy harvesting calculations of photovoltaic generators. *Energy Conversion and Management*, 78:527–536, 2014. ISSN 0196-8904. doi: 10.1016/j.enconman.2013.11.006. URL `http://dx.doi.org/10.1016/j.enconman.2013.11.006`.

N. Sadeghianpourhamami, N. Refa, M. Strobbe, and C. Develder. Quantitive analysis of electric vehicle flexibility: A data-driven approach. *International Journal of Electrical Power and Energy Systems*, 95:451–462, 2018. ISSN 01420615. doi: 10.1016/j.ijepes.2017.09.007. URL `http://dx.doi.org/10.1016/j.ijepes.2017.09.007`.

Julian Sainz, Andres Cortes, Julia Merino, and Esther Torres. A voltage sensitivity-based method for assessment of distributed energy resources impact in unbalanced low-voltage grids. In *2020 IEEE International Conference on Environment and Electrical Engineering and 2020 IEEE Industrial and Commercial Power Systems Europe (EEEIC / I&CPS Europe)*, pages 1–6. IEEE, 6 2020. ISBN 978-1-7281-7455-6. doi: 10.1109/EEEIC/ICPSEurope49358.2020.9160857. URL `https://ieeexplore.ieee.org/document/9160857/`.

Sérgio F. Santos, Desta Z. Fitiwi, Miadreza Shafie-khah, Abebe W. Bizuayehu, and João P.S. Catalão. Introduction to Renewable Energy Systems. In *Optimization in Renewable Energy Systems*, pages 1–26. Elsevier, 3 2017. ISBN 9780081012093. doi: 10.1016/B978-0-08-101041-9.00001-6. URL `https://linkinghub.elsevier.com/retrieve/pii/B9780081010419000016`.

Siyamak Sarabi, Arnaud Davigny, Vincent Courtecuisse, Yann Riffonneau, and Benoît Robyns. Potential of vehicle-to-grid ancillary services considering the uncertainties in plug-in electric vehicle availability and service/localization limitations in distribution grids. *Applied Energy*, 171:523–540, 2016. ISSN 03062619. doi: 10.1016/j.apenergy.2016.03.064.

Jonattan E. Sarmiento, Cristian A. Alvez, Bruno N. De Nadai, Antonio Carlos Zambroni De Souza, Edgar M. Carreno, and Paulo F. Ribeiro. A Complex-Valued Three-Phase Load Flow for Radial Networks: High-Performance and Low-Voltage Solution Capability. *IEEE Transactions*

*on Power Systems*, 34(4):3241–3249, 2019. ISSN 15580679. doi: 10.1109/TPWRS.2019.2892014.

Nupur Saxena, Ikhlaq Hussain, Bhim Singh, and Anoop Lal Vyas. Implementation of a Grid-Integrated PV-Battery System for Residential and Electrical Vehicle Applications. *IEEE Transactions on Industrial Electronics*, 65 (8):6592–6601, 8 2018. ISSN 0278-0046. doi: 10.1109/TIE.2017.2739712. URL http://ieeexplore.ieee.org/document/8023763/.

Kevin P. Schneider, Yousu Chen, David P. Chassin, Robert G. Pratt, David W. Engel, and Sandra E. Thompson. Modern Grid Initiative Distribution Taxonomy Final Report. Technical report, Pacific Northwest National Laboratory (PNNL), Richland, WA (United States), 11 2008. URL http://www.osti.gov/servlets/purl/1040684/.

Miadreza Shafie-Khah, Ehsan Heydarian-Forushani, Gerardo J. Osorio, Fabio A.S. Gil, Jamshid Aghaei, Mostafa Barani, and Joao P.S. Catalao. Optimal Behavior of Electric Vehicle Parking Lots as Demand Response Aggregation Agents. *IEEE Transactions on Smart Grid*, 7(6):2654–2665, 2016. ISSN 19493053. doi: 10.1109/TSG.2015.2496796.

Shahab Shokrzadeh, Hajo Ribberink, Issa Rishmawi, and Evgueniy Entchev. A simplified control algorithm for utilities to utilize plug-in electric vehicles to reduce distribution transformer overloading. *Energy*, 133:1121–1131, 2017. ISSN 03605442. doi: 10.1016/j.energy.2017.04.152. URL http://dx.doi.org/10.1016/j.energy.2017.04.152.

Santiago Silvestre. *Review of system design and sizing tools*. Elsevier Ltd, 2018. ISBN 9780128103975. doi: 10.1016/B978-0-12-809921-6.00018-5. URL http://dx.doi.org/10.1016/B978-0-12-809921-6.00018-5.

Branimir Škugor and Joško Deur. A novel model of electric vehicle fleet aggregate battery for energy planning studies. *Energy*, 92, Part 3:444–455, 2015a. ISSN 0360-5442. doi: https://doi.org/10.1016/j.energy.2015.05.030. URL https://www.sciencedirect.com/science/article/pii/S0360544215006118.

Branimir Škugor and Joško Deur. Dynamic programming-based optimisation of charging an electric vehicle fleet system represented by an aggregate battery model. *Energy*, 92:456–465, 12 2015b. ISSN 03605442. doi: 10.1016/j.energy.2015.03.057. URL http://linkinghub.elsevier.com/retrieve/pii/S036054421500362X.

Eric Sortomme, Mohammad M Hindi, S. D.James MacPherson, and S S Venkata. Coordinated charging of plug-in hybrid electric vehicles to minimize distribution system losses. *IEEE Transactions on Smart Grid*, 2(1): 186–193, 3 2011. ISSN 19493053. doi: 10.1109/TSG.2010.2090913. URL `http://ieeexplore.ieee.org/document/5664815/`.

Alfio Spina, Kalle Rauma, Christoph Aldejohann, Mara Holt, Jonas Maasmann, Patrick Berg, Ulf Hager, Fritz Rettberg, and Christian Rehtanz. Smart Grid Technology Lab - A Full-Scale Low Voltage Research Facility at TU Dortmund University. In *2018 110th AEIT International Annual Conference, AEIT 2018*. Institute of Electrical and Electronics Engineers Inc., 12 2018. ISBN 9788887237405. doi: 10.23919/AEIT.2018.8577378.

G. Strbac and J. McDonald. GitHub - sedg/ukgds: United Kingdom Generic Distribution System, 2015. URL `https://github.com/sedg/ukgds`.

Kai Strunz, Ehsan Abbasi, Chad Abbey, Christophe Andrieu, Udaya Annakkage, Stefano Barsali, Ryan C. Campbell, Robert Fletcher, Feng Gao, Trevor Gaunt, Ani Gole, Nikos Hatziargyriou, Reza Iravani, Géza Joos, Hiroo Konishi, Maren Kuschke, Erkki Lakervi, Chen-Ching Liu, Jean Mahseredjian, Farid Mosallat, Dharshana Muthumuni, Antje Orths, Stavros Papathanassiou, Krzysztof Rudion, Zbigniew Styczynski, and Suresh C. Verma. *Benchmark systems for network integration of renewable and distributed energy resources*. Number April. 2014. ISBN 9782858732708.

Xiangjing Su, Mohammad A.S. Masoum, and Peter J. Wolfs. Optimal PV inverter reactive power control and real power curtailment to improve performance of unbalanced four-wire LV distribution networks. *IEEE Transactions on Sustainable Energy*, 5(3):967–977, 2014. ISSN 19493029. doi: 10.1109/TSTE.2014.2313862.

Olle Sundström and Carl Binding. Optimization Methods to Plan the Charging of Electric Vehicle Fleets. In *International Conference on Control, Communication and Power Engineering*, pages 1–6, Chennai, India, 2010. Conference Publishing System. URL `https://www.zurich.ibm.com/pdf/csc/EDISON_ccpe_main.pdf`.

Olle Sundstrom and Carl Binding. Flexible Charging Optimization for Electric Vehicles Considering Distribution Grid Constraints. *IEEE Transactions on Smart Grid*, 3(1):26–37, 3 2012. ISSN 1949-3053. doi: 10.1109/TSG.2011.2168431. URL `http://ieeexplore.ieee.org/document/6112699/`.

Fabian Tamp and Phil Ciufo. A sensitivity analysis toolkit for the simplification of MV distribution network voltage management. *IEEE Transactions on Smart Grid*, 5(2):559–568, 2014. ISSN 19493053. doi: 10.1109/TSG.2014.2300146.

Texas A&M University. Electric Grid Test Case Repository, 2020. URL https://electricgrids.engr.tamu.edu/.

The GridWise Architecture Council. GridWise® Transactive Energy Framework V1.1, 2019. URL https://www.gridwiseac.org/about/transactive_energy.aspx.

Olivier Tremblay and Louis-A. Dessaint. Experimental Validation of a Battery Dynamic Model for EV Applications. *World Electric Vehicle Journal*, 3(2):289–298, 6 2009. doi: 10.3390/wevj3020289. URL http://www.mdpi.com/2032-6653/3/2/289.

Francis K. Tuffner, Michael CW Kintner-Meyer, and Krishnan Gowri. Utilizing Electric Vehicles to Assist Integration of Large Penetrations of Distributed Photovoltaic Generation Capacity. Technical Report November, Pacific Northwest National Laboratory (PNNL), Richland, WA (United States), 11 2012. URL http://www.pnnl.gov/main/publications/external/technical_reports/PNNL-22064.pdfhttp://www.osti.gov/servlets/purl/1060681/.

Pinak J Tulpule, Vincenzo Marano, Stephen Yurkovich, and Giorgio Rizzoni. Economic and environmental impacts of a PV powered workplace parking garage charging station. *Applied Energy*, 108:323–332, 2013. ISSN 03062619. doi: 10.1016/j.apenergy.2013.02.068.

UK Department for Transport. 2017 National Travel Survey, 2018. URL https://www.gov.uk/government/statistics/national-travel-survey-2017.

UNE-EN-50160. Voltage characteristics of electricity supplied by public electricity networks, 2011. URL https://www.une.org/encuentra-tu-norma/busca-tu-norma/norma/?c=N0064209.

U.S. Department of Energy. 2013 Nissan Leaf Advanced Vehicle Testing - Baseline Testing Results. Technical report, 2015. URL http://www.transportation.anl.gov/D3/,.

U.S. Department of Transportation. 2017 National Household Travel Survey. URL https://nhts.ornl.gov/tables09/CodebookBrowser.aspx.

Mart van der Kam and Wilfried van Sark. Smart charging of electric vehicles with photovoltaic power and vehicle-to-grid technology in a microgrid; a case study. *Applied Energy*, 152:20–30, 2015. ISSN 03062619. doi: 10.1016/j.apenergy.2015.04.092. URL http://dx.doi.org/10.1016/j.apenergy.2015.04.092.

Juan Van Roy, Niels Leemput, Frederik Geth, Robbe Salenbien, Jeroen Buscher, and Johan Driesen. Apartment Building Electricity System Impact of Operational Electric Vehicle Charging Strategies. *IEEE Transactions on Sustainable Energy*, 5(1):264–272, 1 2014. ISSN 1949-3029. doi: 10.1109/TSTE.2013.2281463. URL http://ieeexplore.ieee.org/document/6650062/.

Zhiwei Xu, Zechun Hu, Yonghua Song, Wei Zhao, and Yongwang Zhang. Coordination of PEVs charging across multiple aggregators. *Applied Energy*, 136:582–589, 12 2014. ISSN 03062619. doi: 10.1016/j.apenergy.2014.08.116. URL https://linkinghub.elsevier.com/retrieve/pii/S0306261914009398.

Zhiwei Xu, Wencong Su, Zechun Hu, Yonghua Song, and Hongcai Zhang. A Hierarchical Framework for Coordinated Charging of Plug-In Electric Vehicles in China. *IEEE Transactions on Smart Grid*, 7(1):428–438, 1 2016. ISSN 1949-3053. doi: 10.1109/TSG.2014.2387436. URL http://ieeexplore.ieee.org/document/7017597/.

Zhiwei Xu, Tianhu Deng, Zechun Hu, Yonghua Song, and Jianhui Wang. Data-driven pricing strategy for demand-side resource aggregators. *IEEE Transactions on Smart Grid*, 9(1):57–66, 2018. ISSN 19493053. doi: 10.1109/TSG.2016.2544939.

Ruifeng Yan and Tapan Kumar Saha. Voltage variation sensitivity analysis for unbalanced distribution networks due to photovoltaic power fluctuations. *IEEE Transactions on Power Systems*, 27(2):1078–1089, 2012. ISSN 08858950. doi: 10.1109/TPWRS.2011.2179567.

Maziar Yazdani-Damavandi, Mohsen Parsa Moghaddam, Mahmoud-reza Haghifam, Miadreza Shafie-khah, and Joao P. S. Catalao. Modeling Operational Behavior of Plug-in Electric Vehicles' Parking Lot in Multienergy Systems. *IEEE Transactions on Smart Grid*, 7(1):124–135, 1 2016. ISSN 1949-3053. doi: 10.1109/TSG.2015.2404892. URL http://ieeexplore.ieee.org/document/7055363/.

Jia Ying Yong, Vigna K. Ramachandaramurthy, Kang Miao Tan, and N. Mithulananthan. A review on the state-of-the-art technologies of electric vehicle, its impacts and prospects. *Renewable and Sustainable Energy Reviews*, 49:365–385, 2015. ISSN 18790690. doi: 10.1016/j.rser.2015.04.130.

Hongcai Zhang, Zechun Hu, Zhiwei Xu, and Yonghua Song. Evaluation of Achievable Vehicle-to-Grid Capacity Using Aggregate PEV Model. *IEEE Transactions on Power Systems*, 32(1):784–794, 2017. ISSN 08858950. doi: 10.1109/TPWRS.2016.2561296.

Lei Zhang and Yaoyu Li. Optimal Management for Parking-Lot Electric Vehicle Charging by Two-Stage Approximate Dynamic Programming. *IEEE Transactions on Smart Grid*, 8(4):1–9, 2015. ISSN 19493053. doi: 10.1109/TSG.2015.2505298.

Wenjie Zhang, Oktoviano Gandhi, Hao Quan, Carlos D. Rodríguez-Gallegos, and Dipti Srinivasan. A multi-agent based integrated volt-var optimization engine for fast vehicle-to-grid reactive power dispatch and electric vehicle coordination. *Applied Energy*, 229:96–110, 11 2018a. ISSN 03062619. doi: 10.1016/j.apenergy.2018.07.092.

Zedong Zhang, Luis F. Ochoa, and Gustavo Valverde. A Novel Voltage Sensitivity Approach for the Decentralized Control of DG Plants. *IEEE Transactions on Power Systems*, 33(2):1566–1576, 2018b. ISSN 08858950. doi: 10.1109/TPWRS.2017.2732443.

Jinghong Zheng, Xiaoyu Wang, Kun Men, Chun Zhu, and Shouzhen Zhu. Aggregation Model-Based Optimization for Electric Vehicle Charging Strategy. *IEEE Transactions on Smart Grid*, 4(2):1058–1066, 6 2013. ISSN 1949-3053. doi: 10.1109/TSG.2013.2242207. URL `http://ieeexplore.ieee.org/document/6484219/`.

'DIgSILENT GmbH Germany. DIgSILENT PowerFactory, 2019. URL `https://www.digsilent.de/en/`.